UAB
Universitat Autònoma de Barcelona

STUDY OF CHITINASE 3-LIKE 1 AS A PROGNOSTIC BIOMARKER OF NEURODEGENERATION IN MULTIPLE SCLEROSIS

Rucsanda Pinteac

STUDY OF CHITINASE 3-LIKE 1 AS A PROGNOSTIC BIOMARKER OF NEURODEGENERATION IN MULTIPLE SCLEROSIS

Rucsanda Pinteac

PhD thesis, 2024

Supervisors:

Dr. Manuel Comabella López

Prof. Xavier Montalban Gairín

Tutor:

Dr. Manuel Comabella López

Programa de Doctorado en Medicina, Departamento de Medicina, Universitat Autònoma de Barcelona

Vall d'Hebron

Vall d'Hebron Institut de Recerca VHIR

UAB Universitat Autònoma de Barcelona

Cemcat Centre d'Esclerosi Múltiple de Catalunya

Science is the poetry of reality.

Richard Dawkins

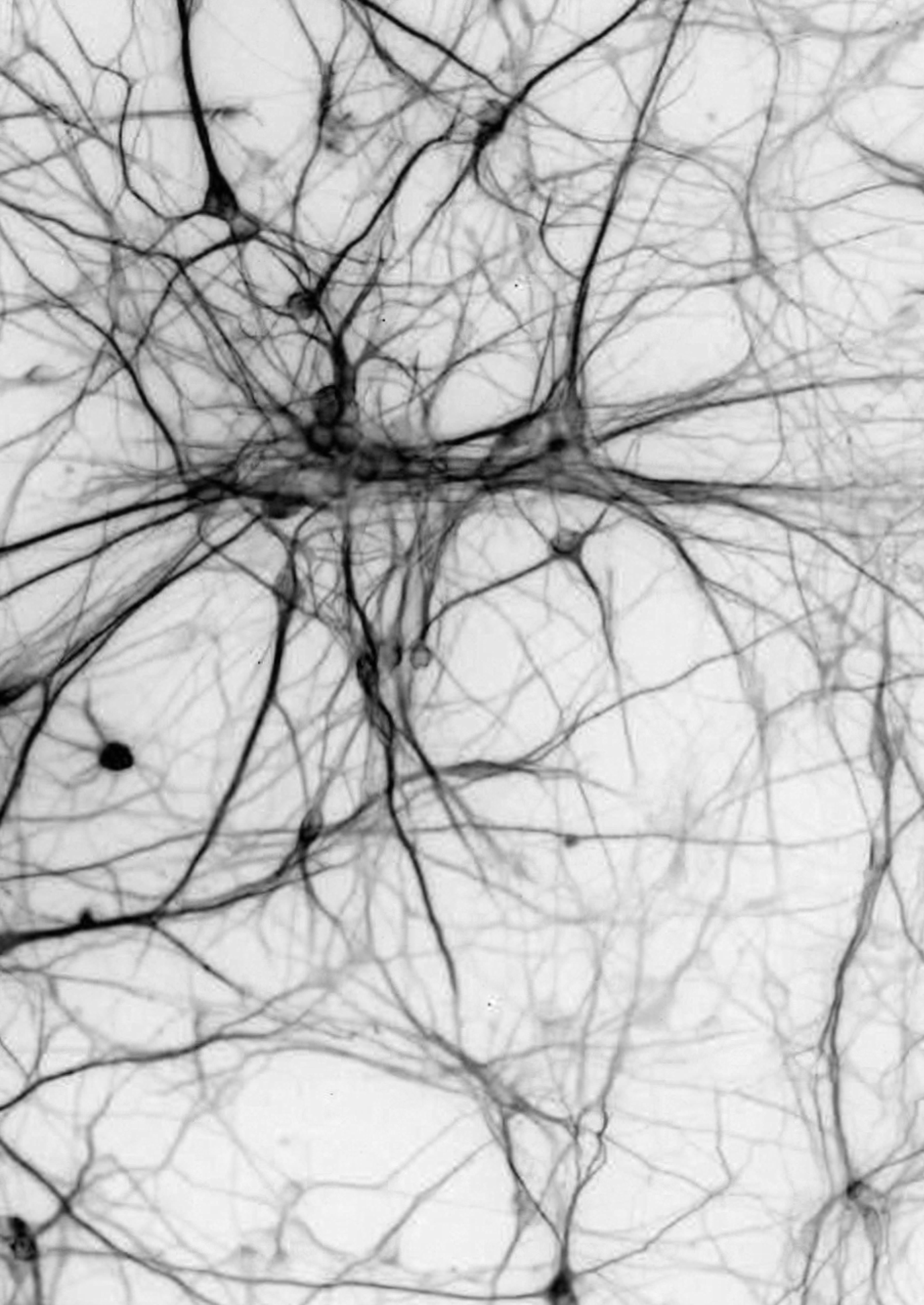

Agradecimientos

En primer lugar, me gustaría expresar mi sincero agradecimiento a mi jefe, Manuel Comabella, por brindarme la valiosa oportunidad de llevar a cabo esta tesis. Sus enseñanzas, orientación y la paciencia que ha demostrado a lo largo de este proceso han sido fundamentales para mi desarrollo académico y profesional. Su apoyo inquebrantable ha sido un faro guía, y estoy profundamente agradecido por la confianza que ha depositado en mí. Continuando, deseo expresar mi más sincero agradecimiento al profesor Xavier Montalbán por ofrecerme la oportunidad de realizar mi tesis en el CEMCAT. Su compromiso con la investigación y su dedicación diaria para mejorar la calidad de vida de los pacientes con esclerosis múltiple son inspiradores. Agradezco su liderazgo visionario, así como la invaluable labor que él y su equipo llevan a cabo. Trabajar bajo su dirección ha sido una experiencia enriquecedora que ha dejado una marca indeleble en mi formación académica y profesional.

En tercer lugar, deseo expresar mi profundo agradecimiento a Jordi Soriano por toda su invaluable ayuda y, especialmente, por el apasionado amor que transmite hacia la ciencia. La colaboración que hemos mantenido ha sido excepcionalmente enriquecedora tanto desde una perspectiva profesional como personal. Su orientación y apoyo constante han contribuido significativamente a mi crecimiento académico. Además, quiero agradecerle por compartir experiencias más allá del ámbito científico, como la inolvidable ocasión en la que me llevó a presenciar mi primer espectáculo de flamenco. Naturalmente no me puedo olvidar de Clara, gracias por los ratitos que hemos compartido en el laboratorio y fuera de él, hablando de nuestros adorables gatos y sobre los cultivos de neuronas, etc. Gracias!

A mis queridos compis del laboratorio,

No puedo finalizar estos agradecimientos sin dedicar unas palabras a aquellos que han sido más que colegas, han sido amigos y una parte fundamental de esta travesía científica. Nico, gracias por abrirme las puertas del grupo; tu amabilidad y orientación han sido clave. Clara, tu ausencia se siente profundamente, y agradezco todo lo que me enseñaste, tanto en lo profesional como en lo personal. Mireia, estos años compartiendo despacho han sido pura diversión. Eres como una hermana mayor y el alma del laboratorio. Maria, nuestra amistad es un tesoro que espero perdure por muchos más años. A Llucía, a pesar de nuestros roces, sabes que es con todo el cariño del mundo. Lucía, gracias por los cafés y los ratitos juntas; nuestra relación de "amigas de despacho, enemigas de poyata" siempre será recordada con cariño. Sunny, tu buena vibra es inspiradora, y Gloria, aunque llevas poco, ya eres imprescindible. Gracias también a Elisa, Andrés y al equipo CER, Carmen y Herena, por su valioso aporte al grupo. No olvido a Laura Calvo y a Elia, grandes compañeras desde las primeras etapas.

A mis amigos, auténticos pilares durante esta intensa etapa, quiero expresar mi gratitud. Ani, eres la mejor compañera, y tu constante presencia ha sido mi mayor fortaleza. Pilar, agradezco tu capacidad para equilibrar mi energía y por estar siempre ahí en cada paso del camino. Gloriya, gracias por ser incondicional durante nuestros 20 años de amistad; tu amistad es un tesoro que valoro profundamente. A Dani y Joel, más que amigos, sois fuente de inspiración y grandes artistas. Vuestra presencia ha iluminado mis días y enriquecido mi vida de manera inigualable.

A mi familia, pilar fundamental de mi existencia, quiero expresar mi eterna gratitud. Mama, tata, Vasile, abuela, tíos Olga y Marcos, y a Marina y Sofi, nunca podré agradecer lo suficiente su inquebrantable apoyo, paciencia y amor incondicional. Cada uno de vosotros ha sido un gran apoyo en los momentos más desafiantes, y vuestra presencia ha hecho de este viaje una experiencia aún más valiosa.

Por último, quiero dirigirme a mí misma con un sincero agradecimiento. A lo largo de esta travesía, he aprendido a valorar cada pequeño paso hacia adelante, incluso en las montañas rusas emocionales. Sin prisa, pero sin pausa, he perseverado día a día, creciendo y mejorando constantemente. Este agradecimiento personal es un recordatorio de la importancia de la autoapreciación en el camino de la autorrealización.

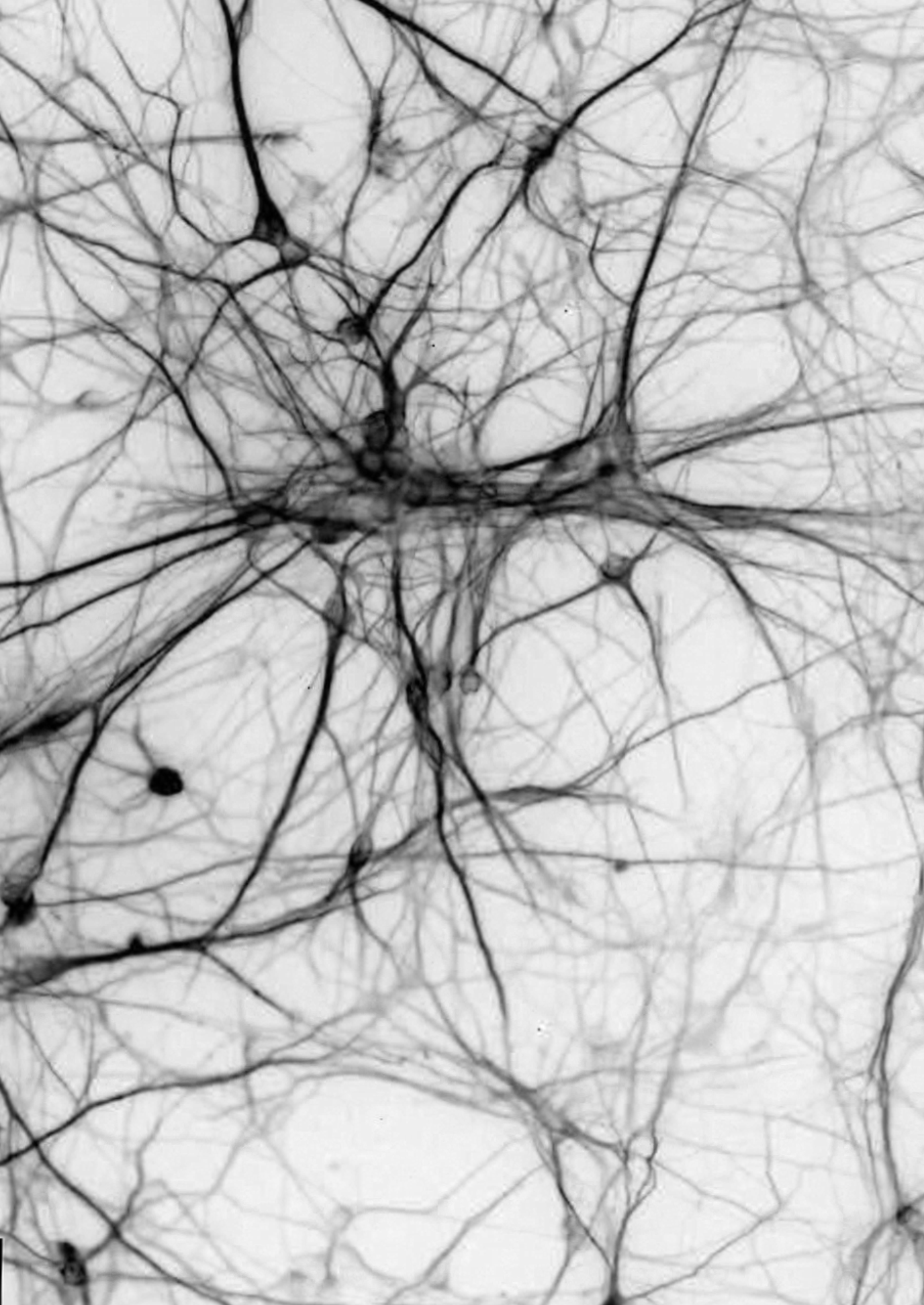

Abbreviations

AD - Alzheimer's disease

AFP – α-fetoprotein

ALS – amyotrophic lateral sclerosis

AMPA - α-amino-3-hydroxy-5-methyl-4-isoxazolepropionic acid

APC – antigen presenting cell2

ASA – α-sarcomeric actin

ASMA – α-smooth muscle actin

ATP – adenosine triphosphate

AU – Airy Unit

BBB – blood-brain barrier

BDNF – brain derived neurotrophic factor

BMP – bone morphogenetic protein

BSA – bovine serum albumin

cAMP – cyclic adenosine monophosphate

CCI – cortical controlled impact

CHI3L1 – chitinase-3 like 1

CLPs – chitinase-like proteins

CIS – clinically isolated syndrome

CRTH2 – prostaglandin D2 receptor 2

CJD – Creutzfeldt-Jakob disease

CNS – central nervous system

CSF – cerebrospinal fluid

CTIP2 – COUP-TF interacting protein 2

DAPI - 4',6-diaminido-2-phenylindole

DCX – doublecortin

DEGs – differentially expressed genes

DMTs – disease modifying treatments

EBs – embryoid bodies

EGF – epidermal growth factor

EAE – experimental autoimmune encephalomyelitis

ERK – extracellular signal-regulated kinase

FACS – fluorescence activated cell sorting

FBS – fetal bovine serum

FC – fold change

FGF – fibroblast growth factor

FGFR4 – fibroblast growth factor receptor 4

FOXA2 – forkhead box A2

FTD – frontotemporal dementia

GABA - γ-aminobutyric

GH18 – glycosyl hydrolase family

GM – grey matter

GM-CSF – granulocyte-macrophage colony stimulating factor

GNA – global network activity

GO – Gene Ontology

GSEA – Gene set enrichment analysis

GFAP – glial fibrillary acidic protein

hiPSCs – human induced pluripotent stem cells

HRP – horse radish peroxidase

IBI – interburst-interval

ICQ - immunocytochemistry

IF - immunofluorescence

IFN-β – interferon-β

IFN-γ – interferon – γ

IL-1β – interleukin-1β

IL-2 – interleukin-2

IL-6 – interleukin-6

IL-13Rα2 – interleukin-13 receptor α2

IL-17 – interleukin-17

IL-27 – interleukin-27

IRF1 – interferon responsive factor 1

KEGG – Kyoto encyclopedia of genes and genomes

KLF4 – KLF transcription factor 4

LAA – large artery atherosclerotic stroke

MAP2 – microtubule associated protein 2

MAPK – mitogen activated protein kinase

MCAO – middle cerebral arterial occlusion

MCI – mild cognitive impairment

MHC – major histocompatibility complex

MRI – magnetic resonance imaging

MS – Multiple sclerosis

mtDNA – mitochondrial DNA

MYC - MYC Proto-Oncogene, BHLH Transcription Factor

NAWM – normal-appearing white matter

NABA – novel angiogenesis biologically active peptides

NDS – normal donkey serum

NES – normalized enrichment score

NfL – neurofilament light chain

NGS – normal goat serum

NIM – neural induction medium

NMDA – N-methyl-D-aspartate

NOX - NADPH oxidases

NPCs – neural progenitor cells

NSCs – neural stem cells

OCT3/4 - POU Class 5 Homeobox 1

OPCs – oligodendrocyte progenitor cells

OXPHOS – oxidative phosphorylation

PBS – phosphate-buffered saline

PCS – post-contusion syndrome

PD – Parkinson’s disease

PFA – paraformaldehyde

PLO – poly-L-ornithine

POLAM – Poly-L-Ornithine/Laminin

PMS – progressive multiple sclerosis

PPMS – primary progressive multiple sclerosis

PSD-95 – postsynaptic density protein 95

PVCA – principal variance component analysis

PVDF – polyvinylidene fluoride

RA – retinoic acid

RAGE – advanced glycation end products

RAF – rapidly accelerated fibrosarcoma

RB – retinoblastoma

ROI – region of interest

ROS – reactive oxygen species

RRMS – relapsing-remitting multiple sclerosis

SMAD – suppressor of mothers against decapentaplegic

SMA – spinal muscular atrophy

SOX1 – SRY-box transcription factor 1

SOX2 – SRY-box transcription factor 2

SPMS – secondary progressive multiple sclerosis

STAT – signal transduced and activator of transcription

TBS – Tris buffered saline

TBI – traumatic brain injury

Tbr1 – T box brain transcription factor 1

TGF-β1 – transforming growth factor β1

TMEM219 – transmembrane protein 219

TNF – tumour necrosis factor

TMEM219 – transmembrane protein 219

vGAT – vesicular GABA transporter

vGLUT1 – vesicular glutamate transporter 1

WB – western blot

INDEX

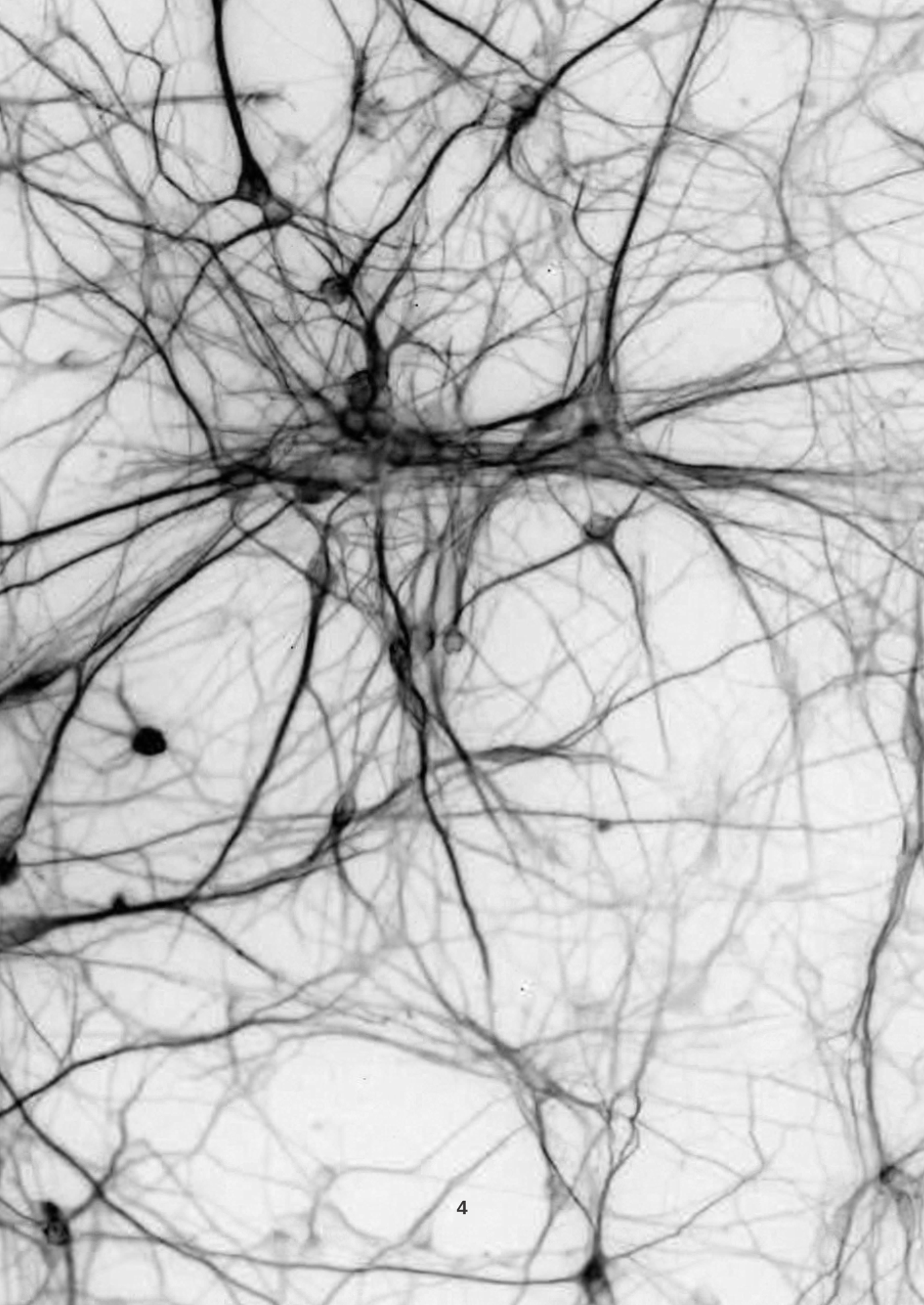

ABSTRACT

Multiple sclerosis (MS) is a chronic autoimmune disorder affecting the central nervous system (CNS), characterized by demyelination and neurodegeneration. Despite current therapeutic efforts focusing on anti-inflammatory and immune-modulatory strategies, the progressive phase of the disease still presents challenges in treatment. There is therefore an imperative need for biomarkers capable of capturing the diverse aspects of the heterogeneity of MS, serving as essential tools for understanding disease progression and potentially identifying therapeutic targets.

Chitinase-3 like 1 (CHI3L1) emerges as a promising biomarker in MS, with elevated levels in the cerebrospinal fluid (CSF) linked to the conversion from clinically isolated syndrome (CIS) to MS and rapid disability progression. Furthermore, increased CHI3L1 levels are associated with increased risk of neurological disability, development of a secondary progressive phase of MS, and cognitive dysfunction in early MS.

Building upon these clinical observations, our research group conducted in the past a preliminary study on murine cortical neurons, revealing reduced viability and dendrite retraction induced by CHI3L1. This crucial exploration prompted a transition to human neurons derived from human induced pluripotent stem cells (hiPSCs) of relapsing-remitting MS (RRMS) patients. In this model, CHI3L1 induced dendrite retraction and reduced dendritic arborization. Synaptic alterations were also evident, with decreased synapsin, a pre-synaptic marker, and active synapses, along with a trend for reduced PSD-95, a post-synaptic marker. Notably, CHI3L1 induced dynamic changes in neuronal network behaviour and increased neuronal excitability, as demonstrated by calcium imaging studies.

Comprehensive transcriptomic and bioinformatic analyses unveiled modifications in synaptic-related processes and signalling, aligning with the observed changes in synaptic function and excitability. Additionally, we detected alterations associated with inflammatory pathways and cytoskeleton remodelling, consistent with the pleiotropic nature of CHI3L1. RT-qPCR validation showed the differential expression

patterns of genes previously implicated in neurodegenerative and synaptic processes (such as UHMK1) or linked to neuropsychiatric diseases and cellular methylation processes (such as GNMT). Molecular investigations revealed the activation of the JAK/STAT1 pathway by CHI3L1, specifically through the phosphorylation of STAT1 at the Y701 residue. Transcription factor enrichment analysis implicated IRF1 and STAT1 as potential regulators, establishing a direct link between CHI3L1 and the interferon response pathway.

Altogether, the research conducted in this thesis integrates clinical observations with mechanistic insights, pointing at CHI3L1 as a valuable biomarker in MS progression and elucidating its neurotoxic effects on human neurons. These findings contribute to a broader understanding of the role of CHI3L1 in MS pathogenesis, offering potential avenues for targeted therapeutic interventions.

RESUMEN

La esclerosis múltiple (EM) es un trastorno autoinmune crónico que afecta el sistema nervioso central (SNC), caracterizado por desmielinización y neurodegeneración. A pesar de los esfuerzos terapéuticos actuales centrados en estrategias antiinflamatorias e inmunomoduladoras, la fase progresiva de la enfermedad sigue presentando desafíos en el tratamiento. Existe una necesidad imperativa de biomarcadores capaces de capturar los diversos aspectos de la heterogeneidad de la EM, sirviendo como herramientas esenciales para comprender la progresión de la enfermedad y potencialmente identificar dianas terapéuticas.

La proteína 1 similar a la quitinasa-3 (CHI3L1) emerge como un biomarcador prometedor en la EM, con niveles elevados en el líquido cefalorraquídeo (LCR) relacionados con la conversión del síndrome clínicamente aislado (SCA) a la EM y la rápida progresión de la discapacidad. Además, niveles elevados de CHI3L1 se asocian con un mayor riesgo de discapacidad neurológica, desarrollo de una fase de EM secundariamente progresiva y disfunción cognitiva en las etapas iniciales de la EM.

Basándonos en estas observaciones clínicas, nuestro grupo de investigación llevó a cabo un estudio preliminar en neuronas corticales murinas, revelando una reducción en la viabilidad y retracción de dendritas inducidas por CHI3L1. Esta exploración crucial condujo a una transición a neuronas humanas derivadas de células madre pluripotentes inducidas (hiPSCs) de pacientes con EM remitente-recurrente (EMRR). En este modelo, CHI3L1 indujo retracción de dendritas y reducción de la arborización dendrítica. También se observaron alteraciones sinápticas, con disminución de la sinapsina, un marcador presináptico, y sinapsis activas, junto con una tendencia a la reducción de PSD-95, un marcador postsináptico. Notablemente, CHI3L1 indujo cambios dinámicos en el comportamiento de la red neuronal y aumentó la excitabilidad neuronal, según lo demostrado por estudios de imágenes de calcio.

Análisis transcriptómicos y bioinformáticos revelaron modificaciones en procesos y señalización relacionados con las sinapsis, en línea con los cambios observados en

la función sináptica y la excitabilidad. Además, detectamos alteraciones asociadas con vías inflamatorias y remodelación del citoesqueleto, coherentes con la naturaleza pleiotrópica de CHI3L1. La validación mediante RT-qPCR mostró patrones de expresión diferencial de genes previamente implicados en procesos neurodegenerativos y sinápticos (como UHMK1) o vinculados a enfermedades neuropsiquiátricas y procesos de metilación celular (como GNMT). Las investigaciones moleculares revelaron la activación de la vía JAK/STAT1 por CHI3L1, específicamente mediante la fosforilación de STAT1 en el residuo Y701. El análisis de enriquecimiento de factores de transcripción implicó a IRF1 y STAT1 como posibles reguladores, estableciendo un vínculo directo entre CHI3L1 y la vía de respuesta a interferones.

En resumen, la investigación desarrollada en esta tesis integra observaciones clínicas con estudios de los mecanismos, señalando a CHI3L1 como un valioso biomarcador en la progresión de la EM y elucidando sus efectos neurotóxicos en neuronas humanas. Estos hallazgos contribuyen a una mayor comprensión del papel de CHI3L1 en la patogénesis de la EM, ofreciendo posibles vías para intervenciones terapéuticas específicas.

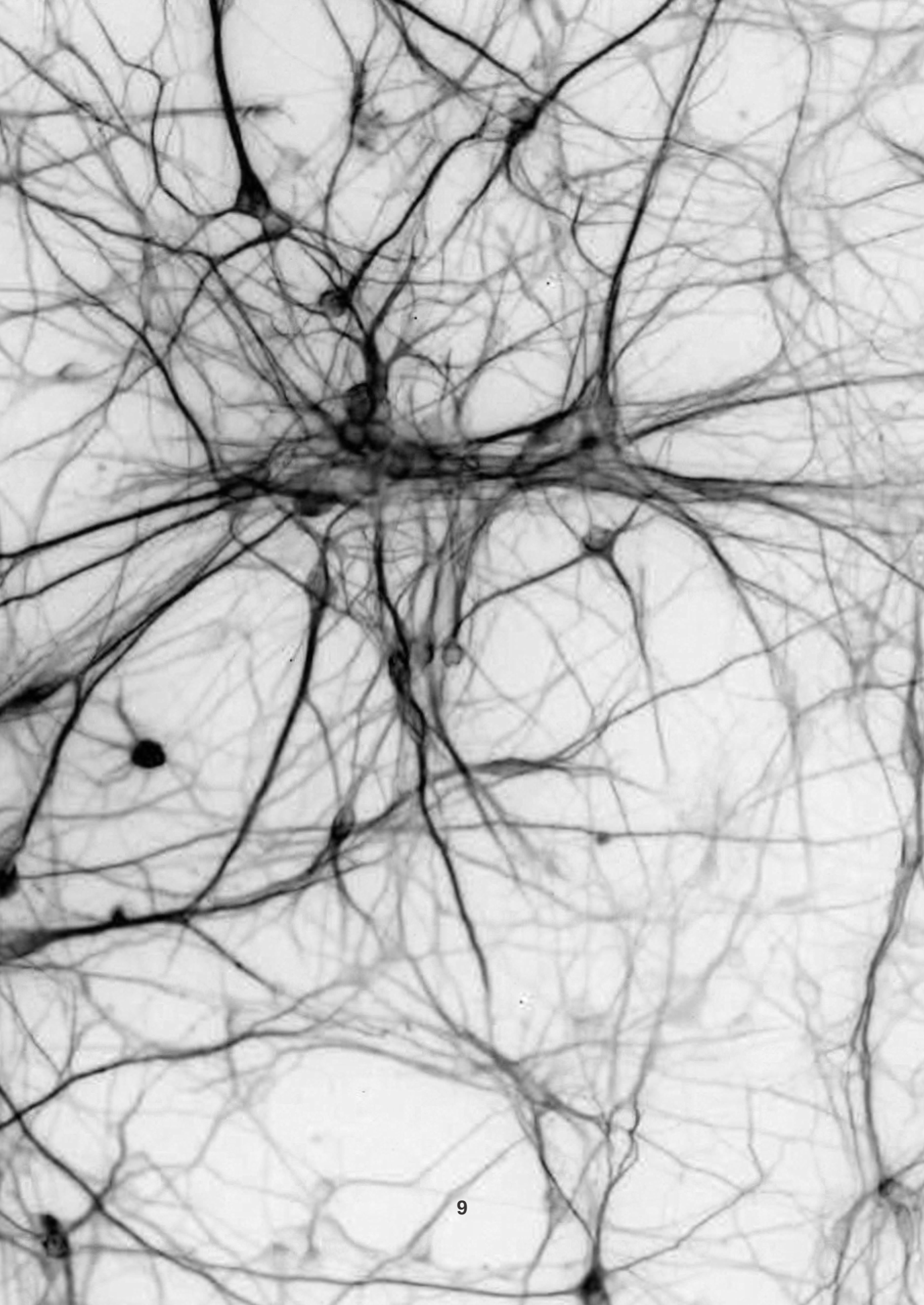

INTRODUCTION

1. INTRODUCTION

1.1 Multiple sclerosis

Multiple sclerosis (MS) is a chronic inflammatory demyelinating disease of the central nervous system (CNS), and is the leading cause of non-traumatic neurological disability in young adults in Europe and North America, affecting 2.5 million people worldwide.[1]

1.1.1 Aetiology

The aetiology of MS remains unclear, yet it is recognized as a complex, multifactorial disease influenced by both genetic and environmental factors. MS is a polygenic condition with a modest inherited risk for disease susceptibility.[2] Incomplete penetrance and moderate individual effect of each *loci* hint at the presence of epistatic interactions and subsequent postgenomic events.[3] The loci associated with the disease are mostly related to the major histocompatibility complex class II (MHC II)-mediated antigen presentation. Nevertheless, genetics alone cannot explain disease development; additional environmental factors are likely involved.[4] Viral infections, through mechanisms like molecular mimicry or bystander activation, have been postulated to trigger autoimmune T cell activation.[5] This hypothesis is supported by research showing a correlation between Epstein-Barr infection and an increased risk of MS.[6] Moreover, gender disparities in MS incidence, with women being affected more frequently at a ratio of 2.3-3.5:1, suggest the potential involvement of hormonal factors.[5,7] Additionally, well-established risk factors such as smoking, vitamin D deficiency, and childhood obesity have been associated with an increased probability of developing MS.[8]

1.1.2 Clinical aspects

MS typically manifests in young adults, predominantly affecting individuals between the ages of 20 and 40.[1] However, a subset of approximately 5% of diagnosed patients experience their initial symptoms either during childhood or adolescence,[9] or in late adulthood,[10] exceeding 50 years of age.

The initial manifestations of MS exhibit significant variability among patients, commonly involving a range of neurological symptoms such as limb weakness, sensory disruptions, optic neuritis, gait instability, and ataxia.[3] Likewise, the clinical course of MS is heterogeneous, with several phenotypes that are defined depending on clinical patterns and additional descriptors as disease activity and disease progression, which reflect ongoing inflammatory and neurodegenerative processes, respectively.[11] Four clinical courses have been defined, and can be classified as relapsing or progressive: (1) clinically isolated syndrome (CIS), (2) relapsing-remitting MS (RRMS), (3) primary progressive MS (PPMS), and (4) secondary progressive MS (SPMS)[11] (**Figure 1**).

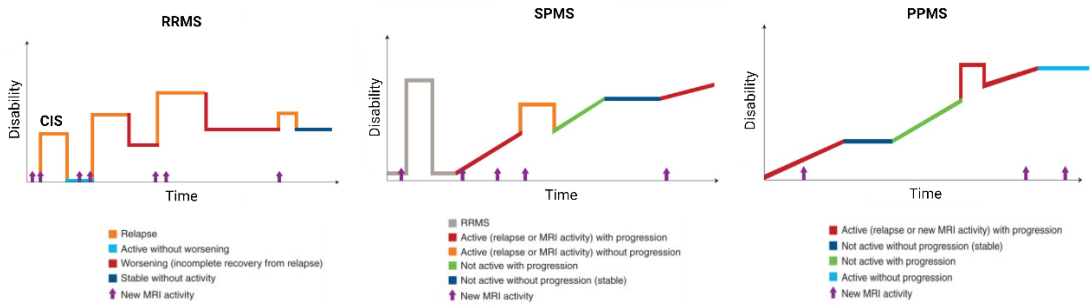

Figure 1. Clinical courses of MS. Adapted from *Klineova S, Lublin FD. Clinical Course of Multiple Sclerosis. Cold Spring Harb Perspect Med. 2018 Sep 4;8(9):a028928.*

Abbreviations: RRMS – relapsing-remitting multiple sclerosis, SPMS – secondary progressive multiple sclerosis, PPMS – primary progressive multiple sclerosis, MRI – magnetic resonance imaging

Most patients, approximately 85-90%, initially debut with a first acute clinical attack, a CIS. This episode strongly indicates inflammatory demyelination and could allow diagnosing RRMS if additional criteria are met.[12] Such criteria may be clinical (i.e., presenting a second attack over time), radiological (presence of typical demyelinating lesions in several brain or spinal cord topographies), or biological (determination of oligoclonal bands in cerebrospinal fluid, CSF).[12] RRMS is defined

by a pattern of alternating phases: relapses marked by the emergence of new neurological symptoms, followed by remissions during which clinical stability may or may not involve complete recovery after relapses. Over time, if such episodes continue to occur, this remission ability becomes increasingly incomplete, resulting in the gradual accumulation of neurological disability and cognitive decline.[13,14] This results in a proportion of patients developing the SPMS clinical form, characterized by ongoing neurological disability independent of relapse activity.[15] Conversely, 10-15% of patients experience a progressive course since disease onset, known as PPMS, characterized by cumulative neurological disability without relapses.[15] The underlying pathological mechanisms in MS differ depending on whether the disease exhibits a progressive course or not. In its earlier stages, RRMS is primarily characterized by an inflammatory component, while in the progressive forms of the disease, neurodegeneration becomes the predominant feature.[13]

1.1.3 Pathology

The primary pathological hallmarks of MS are focal demyelinated regions, referred to as plaques or lesions, affecting both white matter (WM) and grey matter (GM), along with diffuse neurodegeneration.[13] Clinical and magnetic resonance imaging (MRI) data indicate that immune-driven demyelination and the formation of new lesions are common in RRMS. Active lesions are characterized by disruption of the blood-brain barrier (BBB), immune infiltration, reactive gliosis, axonal transection and loss, and expression of pro-inflammatory molecules[13] (**Figure 2**).

The demyelination process involves the activation of astrocytes in active lesions and the development of gliotic scars within inactive lesions.[14] Early in the disease course, axonal transection and axonal loss become apparent and occur in the context of acute inflammation and also as a consequence of demyelination.[15] Some lesions can in part be remyelinated as a result of recruitment and differentiation of oligodendrocyte progenitors. However, during the progressive phases of the disease, new demyelinating lesions become rare. Instead, there is a prominence of diffuse neurodegeneration in both the WM and GM, along with alterations in the normal-appearing white matter (NAWM),[16] and slow expansion of pre-existing lesions.[17]

Inflammation and reactive gliosis are observed in all stages of the disease, being more pronounced in active lesions, but also seen in inactive plaques, remyelinated lesions or NAWM[18] (**Figure 2**). Moreover, meningeal ectopic lymphoid structures are detected in progressive MS patients, and are associated with neurodegeneration and cortical pathology.[19]

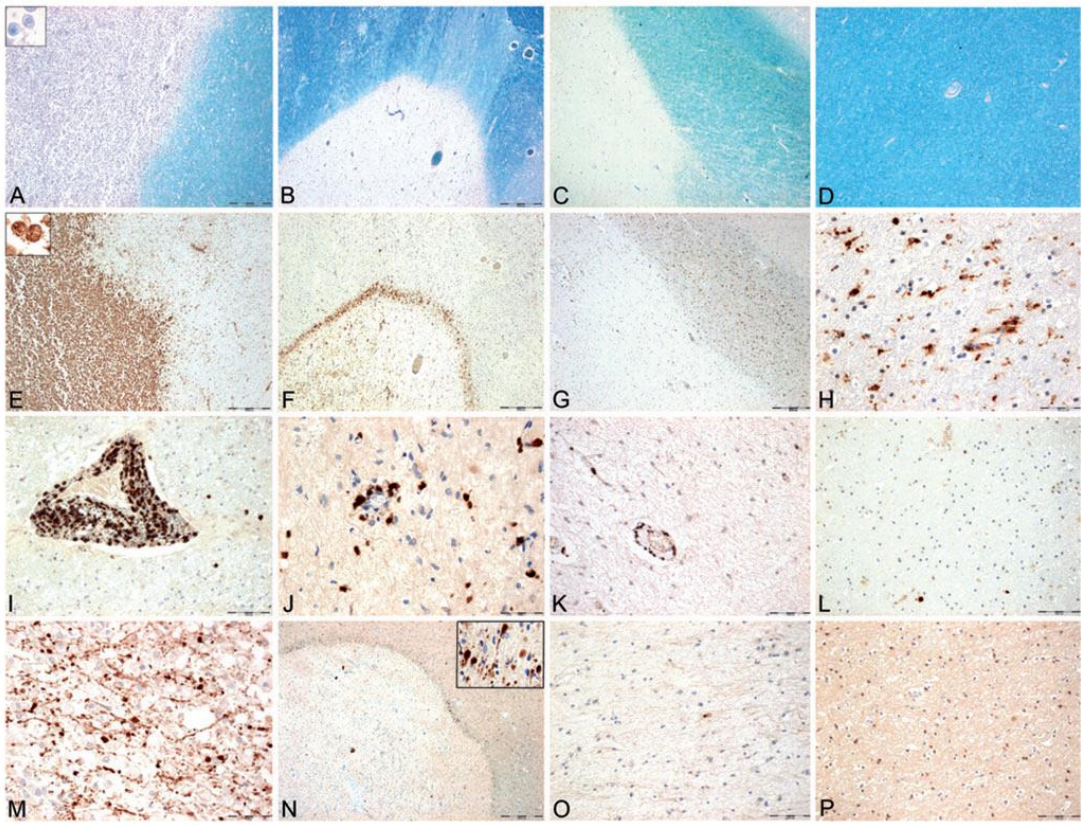

Figure 2. Pathological features in MS lesions and NAWM. (**A, E, I**, and **M**) Panels depict an active lesion in a patient with RRMS displaying active demyelination (**A**), immune cell infiltration (**E** and **I**), and acute axonal injury (**M**). (**B, F, J**, and **N**) Panels illustrate an expanding lesion in a patient with SPMS, featuring focal demyelination (**B**), presence of CD68-positive cells at the lesion edge (**F**), T cell immune infiltration (**J**), and acute axonal injury (**N**). (**C, G, K**, and **O**) Panels show an inactive lesion in a patient with SPMS, exhibiting focal demyelination sharply delineated from the surrounding NAWM (**C**), some CD68-positive cells (**G**), moderate T cell immune infiltration (**K**), and axonal transection within the inactive lesion (**O**). (**D, H, L**, and **P**) Panels reveal the NAWM in a patient with RRMS without demyelination (**D**), the presence of some CD68-positive cells (**H**), a few infiltrating T cells (**L**), and no axonal transection (**P**). The myelin staining using Luxol fast blue with periodic acid-Schiff (PAS) reaction

is utilized for demyelination and myelin visualization in panels (**A-D**). Immunohistochemistry is employed for CD68 staining in panels (**E-H**), for CD3 staining in panels (**I-J**), and for amyloid precursor protein staining in panels (**M-P**) to visualize axonal damage. Adapted from *Frischer JM, Bramow S, Dal-Bianco A, Lucchinetti CF, Rauschka H, Schmidbauer M, Laursen H, Sorensen PS, Lassmann H. "The relation between inflammation and neurodegeneration in multiple sclerosis brains." Brain. 2009 May;132(Pt 5):1175-89*.

Abbreviations: MS – multiple sclerosis, NAWM – Normal appearing white matter, RRMS – relapsing-remitting multiple sclerosis, SPMS – secondary progressive multiple sclerosis, CD68 – cluster of differentiation 68, CD3 – cluster of differentiation 3

1.1.4 Pathogenic Mechanisms

Over the past three decades, significant progress has been made in understanding MS pathogenesis. The traditional view that early stages of MS are defined by neuroinflammation and late stages by neurodegeneration has now evolved, and it is recognized that both components coexist throughout all disease stages differing in quantitative parameters.[17] Despite various hypotheses, the precise mechanisms driving disease progression remain unclear. One traditional theory supports that MS starts as an inflammatory disease, but after years of chronic inflammation, an independent neurodegenerative process takes over, leading to disease progression. Evidence supporting an autoimmune theory originates from research on experimental autoimmune encephalomyelitis (EAE), a condition in animals that can be triggered through sensitization with CNS antigens.[20] In recent years, evidence supporting the inside-out hypothesis has grown, suggesting that MS is primarily a neurodegenerative disease with secondary inflammation amplifying its progression.[21,22]

Immunopathogenesis

The question of whether MS originates in the peripheral or CNS is still unresolved. In the peripheral model, autoreactive T cells are activated at peripheral sites and migrate to the CNS, accompanied by monocytes and B cells, where they exert their effector functions.[5] Alternatively, CNS-specific events could initiate a secondary immune system infiltration.[23] Nevertheless, the immune system assumes a pivotal role in the pathogenesis of MS, and key contributors to the inflammatory process

have been identified. Autoimmune inflammation in early MS is primarily caused by an adaptive immune response that involves T and B lymphocytes, and autoantibodies. Peripheral immune cell infiltration through the BBB promotes relapses and focal demyelinating plaques formation.[24] Autoreactive lymphocytes infiltrate into the CNS through the choroid plexus, the subarachnoid space or crossing the BBB. Once in the CNS, T cells recognize myelin antigens presented by perivascular macrophages. This recognition prompts the T cells to secrete pro-inflammatory cytokines and chemokines, which result in reactive gliosis and the subsequent breakdown of the BBB. Consequently, this allows for the recruitment of additional immune cells into the CNS. This coordinated response involving the peripheral immune infiltrate, along with the activation of microglia and astroglia, perpetuates neuroinflammation, ultimately leading to demyelination and axonal injury[25] (**Figure 3A**).

Multiple immune cell types play crucial roles in the complex immunopathogenesis of MS. Among these, CD4+ T cells of Th1 phenotype contribute to the initiation of acute lesions through the secretion of pro-inflammatory mediators as interferon-γ (IFN-γ), interleukin-2 (IL-2) and tumour necrosis factor α (TNF-α).[26] Concurrently, Th17 cells mediate pathogenic mechanisms through the production of interleukin-17 (IL-17).[27] Elevated levels of IL-17 have been detected in both demyelinated plaques and CSF of patients with MS, and are associated with active disease. [28,29,30] Studies using *in vivo* imaging in the EAE model showed that Th17 cells can establish direct contact with neurons, causing dysfunction and neuronal death.[31] Interestingly, interleukin-27 (IL-27), a negative regulator of the differentiation of Th17, can prevent inflammatory demyelination in the EAE model.[32]

Moving on to CD8+ T cells, which are the predominant T cell population within MS lesions[33], they exhibit both immune-suppressive and pathogenic features. For instance, CD8+ T cells can mediate suppression of CD4+ T cells through the secretion of perforin, which exerts cytotoxic effects leading to the inactivation of T cells. Conversely, CD8+ T cells can directly mediate axonal damage through the recognition of MHC I epitopes on the surface of axons.[34] Notably, CD8+ T cells can

transect axons, directly killing of glia, induce oligodendrocyte death, and also increase vascular permeability.[4]

B cells have accumulated increasing attention due to their multifaceted roles in MS pathology. Beyond antibody production, B cells can present antigens to T cells, secrete cytokines, and form ectopic germinal centers.[26] Treatment with rituximab (an anti-CD20 therapy) demonstrated efficacy in MS patients and is widely used.[35] Macrophages exhibit dual functions in MS, where they can either play a neuroprotective role and support tissue repair or contribute to tissue damage through the secretion of pro-inflammatory molecules and antigen presentation.[36]

Conversely, chronic stages of MS present a compartmentalized immune response within the CNS with activated glia and macrophages, and meningeal immune cell infiltrates that can form lymphoid-like structures.[5] The continuous inflammation, perpetuated by both immune cells and CNS-resident microglia and astrocytes, promotes the release of a wide range of neurotoxic inflammatory mediators. Prolonged neuronal and oligodendrocyte exposure to this ongoing inflammatory milieu fosters neuroaxonal injury and oligodendrocyte damage, ultimately driving irreversible neurodegenerative processes[37] (**Figure 3B**).

A

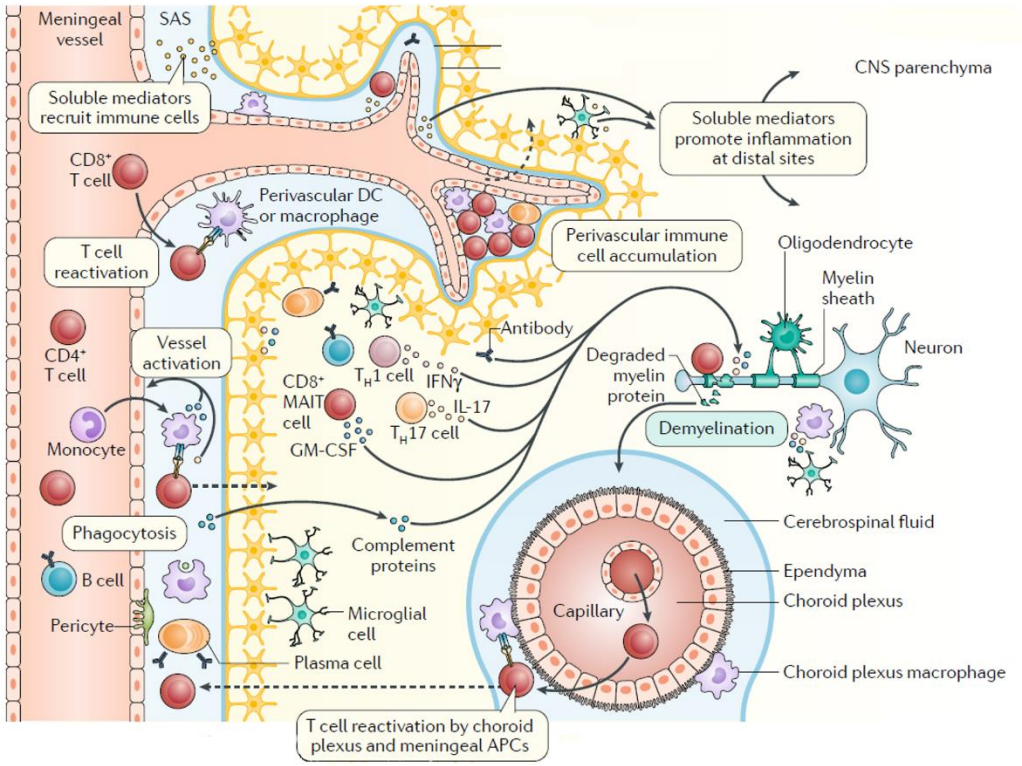
Meningeal vessel
SAS
Soluble mediators recruit immune cells
CD8+ T cell
Perivascular DC or macrophage
T cell reactivation
CD4+ T cell
Vessel activation
Monocyte
Phagocytosis
B cell
Pericyte
CD8+ MAIT cell
TH1 cell
IFNγ
IL-17
TH17 cell
GM-CSF
Antibody
Complement proteins
Microglial cell
Plasma cell
T cell reactivation by choroid plexus and meningeal APCs
CNS parenchyma
Soluble mediators promote inflammation at distal sites
Perivascular immune cell accumulation
Oligodendrocyte
Myelin sheath
Neuron
Degraded myelin protein
Demyelination
Cerebrospinal fluid
Ependyma
Choroid plexus
Capillary
Choroid plexus macrophage

B

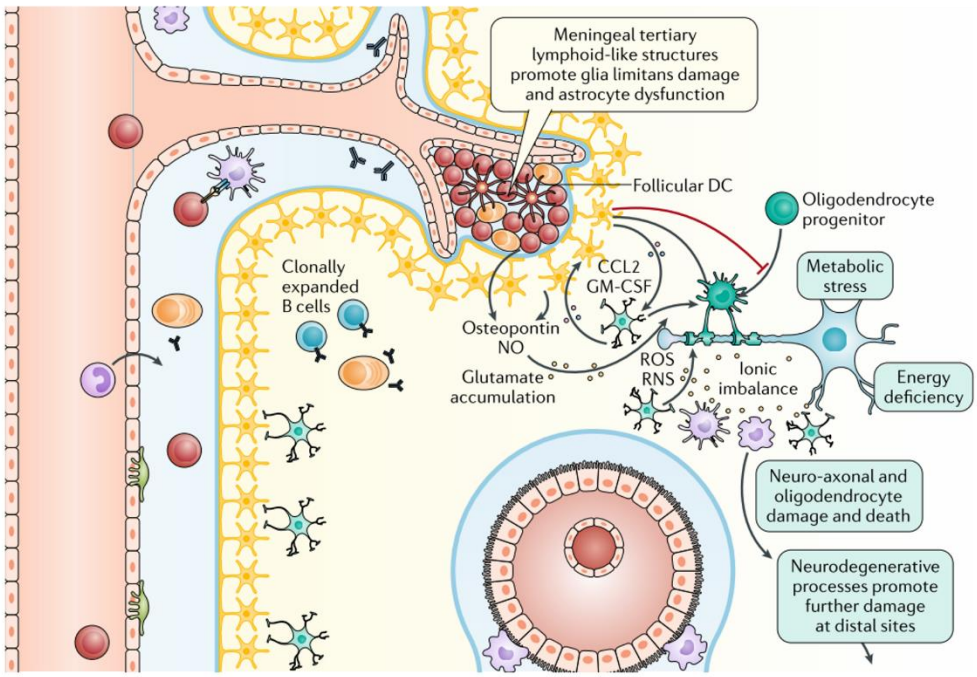
Meningeal tertiary lymphoid-like structures promote glia limitans damage and astrocyte dysfunction
Follicular DC
Oligodendrocyte progenitor
Clonally expanded B cells
CCL2
GM-CSF
Metabolic stress
Osteopontin
NO
Glutamate accumulation
ROS
RNS
Ionic imbalance
Energy deficiency
Neuro-axonal and oligodendrocyte damage and death
Neurodegenerative processes promote further damage at distal sites

Figure 3. Immunopathogenesis in early and late MS. (A) Peripheral immune cells enter the CNS parenchyma trough the blood vessels of the BBB, the subarachnoid space, or the choroid plexus (dashed arrows). In the early inflammatory phase of MS, adaptive immune system cells as T cells CD4+ or CD8+, along with B cells infiltrate the CNS and perpetuate inflammation and contribute to oligodendrocyte and neuronal injury, and demyelination through cell contact-dependent mechanisms and secretion of soluble factors. **(B)** Ongoing tissue injury and clinical manifestations of progressive disease are attributed to neurodegeneration, specifically neuroaxonal damage and oligodendrocyte injury. This damage results from oxidative stress, immune cell activation, mitochondrial dysfunction that led to metabolic stress and energy deficiency, altered glutamate balance, and a pro-inflammatory environment, potentially involving cytotoxic factors and complement activation. Chronic inflammation is facilitated by CNS-compartmentalized inflammation involving meningeal immune cell infiltrates forming lymphoid-like structures and resident CNS cells. For instance, astrocytes secrete CCL2 and GM-CSF which recruit and activate microglia and inhibit remyelination by impeding oligodendrocyte differentiation. Adapted from *Filippi, M., Bar-Or, A., Piehl, F. et al. Multiple sclerosis. Nat Rev Dis Primers 4, 43 (2018)*

Abbreviations: APC – antigen presenting cells, BBB – blood-brain barrier, CCL2 – chemokine ligand 2, CD4 – cluster of differentiation 4, CD8 – cluster of differentiation 8, CNS – central nervous system, DC – dendritic cells, GM-CSF – granulocyte-macrophage colony stimulating factor, IFN-γ – interferon γ, IL-17 – interleukin 17, Th – T helper, MS – multiple sclerosis

Mechanisms of Neurodegeneration in MS

The neurodegenerative process in MS starts early in the disease and is the main cause of irreversible neurological disability and cognitive deficits in MS patients.[22] Several mechanisms of neurodegeneration have been proposed, for instance, exhaustion of oligodendrocyte and neuronal compensatory mechanisms, lack of trophic support, chronic microglial activation, altered expression of ion channels in demyelinated axons as well as oxidative stress, synaptopathy, glutamate excitotoxicity and mitochondrial injury.[17]

During an acute MS attack, the release of proinflammatory cytokines leads to increased glutamate synaptic transmission and a concurrent decrease in γ-aminobutyric (GABA) mediated synaptic signalling thus resulting in heightened synaptic hyperexcitability and potentially contributing to the neurodegenerative process. Furthermore, it appears that the inflammatory microenvironment has a direct impact on the structural alterations and subsequent loss of both presynaptic

and postsynaptic components.[38] Proinflammatory cytokines, such as TNF-α and interleukin-1β (IL-1β), modulate neuronal excitability and, therefore, neuronal function[39] (**Figure 4**). Studies conducted using murine striatal slices incubated in CSF obtained from individuals with active RRMS provide evidence suggesting the involvement of cytokines in disrupted synaptic hyperexcitability and, potentially, excitotoxic neurodegeneration.[40,41]

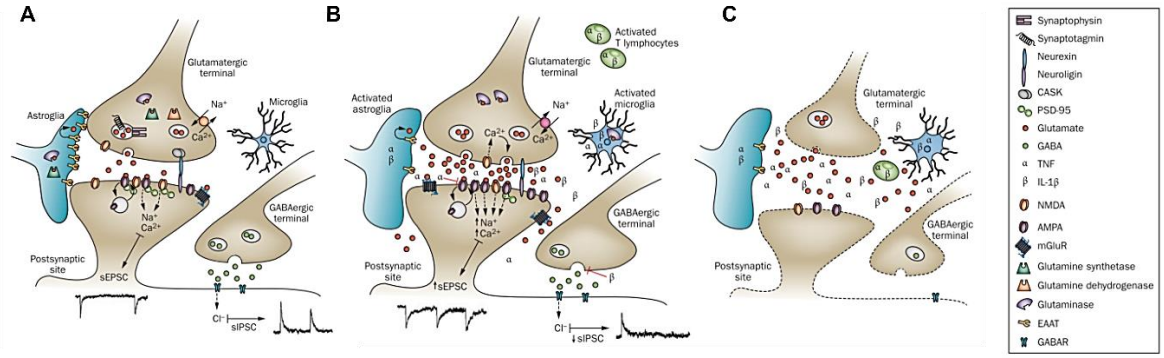

Figure 4. Inflammatory synaptopathy in MS. The figure illustrates the concept of inflammatory synaptopathy in the context of MS, shedding light on the impact of inflammation on synaptic function and structural integrity in the CNS. **(A)** In a healthy synapse, precise control mechanisms regulate the concentrations of excitatory (glutamate) and inhibitory (GABA) neurotransmitters at the synaptic cleft through transmitter release, degradation, and reuptake. **(B)** Proinflammatory cytokines, released by autoreactive lymphocytes and activated microglia, disrupt synaptic function in both the glutamatergic and GABAergic systems in MS. **(C)** Additionally, inflammation can lead to structural alterations, including synaptic loss characterized by the degeneration of the presynaptic and/or postsynaptic components, as well as changes in the glial environment. The figure also provides representative electrophysiological traces (sEPSC and sIPSC) in each panel to underscore these changes. Adapted from *Mandolesi G, Gentile A, Musella A, Fresegna D, De Vito F, Bullitta S, Sepman H, Marfia GA, Centonze D. Synaptopathy connects inflammation and neurodegeneration in multiple sclerosis. Nat Rev Neurol. 2015 Dec;11(12):711-24.*

Abbreviations: AMPA – α-amino-3-hydroxy-5-methyl-4-isoxazolepropionic acid, CASK – Ca^{2+}-calmodulin-dependent protein kinase II, EAAT – excitatory amino acid transporter, EAE – experimental autoimmune encephalomyelitis, GABA – γ-aminobutyric acid, GABAR – GABA receptor, MS – multiple sclerosis, mGluR – metabotropic glutamate receptor, NMDAR – N-methyl-D-aspartate receptor, PSD-95 – postsynaptic density protein 95, sEPSC – spontaneous excitatory postsynaptic current, sIPSC – spontaneous inhibitory synaptic current, TNF – tumor necrosis factor.

The acute clinical impairment associated with new focal inflammatory lesions in MS is linked to axonal transection, subsequent Wallerian degeneration, and loss of synapses.[15] Demyelinated axons are more vulnerable to premature degeneration due to excessive metabolic demands and axonal excitotoxicity from the pro-inflammatory environment in MS lesions.[42] Glutamate is the major neurotransmitter in the CNS, and it has a major role in the communication among neurons and glia.[43] Increased glutamate levels in the CSF of MS patients were observed in several studies[44,45], originating from activated microglia and macrophages, astroglia via diverse mechanisms, neurons in response to intracellular calcium fluctuations, and alterations in glutamate uptake.[46] Excessive glutamate exerts its effects by binding to ionotropic receptors, mainly the N-methyl-D-aspartate (NMDA), and metabotropic receptors, and eliciting the influx of extracellular and intracellular calcium into the axoplasma, thus contributing to neurotoxicity[46,47] (**Figure 5B**). Excitotoxic synapse damage can cause cortical network dysfunctions, cognitive disabilities, neurodegeneration, and neuronal cell death that could lead to irreversible disease progression.[48]

Ectopic and abnormal expression of axonal ion channels has been observed in both MS and EAE model.[49] The increased expression of sodium channels in demyelinated axons first establish a molecular basis for the restoration of action potential conductions as a compensatory mechanism, but non-inactivating sodium conductance can elicit a calcium-mediated neuronal lesion through reverse sodium-calcium exchange[50] (**Figure 5B**).

While it is evident that axonal degeneration is partly attributed to demyelination and the subsequent loss of trophic support from oligodendrocytes, it is essential to note that axonal and neuronal damage can manifest independently of demyelination as well.[51] Moreover, alterations in synaptic transmission manifest early in the course of MS, regardless of the presence of demyelination or axonal loss.[52] Prolonged perturbations in synaptic homeostasis can give rise to excitotoxicity and eventual neuronal death. GM damage, a prominent feature of MS, begins early in the disease process, and it exhibits partial independence from demyelination.[53,54] The GM

damage is closely correlated with clinical disability and cognitive dysfunction. Autopsies of progressive MS patients have provided insights into the molecular changes associated with this condition, revealing a decreased expression of neurexin/neuroligin, synaptophysin, synaptotagmin, and PSD-95.[55] Notably, a substantial reduction in synaptophysin levels has been observed in the MS neocortex, and this reduction was unrelated to local demyelination.[52]

Oxidative damage represents an early and pivotal event in the pathogenesis of MS, exerting a substantial influence on the development of MS lesions and the ensuing neurodegeneration. This oxidative stress induces extensive damage to lipids and proteins through peroxidation and nitration processes.[56] During oxidative bursts, activated microglia and macrophages produce reactive oxygen species (ROS) via NADPH oxidases (NOX) enzymes[57], thereby contributing to mitochondrial impairment, which, in turn, triggers further ROS production as a result of respiratory chain dysfunction. The accumulation of iron associated with aging exacerbates neuroinflammatory oxidative stress[58], and the release of iron from ferritin stores, occurring upon oligodendrocyte damage and in conjunction with ROS, generates highly hazardous hydroxyl radicals[59]. Neurons exhibit heightened sensitivity to oxidative stress, with observable accumulation of oxidized phospholipids and DNA strand breaks in cortical MS lesions.[60] Additionally, there is compelling evidence supporting a positive feedback loop between excitotoxicity and oxidative stress.[61]

Mitochondrial injury with its subsequent energy deficiency and failure is another central player in MS pathogenesis. Significant alterations in mitochondrial structure and function have been clearly identified within MS lesions.[62] A noteworthy aspect of mitochondrial DNA (mtDNA) is that lacks protective histones and prolonged exposure to ROS can induce mutations in mtDNA, ultimately undermining the overall functionality of mitochondria.[63] Furthermore, mitochondrial permeability transition can lead to mitochondrial damage and death because of the dysregulation of the mitochondrial transmembrane potential and subsequent collapse of the oxidative phosphorylation (OXPHOS). The consequences of this disrupted OXPHOS cascade are profound. As a result of altered mitochondrial OXPHOS, the high demands for

neuroaxonal adenosine triphosphate (ATP) can no longer be met, giving rise to a state of chronic hypoxia[63] (**Figure 5A**).

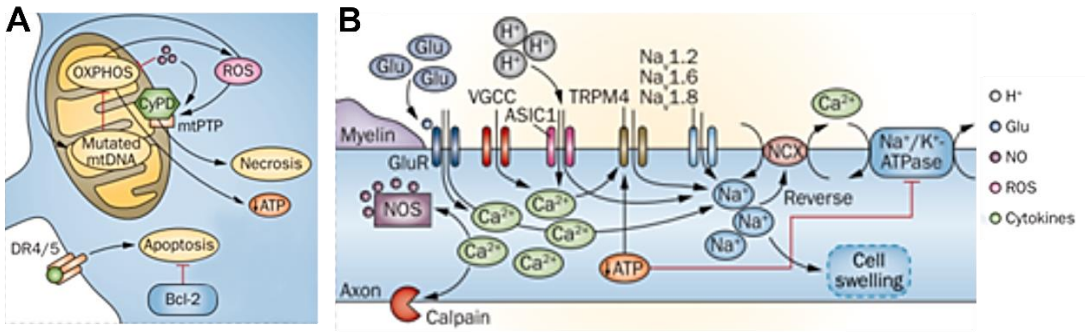

Figure 5. Neuronal injury mechanisms in chronic CNS inflammation. (A) Inflammatory production of ROS and NO triggers the opening of the mtPTP, leading to the accumulation of mitochondrial DNA (mtDNA) mutations, oxidized and misfolded proteins, and necrosis. Impaired mitochondria disrupt oxidative phosphorylation (OXPHOS), resulting in elevated ROS levels and reduced adenosine triphosphate (ATP) production. Apoptosis is partly induced by the engagement of death receptors DR4/5. **(B)** Excessive extracellular glutamate (Glu) activates Glu receptors, causing calcium (Ca^{2+}) influx into neuroaxons. Membrane depolarization activates VGCC and enhances sodium channel (Nav) activity. ASIC1 contributes to further Ca^{2+} influx, and both ASIC1 and TRPM4 enhance sodium (Na^{+}) influx. Reduced ATP levels diminish sodium-potassium ATPase (Na^{+}/K^{+}-ATPase) activity, resulting in the reverse operation of the NCXand a critical increase in intracellular Ca^{2+} and Na^{+} levels. Prolonged elevation of Ca^{2+} activates degradative enzymes and nitric oxide synthase (NOS), ultimately leading to neuronal apoptosis and necrosis. Adapted from *Friese MA, Schattling B, Fugger L. Mechanisms of neurodegeneration and axonal dysfunction in multiple sclerosis. Nat Rev Neurol. 2014 Apr;10(4):225-38.*

Abbreviations: ASIC1 - acid-sensing ion channel 1, CyPD - cyclophilin D, DR4/5 - death receptor 4 and 5, Glu - glutamate, mtDNA - mitochondrial DNA, mtPTP - mitochondrial permeability transition pore, Nav - voltage-gated sodium channel, NCX - sodium-calcium exchanger, NO - nitric oxide, NOS - nitric oxide synthase, OXPHOS - oxidative phosphorylation, ROS - reactive oxygen species, TRPM4 - transient receptor potential cation channel subfamily M member 4, VGCC - voltage-gated calcium channels.

1.1.5 Treatment

Exploring immunopathogenic mechanisms has led to the development of therapies aimed at reducing the frequency and severity of clinical relapses through anti-inflammatory and immune-modulatory approaches. However, when patients enter the progressive disease phase, treatment options are reduced. The disease has an important neurodegenerative component that does not respond to the immune-modulatory and anti-inflammatory treatment. There are approved disease modifying treatments (DMTs) that modify the disease course shortening the duration of the relapses and their frequency, and can be roughly classified into injectables, oral therapies and monoclonal antibodies.[64]

Injectable DMTs include interferon-β (IFN-β) and glatiramer acetate, and exhibit anti-inflammatory and immunoregulatory effects, although their exact mechanisms of action remain unclear.[65,66]

Oral therapies include fingolimod, dimethyl fumarate, teriflunomide and cladribine. Fingolimod is an analogue of sphingosine 1-phosphate and it primarily works by preventing T cell egress from secondary lymphoid organs, thereby reducing the autoimmune attack on the CNS.[67] Other sphingosine 1-phosphate modulators with similar mechanism of action such as ozanimod[68] and ponesimod[69] are also currently available. Dimethyl fumarate has immunomodulatory properties by shifting from a proinflammatory to an anti-inflammatory cytokine profile.[70] Teriflunomide is an anti-mitotic agent that inhibits the proliferation of activated lymphocytes.[71] Cladribine is a purine analogue that ultimately inhibits DNA synthesis and reparation, and depletes populations of activated lymphocytes.[72]

Regarding monoclonal antibodies, they target specific proteins or immune cell populations involved in the pathogenesis of MS. For instance, natalizumab (an anti VLA-4 therapy) interferes with the migration of immune cells across the BBB[73], while anti-CD20 therapies such as ocrelizumab, rituximab or ofatumumab deplete B cells[74].

Furthermore, emerging therapeutic targets are focusing on addressing smouldering inflammation, such as Bruton's Tyrosine Kinase inhibitors, which target B cells and

microglial activation. These newer therapies may hold promise for progressive MS patients.[75]

1.1.6 Biomarkers

Biomarkers, defined as quantifiable indicators of biological conditions, serve as critical tools for distinguishing diseases with similar clinical phenotypes or shared pathophysiological mechanisms. Additionally, biomarkers are essential for monitoring and stratifying patients according to disease activity and progression, as well as for predicting responses to therapeutic interventions. These indicators also contribute to a deeper understanding of disease etiopathogenesis and, in some cases, may evolve into therapeutic targets for specific conditions.[76]

MS, a disease characterized by its heterogeneity, has a significant need for biomarkers capable of capturing the diverse aspects of the condition. These biomarkers can be classified into four distinct groups: predictive, diagnostic, disease activity, and treatment-response markers.[77] Predictive biomarkers have the potential to identify individuals at a higher risk of developing MS. Meanwhile, diagnostic biomarkers, in conjunction with clinical and radiological findings, may support the differential diagnosis of the disease. Disease activity biomarkers can be measured in patients with relapsing-remitting and progressive disease courses and may help in the distinction between MS patients with benign and aggressive disease courses based on the presence, for instance, of clinical activity, radiological inflammatory activity, or development of brain atrophy.

Treatment-response biomarkers are indispensable for assessing a patient's response to medication and optimizing their treatment regimen.[77] In the current landscape of MS, the biomarkers routinely used in clinical practice are CSF-IgG oligoclonal bands, IgG index and MRI.[78]

Despite the dynamic nature of biomarker research in the field of MS, the clinical integration of validated biomarkers remains limited.[77] Two particularly promising biomarkers that are gradually finding its way into routine MS clinical practice are the levels of the neurofilament light chain (NfL) and glial fibrillary acidic protein (GFAP)

in blood.[79,80] These biomarkers serve as valuable indicators of ongoing neurodegeneration and astrocytic activation in MS patients. Besides, elevated levels of CSF chitinase-3 like 1 (CHI3L1) have been linked to the conversion from CIS to MS, as well as to early and rapid disability progression.[81–83] However, it is essential to emphasize the requirement for additional research and validation in this regard.

1.2 Chitinase 3-like 1 (CHI3L1)

1.2.1 CHI3L1 as Biomarker of Neuroinflammation

CHI3L1 has been extensively described as a biomarker indicative of neuroinflammation, not only in MS but also in other neurodegenerative diseases as Alzheimer's disease (AD), amyotrophic lateral sclerosis (ALS) or Creutzfeldt-Jakob disease (CJD), as well as in acute neuroinflammatory scenarios such as stroke or traumatic brain injury (TBI). **Table 1** provides a summary of studies focusing on CHI3L1 and its involvement in various neurological disorders.

Table 1. Summary of CHI3L1 studies in neurological disorders. Adapted from *Pinteac et al., 2021*

Disease	Comments – findings	CNS expression
Multiple sclerosis (MS)	- High levels in early phases are associated with ↑ risk for MS and neurological disability (CSF) [83–86] - Levels correlate with clinical and radiological disease activity (CSF) [87] - Levels are increased in progressive forms of the disease (CSF and blood) [82,84,88] - Predictor of progression to a SPMS phase of the disease (CSF) [88] - Associated with brain volume loss (CSF) [83,89] - Associated with the therapeutic response to interferon-beta (CSF) [90]	Astrocytes and macrophage /microglial cells from chronic active lesions with high and low inflammatory activity
Alzheimer's disease (AD)	- Levels are ↑ in preclinical, prodromal, and demential cases of AD versus cognitively normal controls (CSF)[91–94] - High levels are associated with ↑ risk of AD in cognitively unimpaired individuals or MCI patients (CSF)[94–96]	In a subset of astrocytes from frontal cortex

	- Levels increase over time in patients with AD and MCI (CSF)[96] - High levels are associated with cortical thinning in parietal and temporal areas (CSF)[94,97] - Controversial results as diagnostic biomarker to distinguish AD from FTD (CSF)[91–93,95,98] - Levels ↑ in AD versus α-synucleinopathies (CSF)[93,99]	
Amyotrophic lateral sclerosis (ALS)	- Levels are ↑ in ALS versus ALS mimics, healthy controls and other disease controls (CSF) [100–104] - Controversial results as prognostic biomarker [100–102,104–106] - Levels are longitudinally stable or slightly increase over time [100,101,103,104] - Associated with cognitive impairment (CSF)[101]	Astrocytes from spinal cord and frontal cortex
Stroke	- Levels correlate with infarct volume, stroke severity, and functional outcome (blood)[107] - Independent predictor of the clinical outcome of the LAA stroke (blood)[108] - High baseline levels are associated with increased risk of stroke (blood)[109–112]	Transient expression in astrocytes proximal to the injury during the acute stage
Traumatic brain injury (TBI)	- Levels increase at day 1 post injury, peak at day 4, and decrease by day 6 (CSF)[113] - May be predictor of worse survival outcome (CSF)[113] - Levels correlate with volume of intracranial lesion (blood)[114] - Associated with level of consciousness after TBI (blood)[114] - Levels are ↑ in PCS patients versus healthy controls and correlate with symptom severity and lifetime number of contusions (CSF)[115]	Transient expression in astrocytes in the contusional and pericontusional area†
Creutzfeld-Jakob disease (CJD)	- Levels are ↑ in CJD patients versus patients with Alzheimer's disease, FTD, and controls (CSF) [116,117] - Levels are ↑ in CJD patients versus patients with neurodegenerative dementias, neurological controls and healthy subjects (blood)[118]	Reactive protoplasmic and perivascular astrocytes and fibrillar astrocytes in the white matter

Abbreviations: CSF - cerebrospinal fluid, FTD: frontotemporal dementia, LAA - large-artery atherosclerotic stroke, MCI - mild cognitive impairment, SPMS - secondary progressive MS, PCS - post-contusion syndrome, † - cortical controlled impact model

In conclusion, CHI3L1 has emerged as an interesting biomarker for neuroinflammation, demonstrating its significance not only in MS but also in various other neurodegenerative conditions where CHI3L1 levels have been associated with increased risk and severity, disease progression and cognitive decline.

1.2.2 CHI3L1: Structure and Function

CHI3L1, also known as YKL-40 in humans or BRP-39 in mice, is a 40 kD glycoprotein pertaining to the 18 glycosyl hydrolase family (GH18).[119] GH18 family comprises both active chitinases capable of chitin hydrolysis and chitinase-like proteins (CLPs), including CHI3L1, lacking enzymatic activity but exhibiting strong chitin binding affinity.[120] While true chitinases primarily physiological function is the chitin and chitinous organism clearance,[121] the precise role of CLPs is not yet completely understood. Nevertheless, they appear to be involved in a plethora of biological processes related to inflammation, regulation of immune response, and tissue remodeling.[76] In this regard, upregulation of CHI3L1 is a shared biomarker of numerous inflammatory conditions as inflammatory bowel disease[122], rheumatoid arthritis[123], chronic obstructive pulmonary disease[124], diabetes[125] and cancer[126–128].

CHI3L1 exhibits widespread cellular expression, encompassing chondrocytes[129], macrophages[130], osteoclasts[131], microglia and astrocytes[132], among others. CHI3L1 acts as an acute phase reactant, secreted by immune cells when exposed to pro-inflammatory molecules as interleukin-6 (IL-6), IFN-γ, IL-1β or TNF-α.[123] CHI3L1 is expressed in a time dependent manner during the differentiation and maturation of dendritic cells.[131] Intriguingly, increased expression of CHI3L1 has been described in both M1 and M2 polarized macrophages, suggesting multifaceted roles in inflammation.[133] Furthermore, CHI3L1 appears to play a role in modulating the Th1/Th2 inflammatory balance.[134]

1.2.3 CHI3L1: Receptors and Signalling

CHI3L1 signalling is intricate and context-dependent, with emerging insights into its ligands interactions and cellular signalling pathways (**Figure 6**). Recently, hyaluronan was described as the physiological ligand of CHI3L1[135], although it has the ability to bind to several known receptors.

Several studies demonstrated interaction of CHI3L1 with the interleukin-13 receptor α2 (IL-13Rα2) and transmembrane protein 219 (TMEM219), activating mitogen-activated protein kinase (MAPK), protein kinase B/Akt and Wnt/β-catenin pathways, and mediating a variety of effector responses including regulation of lung oxidant injury response and apoptosis, macrophage pyroptosis and inflammasome activation, transforming growth factor β1 (TGF-β1) induction, and melanoma metastasis.[136,137] Moreover, M2 macrophage-secreted CHI3L1 promoted gastric and breast cancer metastasis through interaction with IL-13Rα2 and activation of MAPK pathway, thus leading to an up-regulation of matrix metalloproteinases genes that facilitate extracellular matrix degradation.[133]

Besides, CHI3L1 has been described to interact with prostaglandin D2 receptor 2 (CRTH2) and with galectin-3 promoting an exaggerated fibroproliferative response and dysregulation of apoptosis in Hermansky-Pudlak syndrome[138,139], and in idiopathic pulmonary fibrosis.[140]

Furthermore, CHI3L1 has been reported to interact with the side-chain molecules of syndecan-1 and integrin αγβ3 activating down-stream focal adhesion kinase (FAK) and MAPK and inducing tumour angiogenesis.[141] CHI3L1 interaction with CD44 induced epithelial to mesenchymal transition in gastric cancer through several pathways as β-catenin, extracellular signal-regulated kinase (ERK) and Akt.[127] In addition, CHI3L1 has been described to interact with receptor for advanced glycation end products (RAGE) activating signal transduced and activator of transcription 3 (STAT3), β-catenin and NF-κB (nuclear factor κB) pathways and inducing proliferation of intestinal epithelial cells.[142]

In summary, the binding of CHI3L1 to its receptors activates multiple and heterogeneous signalling pathways resulting in different cellular outcomes.

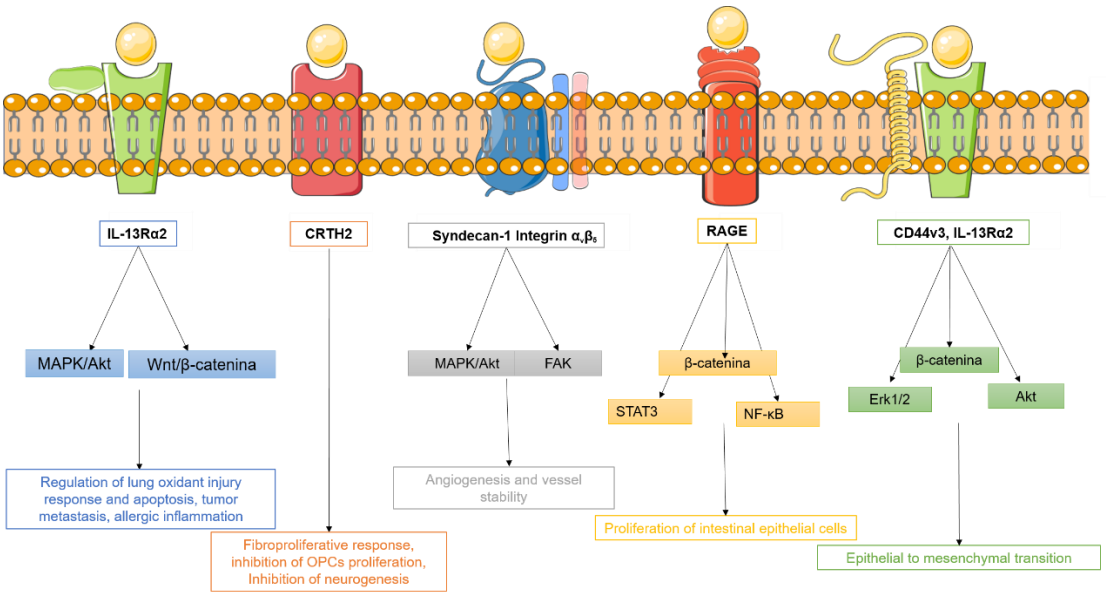

Figure 6. **Signalling pathways and effector responses regulated by CHI3L1 binding to its receptors.** CHI3L1 engages with various receptors and molecules to activate multiple intracellular signaling cascades. These pathways lead to a wide array of cellular responses, including the regulation of lung oxidant injury response, apoptosis, tumour metastasis, allergic inflammation, fibroproliferative responses, and others. CHI3L1 interacts with IL-13Rα2 and TMEM219, triggering MAPK, protein kinase B/Akt, and Wnt/β-catenin pathways, influencing processes such as apoptosis, tumor metastasis, and allergic inflammation. CHI3L1 binding to CRTH2 leads to fibroproliferative responses and apoptosis dysregulation, as seen in Hermansky-Pudlak syndrome, along with the inhibition of oligodendrocyte progenitor cell (OPC) proliferation in a human cellular model, and inhibition of neurogenesis in a mice model. CHI3L1 can induce the activation of FAK and MAPK by binding to syndecan-1 side chain molecules and integrin αvβ5, leading to angiogenesis. Interaction of CHI3L1 with RAGE activates STAT3, Wnt/β-catenin, and NF-κB pathways, promoting intestinal epithelial cell proliferation. Finally, when CHI3L1 engages with CD44v3 and IL-13Rα2, it triggers epithelial to mesenchymal transition through Erk1/2, Wnt/β-catenin, and Akt signaling. Adapted from *Pinteac R, Montalban X, Comabella M. Chitinases and chitinase-like proteins as biomarkers in neurologic disorders. Neurol Neuroimmunol Neuroinflamm. 2020 Dec 8;8(1):e921.*

Abbreviations: CHI3L1 - chitinase-3-like 1, CRTH2 - prostaglandin D2 receptor 2, Erk - extracellular signal–regulated kinase, IL-13Rα2 - interleukin-13 receptor α2, MAPK - mitogen-activated protein kinase, OPC - oligodendrocyte progenitor cell, TMEM219 = transmembrane protein 219

1.2.4 CHI3L1 in the CNS

Several *in vitro*, *in vivo,* and post-mortem investigations have explored the expression and the impact of CHI3L1 on various cellular types of the CNS as summarized in **Figure 7**.

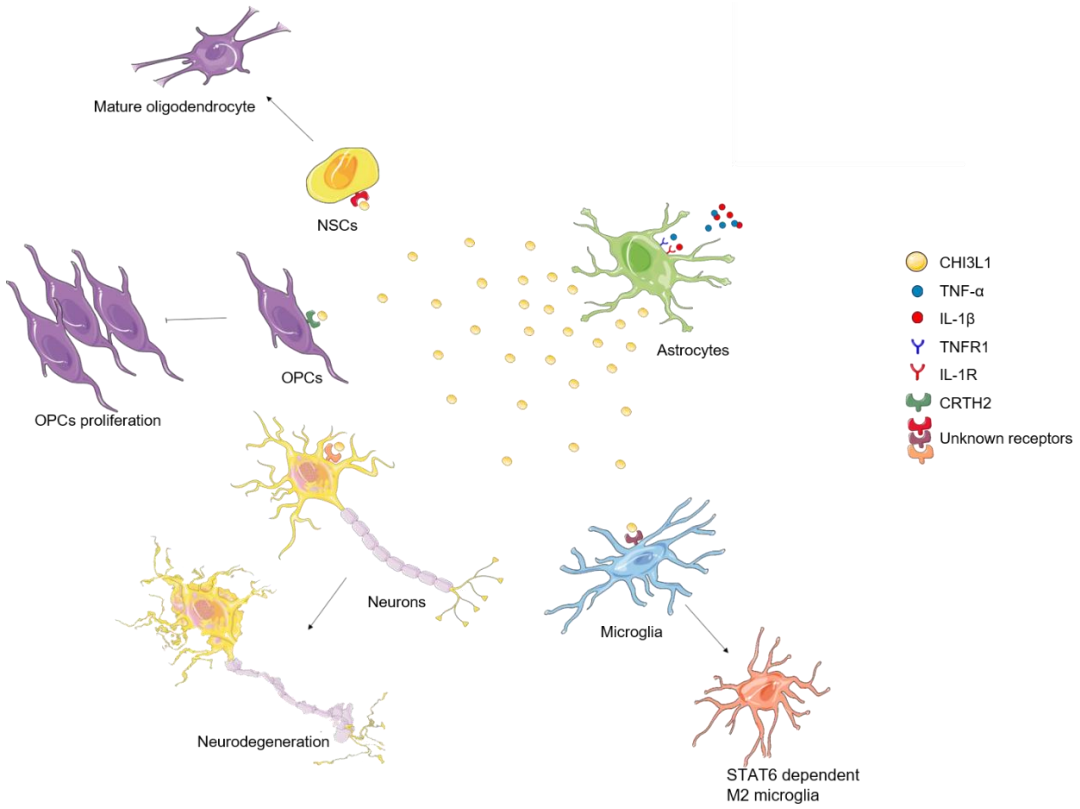

Figure 7. Overview of CHI3L1 effects and signaling on various CNS cell types. Astrocytes are the primary producers of CHI3L1 within the CNS. Upon secretion, CHI3L1 can elicit diverse responses depending on the specific cellular context. *In vitro* investigations have revealed the following outcomes: CHI3L1 enhances the migratory capacity and radiation resistance of human astrocyte cultures; CHI3L1 expression is induced in astrocytes associated with glioblastoma, promoting tumor proliferation and migration via IL-13Rα2 signaling; CHI3L1 inhibits the proliferation and myelination of oligodendrocyte progenitor cells (OPCs); CHI3L1 augments oligodendrogenesis in neural stem cells (NSCs); and CHI3L1 demonstrates neurotoxicity in primary cultured mouse neurons. In an *in vivo* study, the absence

of CHI3L1 leads to reduced STAT6 microglial activation following cortical controlled impact (CCI). Adapted from *Pinteac R, Montalban X, Comabella M. Chitinases and chitinase-like proteins as biomarkers in neurologic disorders. Neurol Neuroimmunol Neuroinflamm. 2020 Dec 8;8(1):e921.*

Abbreviations: CHI3L1 - chitinase-3–like 1, CNS – central nervous system, CRTH2 - prostaglandin D2 receptor 2, IL-1β – interleukin 1β, IL-1R – Interleukin 1 receptor, IL-13Rα2 - interleukin-13 receptor α2, NSC - neural stem cell, OPC - oligodendrocyte progenitor cell, TNF-α – tumour necrosis factor α, TNFR1 – tumour necrosis factor receptor 1

The source of CHI3L1 in the human CNS has been primarily linked to reactive astrocytes in various neuroinflammatory scenarios.[113,143–145] Furthermore, CHI3L1 expression has been observed during the differentiation of human astrocytes from neural progenitor cells (NPCs) *in vitro*.[146] Exposure to the pro-inflammatory cytokines IL-1β and TNF-α has been shown to elicit the expression of CHI3L1 in primary human astrocytes[145] and in astrocytes derived from human induced pluripotent stem cells (hiPSCs)[147]. The IL-1β and TNF-α induced transcription was effectively inhibited by IL-1R and TNF-αR antagonists, and partially supressed by NF-κB inhibitors.[145] Additionally, CHI3L1 has been identified as a factor influencing migration in human primary astrocytes[145,148], and astrocytes transfected with CHI3L1 showed radiation resistance and increased invasion of glioma cells[149].

CHI3L1 expression was observed mainly in astrocytes within chronic active lesions from MS patients, while it was notably absent in brain tissue from individuals without neurological conditions.[83] Within CNS lesions, CHI3L1 expression was evident in both macrophages/microglial cells and astrocytes.[83] In the context of AD, CHI3L1 expression predominantly resides in a subset of astrocytes in the frontal cortex of affected patients. These astrocytes are sometimes found in close proximity to amyloid plaques, although CHI3L1 expression can also occur independently of plaque pathology.[116,144,150] CNS expression studies have revealed significant upregulation of CHI3L1 in the motor cortex of sporadic ALS patients when compared to neurologically healthy controls.[151] In separate investigations, increased CHI3L1 expression was observed in the anterior horn of the spinal cord in sporadic ALS patients.[105] Notably, CHI3L1 immunoreactivity was primarily confined to glial fibrillary acidic protein (GFAP)-positive astrocytes in the frontal cortex and spinal cord of ALS

patients, indicating that reactive astrocytes are the principal cellular source of CHI3L1 expression within the CNS.[104,105]

The upregulation of CHI3L1 in tumour-associated astrocytes surrounding glioblastoma has been described to promote both proliferation and migration through binding to IL-13Rα2 and activation of MAPK signalling.[152] Interestingly, astrocyte-secreted CHI3L1 inhibited the proliferation of oligodendrocyte progenitor cells (OPCs) and myelination through CRTH2 signaling in a cellular model of Alexander disease, a leukodystrophy resulting from mutations in the GFAP gene.[153] Moreover, CHI3L1 interaction with CRTH2 in neural stem cells dampens β-catenin pathway and inhibits neurogenesis.[154] Conversely, another study conducted by Starossom and colleagues reported that CHI3L1 promoted oligodendrogenesis in human neural stem cells *in vitro*.[155] Regarding CHI3L1 effects on neurons, two independent studies revealed that CHI3L1 elicits neuronal death[132,156], and neurite retraction[156].

In the middle cerebral arterial occlusion (MCAO) model of stroke, CHI3L1 knockout mice exhibited accelerated stroke progression due to enhanced neuroinflammation, which was linked to reduced STAT6-dependent microglial activation.[157] Similarly, in the cortical controlled impact (CCI) model of traumatic brain injury, CHI3L1 knockout mice displayed more severe pathology and more pronounced reactive gliosis compared to their wild-type counterparts.[158] This supports the idea that CHI3L1 may play a protective role in the context of acute neuroinflammation by modulating astrocytic and microglial reactive gliosis.

Nevertheless, there are conflicting results regarding the EAE model in CHI3L1 knockout mice. Bonneh-Barkay et al. reported that CHI3L1 knockout mice exhibited exacerbated clinical EAE, increased inflammation, gliosis, and demyelination[159], while Cantó et al. found no differences in EAE progression and gliosis between CHI3L1 knockout mice and their wild-type counterparts[160]. Besides, in a model of AD involving Aβ1-42-infused mice, treatment with K284-6111, a CHI3L1 inhibitor, resulted in reduced neuroinflammation and improved memory.[161]

These diverse outcomes highlight the complexity of the CHI3L1 signaling networks within the CNS. Further research is necessary to unravel the specific roles of CHI3L1 in CNS signaling and its involvement in different pathologic contexts.

1.3 hiPSC-derived Neuronal Cultures

In the last century, researchers have successfully developed techniques for isolating, culturing and dynamically observing mammalian neuronal networks *in vitro*. The development of *in vitro* cultures for neuronal cells has been essential in advancing our understanding of the physiology and pathology of the CNS. Neuronal *in vitro* models offer controlled environments to investigate neuronal physiological and pathological processes. Cultivating neuronal cells presents a unique set of challenges, primarily due to the absence of cell division in mature neurons.[162]

For many years, researchers obtained primary neuronal cultures from rodents, and these neurons have been used for a wide range of applications including study of fundamental aspects of neuronal function and signaling[163–168], and disease modelling[169–171]. Murine and rat neuronal cultures, while valuable for basic and mechanistic research, have limitations in their translatability to human physiology and pathologies. The species-specific differences in neural development, function, and disease restrict the applicability of findings to humans.[172]

The inaccessibility of the human CNS is a significant challenge in the study of neuropathological processes. Human neuronal cultures derived from aborted foetuses or neurosurgical resections provide insight into human-specific neural development and disorders, but they are ethically and logistically challenging.[162] While post-mortem brain tissue is more accessible compared to fresh tissue, it is important to note that neural cells are highly vulnerable to fluctuations in oxygen and nutrient availability. As a result, the process of isolating and culturing human primary neural cells poses significant technical challenges.

Advances in stem cell and reprogramming biology offer a novel platform for modelling human neurological conditions. hiPSCs are adult pluripotent stem cells that are generated from somatic cells by the ectopic expression of the Yamanaka reprogramming factors (OCT3/4, SOX2, KLF4 and MYC).[173] hiPSCs are typically derived from readily accessible cell types like skin fibroblasts or peripheral blood mononuclear cells, although they, theoretically, can originate from any cell type.[174] During the reprogramming process, somatic cells are usually transduced with a virus carrying reprogramming factors. There are multiple methods using virus for cell reprogramming, including older ones involving the integration of viruses into the genome, while newer approaches, such as the use of the Sendai virus, avoid this genomic integration.[175] Once reprogrammed, hiPSCs are pluripotent, and under the influence of an adequate combination of growth factors and precise cell culture conditions, can virtually differentiate into every terminally differentiated cellular type, including neurons.[176] hiPSCs-derived neuronal cultures offer a unique platform for studying underlying neuronal mechanisms of neurodegenerative diseases, identify potential targets, and screen drug-candidates in a human model.

1.3.1 Strategies for Neuronal Differentiation from hiPSCs

The *in vivo* development of the CNS is intricately regulated, maintaining a delicate equilibrium between the proliferation of neural stem cells (NSCs) and their differentiation into mature cell types. The primary strategies for neuronal differentiation aim to replicate the *in vivo* developmental processes, which include the formation of the neuroectoderm and the specialization of NSCs resulting in further differentiation into intermediate cell types as NPCs and radial glia, and eventually leading to the generation of a diverse array of neurons and glial cells.[177] *In vitro* neuronal differentiation and maturation requires the application of specific combinations of growth factors and morphogens, with the appropriate concentration and timing determined by the targeted neuronal subtype[178] (**Figure 8**).

In summary, the neural induction process involves the suppression of signalling pathways like bone morphogenetic protein (BMP) and Wnt to prevent non-neural cell fate determination, as well as the inhibition of TGF-β and canonical Wnt pathways to

deter pluripotency.[179] Throughout neurodevelopment, NSCs are organized along the dorsoventral and anteroposterior axes of the neural tube to give rise to the precursor cells responsible for generating the diverse neuronal subtypes.[180] Subsequent to specifying a forebrain identity, gradients of TGFβ and BMP signaling further specify a dorsal NPC identity, ultimately leading to the generation of cortical neurons.[178,181] Neuronal maturation involves progressive gain of neuronal properties as excitability, and ability to generate and transmit action potentials, and it depends on the coordinated action of transcription factors, cellular signaling pathways, cell-cell interactions and concentrations of growth factors and ions.[178,182]

The most common method for generating NPCs from hiPSCs involves the formation of three dimensional embryoid bodies[183] (EBs) which leads to the formation of radially organized structures called neural rosettes. The neural rosettes serve as an *in vitro* representation of early neurodevelopment, resembling the neural tube and serving as a reservoir of NSCs.[177] At this stage, NSCs can be isolated manually, enzymatically or using fluorescence activated cell sorting, and expanded *in vitro* without losing their characteristics, or can be terminally differentiated into either neurons or glial cells. Dual inhibition of SMAD signaling in hiPSCs or EBs through the synergistic action of the morphogen noggin and the small molecule SB431542 is a high efficiency protocol for neuroectoderm differentiation and NSCs/NPCs generation.[184] Other less efficient neural induction protocols include spontaneous differentiation, stromal feeder co-culture, treatment with retinoic acid (RA), or culture in defined media containing EGF (epidermal growth factor) and FGF2 (fibroblast growth factor 2).[185]

Isolated neural rosettes or NPCs at low densities can spontaneously differentiate into neurons when not in a self-renewing environment complemented with growth factors as EGF and FGF2.[177] Nevertheless, neuronal differentiation can be directed towards specific neuronal types by adding specific growth factors as brain derived neurotrophic factor (BDNF), cyclic adenosine monophosphate (cAMP), or RA, as well as by employing small molecules that activate/inhibit specific developmental pathways.[177] Recently, new strategies have been developed of fast neuronal direct

reprogramming from hiPSCs through the forced expression of specific transcription factors as NGN2.[186] The iNeurons recapitulate neuronal characteristics as expression of synaptic markers and integration into the mouse brain.[186]

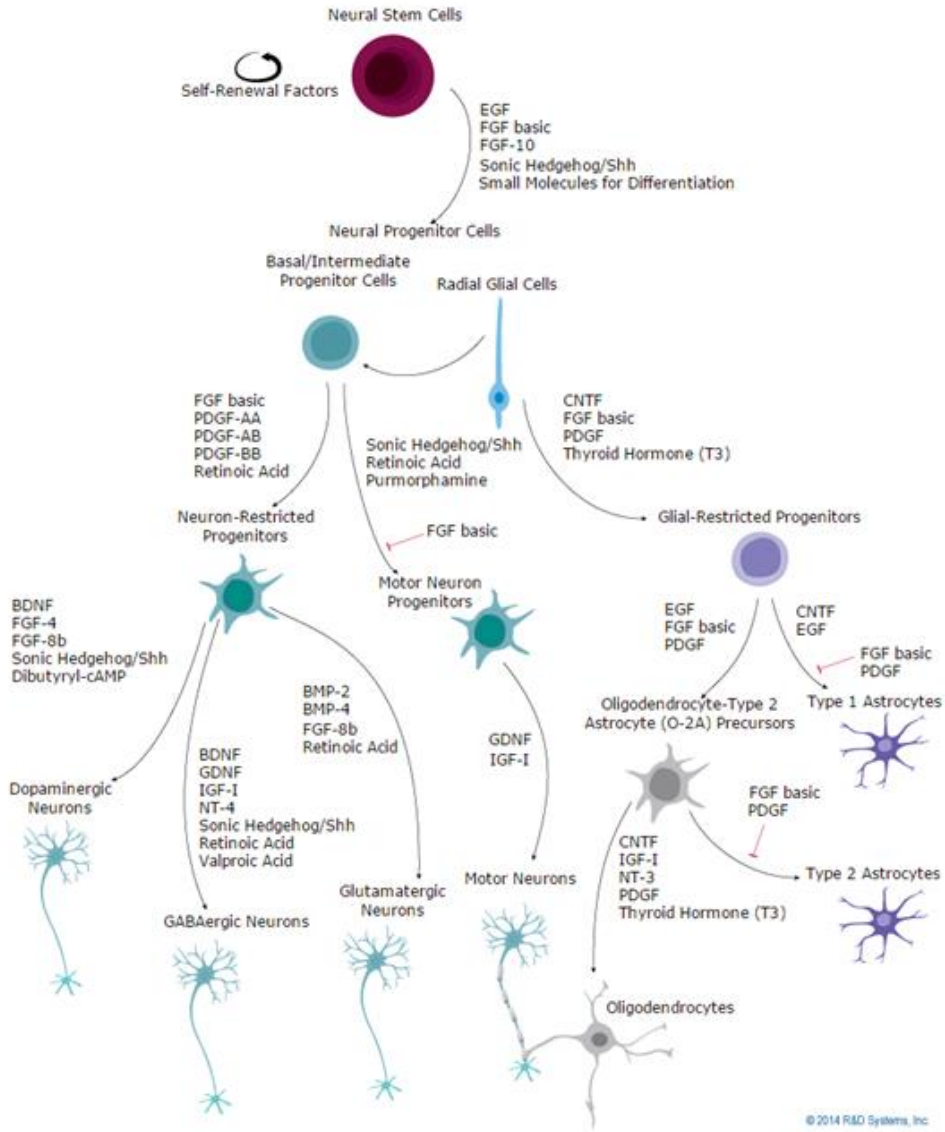

Figure 8. Overview of neural stem cell (NSCs) differentiation pathways. NSCs are undifferentiated precursor cells characterized by their ability for self-renewal and multipotency. During the development of the CNS, NSCs undergo proliferation and division, giving rise to clonally related progeny that

subsequently differentiate into neurons, astrocytes, and oligodendrocytes. The regulation of NSC self-renewal and differentiation relies on a precise temporal sequence of growth factor exposure, intracellular signaling, and the expression of transcription factors. Distinct combinations of growth factors and small molecules are used to induce differentiation to the CNS lineages starting from hiPSCs. Adapted from *R&D Systems*.

Abbreviations: BDNF – brain derived neurotrophic factor, cAMP – cyclic adenosine monophosphate, CNS – central nervous system, CNTF- ciliary neurotrophic factor, EGF – epidermal growth factor, FGF-fibroblast growth factor, IGF – insulin-like growth factor, NT – neurotrophin, PDGF – platelet derived growth factor

Given that many phenotypes associated with neurological diseases are believed to arise from changes in neuronal membrane excitability and/or synaptic communication or plasticity, it is crucial to emphasize that neuronal models employed to investigate neuropathological processes should exhibit functional activity defined by the ability to fire action potentials and synaptic communication among neurons.[182] hiPSCs-derived cortical neurons exhibit maturation over time, with emergence of spontaneous and synchronous activity, and formation of large scale networks.[187,188] Long-term calcium-imaging revealed that hiPSC-derived neuronal cultures self-assemble, and that there is a gradual emergence of functional complex organization, exhibiting rich patterns of network activity.[187]

1.3.3 Modelling Neurologic Diseases with hiPSC-derived Neurons

hiPSCs have the capacity to differentiate into a wide range of neural cell types, providing the opportunity to study specific neuronal subtypes pertinent to various pathologies. For instance, the differentiation into motor neurons can serve as a valuable platform for investigating diseases like ALS[189] and spinal muscular atrophy[190] (SMA), while the differentiation into dopaminergic midbrain neurons[191] offers insights into Parkinson's disease (PD). Differentiation into cortical forebrain neurons can serve as a model for studying neurodegeneration and cognitive dysfunction in the context of various neurodegenerative diseases as AD[177] or MS.

hiPSCs capture the genetic diversity of the patient, thus offering a powerful tool for disease modelling and personalized medicine. hiPSCs-derived neuronal cultures can

be used to identify neuronal phenotypes associated to neurological or neurodevelopmental diseases. In this regard, hiPSCs-derived neuronal cultures from patients with Rett's syndrome exhibited smaller neuronal soma and reduced number of synapses, as well as functional alterations at the neural network level.[192,193] Moreover, hiPSCs-derived dopaminergic neurons from PD patients carrying LRRK2 mutations revealed increased susceptibility to stress, caspase-3 activation, as well as early functional alterations in neuronal connectivity.[194,195] A functional analysis of hiPSC-derived neurons from patients with Timothy syndrome, which is caused by non-sense mutations in the voltage gated calcium channel CACNA1C, revealed that Timothy syndrome neurons displayed significant alterations in action potential duration as well as greater elevations of intracellular calcium.[196] Another successful example of modelling neurodegenerative diseases with neurons derived from hiPSCs is the case of the motor neuron model derived from patients with SMA. In this case, Ebert and his team described a decrease in the number of cholinergic motor neurons derived from hiPSCs of SMA patient, as well as a smaller soma size.[190] Additionally, they pharmacologically increased the expression of the disease-causing gene SMN using valproic acid and tobramycin, rescuing gene expression in SMA-motor neurons.[190] Neurons derived from hiPSCs bearing α-synuclein (SNCA) gene triplication develop α-synuclein aggregates that interact with mitochondrial ATP synthase, resulting in the opening of the permeability transition pore and, ultimately, neuronal cell death.[197] In the context of AD, forebrain cholinergic neurons derived from hiPSCs from APOE3/APOE4 genotypes revealed distinctive AD features, altered drug response, and increased vulnerability to cell death, thus offering insights in both disease pathogenesis and drug screening.[198] Moreover, Liu et al. demonstrated that treating hiPSC-derived neurons from AD patients carrying presenilin 1 (PSN1) with γ-secretase modulators revealed a new unique biomarker signature that can more accurately mirror the biomarker changes observed in real patients.[199]

In conclusion, the versatility of hiPSCs in differentiating into specific neuronal subtypes has enabled the study of various neurological diseases. These models

have yielded valuable insights into disease mechanisms, demonstrated the potential for personalized medicine, and provided a platform for drug screening.

1.3.3 Limitations of hiPSC-derived Neuronal Cultures

One of the primary challenges associated with hiPSC-derived neuronal cultures is the variability observed between hiPSC cell lines.[200] This variability often results in neuronal cultures displaying distinct properties and compositions, even when the same differentiation protocol is applied.[201] Additionally, another significant constraint lies in the considerable amount of time (months) required to produce neuronal cultures that demonstrate functional activity and the complexity of the differentiation protocols.[185]

Variations in the methods of derivation, the quality and source of initial materials, as well as differences in culture conditions and differentiation protocols among research laboratories, introduce complexity to the interpretation of data generated from hiPSC models.[202] It is crucial to combine robust clinical information with *in vitro* data to construct valuable predictive models. The *in vitro* discovery of new phenotypes should be subsequently validated in patients.[202]

Furthermore, hiPSC-derived neurons achieve functional phenotypes that resemble fetal neurons more than adult neurons as revealed by high-throughput transcriptomic studies.[203] The almost complete removal of the age-related epigenetic hallmarks by the reprogramming process[204], limits the capacity to model late-onset neurodegenerative diseases effectively. The use of cellular stressors as ROS to increase the aging of the derived cells may be a feasible solution for modelling late-onset diseases.

1.4 Rationale

The rationale for this thesis is rooted in the studies conducted by our group demonstrating the prognostic significance of CHI3L1 in the context of MS. Initially identified through mass spectrometry-based proteomics as an elevated protein in the CSF of CIS patients with worse prognosis, CHI3L1 exhibited associations with the number of brain lesions, disability progression during follow-up, and a shorter time of conversion to clinically definite MS.[81]

Subsequent studies, both conducted by our group and independent researchers, further affirmed the prognostic value of CHI3L1 in the early stages of MS, highlighting its correlation with an increased risk of neurological disability.[83,85,86] Remarkably, elevated CSF CHI3L1 levels in RRMS patients demonstrated significant correlations with brain volume loss, further reinforcing its negative role in disease progression.[83,89] Additionally, increased CHI3L1 levels independently predicted worsening neurologic disability and progression to SPMS.[88]

Notably, CSF CHI3L1 levels were also associated with cognitive dysfunction in early MS[205] and long-term cognitive impairment in CIS patients[85], suggesting a broader impact on neurological function.

Building on this foundation, our group conducted an initial study assessing the effects of CHI3L1 on murine cortical neurons, revealing decreased neuronal viability and neurite retraction following CHI3L1 treatment[156] – a direct indication of the neurotoxic effects of CHI3L1. This crucial insight prompted our transition to human neurons, where we aim to explore the translatability of the neurotoxic impact of CHI3L1.

By delving into the neuronal effects of CHI3L1, this thesis aspires to provide valuable insights into the underlying mechanisms of CHI3L1-induced neurotoxicity. Our ultimate goal is to contribute to a deeper understanding of CHI3L1's role in MS pathogenesis and pave the way for targeted therapeutic strategies in MS.

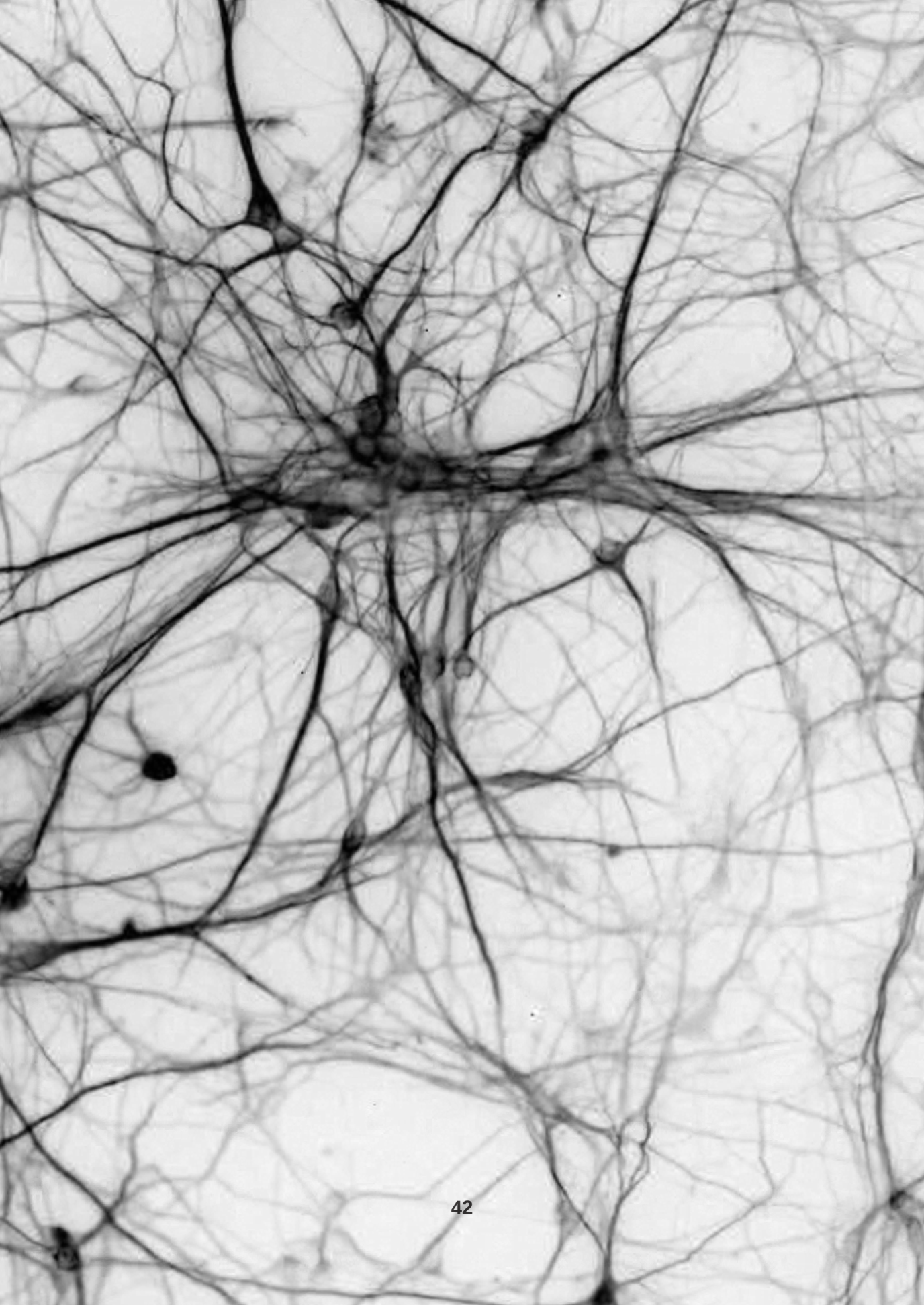

HYPOTHESIS

2. HYPOTHESIS

CHI3L1 exerts a neurotoxic impact, influencing neuronal function at various levels, including morphological, synaptic, and neuronal activity. It exhibits binding affinity to a specific neuronal receptor or receptors, which mediate its neurotoxic effects by modulating cellular signalling and gene expression pathways. The elucidation of the role of CHI3L1 receptor(s) could potentially pave the way for therapeutic interventions aimed at its blockade.

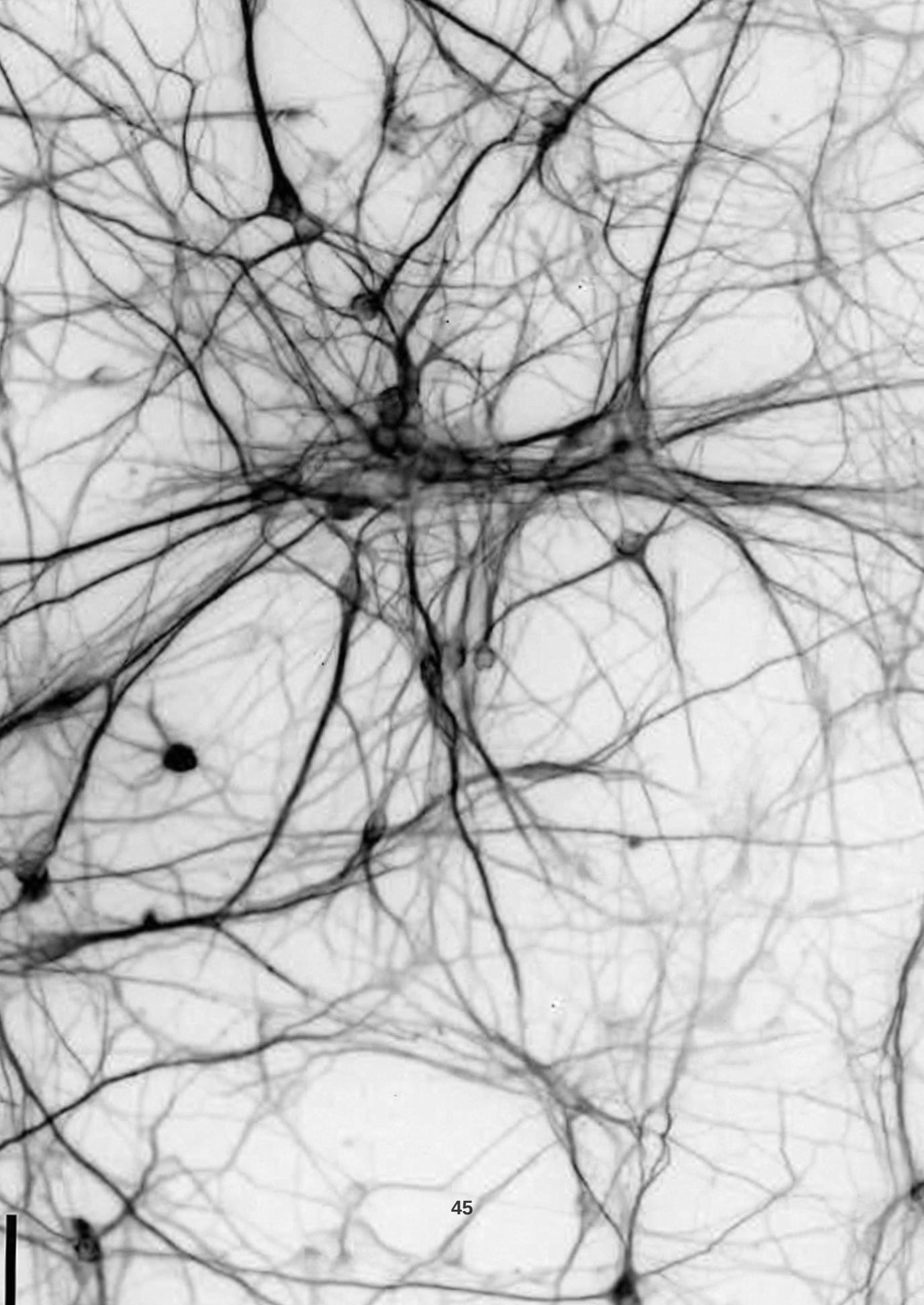

OBJECTIVES

3. OBJECTIVES

3.1 Main objective

The primary aim of this study is to describe in a comprehensive manner the neurotoxic effects of CHI3L1 on neurons and to elucidate the underlying mechanisms mediating its action.

3.2 Secondary objectives

1. Morphological and functional characterization of CHI3L1-induced neuronal damage.

a. Establishment of hiPSC-derived neuronal cultures.

b. Assessment of the impact of CHI3L1 on neuronal morphology.

c. Investigation of the effect of CHI3L1 on synaptic function.

d. Evaluation of the influence of CHI3L1 on neuronal activity and the dynamics of neuronal networks.

2. Dissection of the molecular pathways mediating the neurotoxic effects of CHI3L1.

a. Examination of the gene expression signature induced by CHI3L1 in hiPSC-derived neuronal cultures.

b. Identification of the cellular pathways activated by CHI3L1 in hiPSC-derived neuronal cultures.

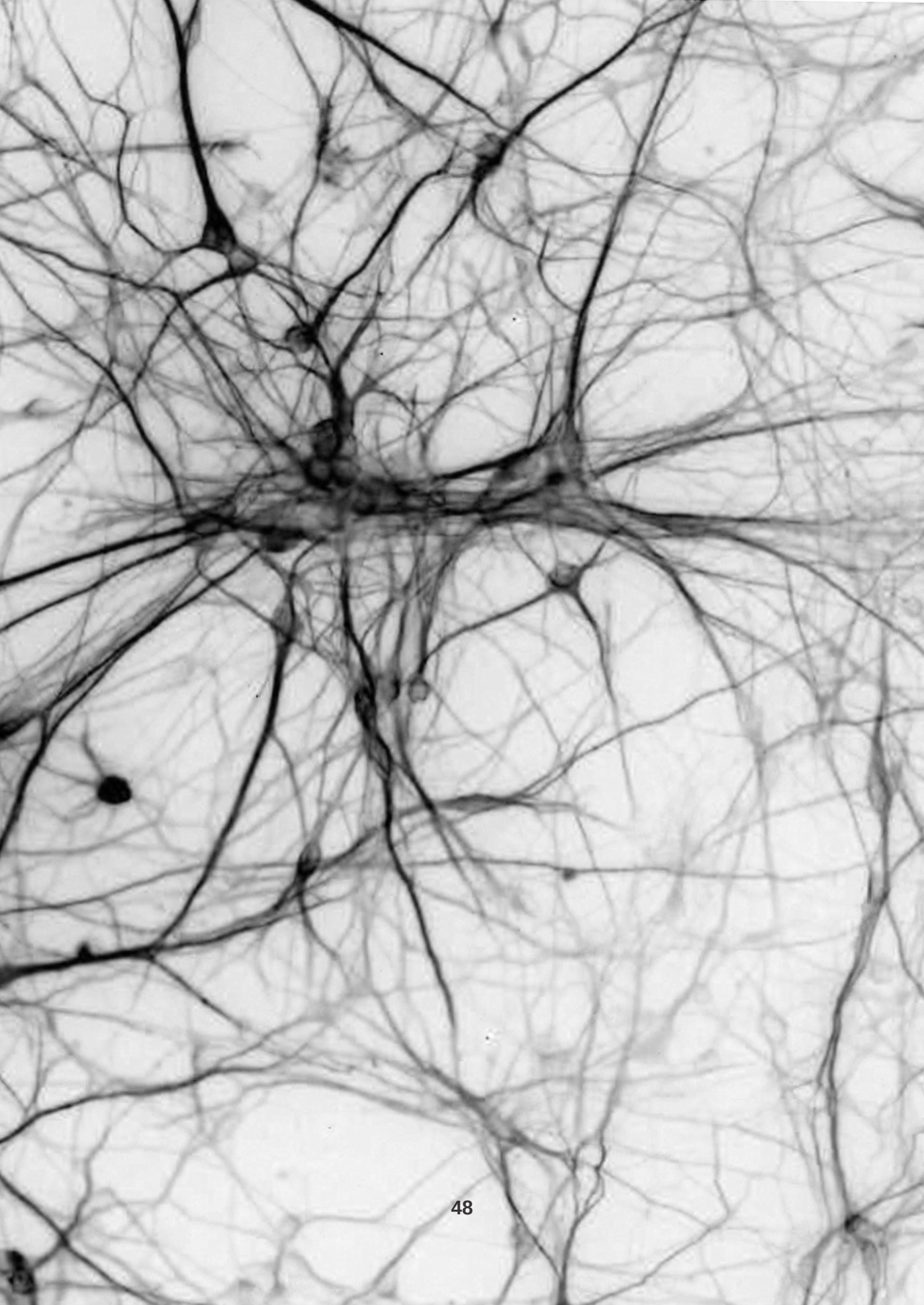

METHODS

4. METHODS

4.1 Cell Culture

All cell culture procedures were performed on sterile techniques and careful handling under a laminar hood cabin type II (Telstar Bio II A). This biosafety containment system provided a controlled environment, minimizing the contamination risk and safeguarding the integrity of cultured cells. A schematic overview of the differentiation process from hiPSCs to neurons is illustrated in **Figure 9**.

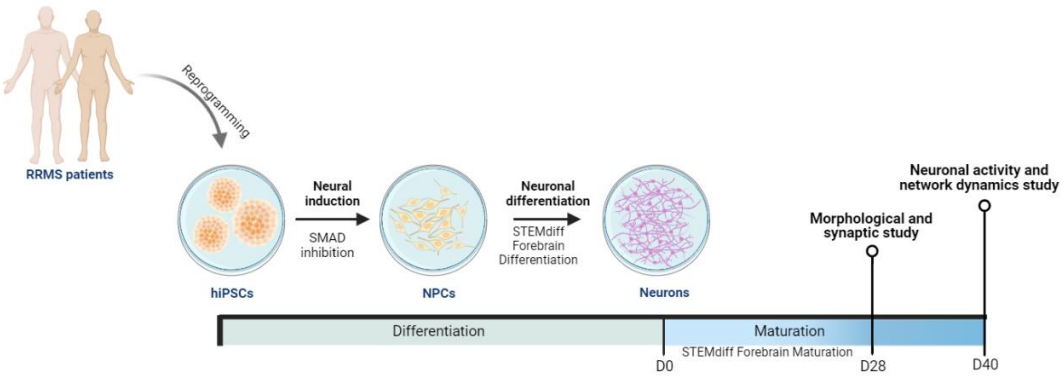

Figure 9. Overview of the hiPSC differentiation process

Abbreviations: hiPSCs – human induced pluripotent stem cells, NPCs – neural progenitor cells, RRMS – relapsing-remitting multiple sclerosis

4.1.1 Coatings

4.1.1.1 Geltrex

hiPSCs were cultured on Geltrex-coated plates. First, Geltrex (ThermoFisher) was thawed overnight at 2-8ºC, and the tube was transferred to an ice container to avoid premature gelling of the matrix. Then, Geltrex was diluted into cold DMEM/F12 (Gibco) to a ratio of 1:100 and the dilution was immediately transferred to the culture ware and incubated at 37ºC for at least 4 hours. Before use, plates were seeded out to room temperature for 1 hour.

4.1.1.2 Poly-L-Ornithine/Laminin (POLAM)

NPCs, neuronal precursors and neurons were cultured on POLAM-coated culture wares. For the POLAM coatings, poly-L-ornithine (PLO, Sigma) was diluted in phosphate-buffered saline (PBS, Biowest) to reach a final concentration of 15 µg/ml. Then, the PLO solution was added to culture-treated culture ware and culture wares were swirled to spread the PLO solution and incubated at 37ºC for at least 2 hours. Culture wares were washed with PBS, and laminin (Sigma) diluted in DMEM-F12 at a final concentration of 5 µg/ml was added to the PLO-coated culture ware and incubated for at least 2 hours at 37ºC.

4.1.2 Media Preparation

4.1.2.1 mTESR1

mTESR1 (StemCell Technologies) is a defined, feeder-free maintenance medium for human hiPSCs. For preparation of mTESR1 complete medium (Basal Medium + 5x Supplement), the supplement was thawed at room temperature or overnight at 2-8ºC and mixed thoroughly with the basal medium. The complete medium was used and stored for up to 2 weeks at 2-8ºC or aliquoted and stored at -20ºC for up to 6 months.

4.1.2.2 STEMdiff SMADi Neural Induction Medium

For the neural induction protocol, we used STEMdiff SMADi Neural Induction (StemCell Technologies) or neural induction medium (NIM) which directs neural fate through the inhibition of TGF-β/BMP-dependent SMAD signalling. The complete medium was constituted by STEMdiff™ NIM and STEMdiff™ SMADi Neural Induction Supplement. First, the basal medium and the supplement were thawed at room temperature or overnight at 2-8ºC. Then, 0.5 ml of the supplement was added to 250 ml of the basal medium and mixed thoroughly. The complete medium was used and stored for up to 2 weeks at 2-8ºC or aliquoted and stored at -20ºC for up to 6 months.

4.1.2.3 STEMdiff Forebrain Differentiation

STEMdiff™ Forebrain Neuron Differentiation Kit was used to generate neuronal precursors from NPCs. The complete medium was constituted by Differentiation

Basal Medium + Differentiation Supplement. First, the supplement was thawed at room temperature or overnight at 2-8ºC and mixed thoroughly with the differentiation basal medium. The complete medium was stored at 2-8ºC for up to two months.

4.1.2.4 STEMdiff Forebrain maturation

The STEMdiff™ Forebrain Neuron Maturation Kit was employed to induce maturation in neuronal precursors, resulting in the generation of a mixed population primarily composed of neurons with a smaller proportion of astrocytes. The complete medium was constituted by Maturation Basal Medium + Maturation Supplement. Initially, the supplement was thawed at room temperature or overnight at 2-8ºC and mixed thoroughly with the differentiation basal medium. The complete medium was stored at 2-8ºC for up to two months.

4.1.3 hiPSCs

4.1.3.1 hiPSCs information

Two hiPSC cell lines derived from RRMS patients were used in this study. These cell lines were previously generated and characterized at the Center of Regenerative Medicine in Barcelona (CMRB), as described by *Miquel-Serra et al. in 2017*. Detailed patient and hiPSC information can be found in **Table 2**. The generation of these hiPSC lines was conducted following the corresponding ethical approvals from the involved centres, namely the Comité de Ética e Investigación Clínica-CEIC-CMRB (ADD06/2014 17/2012) and the Catalan Authority for Stem Cell Research (Approval number: 326 191 2). Prior to obtaining skin biopsies from the MS patients, written consent was acquired in accordance with the guidelines set forth by the Hospital Universitari Vall d'Hebron Ethics Committee.

Table 2. Information of MS patients and hiPSC cell lines

Unique identifier	Abbreviation in figures	Age	Gender	Ethnicity	Disease
MS_FiPS2_R4F_10 (ESi049-A)	MS-10	44	Male	Caucasian	MS
MS_FiPS5_R4F_6 (ESi052-A)	MS-6	42	Female	Caucasian	MS

hiPSC cell lines were reprogrammed from dermal fibroblasts derived from skin biopsies by an integrative method using retroviral transduction of the Yamanaka factors (OCT4, SOX2, KLF4, c-MYC) encoded by two polycistronic vectors. hiPSC cell lines were characterized for pluripotency-associated markers and differentiation potential towards the three main embryo germ layers.[206] The full characterization is summarized in **Table 3**.

Table 3. Summary of hiPSCs characterization Adapted from *Miquel-Serra et al., 2017*

Classification	Test	Result
Pluripotency	RT-qPCR	OCT4, SOX2, KLF4, cMYC
	Immunocytochemistry	OCT4, SOX2, NANOG, TRA-1-60, TRA-1-81, SSEA-3 and SSEA-4
	Alkaline phosphatase activity	Positive
Genotype	Karyotype	Normal
Identity	STR-analysis	Performed
Differentiation potential	Embryoid bodies formation + immunocytochemistry	α-fetoprotein (AFP) and forkhead box A2 (FOXA2) βIII-tubulin (Tuj1) and glial fibrillary acidic protein (GFAP) α-smooth muscle actin (ASMA) and α-sarcomeric actin (ASA)
Microbiology	Mycoplasma	Negative

4.1.3.2 hiPSCs culture

hiPSCs were cultured as colonies on Geltrex (ThermoFisher) coated plates in mTESR1 medium (StemCell Technologies). For the thawing procedure, the cryovial of hiPSCs was removed from liquid nitrogen storage and immediately placed into a 37ºC water bath for 1 minute by gently swirling the cryovial until a small bit of ice was left in the vial. The content of the vial was transferred into a conical tube containing 5 ml of mTESR1 and centrifuged at 300g for 5 minutes. Then, the cell pellet was resuspended with 1 ml of mTESR1 + 10 µM Y-27632 (StemCell Technologies) and the cell suspension was plated into a well of a 6-well plate with a final volume of 2 ml/well using a wide-bore pipette to not disrupt the hiPSC colonies. The next day, the medium was changed to fresh mTESR1 without Y-27632. hiPSCs were maintained at 37ºC in a humidified atmosphere containing 5% CO_2. The medium was changed every other day, and cells were passaged when 80% confluent at 1:4-1:6 ratios. For the passaging protocol, cells were first washed with PBS (Biowest) and 50 µM EDTA (Invitrogen) was added to the culture to detach the colonies. After 2-3 minutes of incubation, the EDTA was aspired and 2 ml of mTESR1 were roughly added to detach the colonies. Those colonies which were not detached with the flush of medium were manually scrapped from the plate using a pipette tip. The colonies were transferred using a wide-bore pipette to a falcon containing the corresponding volume of mTESR1 to achieve the 1:4-1:6 ratios and plated on fresh Geltrex-coated 6 well-plates.

4.1.4 Neural Induction

The differentiation of hiPSCs into NPCs was undertaken as a means of obtaining a population with the ability to proliferate and give rise to the major differentiated cell types of the CNS. The neural induction protocols utilized in this investigation were adapted from established procedures provided by StemCell Technologies. Two approaches, embryoid body (EB) formation and monolayer protocols, were employed for the generation of NPCs and are illustrated in **Figure 10**.

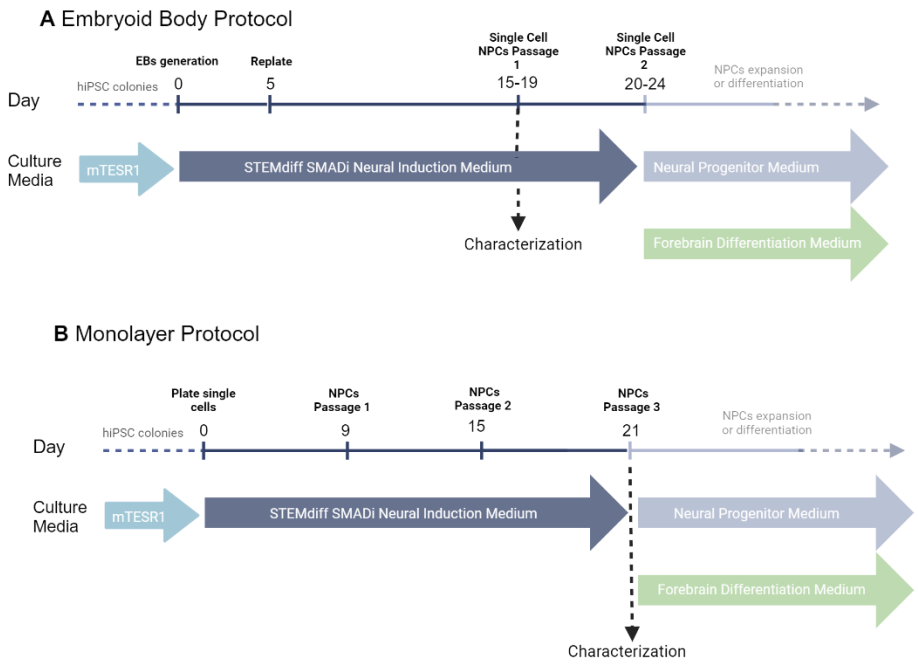

Figure 10. Neural induction protocols. Adapted from *StemCell Technologies Neural Induction Manual*.

4.1.4.1 EBs Protocol

hiPSCs were cultured until they reached 80% confluence, then colonies were detached using EDTA as previously described, and clumps were resuspended in mTESR1. The hiPSCs clumps were seeded into low attachment conical end 96-well plates (ThermoFisher), centrifuged at 500 rpm for 10 minutes and incubated overnight. The following day, 50% of the mTESR1 was changed to NIM and incubated overnight. At 48 hours post-seeding, EBs were round with clearly delimitated borders, and they were transferred to a low attachment dish and grown in suspension for 3 days with daily medium changes. Then, EBs were transferred to a Geltrex-coated dish and cultured for 10-14 days or until they reached confluency. At this point, NPCs were passaged to POLAM-coated plates and the expression of NPCs' typical markers (SOX1, PAX6 and Nestin) and the absence of pluripotency were assessed by immunofluorescence. For the passaging protocol, cells were washed with PBS and incubated with Accutase (ThermoFisher) for 5 minutes at 37ºC.

Then, the cellular suspension was transferred to a falcon containing 5 ml of DMEM-F12 (Gibco) and centrifuged at 300g for 5 minutes. The cellular pellet was resuspended in NIM, and NPCs were plated at a 1.5 - 2 $x10^5$ cells/cm2 density. Cells were maintained at 37ºC in a humidified atmosphere containing 5% CO_2. NPCs were maintained in the NIM medium for 5-7 days with every other day medium changes or until the next passage and then expanded using the Neural Progenitor Medium (StemCell Technologies). For the expansion of NPCs, cells were passaged as described previously and cryopreserved in the cryopreservation medium containing 90% Fetal Bovine Serum (Gibco) and 10% DMSO (Sigma).

4.1.4.2 Monolayer Protocol

One well of a 6-well plate of hiPSCs at 80-90% confluence was washed once with PBS and the colonies were enzymatically dissociated with TryPLE (Gibco) for 5 minutes at 37ºC to obtain a single cell suspension. The cellular suspension was transferred to a falcon containing 5 ml DMEM-F12 (Gibco) and centrifuged at 300g for 5 minutes. The cellular pellet was resuspended into 2 ml of NIM + 10 µM Y-27632 and plated into a POLAM-coated well to a final density of 2.5 $x10^5$ cells/cm^2. The next day, the medium was changed to fresh medium without Y-27632. Cells were maintained at 37ºC in a humidified atmosphere containing 5% CO_2. Daily medium changes were performed until day 9 of neural induction when cells were passaged. For the passaging protocol, cells were washed once with PBS and incubated with Accutase for 5 minutes at 37ºC. The cell suspension was transferred to a falcon containing 5 ml DMEM-F12 and centrifuged at 300g for 5 minutes. The cell pellet was resuspended in 1 ml of NIM medium + 10 µM Y-27632 and plated into POLAM coated culture plate at 2 $x10^5$ cells/cm^2 density. Daily medium changes were performed without Y-27632 until NPCs reached confluency after approximately 7 days and were passaged as described but at a density of 1.5 $x10^5$ cells/cm^2. After the third passage, the neural induction protocol is completed, and NPCs can be expanded using the Neural Progenitor medium as described previously.

4.1.5 Neuronal Differentiation

For the neuronal differentiation protocol, NPCs were passaged as previously described but the cellular pellet was resuspended in STEMdiff Forebrain Differentiation Medium (StemCell Technologies), and cells were plated at a density of 80 - 125,000 cells/cm^2. Daily medium changes were performed until cells reached 80-90% confluence after 6-7 days. Neuronal precursors were maintained at 37ºC in a humidified atmosphere containing 5% CO_2. The resulting neuronal precursors were ready to start neuronal maturation.

4.1.6 Neuronal Maturation

Neuronal precursors were washed once with PBS and incubated with Accutase at 37ºC. The cellular suspension was transferred to a falcon containing 5 ml of DMEM-F12 and centrifuged at 400g for 5 minutes. The cellular pellet was resuspended in STEMdiff Forebrain Maturation Medium (StemCell Technologies), and neuronal precursors were plated in STEMdiff Forebrain Maturation medium at a density of 20,000 cells/cm^2. Neurons were maintained at 37ºC in a humidified atmosphere containing 5% CO_2. Two partial medium changes per week were performed, and neurons were maintained for 28 (D28) or 40 days (D40). The resulting neuronal cultures were extensively characterized by immunofluorescence with neuronal and astrocytic markers and cortical fate markers.

4.2 Immunofluorescence

Cells, either NPCs or neurons, were washed once with PBS and fixed using 4% paraformaldehyde (Sigma) at room temperature for 20 minutes. Subsequently, cells were permeabilized and blocked with a solution containing 0.5% Triton X-100 (Sigma-Aldrich) and 5% Normal Goat Serum (NGS, Millipore) or 5% Normal Donkey Serum (NDS, Millipore) in PBS for 30 minutes at room temperature. Following the blocking step, primary antibodies (**Table 4**) were applied and allowed to incubate overnight at 2-8ºC, diluted in PBS supplemented with 0.1% Triton X-100 and 5% NGS or NDS. After three PBS washes, cells were subjected to incubation for 1 hour at room temperature with secondary antibodies (**Table 5**), diluted in PBS with 0.1%

Triton X-100 and 5% NGS or NDS. To label cell nuclei, 4',6-diaminido-2-phenylindole (DAPI, Sigma) staining was performed, and coverslips were mounted using Fluoromount-G (Invitrogen) as the final step.

Table 4. List of primary antibodies.

Primary antibody	Host	Dilution	Reference	Target
MAP2	Chicken	1:5000	ab5392, Abcam	Mature neurons
MAP2	Mouse	1:500	M1406, Merck	Mature neurons
GFAP	Rabbit	1:500	Z0334, Dako	Astrocytes
Synapsin	Mouse	1:1000	MA5-31919, Thermofisher	Presynaptic compartment
PSD-95	Rabbit	1:250	ab18258, Abcam	Postsynaptic compartment
vGLUT1	Guinea pig	1:1000	135 304, SYSY	Glutamatergic vesicles
vGAT	Guinea pig	1:1000	131 308, SYSY	GABAergic vesicles
βIII-tubulin	Rabbit	1:500	T2200, Merck	Immature post-mitotic neurons
CTIP2	Rat	1:200	ABE1045, Werfen	Neuronal cortical fate
Tbr1	Rabbit	1:100	ab183032, Abcam	Neuronal cortical fate
SOX1	Goat	1:50	AF3369, Invitrogen	NPCs
PAX6	Rabbit	1:50	ab5790, Abcam	NPCs
Nestin	Mouse	1:100	MAB5326A4, Merck	NPCs
OCT3/4	Mouse	1:25	Sc-5279, SantaCruz Biotechnology	Pluripotency

Table 5. List of secondary antibodies.

Secondary antibody	Host	Dilution	Reference
anti-Mouse 488	Goat	1:500	A1101, Invitrogen
anti-Rabbit 488	Goat	1:500	A11034, Invitrogen
anti-Guinea 488	Goat	1:500	A11073, Invitrogen
anti-Mouse 568	Goat	1:500	A11031, Invitrogen
anti-Rabbit 568	Goat	1:500	A11011, Invitrogen
anti-Chicken 647	Goat	1:500	A21449, Invitrogen
anti-Goat 568	Donkey	1:500	A11057, Invitrogen
anti-Rabbit 647	Donkey	1:500	A31573, Invitrogen

4.3 Functional Studies of the Effects of CHI3L1 on Neurons

4.3.1 Morphological Analysis

For the morphological analysis, hiPSC-derived neuronal cultures at D28 were treated with human recombinant CHI3L1 (300 ng/ml, R&D Systems) or vehicle (PBS) diluted in neuronal maturation complete medium for 24 and 72 hours. The effects of CHI3L1 were evaluated by immunofluorescence using α-MAP2 and DAPI to immunostain neurons.

Images were acquired using a Zeiss LSM980 confocal microscope equipped with an x25 oil-immersion objective and a Zoom setting of 0.7. Confocal Z-stacks were obtained at a resolution of 2,048x2,048 pixels, with a slice interval of 1.22 µm. The pinhole size for the MAP2 channel was consistently set to 1 Airy Unit (AU) throughout the study. A total of 4-6 fields were acquired per replicate using the multi-position mode. Each experiment included 3-5 replicates per condition, and a total of 6 experiments were conducted. To avoid bias, image acquisition was performed by the researcher in a condition-blinded manner.

Prior to automated analysis, images were pre-processed using Zen Blue 3.1 software, which applied a "Median" filter. Next, maximum Z-projections from each

channel were processed using FIJI-Image J (NIH) software. The automated quantification of dendrite length, neuronal area, and dendritic arborization was carried out on MAP2 and DAPI Z-projections utilizing a custom pipeline in CellProfiler v4.2.1 software, following the methodology described in the provided reference.[207] A schematic overview of the analysis pipeline is provided in **Figure 11**. First, nuclei were segmented from the DAPI channel using the *IdentifyPrimaryObjects* module. For detection of neuronal bodies, either an adaptive Minimum Cross-Entropy or a Global Robust Background threshold was set in the MAP2 channel. Subsequently, the module *IdentifySecondaryObjects* was applied to define the neuronal soma and dendritic tree, considering DAPI-positive nuclei within the MAP2 mask. The *MorphologicalSkeleton* and *MeasureSkeleton* modules were then employed to derive measurements for dendritic tree length, neuronal area, and the number of ramifications for each neuron. For statistical analysis, mean image values of dendritic length, neuronal area, and number of branches were utilized.

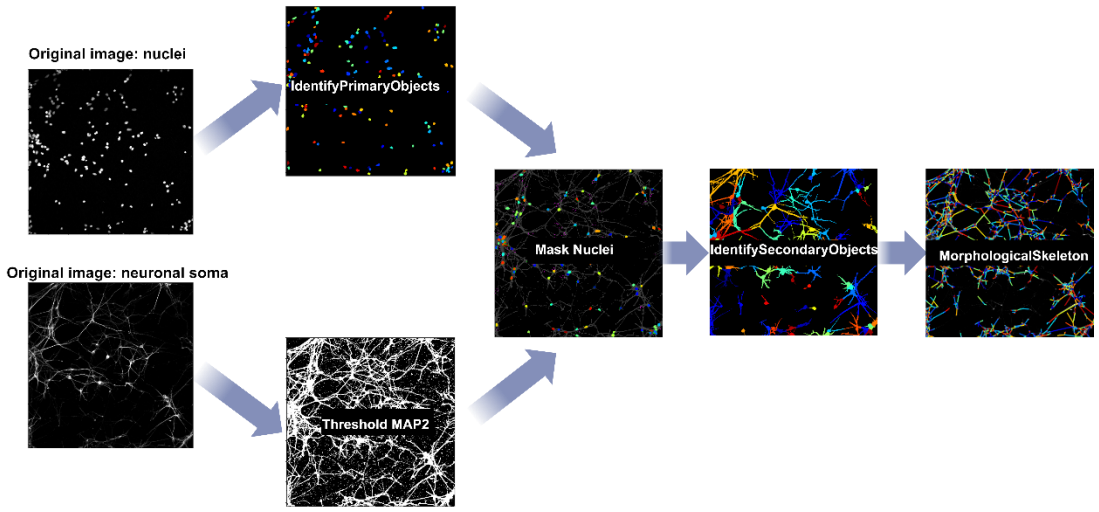

Figure 11. Overview of the morphological analysis pipeline.

4.3.2 Synaptic Plasticity

For the synaptic plasticity study, hiPSC-derived neuronal cultures at D28 were treated with human recombinant CHI3L1 (300 ng/ml, R&D Systems) or vehicle (PBS) diluted in neuronal maturation complete medium for 24 and 72 hours. Then, the

effects of CHI3L1 were evaluated by immunofluorescence and neurons were immunostained with α-MAP2, α-Synapsin, α-PSD-95 and DAPI.

Images were acquired using a Zeiss LSM980 confocal microscope with an x100 oil immersion objective. Confocal Z-stacks were obtained at a resolution of 1,024x1,024 pixels, with a slice interval of 0.5 µm. The pinhole size for the green channel remained constant at 1 Airy Unit (AU) throughout the study. In the multi-position mode, 8-10 fields were captured per replicate, each corresponding to neurites from distinct neurons. For each experiment, a total of 3-5 replicates per condition were analyzed, with 6 experiments conducted in total. Image acquisition was conducted in a condition-blinded manner to minimize bias.

Automated image analysis was carried out using FIJI-Image J in conjunction with a custom-programmed macro developed by the Advanced Optic Microscopy Unit at Hospital Clínic-CCITUB. In the initial step, the images underwent pre-processing to exclude small dendritic segments and cellular debris, thus ensuring the focus on relevant data. Subsequently, dendrites were segmented by employing intensity threshold strategies and binarization techniques. To identify synapsin and PSD-95 vesicles, intensity threshold strategies were applied, and pre- and post-synaptic puncta and area counts were determined within the dendritic mask. For the quantification of active synapses involving co-localization of both synaptic markers, the Co-Localization Highlighter Plugin was used. Active synapses were defined based on two criteria: (a) their respective fluorescence intensities surpassed the threshold values of their corresponding channels, and (b) their fluorescence intensity ratio exceeded 50% of a 0-100% ratio setting value. A schematic overview of the analysis pipeline is provided in **Figure 12**.

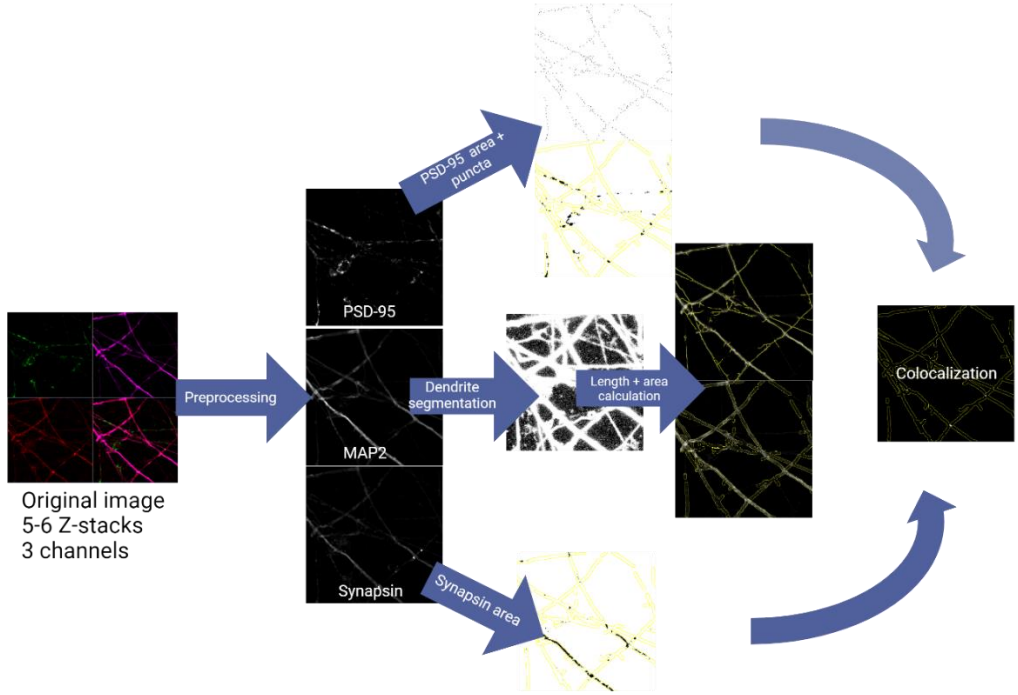

Figure 12. Overview of the synaptic study analysis pipeline

4.3.3 Neuronal Activity and Network Dynamics Study

The Neuronal Activity and Network Dynamics study was carried out in collaboration with Soriano's Lab at the Condensed Matter Physics Department and the Institute of Complex Systems (UBICS), University of Barcelona (UB).

hiPSC-derived neuronal cultures of D40 were treated with human recombinant CHI3L1 (300 ng/ml, R&D Systems) or vehicle (PBS) diluted in neuronal maturation complete medium for 4, 24 and 72 hours and neuronal activity was recorded by Fluorescence Calcium Imaging. This technique allows the detection of neuronal firing through the monitoring of calcium transients using calcium-binding dyes, specifically Fluo-8 (Abcam). After CHI3L1 treatment, the neuronal cultures were incubated with 1 µg/ml of Fluo-8 diluted in an *External Medium* (128 mM NaCl, 1 mM $CaCl_2$, 1 mM $MgCl_2$, 45 mM sucrose, 10 mM glucose, 0.01 M Hepes; pH=7.4) for 20 minutes at 37ºC. Then, the Fluo-8 solution was removed and *BrainPhys* (StemCell Technologies) without supplementing was added to the neuronal cultures. Six

independent experiments were performed (3 for each cell line) with 2-3 replicas per condition.

Neuronal activity was recorded on a Zeiss Axiovert inverted microscope coupled with a high-speed CMOS camera (Hamamatsu Orca Flash 4) using a 20x objective. All recordings were performed at room temperature and were recorded at 20 frames per second (*fps*) for 600 seconds (containing a total of 12,000 frames). Each frame consisted of an 8-bit grey-scale image with a size of 1024x1024 pixels, and a spatial resolution of 1.75 µm/pixel. Each frame allowed the simultaneous monitoring of 100-600 neurons depending on the neuron/glia proportion. The raw fluorescence images were then processed and analyzed to obtain the neuronal activity and network dynamics using the NETCAL software.

Fluorescence Analysis

NETCAL (www.itsnetcal.com)[208,209] is a MATLAB-built software dedicated to analysing high-speed, high-resolution fluorescence calcium imaging experiments. The fluorescence recordings were first pre-processed to remove background, and individual neurons were selected automatically (for the MS-10 line) or manually (for the MS-6) as Regions of Interest (ROIs). Individual fluorescence traces were then extracted by computing the ROI-average signal along time, which were then corrected for drifts and normalized as DFF_i (t) (%) = $100*(F_i(t)-F_{0,i})/F_{0,i}$, where $F_i(t)$ is the raw fluorescence trace of neuron i and $F_{0,i}$ its level of raw fluorescence at rest. Sharp increases in the fluorescence traces depicted neuronal activations. Individual traces were then observed to empirically determine the upper and lower threshold for considering neuronal firing, a method known as Schmitt-trigger.[210] Each experiment had constant thresholds within conditions and replicas. The detection algorithm finally produced raster plots of neuronal activations that portrayed the spatiotemporal behaviour of the neuronal network. At the end of the analysis, the ROIs centres, the smoothed traces, and the neuronal spikes were exported as CSV files to carry out further analyses. These analyses included advanced computational methods to extract the average neuronal activity, the global network activity (GNA), the inter-burst interval, the % of active neurons, and the effective connectivity.

Average Neuronal Activity

It was computed as the number of firings observed in the raster plot divided by the number of neurons and unit time.

Global Network Activity (GNA)

It consisted in the detection of quasi synchronous collective events in the network that indicated strong correlated activity between neurons. To obtain this information, the neuronal activity in the raster plot was summed up by using a sliding window 0.5 seconds wide and neurons within the window that activated synchronously led to peaks denominated A_b that could be detected. The distribution of A_b values thus revealed the tendency of the network to activate synchronously. This exploration of the raster plot led to a graph A(t) that varied between 0 (no coordinated activity) and 1 (the full network activating) as illustrated in **Figure 13**. A threshold of 10% of the neurons firing simultaneously was set for considering collective events.

Inter-burst interval (IBI)

It quantified the time span between consecutive bursting events and it was computed as the duration of the recording divided by the number of significant bursting events.

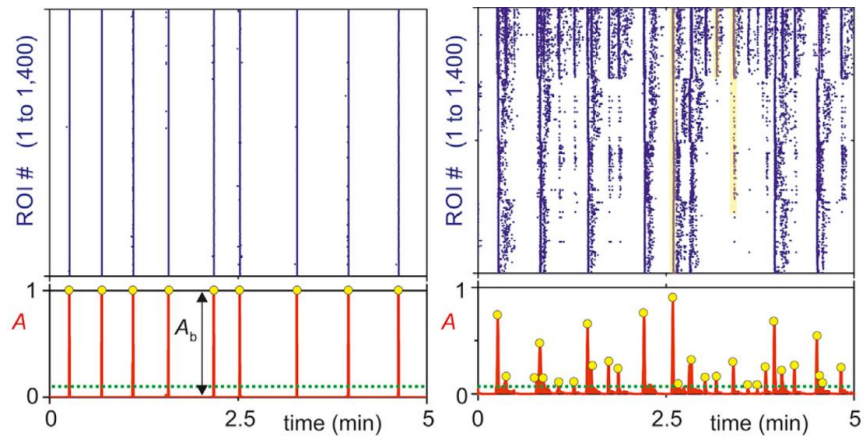

Figure 13. **Examples of raster plots and corresponding global network activity.** Data corresponds to two contrasting networks, one homogeneous on the left, and one designed using neuroengineering on the right. Episodes of strong synchronous activity led to sharp peaks in the global network activity A.

Significant peaks A_b are those that include at least 5% of the network (green horizontal line). Adapted from *Montalà-Flaquer et al., 2022*.

Effective Connectivity

The effective connectivity reflects dynamic interactions between neurons, understood as the likelihood that a neuron was influencing the activity of any another neuron. It was mathematically computed by determining causal relationships among the spike trains of pairs of neurons through a modified version of Generalized Transfer Entropy (GTE)[168,208] run in MATLAB. Since not all computed connections in the analysis were significant, a z-score > 1.5 was introduced as a threshold to capture effective communication both at global and local scales.[209,211] The significant connections were finally set to 1 (effective connection present) or 0 (absence of effective connection), shaping directed yet unweighted connectivity matrices that were visualized in the form of network maps with Gephi[212], as depicted in **Figure 14**. The effective connectivity was used to compute several network measures (see below) that reflected the functional organization of the network and its alteration upon treatment.

Network Properties

The properties defined next provided whole network characteristics that allowed to compare the functional organization of neuronal cultures with and without treatment:

Average connectivity or $\langle k \rangle$

It described the capacity of neurons to directly communicate with others in the network, and it was defined as the sum of the number of effective connections per neuron i, k_i, divided by the number of neurons N in the network.

$$\langle k \rangle = \frac{1}{N} \sum_{\mathrm{i}} k_i \, .$$

Global efficiency or G_E*.*

It described the capacity of neurons to exchange information across the entire network, and it was defined as:

$$G_E = \frac{1}{N(N-1)} \sum_{0 \le i,j \le N} \frac{1}{d(i,j)},$$

where N is the number of neurons and $d(i,j)$ is the length of the shortest topological path connecting neurons. $G_E = 0$ indicated that neurons were essentially isolated and were unable to communicate with one another at global scale, while $G_E = 1$ showed that there was a strong capacity for information exchange at the whole-network scale. **Figure 14** provides an illustrative example for two networks, with the left one exhibiting a lower global efficiency than the right one.

Modularity index or Q

It accounted for the tendency of neurons to form functional modules or communities. It was defined as

$$Q = \frac{1}{2m} \sum_{0 \le i,j \le N} \left(A_{ij} - \frac{k_i k_j}{2m} \right) \delta(c_i, c_j),$$

where N is the number of neurons, A_{ij} represents the weight of the connection between i and j, $k_i = \sum_{j=1}^{N} A_{ij}$ is the sum of the weights of the connections attached to neuron i, c_i is the community to which neuron i belongs, $m = (1/2) \sum_{i,j=1}^{N} A_{ij}$, and $\delta(u,v)$ is the Kronecker Delta with $\delta(u,v) = 1$ for $u = v$ and $\delta(u,v) = 0$ otherwise.

The modularity Q, and optimal community structure, was computed using the Louvain algorithm.[213] Q ranges between 0 (the entire network shapes a unique module) and 1 (each neuron is an isolated module). Values of $Q \simeq 0.3$ indicate the existence of modules in the network with a varying number of ROIs and interconnected to one another. The left network of **Figure 14** exemplifies such a situation.

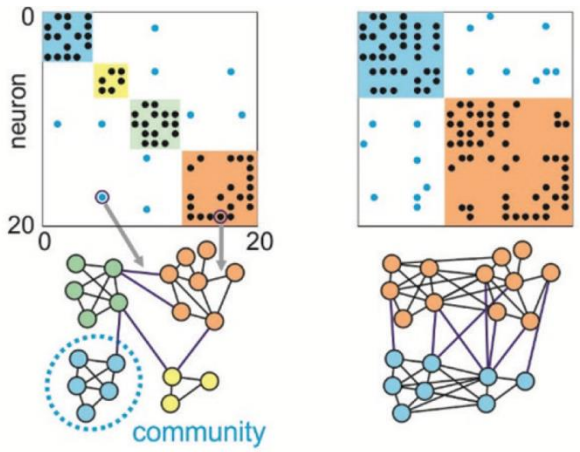

Figure 14. Effective connectivity. Top, effective connectivity matrices, in which each dot is a connection. Bottom, corresponding network maps, in which neurons are placed according to their position in the culture. Two contrasting networks are shown. The one on the left has relatively few connections and is highly modular, with neurons more connected within modules (color boxes) than across modules. The one on the right has more connections and is less modular, overall shaping a highly integrated network.

4.4 Molecular characterization of CHI3L1 signature on hiPSC-derived neurons

4.4.1 Transcriptomic Study

CHI3L1 treatment of hiPSC-derived neurons induced morphological and functional alterations that may have been driven by the interaction of CHI3L1 with one or more neuronal receptors. This ligand-receptor interaction activates or inhibits signalling pathways that ultimately drive a gene expression fingerprint associated with the phenotype observed in the morphologic and functional assays.

To decipher the transcriptomic signature underlying the effects of CHI3L1 on hiPSC-derived neurons, a microarray experiment was conducted. The primary objectives of the microarray analysis were: (1) to identify differentially expressed genes (DEGs) between CHI3L1 and vehicle-treated conditions at various time points; and (2) to find enriched pathways that may mediate the CHI3L1 effects on neuronal cultures. The

microarray experiment was performed using D28 MS-10-derived neuronal cultures, which were subjected to CHI3L1 treatment (300 ng/ml) or vehicle (PBS) for 12 and 24 hours. Additionally, a basal condition of untreated neurons at t=0 was included in the study.

RNA Extraction

Total RNA was isolated from neuronal cultures using TRIzol (ThermoFisher) according to the manufacturer's instructions. Briefly, 1 ml of TRIzol was added to $1x10^6$ cells, pooling three 6-well plates. The cell lysate was homogenated by pipetting and vortexing. Next, the lysate was incubated for 5 minutes at room temperature and 200 µl chloroform (Sigma)/ml TRIzol was added, and the mixture was vigorously shaken and incubated for 3 minutes. Samples were centrifuged at 12,000g for 15 minutes at 4ºC and the upper aqueous phase containing the RNA was transferred to a new tube and 500 µl of isopropanol (Merck) was added to precipitate the RNA. After 10 minutes of incubation at room temperature, samples were centrifuged at 12,000g for 10 minutes at 4ºC and the supernatant was discarded. The RNA pellet was washed in 1 ml of ethanol (Merck) and centrifuged at 14,000g for 10 minutes. Finally, the supernatant was discarded, and the RNA pellet was resuspended in RNAse-free water. RNA quality and concentration were measured by Nanodrop (Thermo Scientific™) and capillary electrophoresis (Bioanalyzer 2100, Agilent Technologies).

Microarray Study

Microarray service was carried out at the High Technology Unit (UAT) of the Vall d'Hebron Research Institut (VHIR), Barcelona (Spain). Affymetrix GCS3000 microarray platform and the GeneChip Human Clariom S array cartridge were used for this experiment. This array analyzes gene expression patterns on a whole-genome scale on a single array with probes covering many exons on the target genomes, thus permitting an accurate expression summarization at the gene level. The starting material was 10 ng of total RNA of each sample. Briefly, sense dsDNA suitable for labelling was generated from total RNA with the GeneChip Pico Reagent Kit from Affymetrix (Thermofisher - Affymetrix, UK) according to the manufacturer's

instructions. Sense dsDNA was fragmented, labelled, and hybridized to the arrays with the GeneChip PicoTerminal Labeling and Hybridization Kit from the same manufacturer. Arrays plates were scanned to obtain .CEL files. The first control of the technical quality was made with the software Expression Control.

Bioinformatics Analysis

The bioinformatics analysis was carried out in the Statistics and Bioinformatics Unit (UEB) at VHIR. Statistical analysis was performed using the statistical language "R" (R version 4.1.0(2021-05-18), Copyright (C) 2018 The R Foundation for Statistical Computing), and the libraries developed for the microarray analysis in the Bioconductor Project (www.bioconductor.org). The analysis pipeline followed standard procedures for microarray data. Initial quality controls (QC) were performed to ensure array suitability for normalization and to verify the appropriateness of the normalized data for differential expression analysis. Pre-processing involved RMA normalization, and exon-level values were averaged to obtain one expression value per gene, facilitating data comparability and eliminating technical biases. To estimate the main sources of variability, Principal Variance Component Analysis (PVCA) was performed using the PVCA Bioconductor Package. The analysis to select DEGs was based on adjusting a linear model with empirical Bayes moderation of the variance.[214] To adjust for the variability derived from the three rounds of cell differentiation, the *CellDiff* factor was included in the linear model. The empirical Bayes analysis employed various performance measures to determine DEGs. Since no DEGs passed the False Discovery Rate method by Benjamini and Hochberg, less restrictive criteria were used. DEGs were considered if they exhibited an absolute logFC >0.3 (fold change) with unadjusted p-values of <0.01, setting the stage for subsequent validation.

Metascape Pathway and Process Enrichment Analysis

DEGs with a p<0.01 from both time points were selected. Next, pathway and process enrichment analyses were conducted for each gene list using the following ontology sources: KEGG Pathway, GO Biological Processes, GO Cellular Components, GO Molecular Functions, Reactome Gene Sets, Canonical Pathways, and

WikiPathways. The entire genome's genes were utilized as the background for enrichment analysis. Enriched terms were identified based on the following criteria: a $p<0.01$, a minimum count of 3, and an enrichment factor>1.5 (where the enrichment factor represents the ratio between observed and expected counts based on chance). These enriched terms were then grouped into clusters based on their similarity of membership. The p-values were computed using the cumulative hypergeometric distribution, while the Benjamini-Hochberg procedure was employed to calculate q-values to account for multiple testing. To perform hierarchical clustering on the enriched terms, Kappa scores were utilized as the similarity metric. Sub-trees with a similarity score greater than 0.3 were considered as belonging to the same cluster. Within each cluster, the term with the most significant statistical outcome was chosen to represent the entire cluster.

Gene Set Enrichment Analysis

The analysis of biological significance has been based on gene set enrichment analysis (GSEA) on two different annotation databases: the GO and the Reactome Pathway knowledge databases. The goal of this analysis was to perform one of the available statistical tests to determine whether a given gene set, usually a particular category of the GO or pathway in Reactome, is over-represented in the list of selected genes (the sample) compared to a reference set (all the genes analyzed in the study) from where it has been selected. In GSEA, all the genes analyzed in the study (altered genes) are ranked by log fold change and used in the analysis. GSEA aggregates the per gene statistics across genes within a gene set, therefore making it possible to detect situations where all genes in a predefined set change in a small but coordinated way.

To summarize the results obtained in the enrichment analysis, a clustering analysis was performed using the R/Bioconductor package simplifyEnrichment.[215] This method allows to cluster terms using different similarity measures and clustering algorithms and visualize the results as Heatmaps. Clusters can be annotated with word cloud or the most representative term within the cluster (eg. term with maximal set size or minimal p-value). Here, the term with minimal p-value was used to

annotate the clusters. - Lists of enriched pathways were summarized separately for each comparison or grouped into multiple comparisons to visualize the terms enriched in common/specifically in each comparison. For each comparison, a maximum of 1000 terms with a raw p-value below 0.05 (GSEA result) were selected for single and multiple comparisons.

4.4.2 Reverse Transcription-Quantitative PCR (RT-qPCR) Studies

RNA samples were obtained from all conditions and all experiments using the TRIzol method as explained previously. Complementary DNA (cDNA) was synthesized using the High-Capacity cDNA Kit (Applied Biosystems) with RNAse Inhibitor (Applied Biosystems) according to the manufacturer's instructions.

For RT-qPCR validation, we selected the top DEGs between CHI3L1 and vehicle-treated conditions at 12 and 24 hours, with an unadjusted p-value < 0.001 and an absolute logFC > 0.3. Additionally, we chose other genes based on their neuronal function from the set of genes with p-values ranging from >0.001 to <0.01. Furthermore, certain genes were selected for validation, even if they did not fully meet the criteria, due to their association with intriguing pathways. Also, the expression of the known receptors of CHI3L1 was assessed by RT-qPCR. GAPDH gene expression was used as an endogenous control in all RT-qPCR studies.

All primers and probes were from Applied Biosystems, and they are summarized in **Table 6**. All RT-qPCR experiments were performed using the TaqMan Gene Expression Master Mix (Applied Biosystems) and assays were run on the QuantStudio™ 7 Pro Real-Time PCR System (Applied Biosystems). The relative level of gene expression was quantified using the $2^{-\Delta\Delta Ct}$ method.[216] Shortly, the expression of the housekeeping gene (GAPDH) was used for normalization and the expression of the genes of interest in the vehicle was used as a calibrator. Results were expressed as logFC in gene expression in CHI3L1-treated condition versus vehicle. All analyses were performed with QuantStudio™ Real-Time PCR Software (Applied Biosystems).

Table 6. Genes and probes assessed by RT-qPCR

Condition	Gene Symbol	Ref
12 hours	AKR1E2	Hs00230170_m1
	LCK	Hs00178427_m1
	SCYL3	Hs00928639_m1
	PDE6G	Hs00159965_m1
	AQP1	Hs01028916_m1
	GNMT	Hs00219089_m1
	ABCA13	Hs01110200_m1
	NR2E1	Hs01128417_m1
	RALGPS2	Hs00404163_m1
	ITPR3	Hs01573539_m1
	AHNAK	Hs01102463_m1
24 hours	CGN	Hs00430426_m1
	CFAP157	Hs00402363_g1
	TMEM161B	Hs00995425_g1
	RIOK2	Hs01084566_m1
	CYLC1	Hs03005816_m1
	DENND2C	Hs00942533_m1
	CD86	Hs01567026_m1
	CFAP61	Hs01037320_m1
	TPTE2	Hs01685755_m1
	TSNAX-DISC1	Hs00962133_m1
	LRRN4	Hs00379905_m1
	GRID2	Hs00910017_m1
	RASA2	Hs01003332_m1
	OR2D2	Hs00999189_s1
	HMSD	Hs00416456_m1
	LRRC66	Hs02386735_m1
	SLC5A6	Hs00951312_m1
	ERAP2	Hs01073631_m1
	VPS54	Hs00212957_m1
	TRIM66	Hs00389418_m1
	UHMK1	Hs00332674_m1
	CDH12	Hs00362037_m1
	CD44	Hs01075861_m1

	GNMT	Hs00219089_m1
	CHRFAM7A	Hs04189909_m1
	EFNA1	Hs00358886_m1
	RHOQ-AS1	Hs04408403_m1
	TNFAIP6	Hs00200180_m1
	MTMR2	Hs01547438_m1
Additional genes with potential interest	APELA	Hs05044590_s1
	GNMT	Hs00219089_m1
	GNG5	Hs00893832_g1
	CAMK2B	Hs00365799_m1
	APC2	Hs00183420_m1
	SYT10	Hs01394304_m1
	CHRM2	Hs00265208_s1
	RHOQ-AS1	Hs04408403_m1
	CD86	Hs01567026_m1
	STUB1	Hs01071598_g1
	CDH12	Hs00362037_m1
	CHRM3	Hs00265216_s1
	CALB1	Hs01077197_m1
Endogenous control	GAPDH	Hs02786624_g1

4.4.3 Human Phospho-Kinase Array

As described previously, CHI3L1 treatment of hiPSC-derived neurons induced alterations that may have been driven by the interaction of CHI3L1 with one or more neuronal receptors. To assess the impact on cellular pathways, we employed The Human Phospho-Kinase Array (R&D Systems), enabling simultaneous detection of the relative levels of phosphorylation of 37 kinase phosphorylation sites and 2 related proteins (**Table 7**). In this experiment, we focused on signalling events that occurred before gene expression and functional changes by analyzing earlier time points (30 minutes, 1, 2, and 4 hours) following CHI3L1 (300 ng/ml) or vehicle treatment in D28 MS-10-derived neurons.

Cell lysates were diluted and incubated overnight at 4ºC with the Human Phospho-kinase Array where capture and control antibodies were spotted in duplicate on

nitrocellulose membranes. Then, the arrays were washed to remove unbound proteins and incubated with a cocktail of biotinylated detection antibodies. Protein detection was performed with Streptavidin-HRP and chemiluminescent substrates, and arrays were revealed on developed films (Fujifilm) with CP-BU (AGFA, Belgium). Pixel intensities were collected by a transmission mode scanner and corresponded to the amount of protein bound at each spot. FIJI was used for array analysis, determining the average signal of pixel intensity for duplicate spots. Relative changes per analyte were derived by comparing CHI3L1 versus vehicle samples at each time point.

Table 7. Human Phospho-Kinase Array targets and Phosphorylation sites

Target	Phosphorylation site
Akt 1/2/3	T308, S473
CREB	S133
EGFR	Y1086
eNOS	S1177
ERK1/2	T202/Y204, T185/Y187
Chk-2	T68
c-Jun	S63
Fgr	Y412
GSK-3α/β	S21/S9
GSK-3β	S9
HSP27	S78/S82
p53	S15, S46, S392
JNK 1/2/3	T183/Y185, T221/Y223
Lck	Y394
Lyn	Y397
MSK1/2	S376/S360
p70 S6 Kinase	T389, T421/S424
PRAS40	T246
p38α	T180/Y182
PDGFRβ	Y751
PLC-γ1	Y783
Src	Y419
PYK2	Y402
RSK1/2	S221/S227

RSK1/2/3	S380/S386/S377
STAT2	Y689
STAT5a/b	Y694/Y699
WNK1	T60
Yes	Y426
STAT1	Y701
STAT3	Y705, S727
β-Catenin	-
STAT6	Y641
HSP60	-

4.4.4 Western Blot (WB)

MS-10-neuronal D28 lysates from basal, CHI3L1 (300 ng/ml), and vehicle-treated conditions at 2 and 4 hours were prepared using cold-ice RIPA buffer supplemented with a protease inhibitor cocktail and phosphatase inhibitors. Protein concentration was determined using the BCA Protein Assay, and protein concentrations were equalized with supplemented lysis buffer and Laemmli Sample Buffer 4x, followed by boiling at 95ºC for 5 minutes. Protein samples were loaded into 7.5% or 10% SDS-PAGE gels and subjected to electrophoresis in Electrophoresis Buffer at 100V for 90 minutes at room temperature. Subsequently, the gel was transferred to a PVDF membrane using the wet transfer technique in Transference Buffer at 100V for 90 minutes at 4ºC. The membrane was blocked for 1 hour at room temperature using either 5% non-fat dry milk in TBST or 5% Bovine Serum Albumin (BSA) in TBST. The blocked membrane was then incubated with the primary antibody (**Table 8**) overnight at 4ºC, followed by washing with TBST and incubation with the corresponding HRP-conjugated secondary (detailed in **Table 9**) antibody for 1 hour at room temperature. After further washing with TBST, the membrane was revealed using the chemiluminescence substrate ECL Clarity on developed films. β-actin was used as the endogenous control in all experiments. Complete buffer recipes are summarized in Supplementary Table 1. The details concerning the Western Blot (WB) primary and secondary antibodies and dilutions, as well as the variable WB conditions, are provided in **Table 8** and **Table 9.**

Table 8. WB targets and primary antibodies

Target	Molecular Weight	% SDS-PAGE	Dilution	Host
STAT1	84, 91 kD	7.5	1:1000	Rabbit
pSTAT1-Y701	84, 91 kD	7.5	1:500	Rabbit
β-actin	42 kD	7.5 or 10	1:3000	Mouse

Table 9. WB secondary antibodies

Secondary antibody	Dilution	Reference
α-Goat HRP	1:3000	HAF017, R&D Systems
α-Rabbit HRP	1:3000	P0448, Dako
α-Rat HRP	1:3000	STAR72, Bio-Rad
α-Mouse HRP	1:300	P0447, Dako

4.5 Statistical Analysis

Statistical analysis details for each experiment are provided in the corresponding figure legends. For all experiments, except microarrays, GraphPad Prism 8 software (San Diego, USA) was used for statistical analysis. For microarray data, R (R version 4.1.0, R Project for Statistical Computing) was employed.

Data were assumed to follow a normal or lognormal distribution. Two-tailed unpaired t-test was used for comparing two experimental groups, while least-square means were used for analyzing three or more experimental groups. For the STAT 1 phosphorylation analysis, two-tailed ratio paired t-test was performed. For the morphological analysis, synaptic plasticity, and neuronal activity and network dynamics studies, one-way ANOVA with Sidak's post hoc test was conducted. In the multiple comparisons tests, each treated condition was compared to its corresponding vehicle, and statistical significance was set at $p<0.05$. For the Proteome Phosphokinase Array, two-way ANOVA (factors time and treatment) with Geisser-Greenhouse correction and Bonferroni post hoc test was performed.

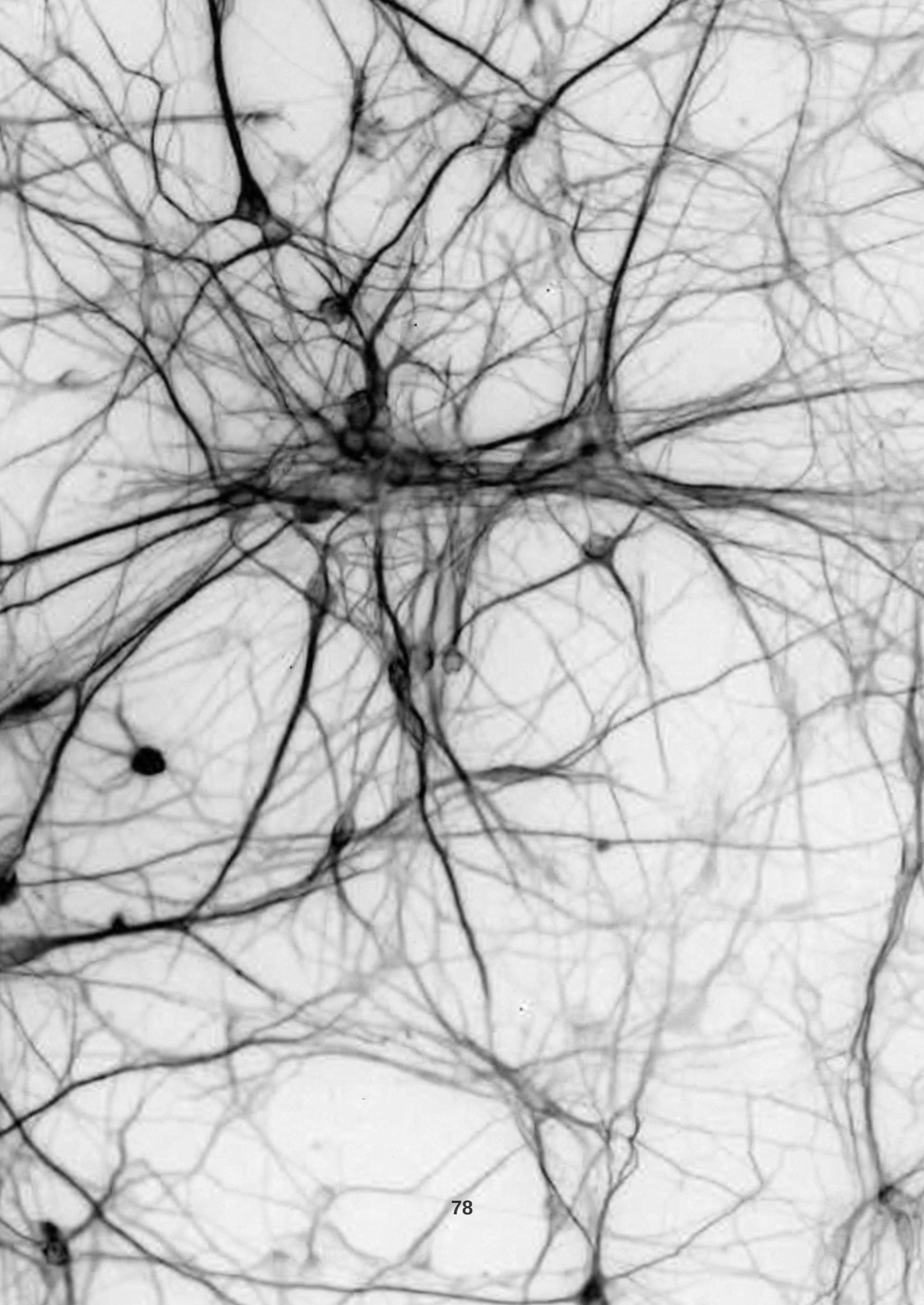

RESULTS

5. RESULTS

5.1 Characterization of NPCs and hiPSC-derived Neuronal Cultures

In this study, we differentiated two RRMS hiPSCs lines towards cortical fate neurons. **Figure 15** presents illustrative bright-field microscopy images that demonstrate the key stages of the differentiation process.

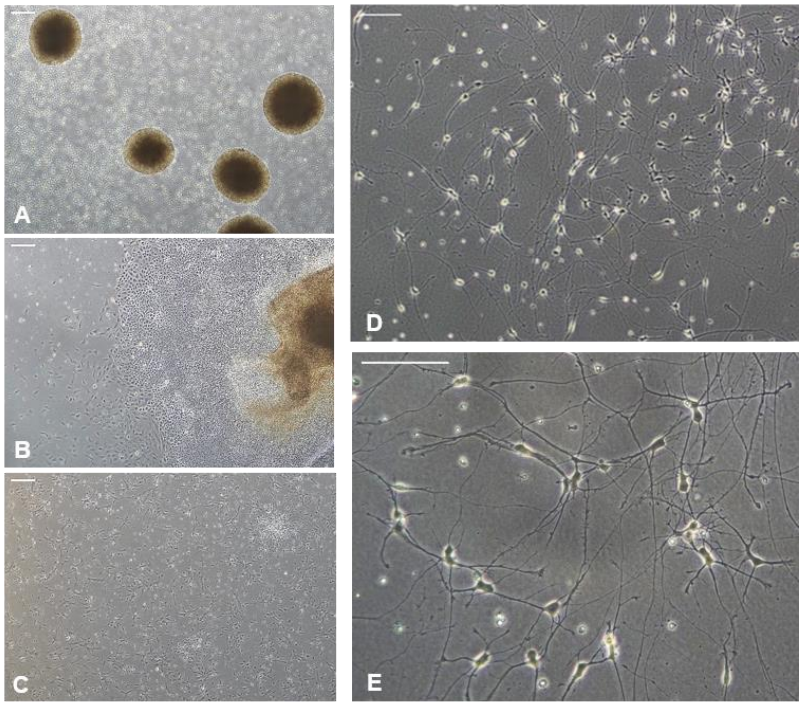

Figure 15. Illustrative bright field microscopy images depicting the differentiation process of hiPSCs and the subsequent maturation of neurons. The neural induction protocol involves culturing hiPSCs until they reach 80% confluence, followed by seeding clumps of hiPSCs in low attachment conical plates containing NIM. At 48 hours, the EBs (**A**) should exhibit a rounded morphology with well-defined borders. Subsequently, the EBs are transferred to a Geltrex-coated plate, facilitating the migration and colonization of NPCs (**B**). NPCs are cultured until they reach confluence, and then they are differentiated into neuronal precursors (**C**). Next, neurons (**D** and **E**) are seeded in the final plate, where they mature until D28 or D40. **A**, **B** and **C** scale bar = 400 µm; **D** and **E** scale bar = 100 µm.

Abbreviations: hiPSCs – human induced pluripotent stem cells; NIM – Neural Induction Medium; EBs – Embryoid Bodies; NPCs – Neural Progenitor Cells

5.1.1 Characterization of NPCs

First, we directed neural fate through inhibition of TGF-β/BMP dependent SMAD signalling in hiPSCs, resulting in cultures enriched for CNS-type NPCs, where most cells expressed SRY-box transcription factor 1 (SOX1), Paired Box 6 (PAX6), and Nestin as detailed in **Figure 16**. Since MS-10-derived NPCs exhibited spontaneous neuronal differentiation, we also evaluated by immunofluorescence the expression of doublecortin (DCX), a marker for immature neurons.

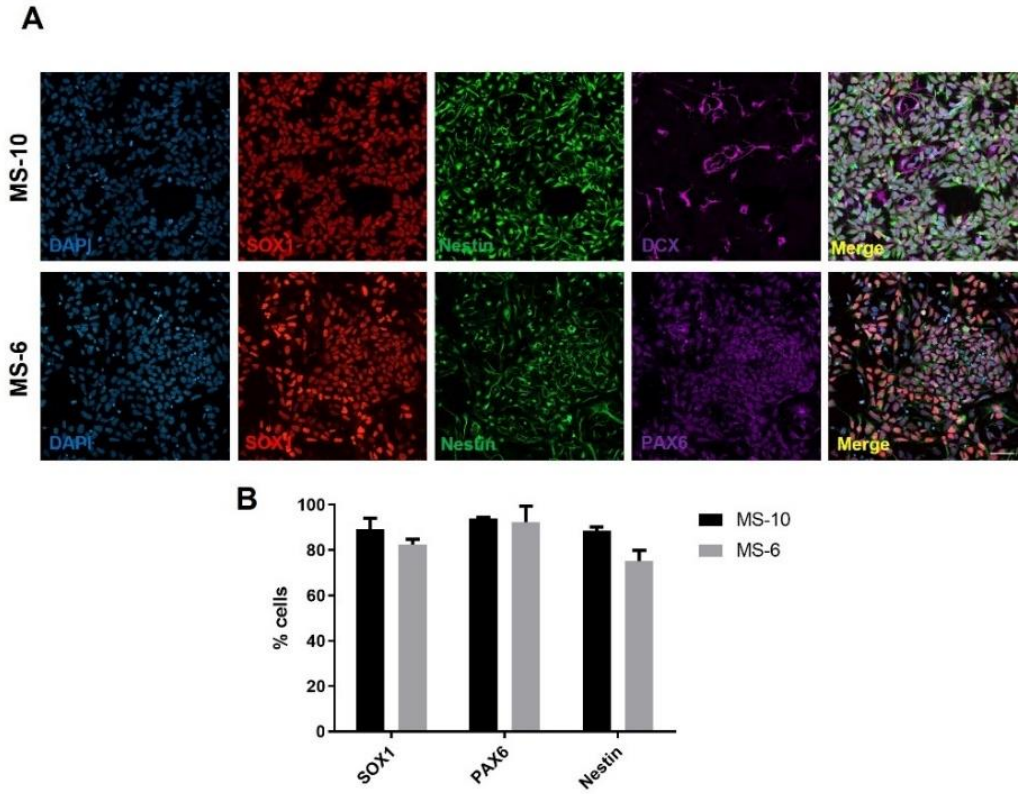

Figure 16. Immunofluorescence analysis of typical NPCs markers in MS-10 and MS-6-Derived cultures. (A) Representative immunofluorescence images of MS-10 and MS-6 cultures showing SOX1 (red), Nestin (green), DCX or PAX6 (magenta), and DAPI (blue) staining. **(B)** Percentage of cells expressing NPCs markers SOX1, PAX6, and Nestin in MS-10 and MS-6 cultures. Two independent cultures were analyzed for each cell line. Scale bar = 50 µm.

Abbreviations: NPCs - Neural Progenitor Cells; SOX1 - SRY-Box Transcription Factor 1; DCX - doublecortin; PAX6 - Paired Box 6; DAPI - 4′,6-Diamidino-2-phenylindole dihydrochloride.

5.1.2 Characterization of hiPSC-derived Neuronal Cultures

As detailed in the Methods section, we directed the differentiation of NPCs towards forebrain fate neuronal precursors and further matured them into cortical-fated neurons. Our first objective was to determine the optimal neuronal maturation time point for conducting the experiments. We evaluated dendrite growth in MS-10-derived neuronal cultures at 8, 15, and 28 days (**Figure 17A**). At D8, most neurons already expressed the dendritic marker MAP2 and displayed continuous growth over time. At D28, neurons displayed densely interconnected networks (**Figure 17B**) and expressed both presynaptic (synapsin) and postsynaptic (PSD-95) markers (**Figure 18**). Based on these findings, we selected D28 as the appropriate time point to conduct our experiments.

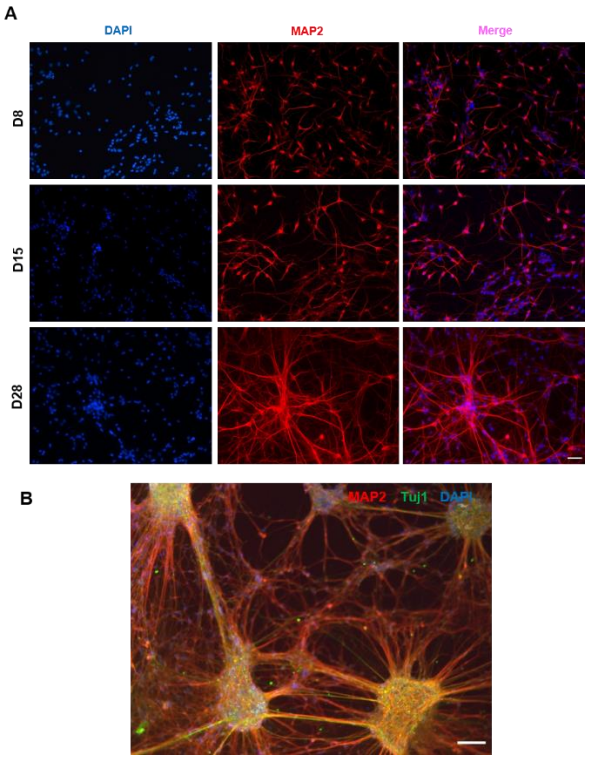

Figure 17. **(A)** Immunofluorescence images of MS-10-derived neuronal cultures at D8, D15, and D28. Neurons were stained for MAP2 (red) and DAPI (blue). Cultures displayed continuous dendrite growth

throughout the assessed time points. Scale bar = 50 µm. (**B**) MS-10-derived neuronal culture at D28 immunostained for MAP2 (red), Tuj1 (green), and DAPI (blue). Scale bar = 400 µm.

Abbreviations: MAP2 – Microtubule Associated Protein 2; DAPI - 4′,6-Diamidino-2-phenylindole dihydrochloride; Tuj1 - β-tubulin III.

Next, we aimed to determine the onset of spontaneous neuronal firing and the development of synchronous activity in our neuronal cultures. We performed a characterization of MS-10-derived neuronal activity at D21, D35, and D40 days of maturation to identify when spontaneous and synchronous activity emerged (**Figure 19**). We observed that some neurons started to fire around D21, and over time, there was a gradual increase in both neuronal activity and synchronicity. By D40, the hiPSC-derived cultures exhibited a pattern of activation that encompassed both sporadic and synchronous activity, consistent with previous observations.[187] Consequently, we selected the D40 time point to conduct CHI3L1 experiments in the study of neuronal activity and neuronal network dynamics.

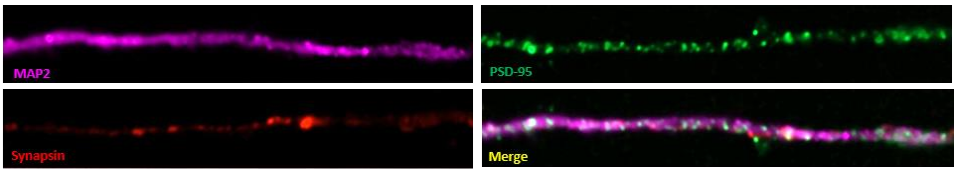

Figure 18. Representative images showing the expression of the presynaptic protein synapsin (in red) and the postsynaptic protein PSD-95 (in green) within MAP2-labeled dendrites (magenta) in D28 MS-10-derived neuronal cultures.

Abbreviations: PSD-95 - postsynaptic density protein 95; MAP2 – Microtubule Associated Protein 2

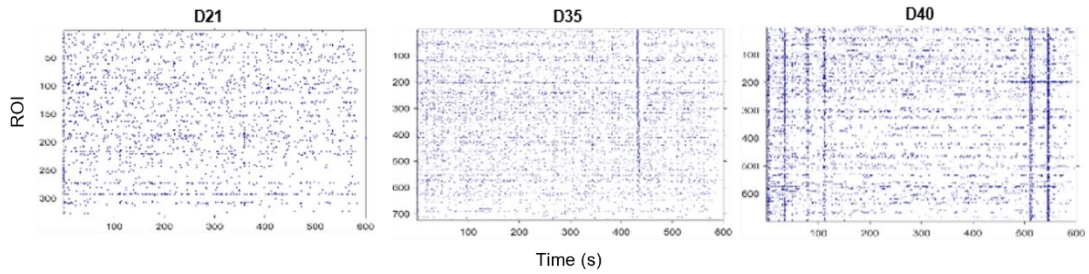

Figure 19. Raster plots representing neuronal activity on D21, D35 and D40 of MS-10 derived neuronal cultures. Blue dots represent Schmitt interference spikes corresponding to neuronal activations obtained from calcium fluorescence variations. The Y-axis indicates the ROI index, and the X-axis represents time in seconds.

We carried out a comprehensive characterization of neuronal cultures at D28 and D40, carefully selected as the neuronal maturation time points for our experiments. Initially, we assessed the neuronal/astrocyte ratio through immunostaining with MAP2 for neurons and GFAP for astrocytes. At D28, MS-10 (**Figure 20I**) and MS-6 (**Figure 20K**) neuronal cultures showed varying percentages of GFAP+ astrocytes, with less than 5% in the MS-10 line and 30% in the MS-6 line. Over time, the proportion of astrocytes significantly increased, reaching more than 10% in the MS-10 line ($p<0.0001$) and 45% in the MS-6 line ($p=0.0251$) at D40.

To evaluate cortical fate, we performed immunofluorescence analysis against Tbr1 and CTIP2, two cortical-specific markers. At D28, most MAP2+ neurons in both MS-10 (**Figure 20J**) and MS-6 (**Figure 20L**) lines were Tbr1-positive with limited expression of CTIP2. At D40, MS-10 (**Figure 20J**) neurons maintained Tbr1 immunoreactivity, while MS-6 (**Figure 20L**) neurons showed decreased Tbr1 expression and increased CTIP2 immunoreactivity.

Additionally, we characterized hiPSC-derived neurons for glutamatergic (vGLUT1) and GABAergic (vGAT) markers (**Figure 21**), observing the expression of both markers at D28 and D40, with a loss of most vGAT immunoreactivity at D40.

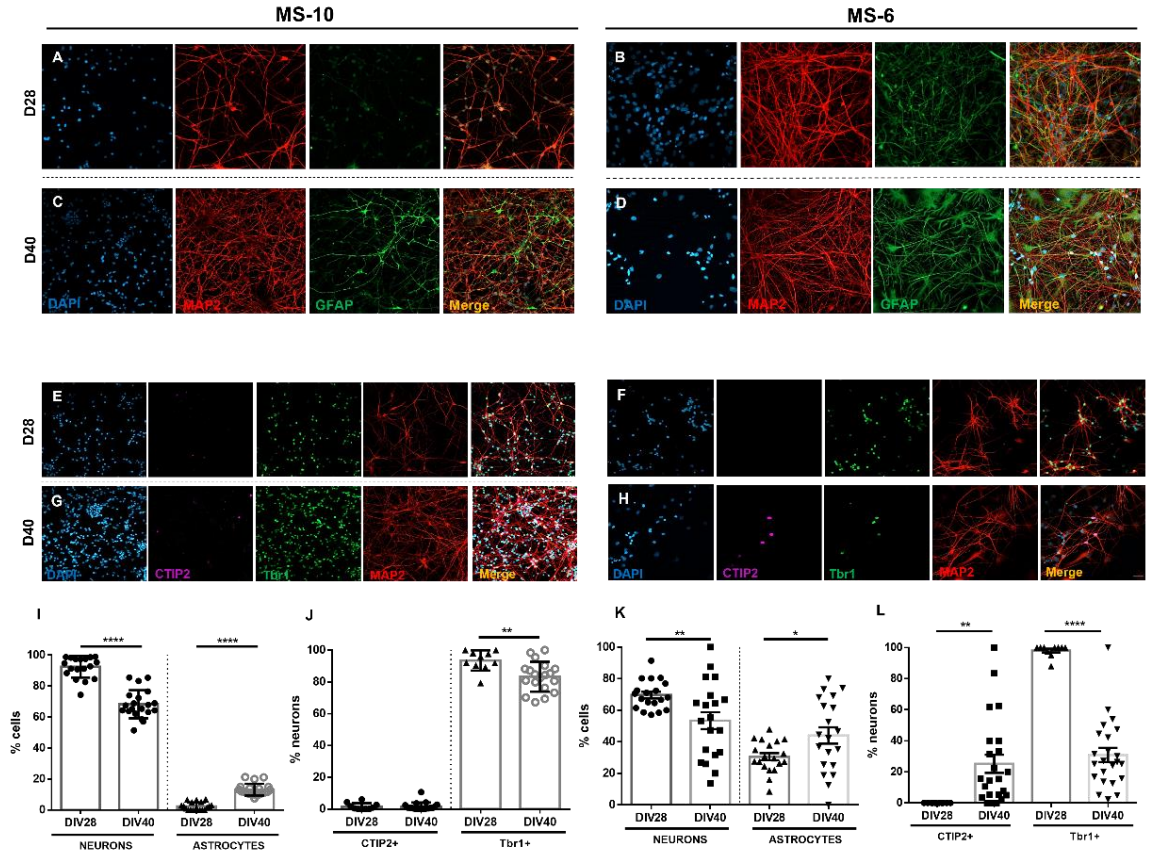

Figure 20. Characterization of hiPSC-derived neuronal cultures. (A, **B**, **C**, and **D**) Immunostaining of hiPSC-derived neuronal cultures with MAP2 (red) and GFAP (green) neuronal and astrocyte markers, respectively, and DAPI (blue) nuclear marker. Representative images of MS-10 at D28 (**A**) and D40 (**C**), and MS-6 at D28 (**B**) and D40 (**D**). (**E**, **F**, **G**, and **H**) Immunostaining of hiPSC-derived neuronal cultures with MAP2 (red), cortical markers Tbr1 (green), and CTIP2 (magenta), along with DAPI (blue) nuclear marker. Representative images of MS-10 at D28 (**E**) and D40 (**G**), and MS-6 at D28 (**F**) and D40 (**H**). Two independent neuronal cultures per cell line were assessed for MAP2+, GFAP+, Tbr1+, and CTIP2+ percentages at D28 and D40. Quantification of neuronal/astrocyte percentages in MS-10 (**I**) and MS-6-derived (**J**) neuronal cultures. Quantification of Tbr1+ and CTIP2+ percentages in MS-10 (**K**) and MS-6-derived (**L**) neuronal cultures. Scale bar = 50 µm. *p<0.05; **p<0.01; ***p<0.001; (*Unpaired t-test*).

Abbreviations: hiPSC – human induced Pluripotent Stem Cells; MAP2 – Microtubule Associated Protein 2; GFAP – Glial Fibrillary Acidic Protein; DAPI - 4′,6-Diamidino-2-phenylindole dihydrochloride; CTIP2 - C-terminal-binding protein 2; Tbr1 - T-Box Brain Transcription Factor 1.

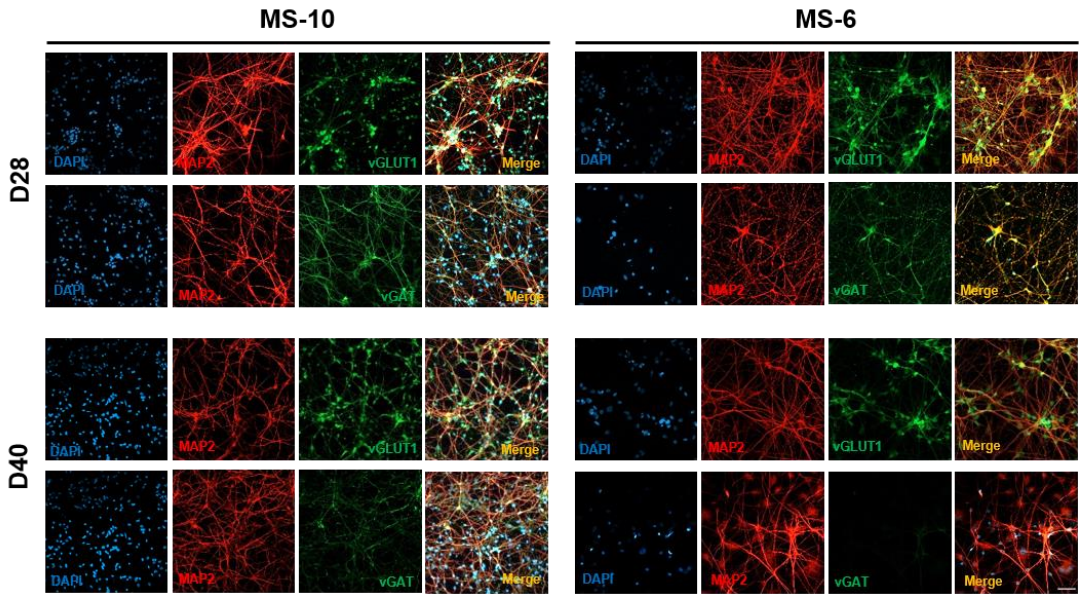

Figure 21. **Immunofluorescence analysis of glutamatergic and GABAergic markers in MS-10 and MS-6 derived neuronal cultures at D28 and D40.** Neurons were immunostained for MAP2 (red), vGLUT1 (green), vGAT (green), and DAPI (blue). Both MS-10 and MS-6 derived neurons expressed glutamatergic and GABAergic markers at D28, and maintained vGLUT1 expression at D40, while vGAT expression was mostly lost. Scale bar = 50 µm.

Abbreviations: MAP2 – Microtubule Associated Protein 2; vGLUT1 – vesicular glutamate transporter 1; vGAT – vesicular GABA transporter; DAPI - 4′,6-Diamidino-2-phenylindole dihydrochloride.

5.2 Morphological Analysis

In this study, we investigated the impact of CHI3L1 on hiPSC-derived neuronal morphology. Neurons from hiPSCs of MS patients were treated with human recombinant CHI3L1 or vehicle (PBS) for 24 and 72 hours. We assessed the morphological alterations by analyzing MAP2+ neurons using confocal microscopy. Total dendrite length, neuronal area, and the number of branch ends were measured to evaluate dendritic complexity. A dose-response experiment revealed no significant differences between 300 and 600 ng/ml of CHI3L1 (data not shown), so we chose the lower dose for further experiments.

At 72 hours, CHI3L1 significantly reduced dendrite length (↓16.5 %, $p=0.0155$) and dendritic arborization (↓19.4 %, $p<0.001$), and reduced neuronal area at the trend level (↓13.9%, $p=0.0735$) (**Figures 22A-C**). At 24 hours, CHI3L1 treatment led to a significant decrease in dendritic arborization (↓17.5 %, $p<0.001$; **Figure 22C**).

The outcomes of this analysis suggest that CHI3L1 exhibits a discernible neurotoxic influence on hiPSC-derived neuronal cultures. This is manifested by a noteworthy reduction in both dendrite length and complexity, implying an impact on the structural integrity of neurons.

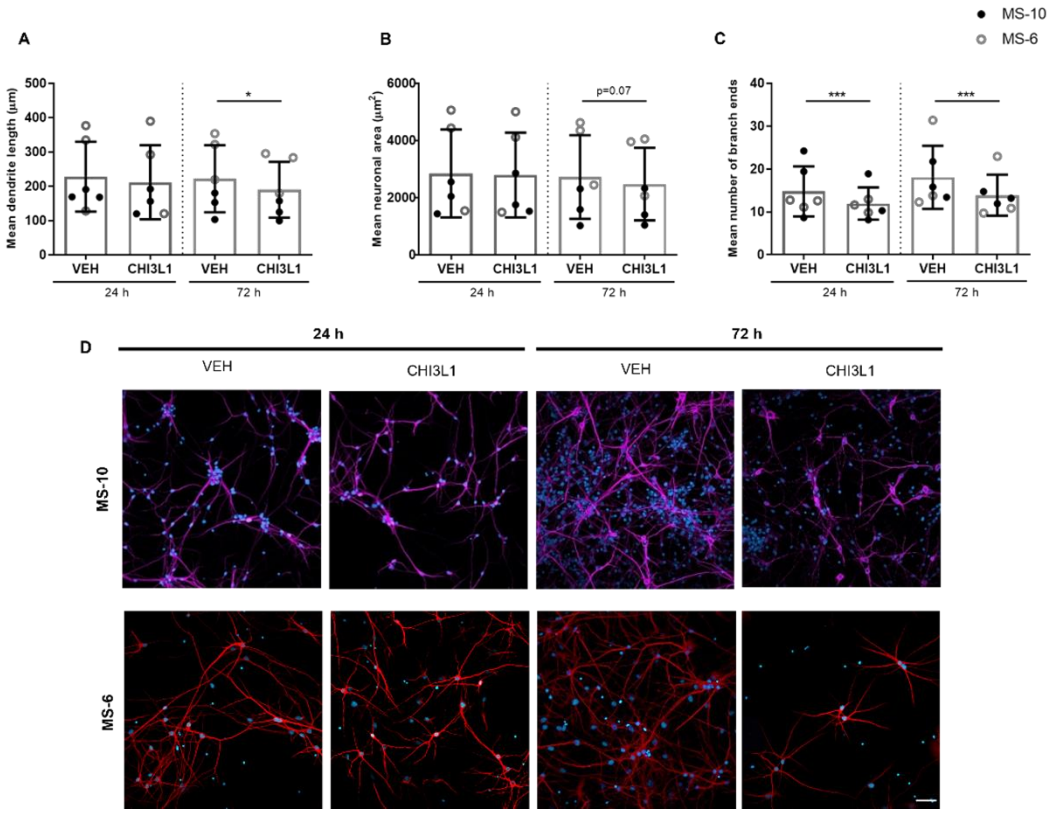

Figure 22. CHI3L1-induced morphological alterations in hiPSC-derived neuronal cultures. Neuronal cultures from MS-10 and MS-6 hiPSC lines were treated with CHI3L1 (300 ng/ml) or vehicle for 24 and 72 hours. Immunofluorescence images of MAP2 (magenta or red) and DAPI (blue) were acquired using confocal microscopy. Representative images are shown in panel (**D)**. Mean values for dendrite length, neuronal area, and the number of branch ends were obtained from each image. Statistical analysis was carried out on mean image values (155-191 images per condition) from both cell lines. Graphs display Dendrite length (**A**), Neuronal area (**B**), and Number of branch ends (**C**). Graph bars represent mean ± SD. Black and grey dots indicate the mean of independent experiments (n=6) performed with MS-10 (n=3) and MS-6 (n=3) lines, respectively. Scale bar = 50 µm.

*p<0.05; ***p<0.001 (*one-way ANOVA* with *Sidak's post hoc*).

Abbreviations: hiPSC – human induced Pluripotent Stem Cells; CHI3L1 – chitinase 3 like 1; MAP2 – Microtubule Associated Protein 2; DAPI - 4',6-diaminido-2-phenylindole

5.3 Synaptic Plasticity Study

We next investigated if synaptic alterations accompanied morphological abnormalities in hiPSC-derived neuronal cultures from MS patients. Neurons were treated with CHI3L1 (300 ng/ml) or vehicle (PBS), and presynaptic (synapsin) and postsynaptic (PSD-95) markers were assessed within MAP2+ dendrites. Co-localization of these markers indicated active synapses.

CHI3L1-induced synaptic alterations were observed only at 72 hours. At this time point, CHI3L1 led to significant reductions in synapsin area (↓23.3 %, p=0.0033) (**Figure 23B**) and active synapses (↓47.9 %, p<0.001) (**Figure 23C**). Additionally, there was a trend towards lower PSD-95 levels at 72 hours (↓8.6%, p=0.0517) (**Figure 23A**). Interestingly, no significant changes were observed at 24 hours, although a trend for increased PSD-95 was observed.

These findings imply that the neurotoxic effects induced by CHI3L1 may play a direct role in influencing early neurodegenerative events within hiPSC-derived neuronal cultures. Specifically, the significant reductions in synapsin area and active synapses at 72 hours point to a potential disruption in synaptic integrity, highlighting a critical time window for CHI3L1-induced alterations. Notably, the observed trend towards lower PSD-95 levels further suggests an impact on postsynaptic elements.

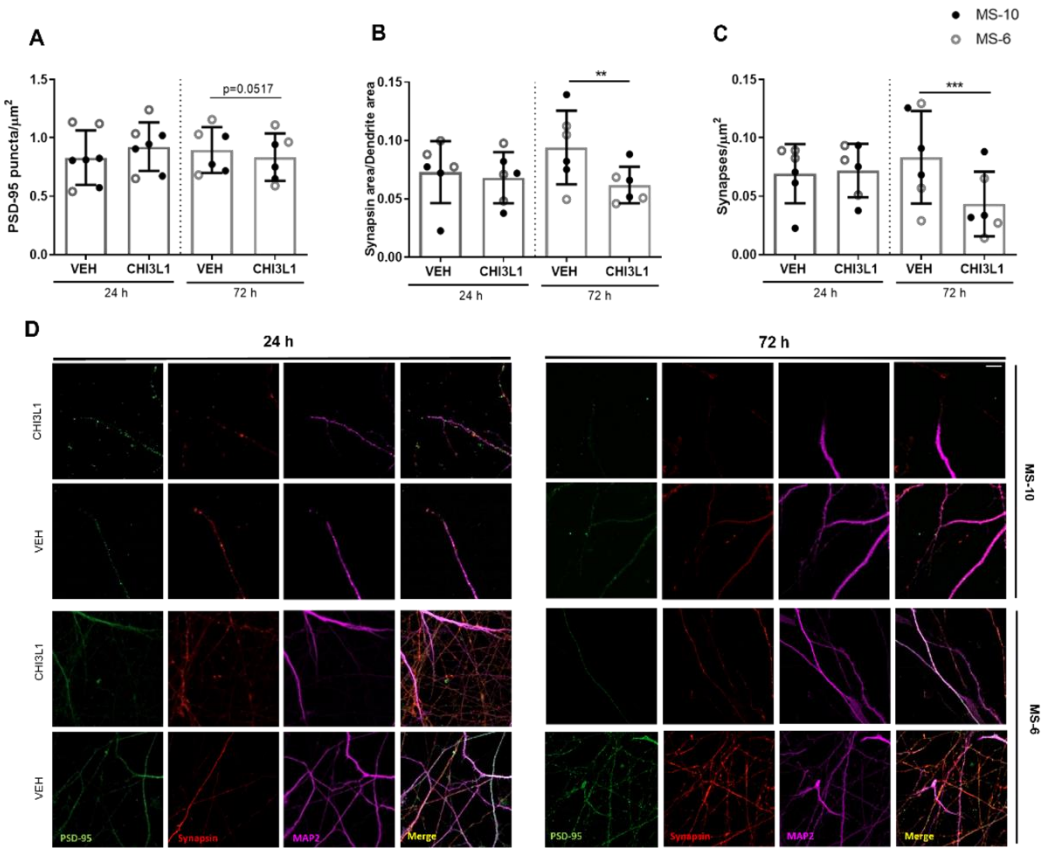

Figure 23. CHI3L1-induced synaptic plasticity alterations in hiPSC-derived neurons. Neurons from hiPSC lines MS-10 and MS-6 were treated with CHI3L1 (300 ng/ml) or vehicle (PBS) for 24 and 72 hours. Immunostaining was performed for MAP2 (magenta), the pre-synaptic marker synapsin (red), and the post-synaptic marker PSD-95 (green). Co-localization of synapsin and PSD-95 indicated active synapses. Automated quantitative analysis was performed using an ImageJ macro on images from both cell lines (164-202 images per condition). Representative images are shown in (**D**). Data acquisition and analysis were blinded to the researcher. Graphs depict PSD-95 puncta density (**A**), Synapsin area/Dendrite area (**B**), and Synapse density (**C**). Black and grey dots represent the mean of independent experiments (n=6) performed with MS-10 (n=3) and MS-6 (n=3) lines, respectively. Data are presented as mean ± SD. Scale bar: 10 µm.

**p<0.01; ***p<0.001. (*one-way ANOVA* with *Sidak's post hoc*)

Abbreviations: hiPSC – human induced Pluripotent Stem Cells; CHI3L1 – chitinase 3 like 1; MAP2 – Microtubule Associated Protein 2; PSD-95 – post synaptic density protein 95.

5.3 Neuronal Activity and Network Dynamics Study

In order to assess the impact of CHI3L1 (300 ng/ml) on neuronal activity and the dynamics of neuronal networks, we performed calcium activity recordings on D40 neurons derived from hiPSCs sourced from individuals with MS. We examined the recordings at specific time points, namely 4, 24, and 72 hours. Subsequently, we employed sophisticated computational techniques to analyze the gathered data.

5.3.1 Neuronal Activity Study

The examination of neuronal activity (**Figure 24B**) indicated that there were no discernible differences between the conditions treated with the vehicle and those treated with CHI3L1 at any of the observed time points. Similarly, the percentage of active neurons (**Figure 24D**) showed no significant variation between the two conditions.

However, the analysis of collective events, specifically the GNA sizes (proportion of the network participating in collective bursts), yielded intriguing findings. In the CHI3L1-treated condition, there was an initial increase in GNA sizes observed at 4 hours, which was followed by a progressive decline at 24 and 72 hours (**Figure 24A**). Conversely, no significant differences were observed in the interval of time between bursts (inter-burst interval, IBI) as depicted in **Figure 24C**.

The investigation of fluorescence amplitude (**Figure 25A**) revealed a notable increase in the CHI3L1-treated condition across all time points, with statistical significance achieved specifically at the 4-hour time point (**Figure 25B**). Since fluorescence amplitude is proportional to the number of elicited action potentials, these results indicate that CHI3L1-treated neurons show an increased excitability that favours an increase in activity. However, such an increase of individual activity does not alter the collective behaviour of the network, for instance, through a higher presence of collective events. In fact, after an initial increase of the GNA sizes at 4 hours, we observed a progressive decrease of collective events at 24 and 72 hours, indicating that increased individual neuronal excitability does not translate in increased communication among neurons. This separation between individual and

collective behaviour may be an interesting result, suggesting that the network as a whole does not overtly change its intrinsic functionality.

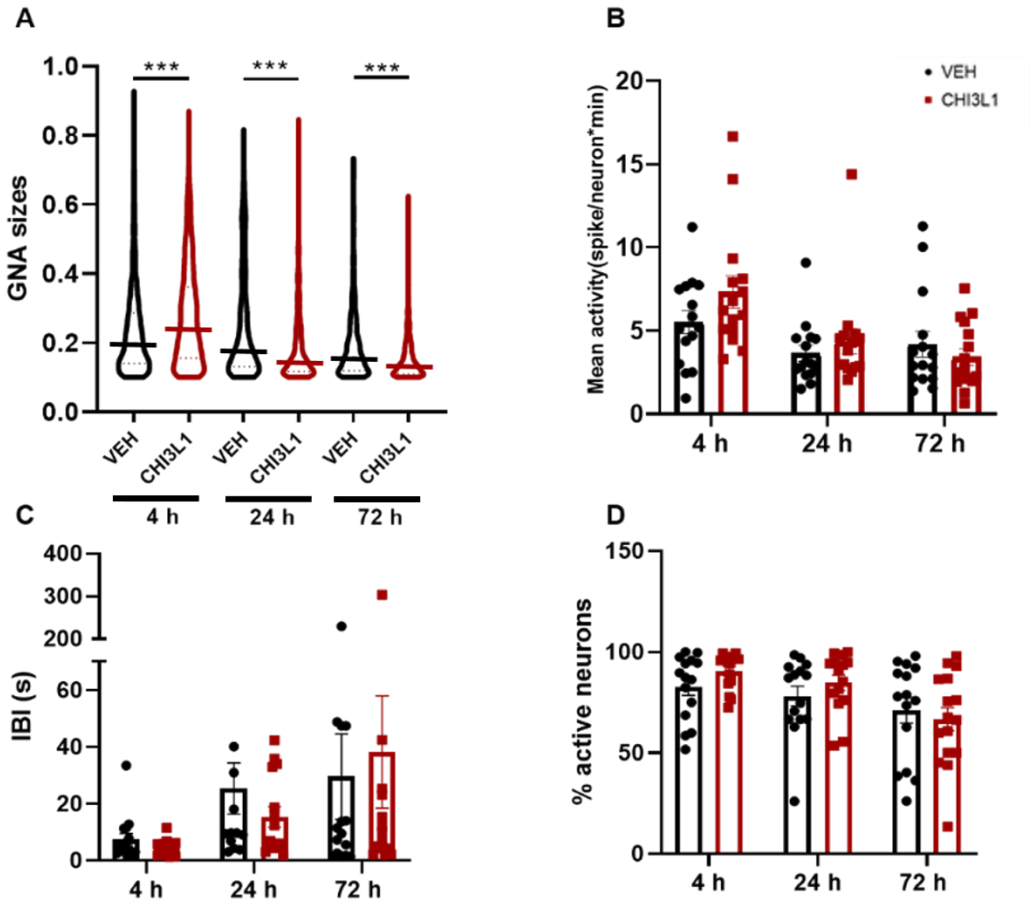

Figure 24. Impact of CHI3L1 on neuronal activity and structural network dynamics in hiPSC-derived neurons from MS patients. Neurons were treated with CHI3L1 (300 ng/ml) or vehicle for 4, 24, and 72 hours. Calcium imaging recordings and advanced computational analysis were used to assess neuronal activity and network dynamics. (**A**) Violin plots display GNA sizes (proportion of the network participating in collective events), with median and quartiles marked by continuous and pointed lines, respectively. (**B**, **C**, and **D)**: Data presented as mean ± SEM for Mean Activity of the culture (**B**), IBI (**C**) and percentage of active neurons (**D).** Six independent experiments were conducted, three with each cell line (MS-10 and MS-6). The dots in (**B)**, (**C)**, and (**D)** represent the mean value of individual replicas from six independent experiments.

***p<0.001. (*one-way ANOVA with Sidak's post hoc*)

Abbreviations: hiPSCs - human induced pluripotent stem cells; CHI3L1 - chitinase 3 like 1; GNA - Global Network Activity; IBI – inter-burst interval

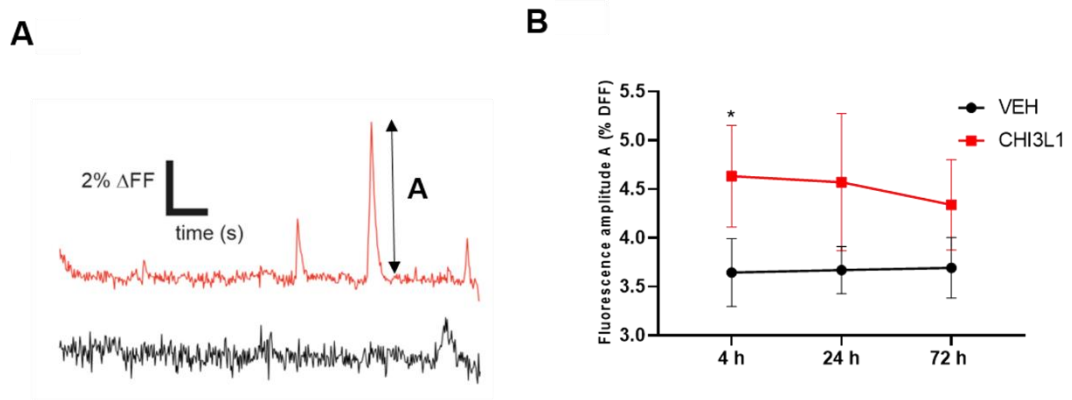

Figure 25. Influence of CHI3L1 on fluorescence amplitude in hiPSC-derived neurons from MS patients. Neurons were treated with CHI3L1 (300 ng/ml) or vehicle for 4, 24, and 72 hours. Calcium imaging recordings and advanced computational analysis were used to assess fluorescence amplitude. (**A**) CHI3L1 increased fluorescence amplitude of neuronal cultures. (**B**) Illustrative example comparing CHI3L1-induced alterations (red) in fluorescence amplitude versus vehicle (black). The data is presented as Mean ± SEM. Six independent experiments were conducted, three with each cell line (MS-10 and MS-6).

*p<0.05; (*one-way ANOVA with Sidak's post hoc*)

Abbreviations: hiPSCs - human induced Pluripotent Stem Cells; CHI3L1 - chitinase 3 like 1; MS – Multiple Sclerosis

5.3.2 Effective Connectivity

To provide further insight into the collective behaviour of the neuronal cultures upon CHI3L1 treatment, we carried out a connectivity analysis using transfer entropy, a mathematical tool that conceptually captures the degree of communication between neurons across the network. Since the most important differences between vehicle and treated conditions appeared at 4 hours post treatment and the endpoint of the analysis was 72 hours, we concentrated the analysis at these time points.

Figure 26 and **Figure 27** show the results of the analysis for representative cultures vehicle and CHI3L1 cultures at 4- and 72-hours post treatment, respectively. In both cases, the number of neurons analyzed was reduced to 70 to properly compare (and average out) network metrics across conditions. The top of the figure highlights the effective connectivity matrices, which inform about the neuronal interactions across the network. Each black dot represents strong communication between a neuronal pair. Matrices are ordered to highlight functional communities along the diagonal (colour boxes), i.e., groups of neurons that tend to communicate more strongly among themselves than with the rest of the network. The bottom graphs of the figure show the actual connectivity of the networks, with the neurons placed as in the microscope's images and coloured according to their community.

To properly compare the vehicle condition (**Figure 26A and Figure 27A)** and the CHI3L1 treated one (**Figure 26B and Figure 27B)**, a set of relevant neuron descriptors that reflect the key characteristics of the shown networks are provided at the bottom of the figure. The global efficiency G_E informs about the strength of global communication across the network, i.e. the tendency of neurons to exchange information with all the network and not just with their neighbours. G_E is higher for CHI3L1 culture as compared to the vehicle one at 4h, indicating an increased global communication. This is also reflected with the average connectivity <k>, which increases by 20%. In the same direction, the modularity Q, which reflects the tendency of the neurons to group into communities, is smaller for the CHI3L1 culture as compared to vehicle at the 4-hour time point, indicating that communities in the CHI3L1 condition have lost relevance in favour of a more global system. Indeed, by looking at the network graphs (bottom panels of **Figure 26**) we can see that, for the vehicle, neurons within a community are physically nearby, e.g., the pink- and yellow-coloured neurons at the bottom-left, whereas this physical proximity is less apparent in the CHI3L1 condition. A contrary situation was observed for the 72-hour time point, where CHI3L1-treated neuronal cultures exhibit a higher modularity combined with a lower G_E and <k>, thus reflecting neurons communicating in smaller groups rather that in an integrated manner. The representation of the network graphs (bottom

panels of **Figure 27**) illustrates the overall smaller neuronal communities in the CHI3L1-treated condition at 72 hours.

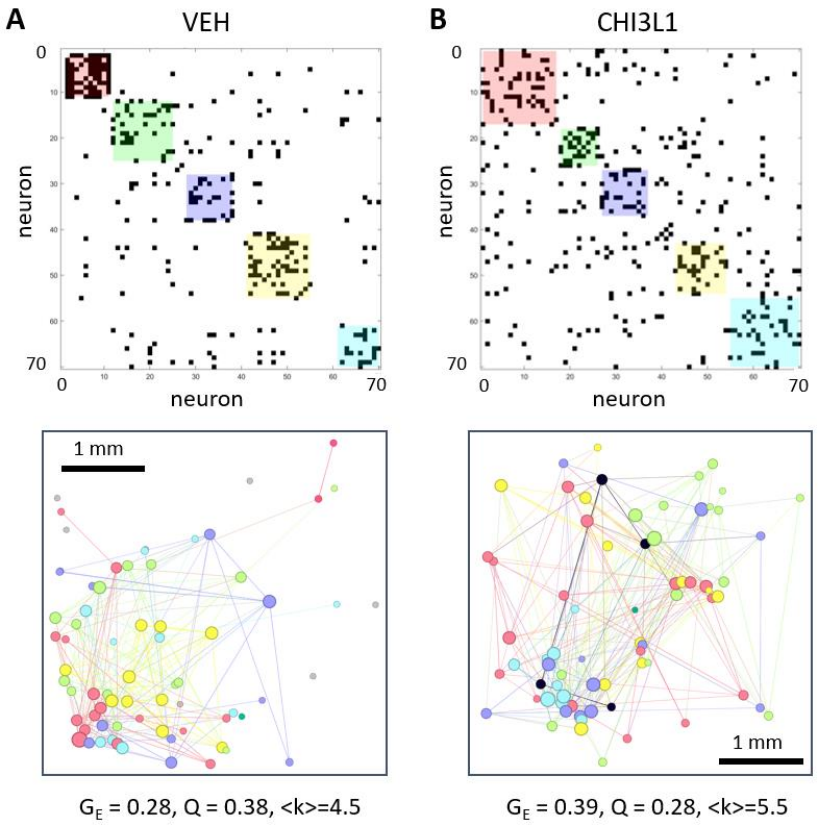

Figure 26. Network analysis. **(A**) Effective connectivity matrix and network map for the vehicle condition 4 hours post-treatment. Black dots indicate the presence of an effective connection (strong communication between neuronal pairs), and colour boxes indicate functional communities. In the below graph, nodes represent neurons, and are placed according to their physical location on the images, and coloured according to the community they belong to. The diameter of the nodes is proportional to their connectivity k. The bottom information summarizes the most important network properties. (**B**) Equivalent analysis for cultures treated with CHI3L1. Overall, the latter network exhibits a stronger connectivity as compared to vehicle, with higher global efficiency GE and average connectivity <K>, and lower Q.

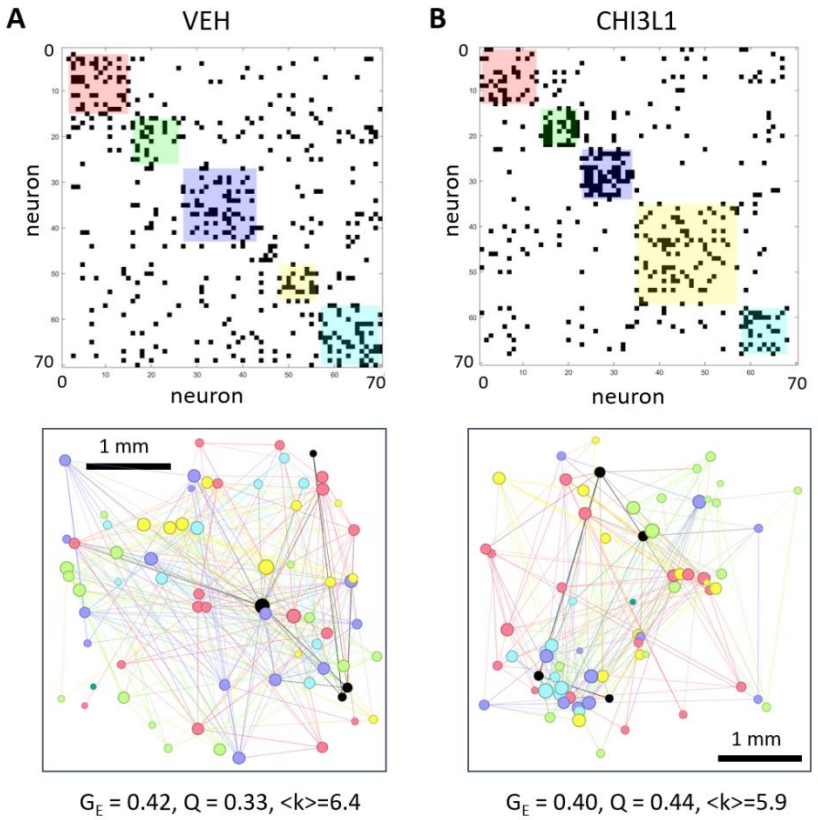

Figure 27. Network analysis. (**A**) Effective connectivity matrix and network map for the vehicle condition 72 hours post-treatment. Black dots indicate the presence of an effective connection (strong communication between neuronal pairs), and colour boxes indicate functional communities. In the graph, nodes represent neurons, and are placed according to their physical location on the images, and coloured according to the community they belong to. The diameter of the nodes is proportional to their connectivity. The bottom information summarizes the most important network properties. (**B**) Equivalent analysis for cultures treated with CHI3L1. Overall, the latter network exhibits a weaker connectivity as compared to the vehicle, with decreased average connectivity <K>, and higher modularity (Q).

The comparison of the above network descriptors, extended to all cultures at 4- and 72-hours post-treatment, is provided in **Figure 28**. The global efficiency increased by 30% on average upon 4 hours of CHI3L1 treatment (**Figure 28A**) but stabilized at 72 hours (**Figure 28D**), with similar values for CHI3L1 and vehicle treated conditions, probably indicating a compensatory mechanism of the network. Although the differences between vehicle and CHI3L1 are not significant, the increase indicates that a tendency toward a more excited network at 4 hours is consistent across

cultures. The modularity (**Figure 28B**) was not substantially altered at 4 hours, but a trend of increase was observed at 72 hours (**Figure 28E**), indicating that neurons may be communicating in smaller groups. Finally, we note that the average connectivity of the networks, <k>, is slightly larger for the CHI3L1 case at 4 hours (**Figure 28C**), again reflecting a tendency towards a more integrated system, and similar for both conditions at 72 hours (**Figure 28F**), suggesting a network compensatory mechanism.

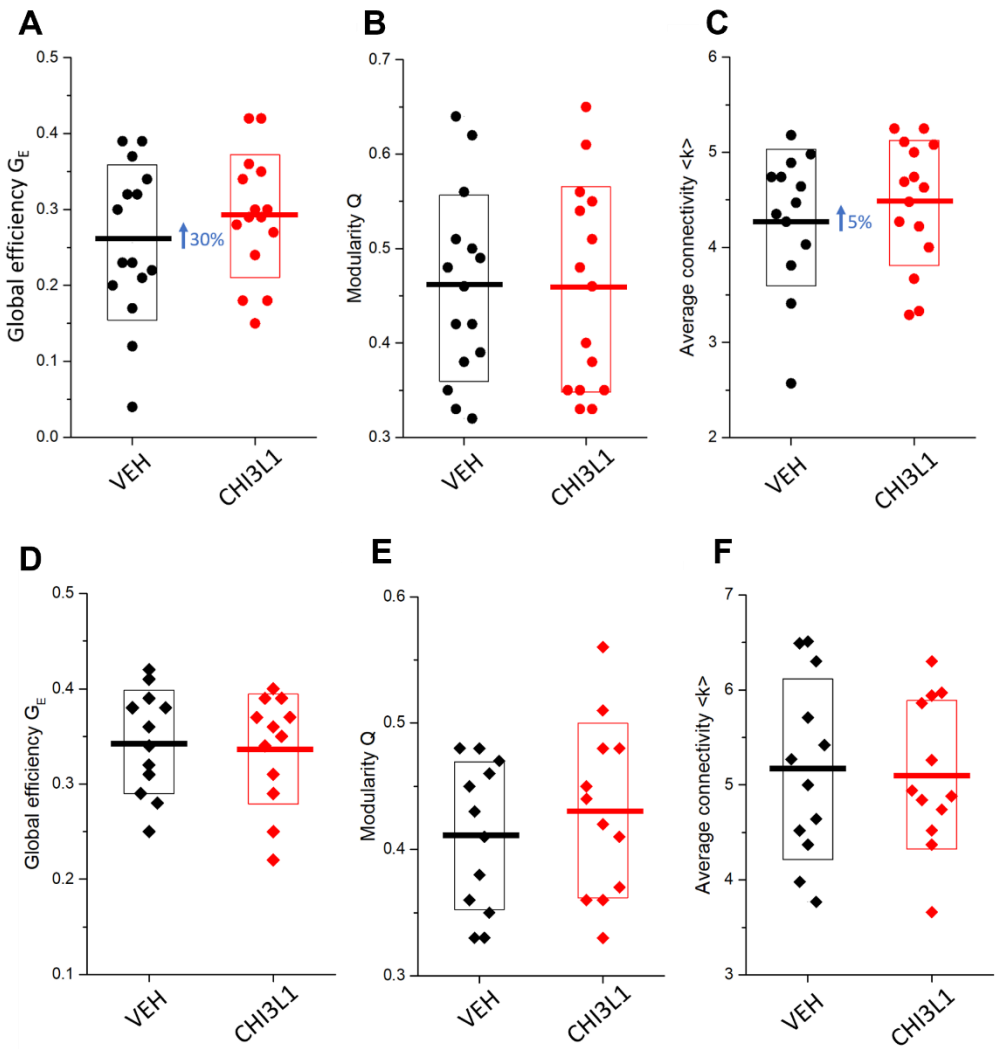

Figure 28. Comparison of different network metrics before and after CHI3L1 treatment for all studied cultures at 4 and 72 hours. (**A** and **B)** panels illustrate Global efficiency, which informs about global network communication, increased 4 hours after treatment (**A**), but stabilized at 72 hours (**D**). (**B** and **E)** depict the Modularity, which informs about the tendency to form neuronal communities, was unaltered on average at 4 hours (**B**), and slightly increased at 72 hours (**E**). (**C** and **F)** show the average connectivity, which informs about the mean number of connected neighbours for a given neuron, slightly increased by 5% (**C**), but stabilized at 72 hours (**F**). Data are presented as Mean (thick horizontal lines) ± SD (*Two-tailed paired t test*)

5.4 Transcriptomic Profiling of CHI3L1 Effects on hiPSCs-derived Neurons

5.4.1 Microarray Experiment

Following the morphological and functional characterization of CHI3L1 effects on hiPSC-derived neuronal cultures from individuals with MS, we aimed to understand the underlying mechanisms of this damage. To achieve this, we conducted a microarray experiment to (I) identify DEGs, and (II) identify enriched pathways that could potentially mediate the effects of CHI3L1. For this purpose, we treated D28 MS-10 derived neuronal cultures with CHI3L1 (300 ng/ml) or vehicle and assessed gene expression at 12 and 24 hours.

Principal Variance Component Analysis (PVCA) identified the major sources of variance, as depicted in **Figure 29**, along with a considerable portion that remained unexplained represented in the residual bar.

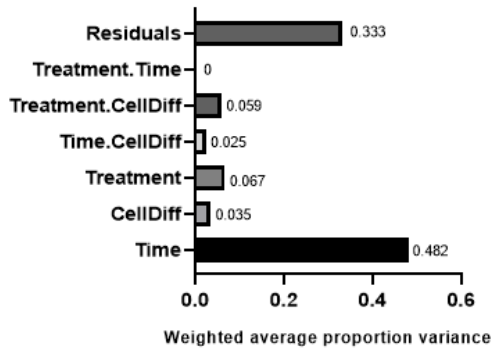

Figure 29. **PVCA Analysis of the microarray experiment performed in this study**.

Abbreviations: PVCA – Principal Variance Component Analysis, CellDiff – Cell Differentiation

Since hiPSC-derived neurons emulate embryonic development, it is expected that a multitude of transcriptional alterations will occur throughout the ongoing maturation process of these neurons. A Heatmap for multiple comparison Effect of Time (**Figure 29**) was performed with genes with an adjusted p-value<0.01 and an absolute log

fold change (FC) >0.5, obtaining a total of 708 genes. Three different clusters were observed, one for each time point.

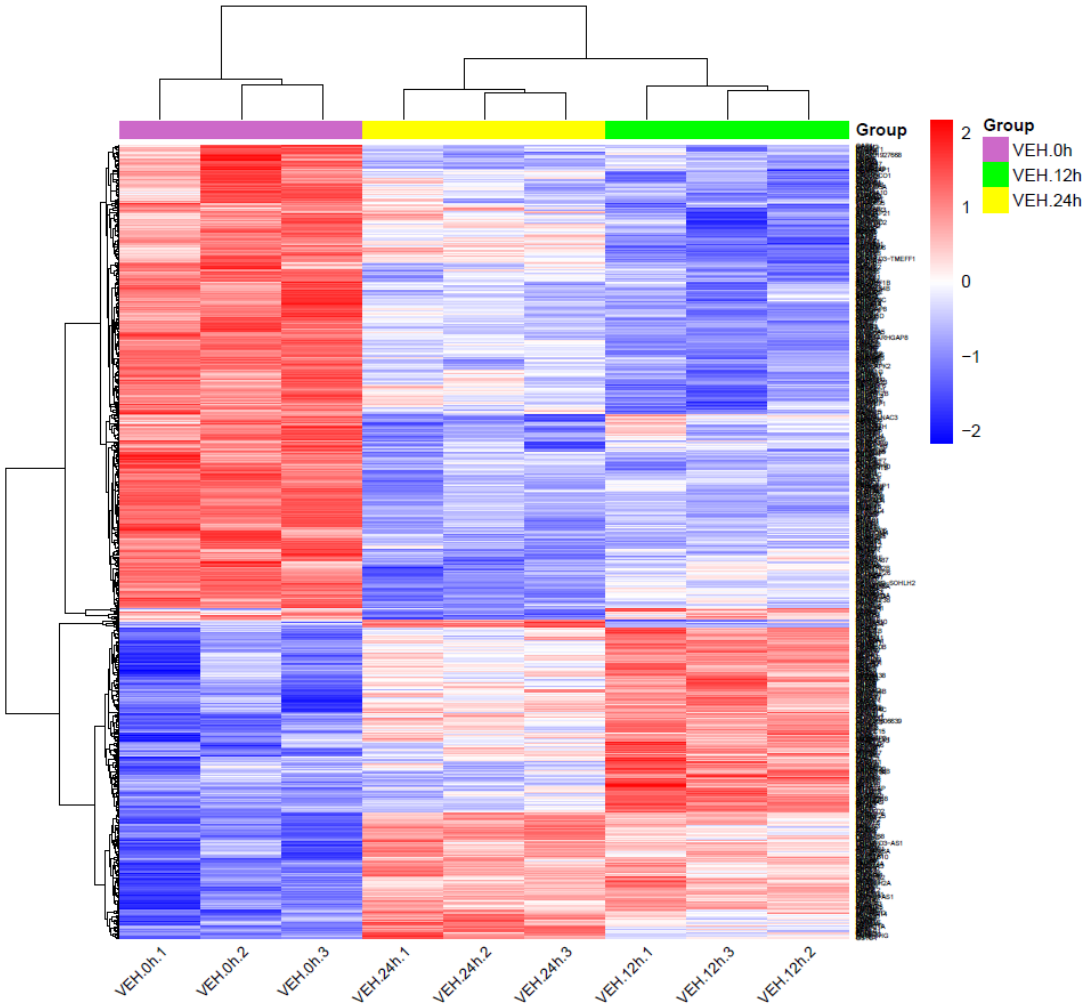

Figure 30. Heatmap illustrating the results of a multiple comparison analysis focusing on the impact of time. Genes meeting the criteria of an adjusted p-value below 0.01 and an absolute log fold change exceeding 0.5 were selected, resulting in a total of 708 genes for inclusion. Three different clusters, one for each time point, were observed.

Selection of the DEGs

During the analysis of DEGs between CHI3L1 and vehicle-treated conditions, none of the DEGs passed the multiple testing corrections. As a result, we focused on genes with an unadjusted p-value<0.01. For the 12 hours' time point, 57 DEGs were selected, and up-regulated and down-regulated genes are summarized in **Table 10** and **Table 11**, respectively. For the 24 hours' time point, 160 DEGs were selected, and up-regulated and down-regulated DEGs are summarized in **Table 12** and **Table 13**, respectively.

Table 10. Top up-regulated (p<0.01) DEGs expressed in the CHI3L1-treated condition versus vehicle at 12 hours.

Gene Symbol	logFC	P.Value	Gene Description
C6orf58	0.455	0.00098947	Chromosome 6 open reading frame 58
SCYL3	0.560	0.00106104	SCY1 like pseudokinase 3
FANCF	0.459	0.00130365	Fanconi anemia complementation group F
DEPDC4	0.624	0.00131163	DEP domain containing 4
AQP1	0.425	0.00154166	Aquaporin 1
IFNA21	0.473	0.00172223	Interferon alpha 21
ZNF30	0.465	0.00279674	Zinc finger protein 30
MLANA	0.404	0.00330623	Melan-A
KLRG1	0.379	0.00348262	Killer cell lectin like receptor G1
ABCA13	0.466	0.00349639	ATP binding cassette subfamily A member 13
BTBD19	0.352	0.00407773	BTB domain containing 19
CARMIL1	0.347	0.00491009	Capping protein regulator and myosin 1 linker 1
GTF3C4	0.345	0.00508083	GTF3C subunit 4
FAM72C	0.338	0.00523658	Family with sequence similarity 72 member C
RALGPS2	0.363	0.00575197	Ral GEF with PH domain and SH3 binding motif 2
INHBE	0.324	0.00602996	Inhibin subunit beta E
TMPRSS11D	0.451	0.00608827	Transmembrane serine protease 11D
ITPR3	0.336	0.00613852	Inositol 1,4,5-trisphosphate receptor type 3
SLC25A30	0.384	0.00652596	Solute carrier family 25 member 30
AREG	0.336	0.00668863	Amphiregulin
TDRD15	0.306	0.00678009	Tudor domain containing 15
STC1	0.408	0.0070882	Stanniocalcin 1
ZWILCH	0.346	0.00731337	Zwilch, kinetochore associated
CCL24	0.342	0.00747813	C-C motif chemokine ligand 24

PRAMEF20	0.347	0.00829835	PRAME family member 20
RAG1	0.371	0.00850275	Recombination activating 1
RASGEF1C	0.333	0.00892504	RasGEF domain family member 1C
DCDC1	0.372	0.00904696	Doublecortin domain containing 1
AP3B2	0.362	0.00935164	Adaptor related protein complex 3 subunit beta 2
EDA	0.361	0.00971221	Ectodysplasin A

Table 11. Top down-regulated (p<0.01) DEGs expressed in the CHI3L1-treated condition versus vehicle at 12 hours.

Gene Symbol	logFC	P.Value	Description
AKR1E2	-0.607	8.23E-05	Aldo-keto reductase family 1 member E2
LCK	-0.443	0.00069905	Lymphocyte-specific protein tyrosine kinase
PDE6G	-0.432	0.00121493	Phosphodiesterase 6G, cGMP-specific rod, gamma
GNMT	-0.368	0.0019048	Glycine N-methyltransferase
BORCS6	-0.396	0.00242834	BLOC-1-related complex subunit 6
C6orf120	-0.371	0.00375067	Chromosome 6 open reading frame 120
MLKL	-0.343	0.00478061	Mixed lineage kinase domain-like protein
SLC38A5	-0.348	0.00484754	Solute carrier family 38 member 5
SMKR1	-0.341	0.00490455	Small lysine-rich protein 1
LOC100506124	-0.524	0.00532272	Uncharacterized protein encoded by gene
TADA1	-0.386	0.00562334	Transcriptional adaptor 1
MRAP2	-0.340	0.00566641	Melanocortin 2 receptor accessory protein 2
MRM2	-0.375	0.00566922	Mitochondrial rRNA methyltransferase 2
NR2E1	-0.433	0.00569621	Nuclear receptor subfamily 2 group E member 1
LRRC66	-0.353	0.00605167	Leucine-rich repeat-containing protein 66
GORAB	-0.396	0.00609479	Golgin, RAB6-interacting
LOC101928436	-0.425	0.00661349	Uncharacterized protein encoded by gene
GPATCH3	-0.311	0.00733912	G-patch domain-containing protein 3
TMEM88B	-0.402	0.00740542	Transmembrane protein 88B
AHNAK	-0.334	0.00776027	AHNAK nucleoprotein
PDCD7	-0.321	0.00785004	Programmed cell death protein 7
PABPC1L2B	-0.457	0.00878467	Polyadenylate-binding protein 1-like 2B
KCNK3	-0.329	0.00884324	Potassium channel subfamily K member 3
MEGF6	-0.333	0.00892342	Multiple epidermal growth factor-like domains
TADA2B	-0.370	0.00952141	Transcriptional adapter 2-beta

GAGE10	-0.367	0.00955803	G antigen 10
NEU4	-0.342	0.00967027	Neuraminidase 4
SOX4	-0.517	0.00995462	SRY-box transcription factor 4
ASB16	-0.360	0.01008612	Ankyrin repeat and SOCS box protein 16

Table 12. Top up-regulated (p<0.01) DEGs expressed in the CHI3L1-treated condition versus vehicle at 24 hours.

Gene Symbol	logFC	P.Value	Description
TMEM161B	0.587	0.00063593	transmembrane protein 161B
RIOK2	0.589	0.00065597	RIO kinase 2
CYLC1	0.631	0.00066315	cylicin 1
DENND2C	0.396	0.00073245	DENN domain containing 2C
CD86	0.429	0.00080773	CD86 molecule
CFAP61	0.729	0.00080835	cilia and flagella associated protein 61
TPTE2	0.519	0.00082156	transmembrane phosphoinositide 3-phosphatase and tensin homolog 2
GRID2	0.487	0.00102925	glutamate ionotropic receptor delta type subunit 2
RASA2	0.502	0.00107523	RAS p21 protein activator 2
OR2D2	0.418	0.00114775	olfactory receptor family 2 subfamily D member 2
HMSD	0.569	0.00127015	histocompatibility minor serpin domain containing
DCDC1	0.480	0.00137422	doublecortin domain containing 1
CD180	0.550	0.00138154	CD180 molecule
CRNDE	0.586	0.00145375	colorectal neoplasia differentially expressed
LRRC66	0.426	0.00146262	leucine rich repeat containing 66
KERA	0.578	0.00147263	Keratocan
ERAP2	0.490	0.00173984	endoplasmic reticulum aminopeptidase 2
VPS54	0.455	0.00203903	VPS54 subunit of GARP complex
UBLCP1	0.427	0.00228041	ubiquitin like domain containing CTD phosphatase 1
SLC9A4	0.406	0.00237543	solute carrier family 9 member A4
ELF1	0.440	0.0025381	E74 like ETS transcription factor 1
SLC13A1	0.461	0.00268302	solute carrier family 13 member 1
PXMP4	0.438	0.00276701	peroxisomal membrane protein 4
MFAP5	0.405	0.00283931	microfibril associated protein 5
PROS1	0.350	0.00285853	protein S

UHMK1	0.416	0.00286597	U2AF homology motif kinase 1
OR8H3	0.400	0.00289189	olfactory receptor family 8 subfamily H member 3
ZNF705G	0.660	0.002894	zinc finger protein 705G
CDH12	0.460	0.00309203	cadherin 12
CALB1	0.452	0.00324353	calbindin 1
TSHB	0.485	0.00338013	thyroid stimulating hormone subunit beta
CHRNA3	0.436	0.00355419	cholinergic receptor nicotinic alpha 3 subunit
CCDC87	0.374	0.00373671	coiled-coil domain containing 87
ATG4A	0.357	0.00388319	autophagy related 4A cysteine peptidase
SLCO1A2	0.541	0.00405189	solute carrier organic anion transporter family member 1A2
GKN1	0.366	0.00407796	gastrokine 1
FBXO5	0.525	0.00453722	F-box protein 5
SKAP2	0.355	0.00459536	src kinase associated phosphoprotein 2
USP17L10	0.313	0.00469516	ubiquitin specific peptidase 17 like family member 10
OR52H1	0.374	0.00477432	olfactory receptor family 52 subfamily H member 1
CHRFAM7A	0.564	0.00503393	CHRNA7 (exons 5-10) and FAM7A (exons A-E) fusion
RHOQ-AS1	0.391	0.00514538	RHOQ antisense RNA 1
TRIM49B	0.460	0.00521803	tripartite motif containing 49B
SFR1	0.441	0.00523994	SWI5 dependent homologous recombination repair protein 1
ZNF404	0.493	0.00529496	zinc finger protein 404
CSN1S1	0.433	0.00533453	casein alpha s1
CPNE4	0.386	0.00540167	copine 4
OR4L1	0.358	0.00553428	olfactory receptor family 4 subfamily L member 1
OR2L13	0.515	0.00579002	olfactory receptor family 2 subfamily L member 13
TMEM35A	0.346	0.00595182	transmembrane protein 35A
ASIC5	0.317	0.00598704	acid sensing ion channel subunit family member 5
GNPNAT1	0.495	0.00602116	glucosamine-phosphate N-acetyltransferase 1
SLC25A46	0.375	0.00624604	solute carrier family 25 member 46
FKTN	0.494	0.00626924	Fukutin
SNX16	0.469	0.0063237	sorting nexin 16
ANO3	0.444	0.00649407	anoctamin 3
CGRRF1	0.479	0.00650804	cell growth regulator with ring finger domain 1
KCND2	0.310	0.00653888	potassium voltage-gated channel subfamily D member 2
TNFAIP6	0.404	0.00661553	TNF alpha induced protein 6
DEFB126	0.439	0.00668255	defensin beta 126
GPR15	0.393	0.00684794	G protein-coupled receptor 15

CHST15	0.334	0.00694344	carbohydrate sulfotransferase 15
OR5F1	0.342	0.00696616	olfactory receptor family 5 subfamily F member 1
CDH13	0.447	0.00722612	cadherin 13
EPB41L5	0.435	0.0073211	erythrocyte membrane protein band 4.1 like 5
CC2D2B	0.383	0.00740025	coiled-coil and C2 domain containing 2B
TEX10	0.422	0.00742631	testis expressed 10
EFCAB1	0.396	0.00768503	Calaxin
KLRB1	0.346	0.00793269	killer cell lectin like receptor B1
SV2C	0.490	0.00797303	synaptic vesicle glycoprotein 2C
TTC5	0.321	0.00809866	tetratricopeptide repeat domain 5
MTMR2	0.537	0.00822868	myotubularin related protein 2
TOR1AIP1	0.339	0.00834325	torsin 1A interacting protein 1
TEC	0.390	0.00846082	tec protein tyrosine kinase
SYT10	0.336	0.00847168	synaptotagmin 10
DUSP19	0.390	0.00857348	dual specificity phosphatase 19
ACOT12	0.539	0.00878722	acyl-CoA thioesterase 12
LINC00266-1	0.344	0.00891099	septin 14 pseudogene 20
OVGP1	0.364	0.00900888	oviductal glycoprotein 1
DCHS2	0.345	0.00911545	dachsous cadherin-related 2
GNPAT	0.394	0.00913637	glyceronephosphate O-acyltransferase
DHX35	0.421	0.009436	DEAH-box helicase 35
C4orf33	0.381	0.00965493	chromosome 4 open reading frame 33
CCDC174	0.304	0.00967993	coiled-coil domain containing 174
PAQR5	0.359	0.00982047	progestin and adipoQ receptor family member 5
SLC10A5	0.342	0.00985671	solute carrier family 10 member 5
NEK10	0.457	0.00986081	NIMA related kinase 10
ZDHHC5	0.370	0.00994998	zinc finger DHHC-type palmitoyltransferase 5

Table 13. Top down-regulated (p<0.01) DEGs expressed in the CHI3L1-treated condition versus vehicle at 24 hours.

Gene Symbol	logFC	P.Value	Description
CGN	-0.487	0.00027254	Cingulin
CFAP157	-0.547	0.00042771	cilia and flagella associated protein 157
TSNAX-DISC1	-0.473	0.00089222	TSNAX-DISC1 readthrough (NMD candidate)
LRRN4	-0.431	0.00092543	leucine rich repeat neuronal 4
ZNF326	-0.560	0.00125904	zinc finger protein 326
RNF126	-0.397	0.00150772	ring finger protein 126
SLC5A6	-0.400	0.00164508	solute carrier family 5 member 6
ABT1	-0.423	0.00177957	activator of basal transcription 1
IKBKG	-0.467	0.0018137	inhibitor of nuclear factor kappa B kinase regulatory subunit gamma
PRSS35	-0.402	0.00185114	serine protease 35
MELTF	-0.442	0.00186731	melanotransferrin
CST6	-0.413	0.00192631	cystatin E/M
BRAT1	-0.396	0.00216621	BRCA1 associated ATM activator 1
TRIM66	-0.476	0.0024558	tripartite motif containing 66
ATP4B	-0.411	0.00266464	ATPase H+/K+ transporting subunit beta
ASMTL	-0.407	0.00270428	acetylserotonin O-methyltransferase like
A3GALT2	-0.452	0.00281207	alpha 1.3-galactosyltransferase 2
MLYCD	-0.351	0.0028679	malonyl-CoA decarboxylase
FOXP3	-0.377	0.00311743	forkhead box P3
KISS1R	-0.458	0.0031541	KISS1 receptor
COQ8B	-0.374	0.00317763	coenzyme Q8B
CD44	-0.425	0.00369255	CD44 molecule (Indian blood group)
KRT14	-0.339	0.00385346	keratin 14
LMNA	-0.376	0.00392716	lamin A/C
GNMT	-0.335	0.00398309	glycine N-methyltransferase
SLC15A3	-0.389	0.0042843	solute carrier family 15 member 3
IL9R	-0.443	0.00440375	interleukin 9 receptor
SIGIRR	-0.376	0.00451397	single Ig and TIR domain containing
FAM71E2	-0.394	0.00483115	golgi associated RAB2 interactor family member 5B
SEMA3G	-0.348	0.00487679	semaphorin 3G
FAM166C	-0.394	0.00489115	family with sequence similarity 166 member C
PAX2	-0.412	0.00493368	paired box 2
EFNA1	-0.423	0.0050473	ephrin A1
CRYBB1	-0.446	0.0050667	crystallin beta B1
C11orf86	-0.373	0.00538842	chromosome 11 open reading frame 86
CRYBB3	-0.348	0.00547955	crystallin beta B3
ZSCAN31	-0.435	0.00560308	zinc finger and SCAN domain containing 31
LRRC75A	-0.367	0.00570868	leucine rich repeat containing 75A

MPP3	-0.317	0.00584033	MAGUK p55 scaffold protein 3
PAFAH2	-0.389	0.00598552	platelet activating factor acetylhydrolase 2
LDHD	-0.363	0.00614585	lactate dehydrogenase D
GEMIN6	-0.354	0.00655666	gem nuclear organelle associated protein 6
ZNF558	-0.320	0.00699557	zinc finger protein 558
ZBTB12	-0.338	0.00767668	zinc finger and BTB domain containing 12
KLHL33	-0.368	0.00769082	kelch like family member 33
PLP2	-0.443	0.007919	proteolipid protein 2
PREX1	-0.347	0.00791906	phosphatidylinositol-3.4.5-trisphosphate dependent Rac exchange factor 1
TNNI1	-0.372	0.00802321	troponin I1. slow skeletal type
TBR1	-0.339	0.00802408	T-box brain transcription factor 1
AIF1L	-0.395	0.00804562	allograft inflammatory factor 1 like
XCR1	-0.345	0.00809632	X-C motif chemokine receptor 1
ZNF786	-0.351	0.00815496	zinc finger protein 786
GRAPL	-0.468	0.00817596	GRB2 related adaptor protein like
OCEL1	-0.364	0.0082239	occludin/ELL domain containing 1
GCAT	-0.321	0.00862087	glycine C-acetyltransferase
NEIL2	-0.358	0.00873637	nei like DNA glycosylase 2
METTL7B	-0.461	0.00882273	thiol methyltransferase 1B
SLC2A1	-0.332	0.00886065	solute carrier family 2 member 1
GPR142	-0.330	0.0089395	G protein-coupled receptor 142
KANK3	-0.341	0.00901053	KN motif and ankyrin repeat domains 3
MMP9	-0.312	0.00902189	matrix metallopeptidase 9
CABP5	-0.459	0.00902857	calcium binding protein 5
TUBA3E	-0.301	0.00903739	tubulin alpha 3e
NGB	-0.344	0.00909084	Neuroglobin
IGF2	-0.384	0.00909385	insulin like growth factor 2
LINC00602	-0.419	0.00925953	long intergenic non-protein coding RNA 602
SLC16A5	-0.309	0.00929426	solute carrier family 16 member 5
PTX4	-0.368	0.00931392	pentraxin 4
PITX3	-0.357	0.00966985	paired like homeodomain 3
HOXB5	-0.341	0.00977787	homeobox B5
CALML5	-0.350	0.0099303	calmodulin like 5
C16orf90	-0.373	0.0099584	chromosome 16 open reading frame 90

5.4.2 Analysis of the Biological Significance

Metascape Analysis

To further gain insight into the molecular pathways and functional neuronal annotations associated with the CHI3L1 signature, we conducted bioinformatics analyses with the software Metascape.[217] We aimed to identify and characterize potential interaction, regulatory networks and neuronal biological processes modulated by CHI3L1.

The functional enrichment analysis of up-regulated DEGs at 12 hours, which is summarized in **Figure 31A** and Supplemental Table 2 (see Annexes), revealed significant processes, with receptor ligand activity (*GO:0048018*) showing the highest significance, followed by signaling receptor activator activity (GO:0030546) and signaling receptor regulator activity (GO:0030545). These enriched processes suggest a potential interaction of CHI3L1 with its receptor. Remarkably, cytokine and inflammatory related processes such as cytokine activity (GO:0005125), cytokine-cytokine receptor interaction (hsa04060), cytokine receptor binding (GO:0005126), and overview of proinflammatory and profibrotic mediators (WP5095) were over-represented. Moreover, NABA (Novel Angiogenesis Biologically Active Peptides), SECRETED FACTORS (M5883) and NABA MATRISOME ASSOCIATED (M5885) processes were enriched. CHI3L1 is a pleiotropic protein that is known to be involved in a plethora of inflammatory and wound-healing processes. CHI3L1 induction of inflammatory mediators has been described in breast cancer metastasis[218], and it has been described as a proangiogenic factor in glioblastoma, colorectal cancer and invasive ductal breast carcinoma.[219] Furthermore, CHI3L1 has been implicated in pulmonary fibrosis as a profibrogenic factor.[138,140] Response to diverse compounds such as cAMP (GO:0051591), organophosphorus (GO:0046683), glucocorticoid (GO:0051384), purine-containing compound (GO:0014074), corticosteroid (GO:0031960) and steroid hormone (GO:0048545) were enriched processes, sharing common hits such as AQP1, AREG and STC1. Additionally, other enriched processes included regulation of GTPase activity (GO:0043547 and GO:0043087), regulation of cellular component size (GO:0032535) and actin filament-based

process (GO:0032970). GTPases are involved in essential cellular processes such as signal transduction and cytoskeleton rearrangements.[220] Functional enrichment analysis conducted on down-regulated DEGs after 12 hours, as depicted in **Figure 31B** and detailed in Supplementary Table 3 (refer to supplementary materials), has unveiled processes that initially appear disparate: regulation of RNA splicing (GO:0043484), along with involvement in lytic vacuoles (GO:0000323) and lysosomes (GO:0005764).

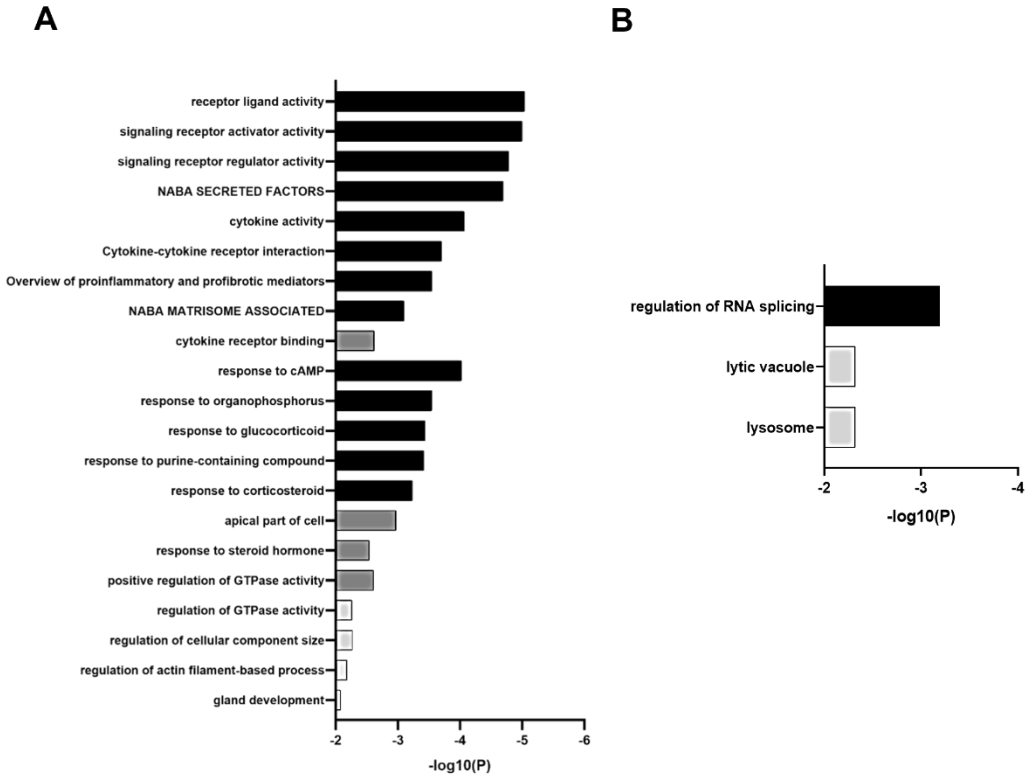

Figure 31. Functional enrichment analysis of 12-hour DEGs. (**A**) Functional enrichment of up-regulated DEGs ($p<0.01$). (**B**) Functional enrichment of down-regulated DEGs ($p<0.01$).

Upon examining the functional enrichment of up-regulated DEGs at 24 hours, which is summarized in **Figure 32** and Supplemental Table 4 (see Annexes), significant

alterations were observed in various processes essential to neuronal function. Notably, the most significant enriched term was chemical synaptic transmission (GO:0007268), suggesting that CHI3L1 may impact the neurotransmitter-based communication between neurons. Anterograde trans-synaptic signalling (GO:0098916) and trans-synaptic signalling (GO:0099537) were as well enriched, indicating potential disruption in neuronal communication pathways. Furthermore, processes related to the regulation of postsynaptic membrane potential (GO:0060078) and synaptic signalling (GO:0099536) exhibited significant enrichment, suggesting alterations in the electrical and chemical transmission. The functional enrichment of the response to calcium ion process (GO:0051592), a tightly regulated process within neurons, may indicate a modulation on intracellular calcium dynamics possibly impacting neuronal dynamics and calcium-dependent signaling pathways. Besides, perturbation in the "sodium ion transport" process (GO:0006814) points to a plausible alteration in neuronal excitability and membrane potential dynamics, key aspects of electric signal generation and propagation.[221] Collectively, these processes indicate that CHI3L1 may impact neuronal communication and signaling. Intriguingly, there were alterations in sensory perception of smell and olfactory pathways (*GO:0007608, GO:0007606, GO:0050911, R-HSA-9752946, R-HSA-381753, hsa04740*). Ectopic expression of odorant receptors has been described in neurodegenerative diseases.[222] Although our neuronal system was forebrain-like, we observed enrichment of cerebellum (GO:0021587) and hindbrain (GO:0021575) morphogenesis. The same genes (GRID2, GNPAT, SLC25A46) were implicated in both processes, suggesting neuronal functions that may extend to forebrain-type neurons. Interestingly, lipid transport (GO:0006869) and localization (GO:0010876) processes emerged as over-represented in the up-regulated DEGs at 24 hours. Dysregulation of lipid transport pathways has been as well associated with neurodegenerative disorders.[223] Lastly, we observed enrichment of genes associated with reproductive processes (GO:2000241) and oogenesis (GO:0048477). The presence of such enrichment might suggest potential crosstalk or shared regulatory elements between neural and reproductive pathways.

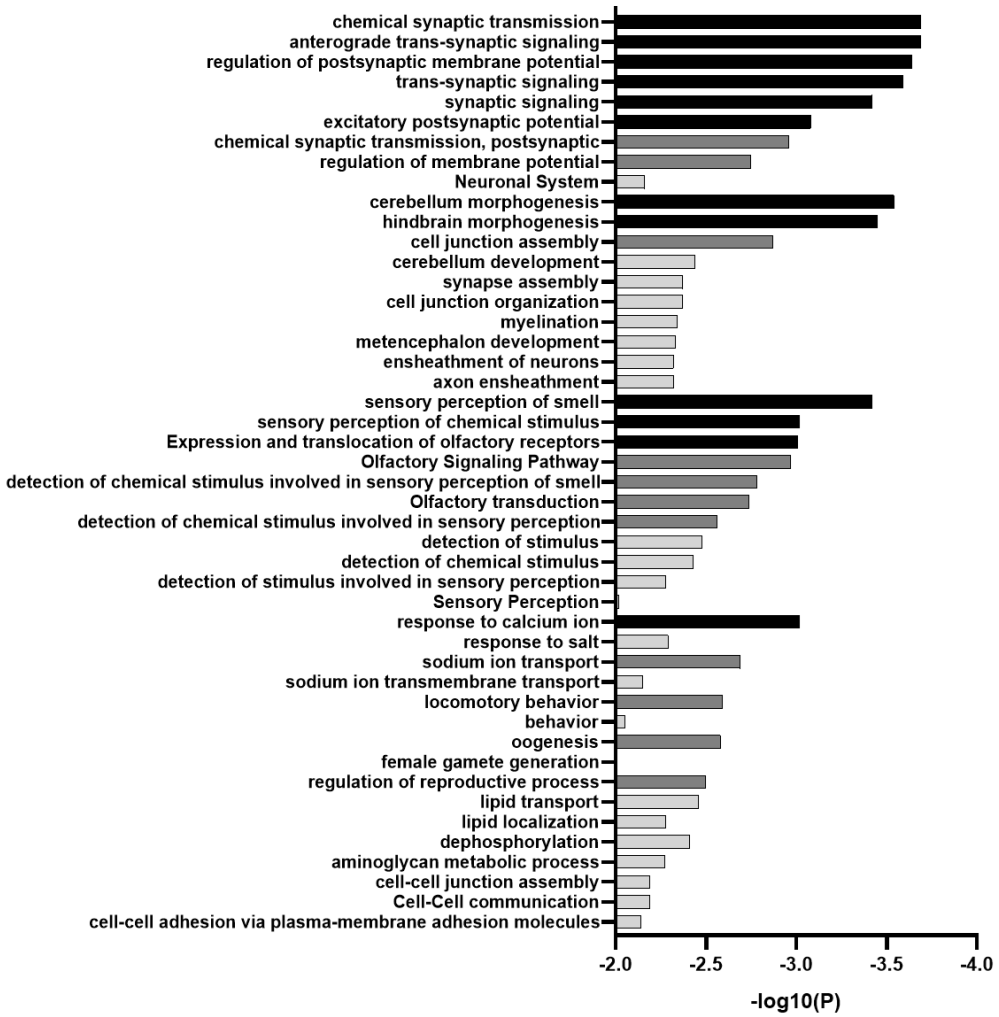

Figure 32. Functional enrichment analysis of 24-hour up-regulated DEGs.

The functional enrichment analysis conducted on down-regulated DEGs at the 24-hour time point, which is summarized in **Figure 33** and Supplemental Table 5 (see Annexes), unveiled a number of significant processes that may contribute to the effects induced by CHI3L1. Notably, one of the most prominently enriched processes was the "negative regulation of cysteine-type endopeptidase activity involved in apoptotic process" (*GO:0043154*). It is worth noting that this enrichment analysis was based on down-regulated DEGs, which might suggest a potential upregulation of the apoptotic process. Interestingly, processes linked to metabolism, such as the

regulation of glucose metabolism (GO:0010906), also exhibited significant enrichment. Besides, processes related with structural components of the cell as the apical plasma membrane (*GO:0016324*) were over-represented. Considering that neurons are highly polarized cells, alterations in these processes can lead to disruptions in neuronal morphology and connectivity.

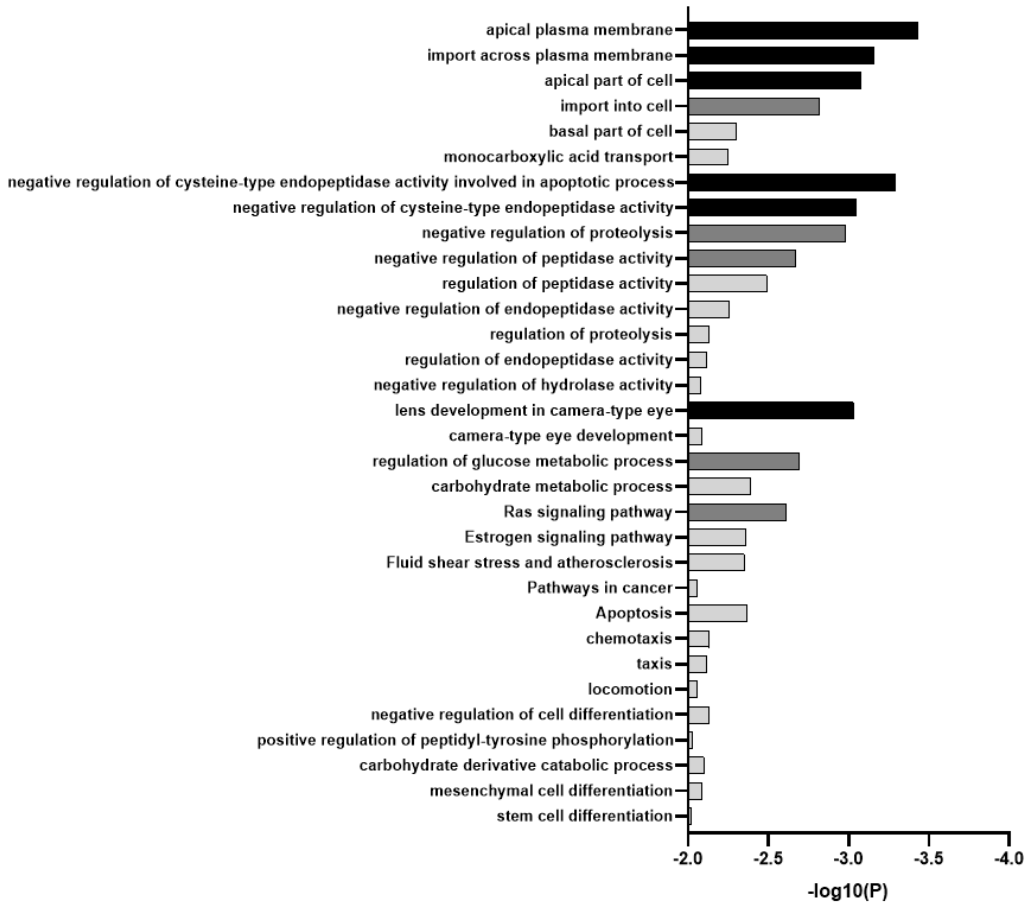

Figure 33. Functional enrichment analysis of down-regulated DEGs at 24 hours.

Gene Set Enrichment Analysis (GSEA)

To gain further insight into the biological significance of the CHI3L1-induced neuronal phenotype, we performed GSEA bioinformatics analysis using the Gene Ontology and Reactome databases.

The GSEA GO Cellular Component (CC) analysis revealed significant molecular alterations at 12 and 24 hours. **Table 14** provides a summary of the top five enriched CC for both time points, including their Normalized Enrichment Score (NES), p-value, and adjusted p-value. The complete tables, including all the significant terms and the core enrichment results for the 12 and 24-hour time points, are available in the Annexes as Supplementary Table 6 and Supplementary Table 7, respectively.

Table 14. Summary of top five GO CC processes at 12 and 24 hours

Timepoint (h)	ID	Description	NES	pvalue	p.adjust
12	GO:0031253	cell projection membrane	1.59679803	2.7904E-05	0.033610249
	GO:0098798	mitochondrial protein-containing complex	-1.65515565	6.3096E-05	0.033610249
	GO:0031526	brush border membrane	1.97805109	7.4359E-05	0.033610249
	GO:0098862	cluster of actin-based cell projections	1.7409846	0.00013648	0.03851084
	GO:0097225	sperm midpiece	2.06704087	0.000142	0.03851084
24	GO:0098982	GABA-ergic synapse	2.40151026	3.8453E-08	3.86889E-05
	GO:0005581	collagen trimer	-2.29703546	5.7063E-08	3.86889E-05
	GO:0097060	synaptic membrane	1.78061265	1.444E-07	6.52695E-05
	GO:0045211	postsynaptic membrane	1.81884976	1.2464E-06	0.000422526
	GO:0098978	glutamatergic synapse	1.72258059	3.1741E-06	0.000860816

At the 12 hours' time point (**Figure 34**), the results revealed affectation of the cell projection membrane (GO:0031253), the brush border membrane (GO:0031526), and the cluster of actin-based cell projections (GO:0098862), suggesting that CHI3L1 treatment alters specialized compartments of the membrane that, in neurons, are usually related to dendritic spines and axonal projections.

Moreover, CHI3L1 had an effect on the mitochondrial protein-containing complex (GO:0098798), indicating an overall decrease in the expression of mitochondrial genes, thereby implying an influence on mitochondrial function.

Interestingly, there was an unusual association of sperm midpiece (GO:0097225) term in the context of hiPSC-derived neurons. This association might hint at the presence of some components with similarities to a sperm midpiece, but it would require further investigation to understand the significance of this term in our context.

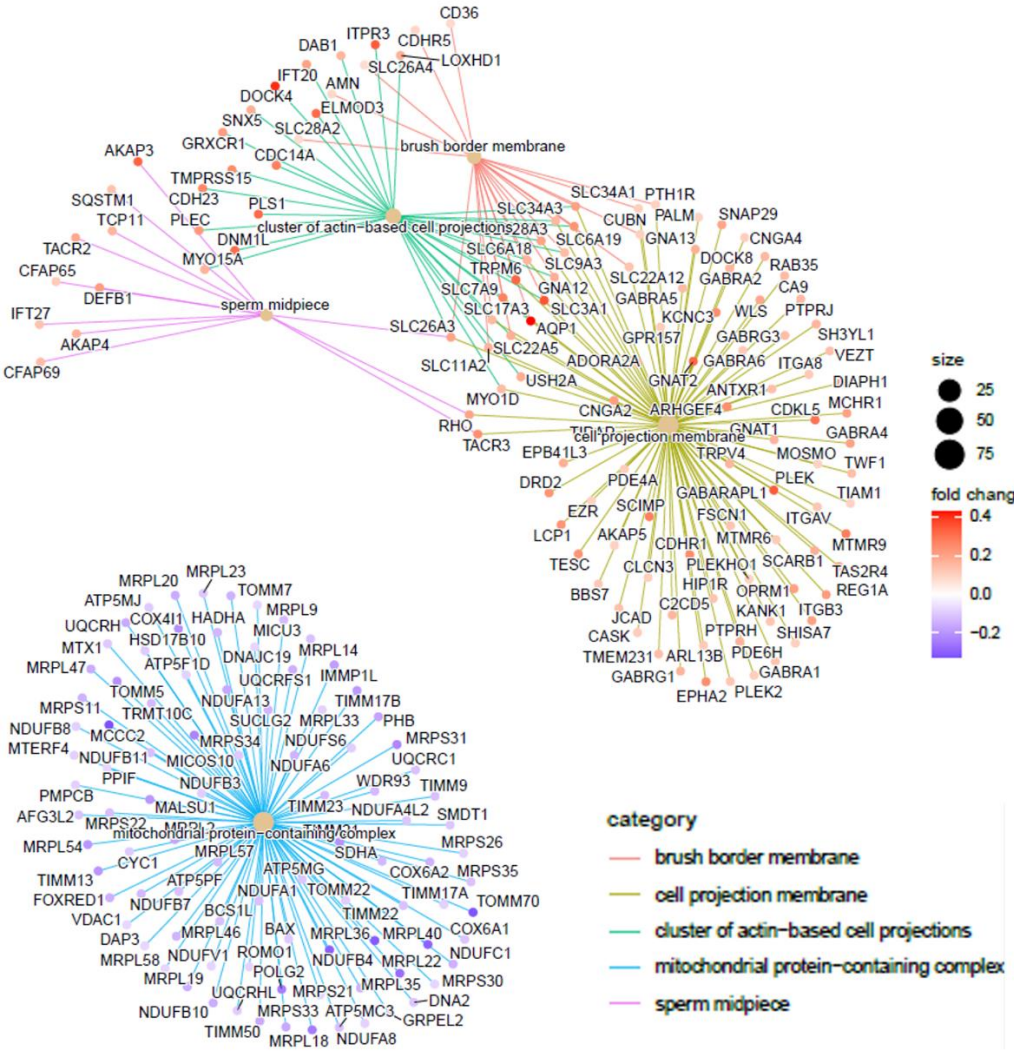

Figure 34. Gene set enrichment analysis (GSEA) uncovers perturbations in membrane and mitochondrial related cellular components at the 12-hour time point. The network plot illustrates the five most enriched pathways in the comparison between VEH and CHI3L1 conditions using the Gene Ontology Cellular Component (GO CC) database.

At the 24-hour time point, the GSEA utilizing the GO Cellular Component database showed the dysregulation of diverse cellular components, particularly those associated with synapses (**Figure 35**). This finding aligns with observed alterations in synaptic plasticity demonstrated in the functional study and is further substantiated by enrichment analysis performed using the Metascape software.

Notably, specific disruptions were identified in GABAergic synapses (GO:0098982) and glutamatergic synapses (GO:0098978), suggesting potential modifications in inhibitory and excitatory synaptic transmission. Concurrently, alterations in the synaptic membrane (GO:0097060) and the postsynaptic membrane (GO:0045211) were observed, indicating potential changes in the structural integrity of synaptic membranes crucial for neurotransmission and synaptic plasticity. These transcriptional changes correspond to the functional studies wherein deviations in synaptic function and collective neuronal activity were noted.

Additionally, there were notable alterations in components related to the collagen trimer (GO:0098978), potentially implicating changes in cell adhesion an extracellular matrix adhesions.

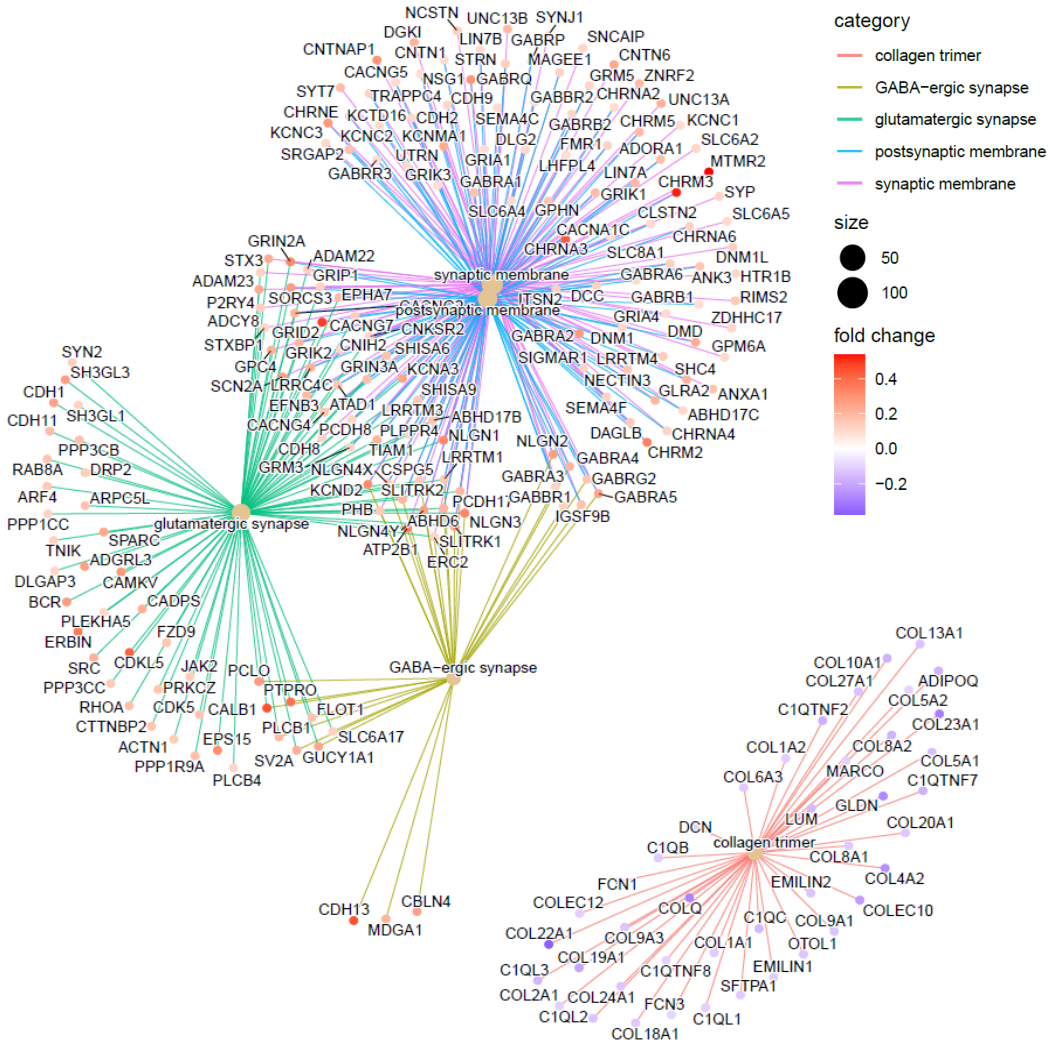

Figure 35. Gene set enrichment analysis (GSEA) uncovers perturbations in synaptic-related processes at the 24-hour time point. The network plot illustrates the five most enriched pathways in the comparison between VEH and CHI3L1 conditions using the Gene Ontology Cellular Component (GO CC) database.

CHI3L1, as a pleiotropic protein that engages with multiple receptors, yielded extensive results in the Reactome pathway analyses. Given the complexity of these outcomes, we conducted a redundancy reduction analysis to gain a clearer insight into the specific pathways and processes modulated by the action of CHI3L1.

The summarization of the Reactome analysis of biological significance at 12 and 24 hours (**Figure 36**) revealed multiple pathways, as well as regulatory and metabolic processes potentially mediating CHI3L1 effects on hiPSC-derived neurons.

Specifically, processes related to RNA translation, encompassed within the peptide chain elongation cluster, were downregulated, suggesting that CHI3L1 may exert influence over the machinery of protein synthesis. Additionally, the analysis identified a downregulation in processes associated with the regulation of RNA stability within the deadenylation dependent mRNA decay cluster. This result may reflect the significance of CHI3L1 in orchestrating modifications in gene expression through the stabilization of mRNA molecules.

Metabolic processes were also found to be altered, revealing an upregulation of pathways related to cholesterol biosynthesis and dysregulation of asparagine glycosylation, thus indicating a potential metabolic shift induced by CHI3L1.

Interestingly, there were alterations in DNA related processes as depicted by the clusters DNA damage/telomere stress induced senescence or aberrant regulation of mitotic G1/S due to RB1 defects. Although neurons are post-mitotic cells that do not entry the cell cycle, aberrant regulation of cell cycle inhibitors as retinoblastoma protein (RB) can lead to DNA damage and genomic instability. Aberrant re-entry of neurons into the cell cycle has been described in neurodegenerative diseases as AD.[224]

Notably, several signaling pathways such as RAF activation, FRS-mediated FGFR4 signaling and RHOD GTPase cycle were upregulated, thus reflecting a dynamic response of neurons to CHI3L1.

Conversely, other pathways such as related to regulated necrosis and the regulation of expression of SLIT and ROBOs were downregulated, suggesting that CHI3L1 might influence the balance between survival and cell death pathways, as well as the regulation of factors involved in axonal guidance.

Furthermore, specific neuronal processes were altered, as evident from the dysregulation of presynaptic depolarization and calcium channel opening. These observations highlight the impact of CHI3L1 on the synaptic level.

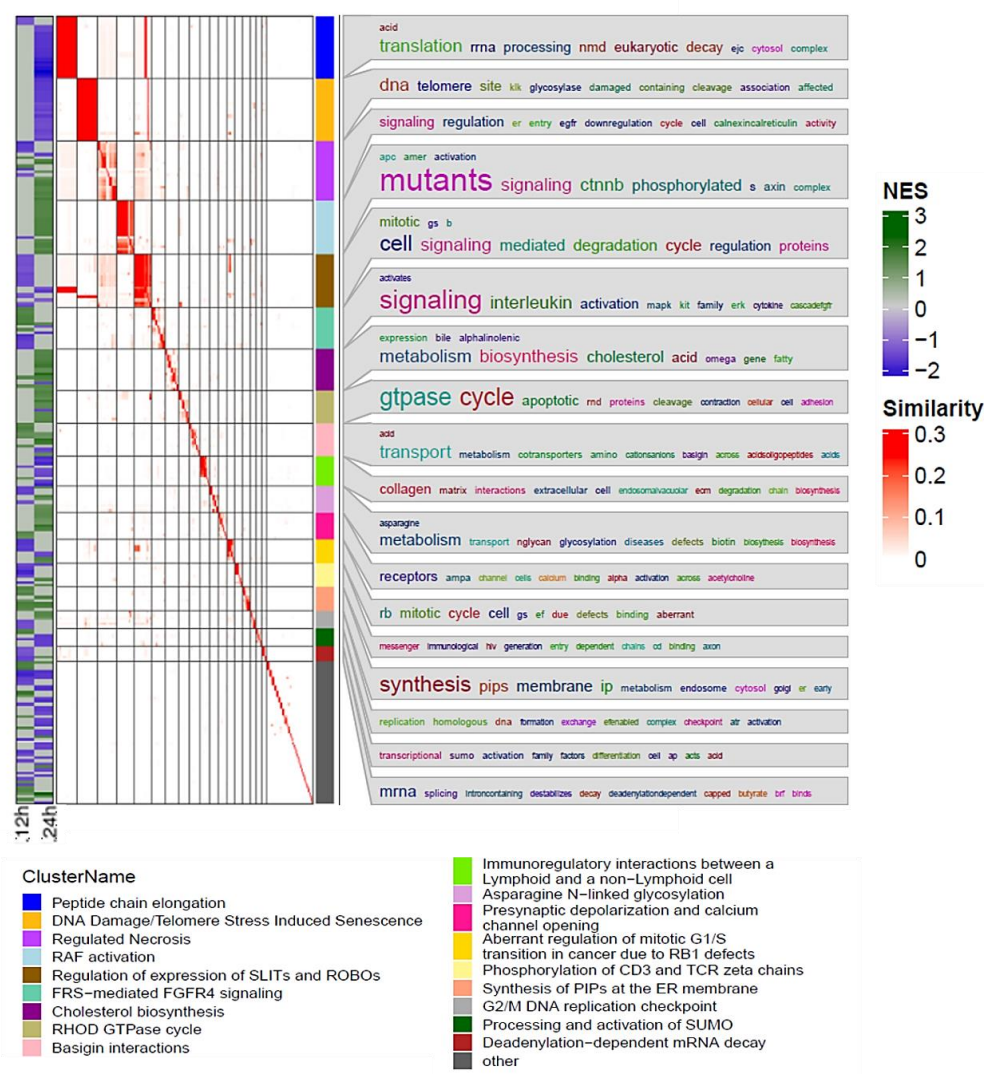

Figure 36. Reactome analysis reveals pathways mediating CHI3L1 effects on hiPSC-Derived neurons. The analysis highlights multiple pathways potentially involved in CHI3L1's impact on hiPSC-derived neurons at 12 and 24 hours. The results are depicted in a heatmap format, with clusters and word annotations providing context. To group similar terms, the analysis employed a Jaccard similarity measure and the fast_greedy clustering method.

5.4.3 Transcriptional Regulators Enrichment

To identify potential transcriptional factors orchestrating the gene expression response to CHI3L1, we included all DEGs ($p<0.01$) at 12 and 24 hours for TRRUST[225] enrichment analysis using Metascape software. Notably, the analysis revealed a prominent transcription factor, Interferon Regulatory Factor 1 (IRF1), which shows significant regulatory potential over gene expression at the 24 hours' time point as depicted in **Figure 37**. No potential regulators were found at the 12 hours' time point.

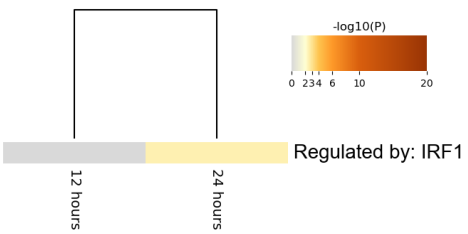

Figure 37. Summary of enrichment analysis in TRRUST.

Abbreviations: IRF1 – Interferon Regulatory Factor 1

To further investigate the involvement of transcription factors at the 24-hour time point, we used the manually curated TRRUST database. We included all DEGs ($p<0.01$), and our transcription factor selection criteria dictated a minimum overlap of three genes and a significance level of $p<0.05$. The TRRUST database recognized only 21/160 DEGs: CALB1, CD44, CD86, CDH13, CHRNA3, ELF1, ERAP2, FOXP3, GNMT, IGF2, KISS1R, KRT14, MELTF, MLYCD, MMP9, PAX2, PROS1, SIGIRR,

SLC2A1, TNFAIP6, and TSHB. The search results, which are summarized in **Table 15**, revealed two transcription factors that met the stipulated criteria: IRF1 and STAT1 (Signal Transducer and Activator of Transcription 1). Remarkably, both transcription factors are implicated in the interferon response pathway.

Table 15. Outcomes of the TRRUST database inquiry for potential transcriptional regulators at the 24 hours' time point.

#	Key TF	Description	# of overlapped genes	P value
1	IKBKB	inhibitor of kappa light polypeptide gene enhancer in B-cells. kinase beta	2	0.00091
2	ASCL1	achaete-scute complex homolog 1 (Drosophila)	2	0.00127
3	HDAC5	histone deacetylase 5	2	0.00168
4	SNAI2	snail homolog 2 (Drosophila)	2	0.0053
5	**IRF1**	**interferon regulatory factor 1**	**3**	**0.00762**
6	SMAD3	SMAD family member 3	2	0.0248
7	**STAT1**	**signal transducer and activator of transcription 1. 91kDa**	**3**	**0.0289**
8	PPARA	peroxisome proliferator-activated receptor alpha	2	0.0379
9	VDR	vitamin D (1.25- dihydroxyvitamin D3) receptor	2	0.0434
10	SIRT1	sirtuin 1	2	0.0552
11	FOS	FBJ murine osteosarcoma viral oncogene homolog	2	0.0746
12	WT1	Wilms tumor 1	2	0.0746
13	HDAC1	histone deacetylase 1	2	0.108
14	AR	androgen receptor	2	0.167
15	RELA	v-rel reticuloendotheliosis viral oncogene homolog A (avian)	4	0.215
16	NFKB1	nuclear factor of kappa light polypeptide gene enhancer in B-cells 1	4	0.218
17	STAT3	signal transducer and activator of transcription 3 (acute-phase response factor)	2	0.309
18	SP1	Sp1 transcription factor	5	0.317

19	JUN	jun proto-oncogene	2	0.329

Entries in regular black font indicate results with a significance level of p<0.05. Entries in bold black font denote results that satisfy the criteria for candidate transcription factors. Entries in grey font indicate results with a significance level of p>0.05. **Abbreviations**: TF - Transcription Factor.

Due to the restricted gene pool within the TRRUST database, we decided to investigate broader databases, such as the Transcription Factor Target Gene Database (REF) which predicts targets for transcription factors. For this purpose, we compared our 24-hour DEGs list to the targets for IRF1 (3285 genes) and STAT1 (2518 genes). The complete target gene lists can be found in the Jaspar repository, namely IRF1_MA0050.1_genes and STAT1_MA0137.2_genes. The comparison of the query gene list to the predicted targets for IRF1 and STAT1 returned 19 hits and 23 hits, respectively, which are summarized in **Table 16.**

Table 16. Comparative analysis of 24-hour DEGs against IRF1 and STAT1 targets

Query gene list	# genes	TF	# predicted targets	# hits	hits
24-hour DEGs	160	IRF1	3285	19	SLC15A3, HOXB5, TBR1, TOR1AIP1, VPS54, CD180, C4orf33, **RASA2**, **RIOK2**, MTMR2, ERAP2, **DENND2C**, CDH12, PAQR5, LMNA, SYT10, **GNMT**, TTC5, ZSCAN31
		STAT1	2518	23	**UHMK1**, TRIM66, LRRN4, ZNF326, MFAP5, FAM166C, PITX3, BRAT1, SNX16, SLC2A1, FAM71E2, VPS54, NEIL2, HMSD, IKBKG, PROS1, TEC, HOXB5, SV2C, CHRNA3, COQ8B, ZSCAN31, C4orf33

Entries in bold font denote successfully validated DEGs by RT-qPCR.

Abbreviations: BRAT1 - BRCA1-associated ATM activator 1, CD180 - CD180 molecule, CDH12 - Cadherin 12, C4orf33 - Chromosome 4 open reading frame 33, CHRNA3 - Cholinergic receptor nicotinic

alpha 3 subunit, COQ8B - Coenzyme Q8B, DENND2C - DENN domain containing 2C, ERAP2 - Endoplasmic reticulum aminopeptidase 2, FAM166C - Family with sequence similarity 166 member C, FAM71E2 - Family with sequence similarity 71 member E2, GNMT - Glycine N-methyltransferase, HMSD - Histocompatibility (minor) serpin domain containing, HOXB5 - Homeobox B5, IKBKG - Inhibitor of nuclear factor kappa B kinase regulatory subunit gamma, LRRN4 - Leucine-rich repeat neuronal 4, LMNA - Lamin A/C, MFAP5 - Microfibril-associated protein 5, MTMR2 - Myotubularin related protein 2, NEIL2 - Nei endonuclease VIII-like 2, PAQR5 - Progestin and adipoQ receptor family member V, PITX3 - Paired-like homeodomain 3, PROS1 - Protein S, RASA2 - RAS p21 protein activator 2, RIOK2 - RIO kinase 2, SLC15A3 - Solute carrier family 15 member 3, SLC2A1 - Solute carrier family 2 member 1, SNX16 - Sorting nexin 16, SV2C - Synaptic vesicle glycoprotein 2C, SYT10 - Synaptotagmin 10, TBR1 - T-box brain transcription factor 1, TEC - Tec protein tyrosine kinase, TOR1AIP1 - Torsin A interacting protein 1, TRIM66 - Tripartite motif containing 66, TTC5 - Tetratricopeptide repeat domain 5, UHMK1 - U2AF homology motif kinase 1, VPS54 - VPS54 subunit of GARP complex, ZNF326 - Zinc finger protein 326, ZSCAN31 - Zinc finger and SCAN domain containing 31, TF – Transcription Factor.

5.4.4 RT-qPCR Validation of Selected DEGs

We next proceeded with the validation of DEGs from the 12-hour and 24-hour time points using RT-qPCR. DEGs were selected based on the fulfilment of the following criteria: (a) statistically significant with a p-value < 0.001 and an absolute logFC > 0.3; (b) statistically significant with a p-value ranging from 0.001 to 0.01 and an absolute logFC > 0.3, accompanied by relevance to neuronal function. Furthermore, a limited number of genes were chosen based solely on their relevance to neuronal function, without adhering to the aforementioned criteria.

At the 12-hour time point, 11 DEGs were selected for RT-qPCR validation (**Figure 37**): 5 were up-regulated (SCYL3, AQP1, ABCA13, RALGPS2, and ITPR3), while 5 were down-regulated (AKR1E2, PDE6G, GNMT, NR2E1, and AHNAK). RT-qPCR validation indicated that most of the DEGs (SCYL3, AQP1, ABCA13, RALGPS2, ITPR3, AKR1E2, NR2E1, and PDE6G) exhibited no significant differences between CHI3L1 and vehicle-treated conditions. Although not statistically significant, both microarray and RT-qPCR analyses indicated downregulation of GNMT. Notably, the AHNAK gene demonstrated differential expression in the CHI3L1-treated condition: microarray analysis indicated down-regulation, while RT-qPCR showed upregulation, achieving statistical significance.

Regarding the RT-qPCR validation for the 24-hour time point (**Figure 38**), we selected 35 DEGs: 25 were up-regulated (TMEM161B, RIOK2, CYLC1, DENND2C, CD86, CFAP61, TPTE2, GRID2, RASA2, OR2D2, HMSD, LRRC66, ERAP2, VPS54, UHMK1, CDH12, CHRFAM7A, TNFAIP6, MTMR2, SYT10, APELA, CAMK2B, CHRM3, CHRM2 and CALB1) and 10 were down-regulated (GNG5, CGN, CFAP157, TSNAX-DISC1, LRRN4, SLC5A6, TRIM66, CD44, GNMT and EFNA1). Subsequent RT-qPCR validation of the upregulated genes demonstrated that the majority of DEGs that were upregulated in the initial microarray experiment were also found to be upregulated in the RT-qPCR validation, with statistically significant findings observed for RIOK2, DENND2C, CFAP61, RASA2, LRRC66, and UHMK1. Conversely, concerning down-regulated genes, there were inconsistencies between the microarray and RT-qPCR validation data for most of the genes (TSNAX-DISC1,

LRRN4, SLC5A6, TRIM66, and EFNA1), except for GNMT, which exhibited consistent validation.

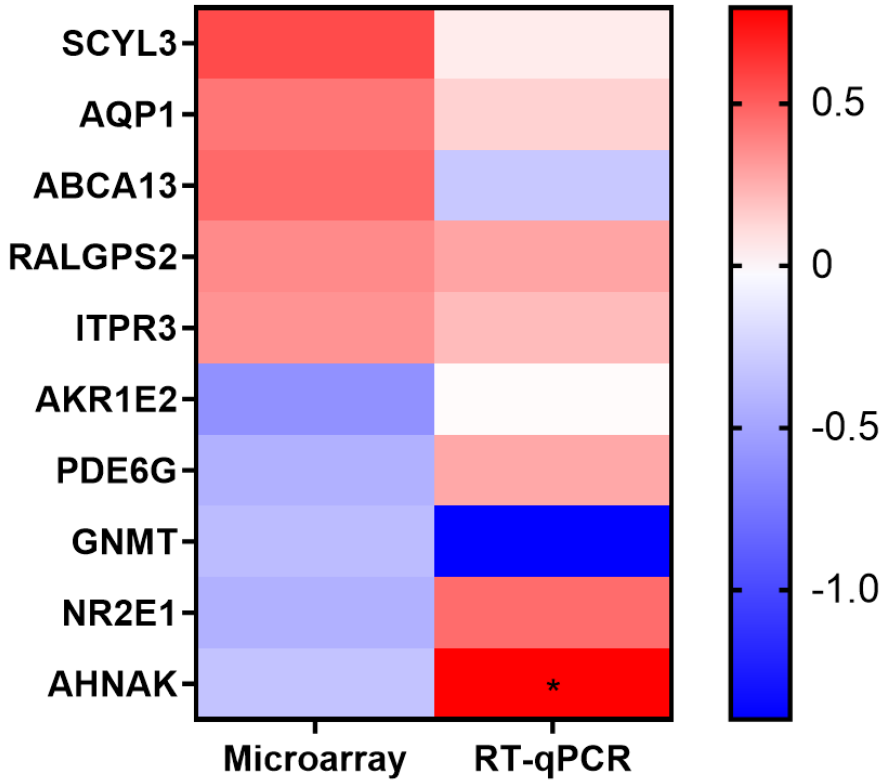

Figure 37. Heatmap presenting expression values obtained from microarray and RT-qPCR validation experiments for selected DEGs at the 12-hour time point. Asterisks mean statistical significance in the RT-qPCR validation experiments. For microarray experiments, 3 independent experiments were conducted. The validation process was performed using the $2^{-\Delta\Delta Ct}$ method, with a comparison between the CHI3L1 condition and its corresponding vehicle control. Each group underwent 3-5 independent experiments. *p<0.05 (*Two-tailed unpaired t-test*)

Abbreviations: ABCA13 - ATP-binding cassette sub-family A member 13, AHNAK - AHNAK nucleoprotein, AKR1E2 - Aldo-keto reductase family 1 member E2, AQP1 - Aquaporin 1, GNMT - Glycine N-methyltransferase, ITPR3 - Inositol 1,4,5-trisphosphate receptor type 3, LCK - Lymphocyte-specific protein tyrosine kinase, NR2E1 - Nuclear receptor subfamily 2 group E member 1, PDE6G - Phosphodiesterase 6G, RALGPS2 - Ral GEF with PH domain and SH3 binding motif 2, SCYL3 - SCY1 like pseudokinase 3

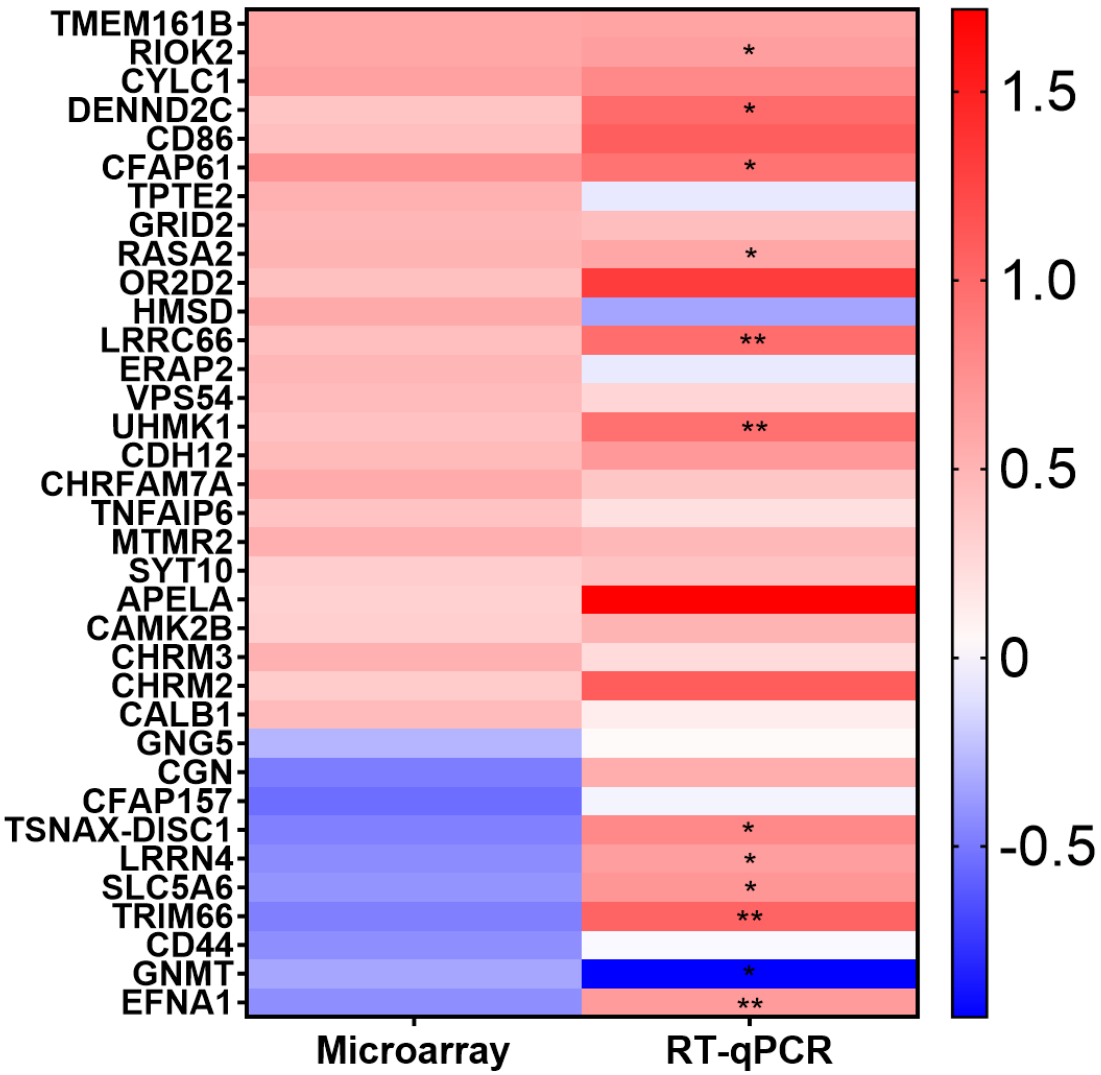

Figure 38. Heatmap presenting expression values obtained from microarray and RT-qPCR validation experiments for selected DEGs at the 24-hour time point. Asterisks mean statistical significance in the RT-qPCR validation experiments. For microarray experiments, 3 independent experiments were conducted. The validation process was performed using the $2^{-\Delta\Delta Ct}$ method, with a comparison between the CHI3L1 condition and its corresponding vehicle control. Each group underwent 3-6 independent experiments. *p<0.05, **p<0.01 (*Two-tailed unpaired t-test*)

Abbreviations: CD44 - Cluster of Differentiation 44, CD86 - Cluster of Differentiation 86, CDH12 - Cadherin 12, CFAP61 - Cilia and Flagella Associated Protein 61, CFAP157 - Cilia and Flagella Associated Protein 157, CGN – Cingulin, CHRFAM7A - Cholinergic Receptor Nicotinic Alpha 7 Subunit

and FAM7A Hybrid, CYLC1 - Cylicin 1, DENND2C - DENN Domain-Containing Protein 2C, EFNA1 - Ephrin-A1, ERAP2 - Endoplasmic Reticulum Aminopeptidase 2, GNMT - Glycine N-Methyltransferase, GRID2 - Glutamate Receptor, Ionotropic, Delta 2, HMSD - Histocompatibility Minor Serpin Domain Containing, LRRC66 - Leucine-Rich Repeat-Containing Protein 66, MTMR2 - Myotubularin-Related Protein 2, OR2D2 - Olfactory Receptor Family 2 Subfamily D Member 2, RASA2 - RAS P21 Protein Activator 2, RIOK2 - RIO Kinase 2, SLC5A6 - Solute Carrier Family 5 Member 6, SYT10 - Synaptotagmin 10, TMEM161B - Transmembrane Protein 161B, TNFAIP6 - Tumor Necrosis Factor Alpha-Induced Protein 6, TPTE2 - Transmembrane Phosphoinositide 3-Phosphatase and Tensin Homolog 2, TRIM66 - Tripartite Motif-Containing Protein 66, TSNAX-DISC1 - TSNAX-Discs Large Homolog 1 Fusion, UHMK1 - U2AF Homology Motif Kinase 1, VPS54 - Vacuolar Protein Sorting 54 Homolog

Figure 39 illustrates the graphical representation of RT-qPCR logFC values of the genes that have undergone successful validation. The validated DEGs hold distinct functional significance within the neuronal context, shaping various aspects of neuronal physiology. RIOK2, is implicated in ribosomal biogenesis and cell cycle regulation suggesting an involvement in neuronal protein synthesis[226] (**Figure 39F**). DENND2C has a role in vesicular trafficking[227] potentially influencing synapse vesicle dynamics and neurotransmitter release in neurons (**Figure 39C**). Both CFAP61 (**Figure 39B**) and LRRC66 (**Figure 39D**) are associated with cilia and may be implicated in signal transduction. RASA2's function as a RAS protein activator indicates its potential contribution to cellular signaling modulation[228] (**Figure 39E**). Particularly intriguing, UHMK1, enriched in neurons, likely contributes to neuronal development, exerting an impact on synaptic plasticity[229] (**Figure 39A**). Interestingly, SYT10 upregulation has been associated with pathological synaptic activity[230] (**Figure 39H**). Lastly, GNMT's involvement in methyl metabolism[231] suggests a role in shaping epigenetic processes and neuronal gene expression (**Figure 39G**).

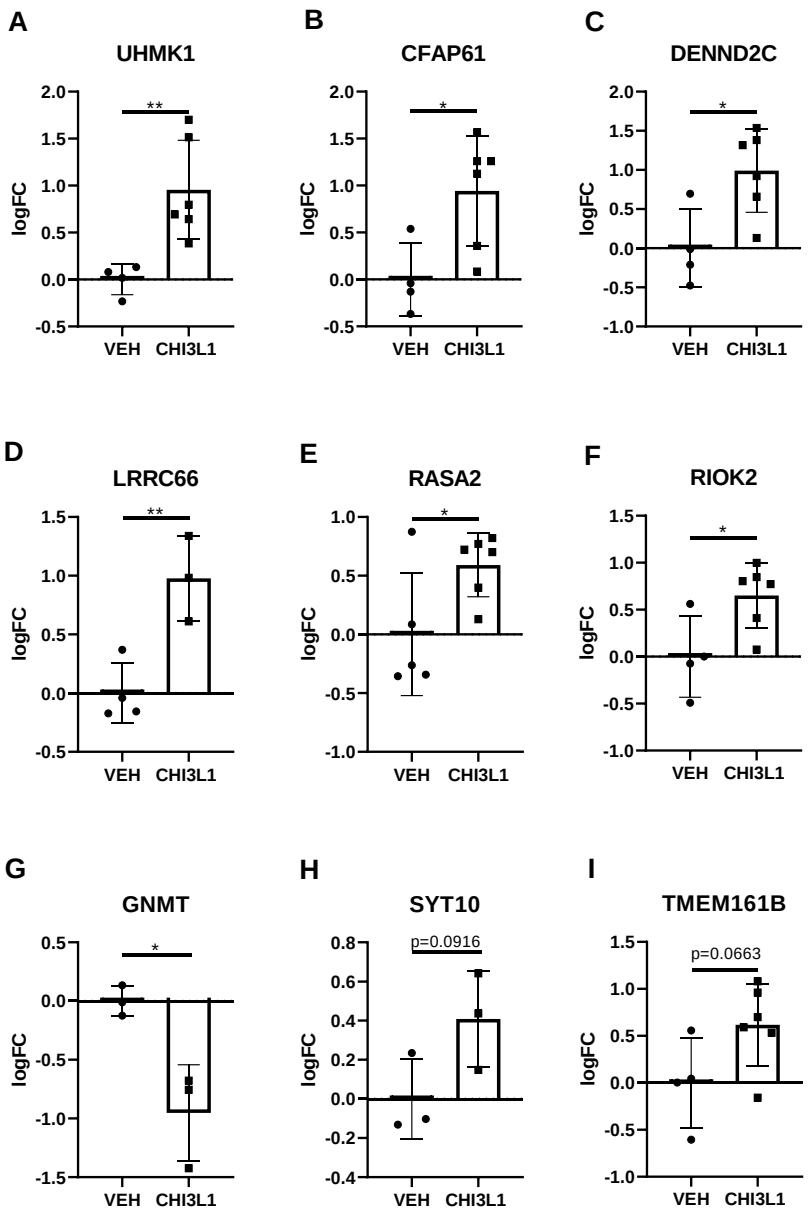

Figure 39. Validated DEGs at the 24-hour time point using RT-qPCR. mRNA expressions levels were measured by RT-qPCR and quantified using the $2^{-\Delta\Delta Ct}$ method. Individual values represent logFC of mRNA expression comparing CHI3L1 versus vehicle control. N=3-6 independent experiments per group. Specifically, graphs show RT-qPCR validation of UHMK1 (**A**), CFAP61 (**B**), DENN2DC (**C**), LRRC66 (**D**), RASA2 (**E**), RIOK2 (**F**), GNMT (**G**), SYT10 (**H**), and TMEM161B (**I**) genes. Data are presented as Mean ± SD. *p<0.05, **p<0.01 (*Two-tailed unpaired t-test*)

Abbreviations: CFAP61 - Cilia and Flagella Associated Protein 61, DENND2C - DENN Domain-Containing Protein 2C, GNMT - Glycine N-Methyltransferase, LRRC66 - Leucine-Rich Repeat-Containing Protein 66, RASA2 - RAS P21 Protein Activator 2, RIOK2 - RIO Kinase 2, UHMK1 - U2AF Homology Motif Kinase 1

5.5 Identification of Neuronal Cellular Pathways Activated by CHI3L1

To gain a more comprehensive understanding of the molecular mechanisms through which CHI3L1 impacts hiPSC-derived neurons, we conducted an exploratory phosphorylation array analysis encompassing key cellular signaling pathways. Given that cellular signalling events precede gene expression and consequential functional changes, we strategically chose four early time points: 30 minutes, 1 hour, 2 hours, and 4 hours.

Our investigation into the activated cellular signaling pathways influenced by CHI3L1 yielded intriguing findings. The complete results are depicted in Supplemental Figure 2 (see Annexes). Notably, we observed a gradual elevation in phosphorylation of STAT1 at Y701 (**Figure 40A**), exhibiting statistical significance at 1 hour and 4 hours post-treatment. We also detected phosphorylation events at STAT2-Y689 (**Figure 40B**) and STAT3-Y705 (**Figure 40C**), manifesting at 2 hours and 1 hour, respectively, although the divergence between CHI3L1-treated and control conditions was less pronounced. Noteworthy observations include phosphorylation at multiple residues of p53—S15 (**Figure 40D**), S46 (**Figure 40E**), and S392 (**Figure 40F**) at 2 hours for S15 and at 30 minutes for S46 and S392. Furthermore, progressive phosphorylation of PYK2 (**Figure 40G**) at Y402 was evident and significant for the 30 minutes, 2 hours and 4 hours' time points. Finally, we identified discrete differences yet significant of GSK-3β-S9 (**Figure 40H**) and PDGFRβ-Y751 (**Figure 40I**) phosphorylation.

Collectively, these results suggest that CHI3L1 may concurrently influence various cellular signaling pathways, aligning with its pleiotropic nature.

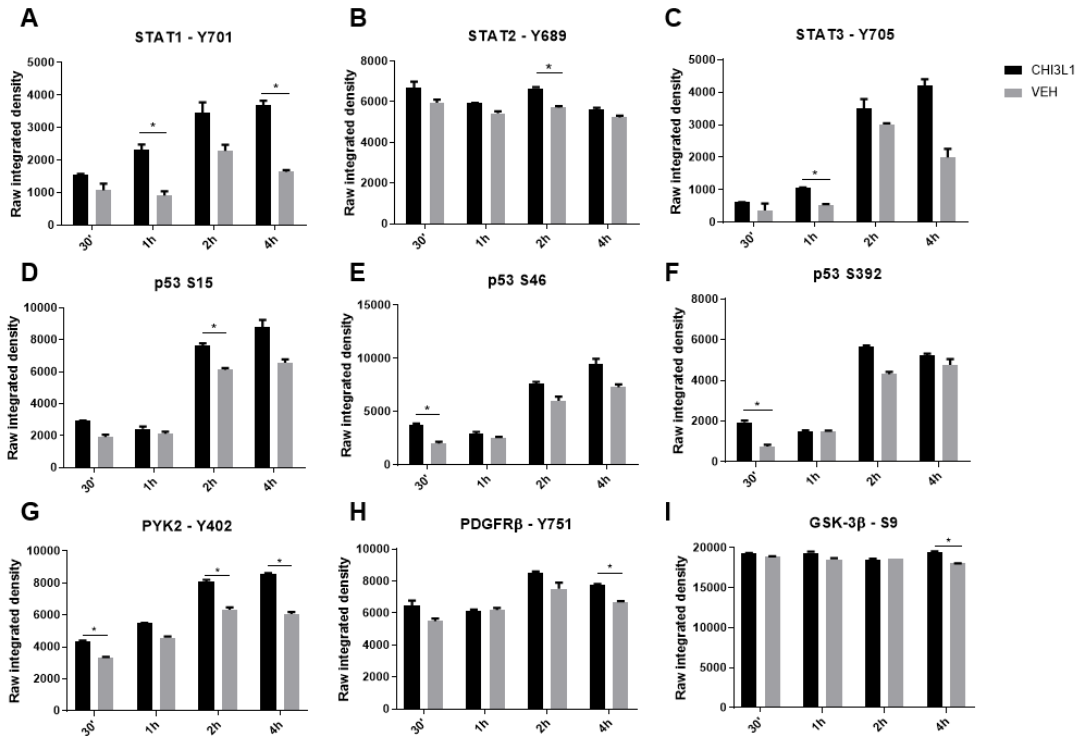

Figure 40. Cellular signaling pathway activation induced by CHI3L1 in hiPSC-derived neurons. hiPSC-derived neurons (MS-10 D28) were exposed to CHI3L1 at a concentration of 300 ng/ml, or vehicle (PBS), for 30 minutes, 1 hour, 2 hours, and 4 hours. The presented graphs display integrated pixel density values, derived from two replicates for each specific condition. Specifically, graphs show phosphorylation of the Y701 residue on STAT1 (**A**), phosphorylation of the Y689 residue on STAT2 (**B**), phosphorylation of the Y705 residue on STAT3 (**C**), the phosphorylation states of p53 at residues S15 (**D**), S46 (**E**), and S392 (**F**), phosphorylation of PYK2 at the Y402 residue (**G**), phosphorylation of the Y751 residue of PDGFRβ (**H**), and phosphorylation of GSK-3beta at the S9 residue (**I**). Statistical analysis was conducted with a Two-Way ANOVA with Greenhouse-Geisser Correction, followed by Bonferroni post hoc analysis. The experimental design encompassed variations in treatment and time. Post hoc comparisons were performed between CHI3L1-treated versus vehicle-treated conditions at each time point. The data are presented as Mean ± SD. *p<0.05

Abbreviations: GSK-3β - Glycogen Synthase Kinase-3β, p53 - Tumor Protein 53, PDGFR-β: Platelet-Derived Growth Factor Receptor beta, PYK2 - Proline-rich Tyrosine Kinase 2, STAT1 - Signal Transducer and Activator of Transcription 1, STAT2 - Signal Transducer and Activator of Transcription 2, STAT3 - Signal Transducer and Activator of Transcription 3

The next step in our investigation was to validate the results obtained in the phosphorylation array. Based on the array results, we chose for validation the phosphorylation of STAT1 at Y701. The WB validation (**Figure 41**) demonstrated a significant increase in the phosphorylation of STAT1-Y701 at the 2-hour time point and a trend at the 4-hour mark.

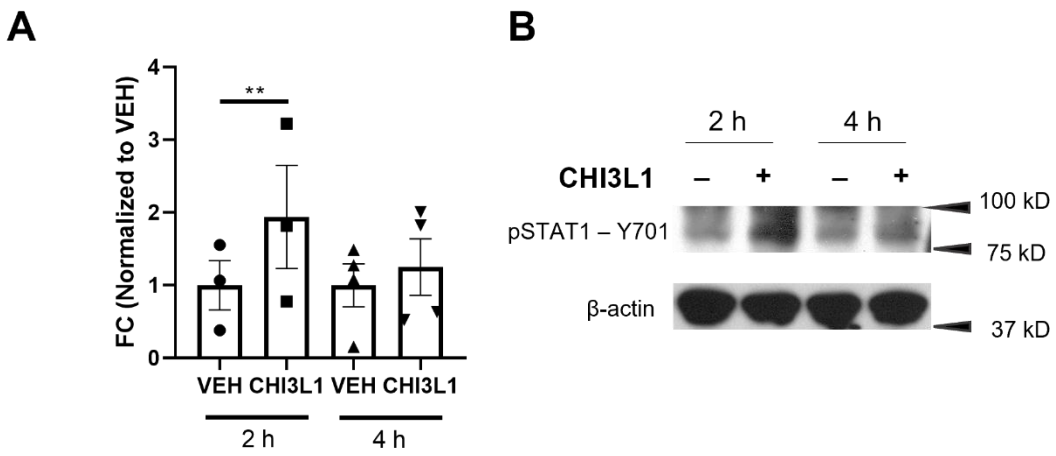

Figure 41. **Western Blot validation of Y701-STAT1 phosphorylation following CHI3L1 treatment in hiPSC-derived neurons at 2 and 4 hours**. (**A)** Graph illustrating the fold change in CHI3L1-treated neurons versus VEH-treated neurons, with fold change values normalized to the vehicle. The data are presented as Mean ± SD, and each dot corresponds to an independent experiment (N=3-4 independent experiments). (**B)** Representative immunoblots showing STAT1-Y701 phosphorylation (80 kD) and the endogenous control β-actin (42 kD). (*Two-tailed ratio paired t-test*) **p<0.01.

Abbreviations: CHI3L1 - chitinase 3-like 1, FC – fold change, VEH – vehicle control, STAT1 – Signal Transducer and Activator of Transcription 1

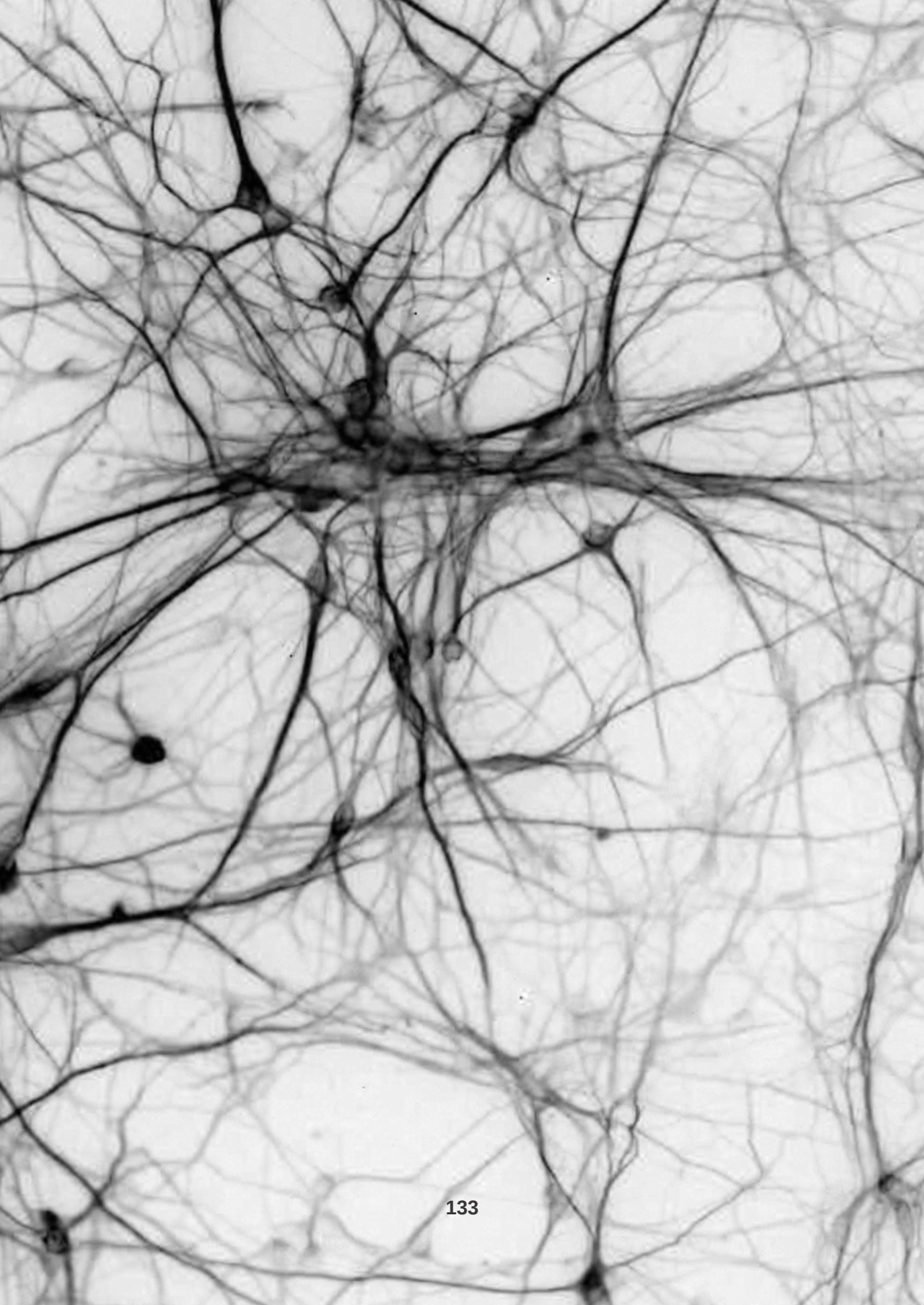

DISCUSSION

6. DISCUSSION

A profound comprehension of the neurodegenerative processes occurring in the CNS during the initial stages of MS pathogenesis is essential for the formulation of targeted therapeutic approaches that may dampen neurodegeneration and progression. This imperative guided our investigation into the prognostic significance of CHI3L1 and the exploration of its role within the neuronal landscape.

Strong evidence supports the prognostic role of CHI3L1 in neurodegenerative processes. In the context of early MS, CHI3L1 was associated with disease parameters such as the number of brain lesions in the MRI, and a shorter time of conversion to MS but, more importantly, CHI3L1 was associated with a more rapid development of neurological disability, thus highlighting its robust prognostic utility.[83,85,86] In patients with RRMS, elevated CSF CHI3L1 levels demonstrated significant correlations with brain volume loss, providing crucial insights into neurodegenerative processes.[83,89] Moreover, increased CHI3L1 levels independently predicted worsening neurological disability and progression to SPMS.[88] Additional facets of CHI3L1 impact include association with cognitive dysfunction, not only in MS[205], but also in other neurodegenerative conditions such as ALS[101], PD[232] and HIV-associated dementia[233], or psychiatric diseases as bipolar disorder[234]. Indeed, increased CHI3L1 levels are observed in various neurological diseases with a neurodegenerative component such as AD, where high levels were associated with cortical thinning.[94]

The histological examination of chronic active lesions in MS patients further supports a prognostic role for CHI3L1, since its expression is notably absent in brain tissue from non-neurologic controls, thus underscoring its specificity as a marker for CNS pathology.[235] Within the CNS lesions, CHI3L1 expression is observed mostly in astrocytes, but also in macrophages and microglia.[235] These histological insights point to CHI3L1 as a player in the intricate neurodegenerative milieu of MS. Based on the finding of a strong association between high CSF CHI3L1 levels and disability progression in patients with CIS; the finding of CHI3L1 as a strong predictor of

development of brain atrophy in CIS and RRMS patients, and the finding of CHI3L1 as an independent predictor of neurological disability worsening and development of a secondary progressive phase of the disease in RRMS patients, our research team wondered *whether* CHI3L1 was just a mere biomarker secreted by astrocytes and microglia to the CSF where it reflects the degree of astrocyte and microglia activation, or CHI3L1 could be neurotoxic by itself. In this context, our group conducted in the past a pivotal study to assess the effects of CHI3L1 on murine cortical neurons, uncovering diminished neuronal viability and neurite retraction after CHI3L1 treatment.[156] Concurrently, independent researchers also documented CHI3L1 neurotoxicity in rodent neuronal cultures.[132] Rodent neuronal cultures have limitations in their translatability to human physiology and pathologies because of species-specific differences in neural development, function and disease.[172] This critical insight reinforced the significance of understanding the detrimental effects of CHI3L1 on human neurons, prompting our shift to hiPSC-derived neurons to explore CHI3L1's impact in a model with high translational value.

In our exploration of CHI3L1's effects on hiPSC-derived neurons from individuals with RRMS, we uncovered multifaceted alterations spanning from neuronal morphology and synaptic function to neuronal network dynamics. The mechanistic investigation of CHI3L1-induced neuronal effects showed that CHI3L1 treatment led to a pleiotropic transcriptomic signature, affecting pathways related to inflammation, synaptic function, and various signaling cascades. Additionally, we described STAT1 activation after CHI3L1 treatment. Overall, we report for the first time an exhaustive morphologic, functional, and molecular characterization of CHI3L1 neurotoxic effects in a human neuronal model.

The rationale for using hiPSC-derived neurons to investigate the effects of CHI3L1 is grounded on two essential considerations. First, the distinctive ability of hiPSCs to differentiate into various cell types, including neurons, renders them a unique human-specific neuronal model.[176] Second, the use of patient-derived hiPSCs ensures the retention of the genetic background of individuals with MS, thus establishing a model that is not only relevant but also personalized for the exploration of disease

mechanisms. By focusing on hiPSC-derived neurons from individuals with RRMS, our study meticulously examines the specific detrimental effects of CHI3L1 within an environment that resembles the nuances of human neurons. This deliberated choice of model facilitates the dissection of CHI3L1-mediated alterations in neuronal morphology, function, and molecular signatures, all of which bear direct relevance to MS pathogenesis. Despite their potential, hiPSC-derived neuronal cultures come with inherent challenges. Variability among hiPSC cell lines, arising from differences in derivation methods and culture conditions, as well as the genetic background of the donors, introduces complexities in data interpretation. Moreover, a considerable time is required for functional maturation of hiPSC-derived neurons, the differentiation protocols are complex, and the resulting cells require exhaustive characterization.

In our pursuit of generating functional cortical neurons from hiPSCs, we reviewed the extensive existing literature describing neural differentiation protocols. Neural differentiation from hiPSCs requires the targeted inhibition of specific signaling pathways to prevent non-neural fate determination, coupled with the precise orchestration of growth factors for the induction of distinct neuronal subtypes. Given the complexity of the differentiation protocols and our commitment to minimizing experimental variability, we opted for performing the differentiation process with commercial kits provided by StemCell Technologies™, known for their rigorous validation.[236,237] For the neural induction, we used the high-efficiency, well established SMADi differentiation protocol, involving dual inhibition of SMADi signaling through small molecules during hiPSCs or EBs formation, faithfully recapitulating early neurodevelopmental events.[184] A key aspect of this protocol is the formation of neural rosettes which *in vitro* resembles the neural tube, and serve as a reservoir of NPCs.[177] Recognizing the critical role that NPCs play in ensuring the desired neuronal fate, we characterized this intermediate stage with key NPCs markers as the neural transcription factors SOX1 and PAX6, and the intermediate filament protein Nestin. By examining and comparing the derived NPCs, we aimed not only to validate the effectiveness of our differentiation protocol, but also to discern variations or unique characteristics between the hiPSC cell lines. At this stage, we

observed that the majority of the cells expressed the desired markers and that were no significant differences between the hiPSC cell lines. In addition, we ensured the loss of pluripotency by assessing the negativity of OCT3/4 marker.

We directed differentiation towards neuronal precursors and subsequently matured the neurons in serum-free supplemented BrainPhys medium. Unlike traditional human neuronal culture media based on DMEM/F12 and/or Neurobasal, which support neuronal survival but impair synaptic and electrophysiological functions, BrainPhys was specifically designed to mimic *in vitro* brain physiological conditions and support optimal neuronal function.[238] This decision underlined our commitment to creating an *in vitro* environment that promoted robust neuronal development.

We then identified the optimal time point for our experiments by assessing the expression of the dendritic marker MAP2 and synaptic markers synapsin and PSD-95. Notably, neurons initiated MAP2 expression at day 8 of maturation; however, their morphology at this stage resembled immature neurons with limited neurites. Over time, these neurons underwent progressive maturation, forming a densely connected network by day 28 of maturation, accompanied by a gradual increase in the expression of synaptic markers. Consequently, we selected this specific time point for conducting most of our experiments. Next, we characterized the emergence of spontaneous and synchronous neuronal activity, finding out that neurons exhibited a pattern of activation that included both sporadic and synchronous activity by day 40, consistent with previous research.[187]

Next, we characterized by immunofluorescence our neuronal cultures. Cortical commitment was verified through the expression of Tbr1 (MS-10 and MS-6 lines) and CTIP2 (MS-6) markers. By day 28, neurons displayed both glutamatergic and GABAergic markers, later shifting towards a predominantly glutamatergic phenotype by day 40. Notably, astrocyte proportions varied between MS-10 and MS-6 at both experimental time points, with MS-10 demonstrating a predominantly neuronal composition (nearly 100% at day 28, ~90% at day 40) and consequently designating this MS-10 cell line as our reference cell line, while MS-6 exhibited a higher astrocytic

presence (~30% at day 28, ~45% at day 40). Astrocytes are reported to positively influence neuronal maturation in hiPSC-derived neuronal cultures.[239] However, considering the documented interactions of CHI3L1 with astrocytes[146,152], a careful consideration was given to our experimental design. In this regard, both MS-10 and MS-6 were employed for morphological and functional experiments, adapting the analysis pipelines to effectively exclude astrocytes. Conversely, for the mechanistic studies involving transcriptomic and proteome array analyses, we deliberately focused on MS-10 alone. This strategic choice aimed to preclude any potential contamination of the CHI3L1-astrocytic response, ensuring a committed investigation of the neuronal response to CHI3L1.

The observed CHI3L1-induced dendrite retraction and decreased arborization align with previous investigations on murine cortical cultures.[156] CHI3L1 also affected synaptic function, leading to significant decreases in synapsin and active synapses, and a trend towards lower levels of the postsynaptic marker PSD-95. Bioinformatic analyses of the DEGs from the microarray experiments revealed a dysregulation of synaptic-related processes at 24 hours, emcompassing chemical synaptic transmission, trans-synaptic and synaptic signaling, and the regulation of postsynaptic membrane potential. GSEA analysis further highlighted dysregulation of various cellular components related to synapses, specifically GABAergic and glutamatergic synapses, as well as synaptic and postsynaptic membranes. Dendritic atrophy and reduced synaptic connectivity, as observed in the CHI3L1-induced effects, are recognized as hallmarks of various neurodegenerative and psychiatric diseases, contributing to impairments in cognition.[240] For instance, in the AD brain there is a significant loss of synapses and dendritic arbor regression that correlates with the degree do cognitive and memory impairment.[241] In MS, synapse dysfunction occurs early and independendtly of demyelination, correlating with cognitive and psychic symptoms.[48]

The interdependence between synapses and dendritic arborization, as highlighted in our study, reflects a well-established neurobiological principle where synapses play a stabilizing role in maintaining dendritic structures.[240] *In vivo,* the loss or reduction

of synaptic inputs can lead to dendritic loss, a phenomenon observed in our CHI3L1-induced effects.[242] Furthermore, the actin cytoskeleton, identified as a structural support for synaptic mainentance, provides a mechanistic link to the alterations in dendrites and synapses induced by CHI3L1.[243] Key regulators of the neuronal actin rearrengements include the Rho family small GTPases[220], in which Rac and Rho play antagonistics roles where Rac activation stimulates actin polymerization, while Rho activation leads to synapse and dendritic loss and dendrite regression.[244] Interestingly, alterations in DEGs associated with the cluster of actin-based cell projections and actin filament-based processes were observed at 12 hours, as well as positive regulation of small GTPase activity. Moreover, the analysis of reduction of the redundancy at 12 and 24 hours showed an upregulation of the RHOD GTPase cycle, which is an atypical small GTPase that is described to play a role in vesicle trafficking, organization of the actin filament system, and cell migration.[245,246]

The analysis of the CHI3L1-induced effects on neuronal activity and neuronal network dynamics yielded intriguing findings, and an interesting temporal pattern of the effects. Despite observing no differences in the mean neuronal activity or the number of active neurons, an evident increase in fluorescence amplitude emerged in the CHI3L1-treated neuronal cultures, specially prominent at the 4-hour time point. Given the direct proportionality of calcium fluorescence amplitude to the number of elicited action potentials, these results imply increased excitability in CHI3L1-treated neurons. Interestingly, this increase in individual activity did not translate into elevated collective behaviour. Following an initial rise in the proportion of the network engaged in collective events (GNA sizes) at 4 hours, a gradual decline in GNA sizes was noted at 24 and 72 hours in CHI3L1-treated neuronal cultures. In contrast, the temporal pattern of collective behaviour in the vehicle-treated condition remained stable over time.

The effective connectivity analysis of the CHI3L1-induced effects showed no significant differences in the studied parameters (global efficiency, modularity and average connectivity) between the CHI3L1 and the vehicle treated conditions at 4 and 72 hours, the time points we selected for the analysis. However, mirroring the

temporal pattern observed in the GNA sizes, CHI3L1 first induced a trend of increase in global communication of the network at 4 hours as depicted by the increase in the global efficiency and the average connectivity. In contrast, at the 72 hours time point, a trend of decrease in the integration of the network was observed, as depicted by the decrease in global efficiency and average connectivity, coupled with an elevated modularity, signifying that neurons tended to communicate in smaller groups.

We hypothesize that the clear reduction of CHI3L1-induced hyperexcitabilty from 4 to 72h is related to plastic effects associated with the intrinsic homeostatic behaviour of neuronal cultures, in which compensatory mechanisms, aimed at maintaninng neuronal culture activity at a set point, activate in response to perturbations. Indeed, and in line with our CHI3L1-induced effects at 4 hours, other studies have shown that acute biochemical perturbation leads to short-time alterations that gradually fade off. For instance, the administration of incremental doses of an antagonist of AMPA excitatory receptors (6-cyano-7-nitroquinoxaline-2,3-dione, CNQX), provoked a gradual reduction of the synaptic excitatory coupling and a dropout in the network spontaneous activity. This action first induced a decrease in global efficiency due to synaptic connectivity degradation, but then the global efficiency boosted beyond normal levels as compensatory mechanisms activated, e.g., by strengthening the excitatory connections.[247] According to the authors in the study, the hyperefficiency situation resulted from a strengthening of the effective connections likely attributed to synaptic scaling - a regulatory mechanism of neuronal circuits in which synaptic strength is adjusted to compensate changes in activity.[247,248] The initial increase in the global efficiency and the GNA sizes in our investigation may reflect a hyperefficiency situation in CHI3L1-treated cultures facing pathologic synaptic activity and subsequent synaptic loss.

In the context of AD, studies reviewed in the provided reference have demonstrated that brain hyperexcitability characterized the early phases of the disease, followed by hypoactivity in later stages of neurodegeneration.[249] It is noteworthy that a growing body of evidence implicates aberrant neuronal synaptic excitability due to inflammatory soluble factors as a contributing factor to synaptic degeneration.[250] For

instance, CSF from active RRMS patients has been shown to enhance glutamate-mediated transmission and excitotoxicity through IL-1β signalling and increased glutamate receptor stimulation in rodent brain slices.[40] Furthermore, a study in MS patients utilizing transcranial magnetic stimulation reported increased brain excitability, likely linked to impaired synaptic inhibition.[251] Notably, the transcriptomic study of CHI3L1 revealed alterations in inflammatory processes related to cytokine activity and signaling at 12 hours, as well as perturbations in the response to calcium and sodium ion transport at 24 hours. These alterations could potentially impact neuronal excitability and membrane potential dynamics, ultimately explaining the mechanistic basis of the observed changes in neuronal excitability.

The transcriptomic profilling of CHI3L1-induced effects on hiPSC-derived neurons unveiled pleiotropic effects potentially impacting multiple pathways and altering neuronal gene expression. However, a notable limitation of the chosen neuronal model became evident during the PVCA analysis of the microarray experiment. This analysis revealed that the primary source of variance in the microarray experiment (approximately 50%) was attributed to the effect of time. Given that hiPSC-derived neurons emulate embryonic development[201], a multitude of transcriptional changes occuring during neuronal maturation diffused the effects of CHI3L1 treatment, which accounted for nearly 7% of the variance. Consequently, during the analysis of DEGs between CHI3L1 and vehicle-treated conditions, no DEGs passed the multiple tests corrections. Therefore, we opted to focus on genes with unadjusted p-value<0.01 for further bioinformatic analyses using Metascape, and for subsequent selection to RT-qPCR validation.

At the 12-hour time point, 11 DEGs were selected for RT-qPCR validation. Although not statistically significant at 12 hours, RT-qPCR revealed GNMT downregulation, becoming significant at 24 hours. GNMT impacts cellular methylation capacity by regulating the S-adenosylmethionine/S-adenosylhomocysteine ratio. Despite its traditional metabolic enzyme role, GNMT is expressed in various brain areas. [252,253] GNMT KO mice showed reduced neurogenic capacity, spatial learning memory

impairment, and decreased pre-pulse inhibition. [252,253] Altered methylation dynamics may contribute to dysregulation of key genes in neurodegenerative disorders.

At the 24-hour time point, we selected 35 DEGs for RT-qPCR validation. Notably, a significant proportion of the upregulated DEGs identified in the microarray experiment exhibited consistent upregulation in the RT-qPCR validation. Particularly, RIOK2, DENND2C, CFAP61, RASA2, LRRC66, and UHMK1 showed statistically significant upregulation. Particularly interesting is the UHMK1 gene, which encodes the KIS protein. Initially recognized as a kinase interacting with stathmin, influencing microtubule dynamics, KIS has also been found to interact with proteins within RNA granules.[254] The knockdown of KIS in mouse cortical neurons resulted in impaired neurite outgrowth and reduced expression levels of PSD-95 and AMPA receptors, leading to both morphological and functional alterations.[229,254] Notably, exposure to CHI3L1 resulted in a increased expression of UHMK1. This dysregulation may potentially contribute to some of the observed functional alterations observed in our study. RIOK2 is implicated in ribosome biogenesis[226], and like CHI3L1 it has been implicated in epithelial mesenchymal transition[255], but no specific neuronal studies have been published. RASA2, or Ras GTPase-activating protein 2, functions as a negative regulator of Ras proteins.[228] The Ras family proteins play a pivotal role in governing diverse cellular processes and its dysregulation has been implicated in various neoplastic diseases. Additionally, this pathways have been involved in neurodegenerative conditions as AD or neurodevelopmental disorders like the Noonan syndrome.[256] DENN2DC has been associated with vesicle trafficking, although its exact function remains elusive.[227] Lastly, CFAP61 and LRRC66 are both proteins predicted to be associated with specific cellular functions, in the context of cilia and flagella. These results highlight the complexity of the CHI3L1-induced gene expression alterations, offering avenues for future investigations.

In addition to the previously mentioned enriched processes at 12 and 24 hours, CHI3L1 significantly impacted the enrichment of multipleprocesses during these time points aligning with its pleiotropic nature. Notably, at 12 hours, upregulated DEGs revealed receptor ligand activity and signaling receptor activator activity, consistent

with a potential interaction of CHI3L1 with its receptors. Inflammatory processes were also upregulated, indicating over-representation of angiogensesis and inflammatory profibrotic mediators. These findings align with CHI3L1's known induction of angiogenesis in various types of cancers[128,219] and its implications as a profibrotic factor in pulmonary fibrosis[138,140]. Additionally, there was an enrichment of responses to diverse molecular components such as cAMP, suggesting potential modulation of signaling pathways by secondary messengers.

Analysis of the upregulated DEGs at 24 hours revealed intriguing findings, including alterations in sensory perception of smell and olfactory pathways. While ectopic expression of odorant receptors has been described in various neurodegenerative diseases[222], the functional consequences of this expression require further investigation. Dysregulation of metabolic processes such as lipid transport and localization were also observed, consistent with observations that associate lipid transport alterations with neurodegenerative diseases.[223] Associations with reproductive processes were highlighted in both Metascape analysis of the upregulated genes at the 24-hour time point, with links to reproductive processes and oogenesis, and the GSEA GO CC analysis of the 12-hours time point, which revealed an association with the sperm midpiece component. These associations might hint at the presence of common genes sharing similarities between the neuronal system and reproductive processes, though their significance would require further investigation.

The summarization of the Reactome GSEA analysis at 12 and 24 hours revealed numerous pathways and processes affected by CHI3L1 in hiPSC-derived neurons. Notably, there were alterations in neuronal cell cycle and DNA-related processes, aligning with findings describing the aberrant re-entry of neurons into the cell cycle in neurodegenerative diseases such as AD.[224] Processes related to RNA modification and translation were also dysregulated, reflecting the capacity of CHI3L1 to modify neuronal gene expression and translation. Dysregulation of cholesterol homeostasis has been described in synaptic degeneration[257], and CHI3L1-induced transcriptomic dysregulation of cholesterol biosynthesis. Remarkably, several signaling pathways,

such as RAF, were positively enriched in the Reactome analysis. Conversely, Ras signaling pathway, which acts upstream RAF, was enriched in the down-regulated DEGs at 24 hours. The Ras family small GTPases are essential players in transmitting extracellular stimuli into neurons, regulating several neuronal processes as survival, cytoskeletal structure or intracellular transport, as well as gene expression.[258] Further investigations validating these associations are needed in order to confirm the activation of the above mentioned pathways and processes and to establish functional significance.

The exploration of the neuronal signaling pathways activated by CHI3L1 uncovered phosphorylation of the Y701 residue of STAT1, indicating activation of STAT1, at 1, 2 and 4 hours. Significantly, we validated this phosphorylation through WB at the 2-hour time point, with an observed trend persisting at the 4-hours mark. Additionally, we performed TRRUST enrichment analysis to identify potental transcriptional factors orchestrating the gene expression response to CHI3L1, and obtained IRF1 and STAT1 as potential regulators at 24-hours. Notably, both transcription factors play a role in the interferon response pathway, and IRF1 has been described to support STAT1 activation.[259] Interestingly, the comparison of the DEGs at 24 hours with the Transcription Factor Target Gene Database[260] returned 19 hits for IRF1, and 23 hits for STAT1, supporting the notion that the interferon response pathway may be mediating the effects of CHI3L1 on hiPSC-derived neurons.

The JAK/STAT1 pathway governs a plethora of physiological processes including cell survival, proliferation, differentiation, inflammation, and innate immune response.[261] IFN-γ is the classic activator of STAT1 signaling, initiating a cascade where phosphorylated STAT1 homodimers migrate to the nucleus, bind to GAS activation sites, and activate transcription of pro-inflammatory, anti-viral and tumour surveillance genes.[262] Increasing evidence suggests that this pathway has neuronal specific functions in the CNS both in physiological and pathological processes, although its signalling is far more complex in neurons than in other cellular types. Neurons exhibit a delayed and extended STAT1 activation when compared to other

non-neuronal cell types[262], consistent with our findings where STAT1 was activated at 2 hours.

The IFN-γ/STAT1 physiological signalling has a role in mantaining proper neuronal excitability.[262] In contrast, pathological IFN-γ mediated STAT1 activation induced both dendritic atrophy and synaptic loss in sensory and hippocampal neuronal cultures.[263] Acute IFN-γ exposure of hiPSC-derived neurons activates STAT1 and alters the expression of major histocompatibility complex I, while simultaneously decreasing synapsin protein expression.[264] Furthermore, pathological molecules like tau and amyloid-β induce STAT1 activation in various *in vitro* and *in vivo* models and functional alterations related to synaptic function. Overexpression of human tau impaired synaptic function through JAK2 activation and phosphorylation of STAT1 at Y701 and its consequent translocation to the nucleus, where it induced supression of NMDA receptor expression.[265] Moreover, amyloid-β induced upregulation of STAT1 through mechanisms that involved downregulation of NMDA receptor subunits contributing to memory deficits observed in models of AD.[266] The activation of STAT1 by CHI3L1 aligns with these observations, correlating with the functional effects observed such as dendritic arbor regression and the loss of synapsin and active synapses.

The impact of CHI3L1 on diverse pathways, including those related to inflammation, angiogenesis, and synaptic signaling, emphasizes its pleiotropic nature. The observed CHI3L1-induced effects on dendritic morphology, synaptic function, and network dynamics point to its neurotoxicity, potentially mediated through the interferon response pathway, as evidenced by STAT1 phosphorylation. These findings align with well-established neurobiological principles, where alterations in synapses and dendrites contribute to neurodegenerative processes observed in diseases like MS. The dysregulation of cholesterol homeostasis and the enrichment of various signaling pathways, such as RAF and Ras, further highlight the intricate network? of molecular events influenced by CHI3L1. Intriguingly, our temporal analysis reveals dynamic changes in excitability and network behaviour over time, emphasizing the complexity of CHI3L1-induced effects. This temporal pattern,

coupled with the unexpected increase in global efficiency in response to synaptic connectivity degradation, suggests a hyperefficiency situation in CHI3L1-treated cultures facing pathological synaptic activity and subsequent loss.

In conclusion, our study expands the understanding of CHI3L1's role in neurodegenerative processes, emphasizing its potential as a prognostic marker in MS and shedding light on its neurotoxic effects on human neurons. Further investigations into the intricate molecular mechanisms and signalling pathways affected by CHI3L1 are warranted, offering new avenues for targeted therapeutic interventions in neurodegenerative diseases.

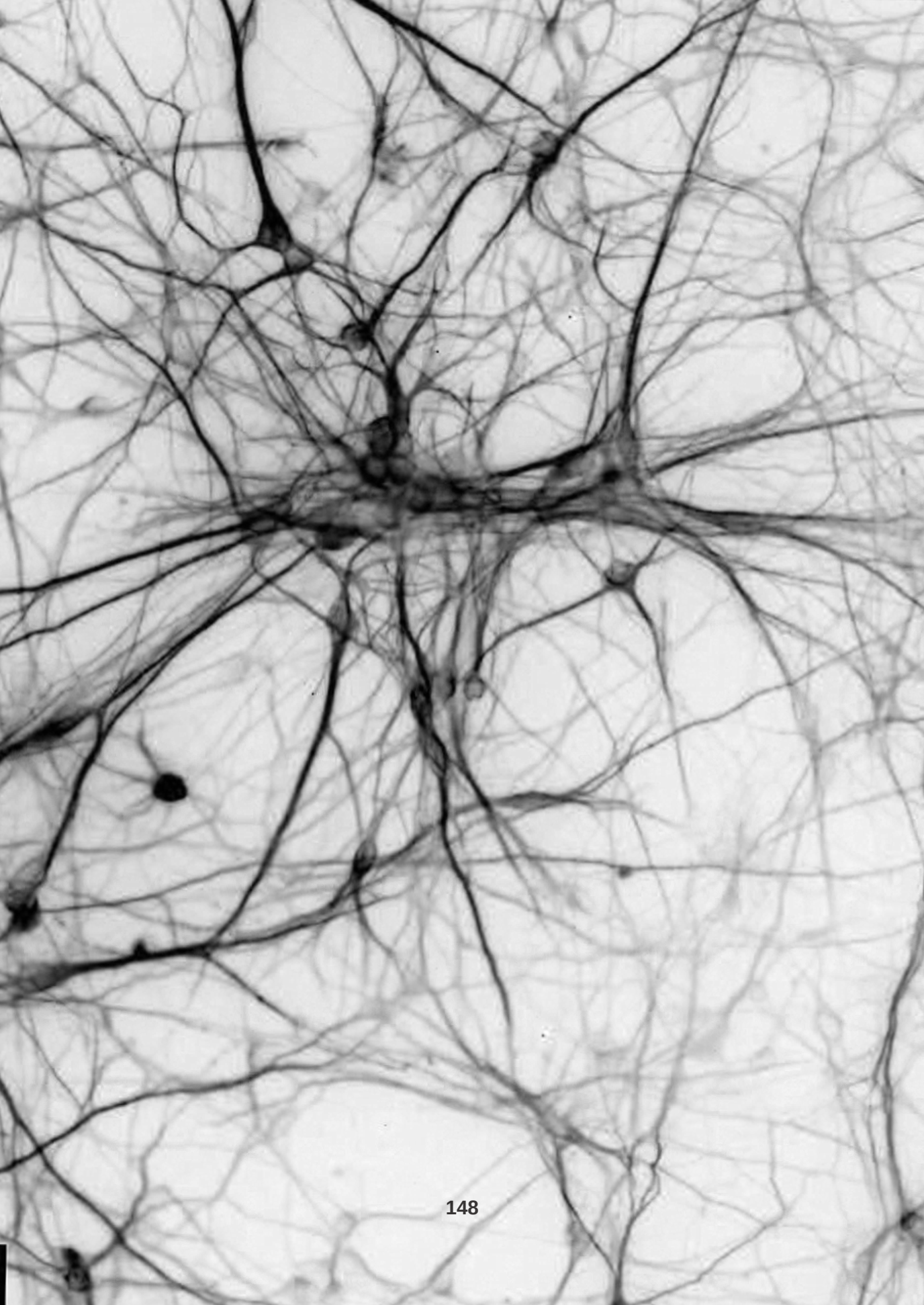

CONCLUSIONS

7. CONCLUSIONS

1. The use of hiPSC-derived neurons provided a human-specific neuronal model, retaining the genetic background of individuals with MS. Despite inherent challenges, the model demonstrated its relevance in studying CHI3L1-induced effects.

2. CHI3L1 induced dendritic retraction and reduced dendritic arborization in hiPSC-derived neurons, aligning with observations in murine cortical neurons. The morphological changes emphasize the neurotoxic impact of CHI3L1 on human neurons.

3. CHI3L1 induced synaptic alterations, including decreased synapsin and active synapses, as well as transcriptomic dysregulation of synaptic-related processes, shedding light on the impact of CHI3L1 on the synaptic function.

4. CHI3L1 induced dynamic changes in neuronal excitability and network behaviour, with a concrete temporal pattern, suggesting a nuanced effect on network dynamics.

5. CHI3L1 pleiotropy highlights its involvement in diverse molecular events, influencing pathways and genes associated with neurodegenerative processes.

6. Activation of the JAK/STAT1 pathway, specifically phosphorylation of STAT1 at the Y701 residue, emerged as a significant molecular event induced by CHI3L1. Additionally, transcription factor enrichment analysis implicated IRF1 and STAT1 as potential regulators, linking CHI3L1 to the interferon response pathway.

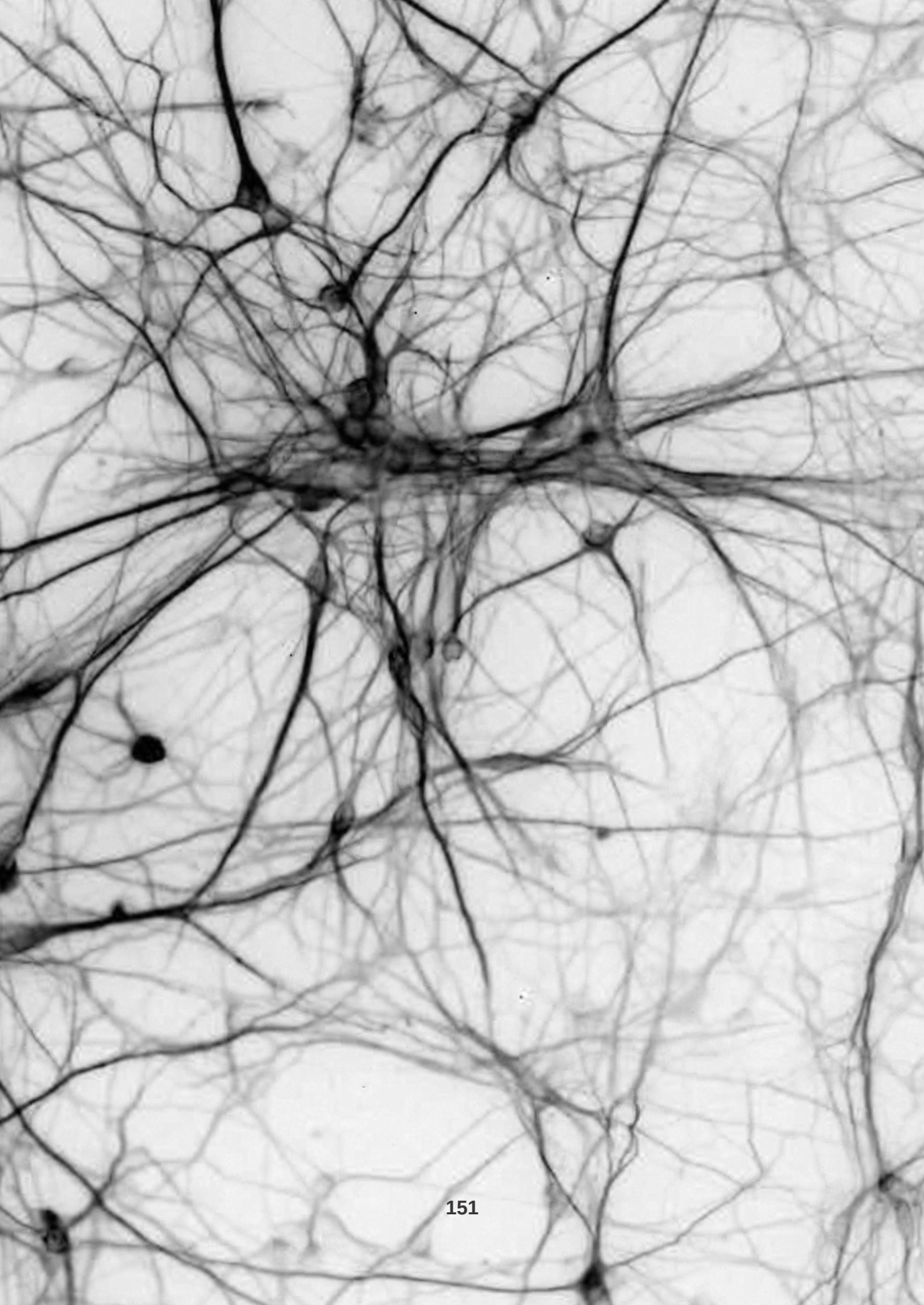

LIMITATIONS AND FUTURE PERSPECTIVES

8. FUTURE PERSPECTIVES

Our study successfully addressed the outlined objectives, providing a comprehensive understanding of CHI3L1-induced effects in a human neuronal model. The observed morphological, functional, and molecular changes highlight the neurotoxicity of CHI3L1, with implications for neurodegenerative processes. The identified molecular pathways, including STAT1 activation, open avenues for further research and targeted therapeutic interventions in neurodegenerative diseases. Despite inherent challenges, the chosen hiPSC-derived neuronal model proved to be a valuable tool in deciphering the complex effects of CHI3L1 on human neurons.

Our transcriptomic profiling revealed pleiotropic effects of CHI3L1 on hiPSC-derived neurons, impacting multiple pathways and altering gene expression. However, the diffuse effects of CHI3L1 treatment on transcription, as evidenced by the PVCA analysis, pose challenges in identifying specific DEGs and concrete pathways. Future studies employing advanced methodologies, such as single-cell RNA sequencing, may provide a more robust understanding of CHI3L1-induced transcriptional changes in individual cell types within the neuronal cultures.

Despite these limitations, our study sets the stage for further investigations into the molecular mechanisms underlying CHI3L1-induced neurotoxicity. Elucidating the intricate signaling pathways affected by CHI3L1 will contribute to the development of targeted therapeutic interventions for neurodegenerative diseases, opening new avenues for precision medicine in MS and beyond.

Future investigations should focus on unravelling the precise mechanisms through which CHI3L1 influences specific molecular pathways and receptors in neurons. The identification and characterization of CHI3L1 receptors will be pivotal, opening avenues for targeted therapeutic interventions. Additionally, a deeper exploration of the temporal dynamics and the signaling events triggered by CHI3L1 is warranted to elucidate the intricate interplay of neurotoxic effects over time.

The comprehensive insights provided by this study pave the way for further research aimed at developing targeted therapeutic approaches to mitigate the

neurodegenerative impact of CHI3L1. Understanding the molecular intricacies of CHI3L1-induced effects on human neurons not only expands our knowledge of MS pathogenesis but also offers potential strategies for intervention in other neurodegenerative diseases.

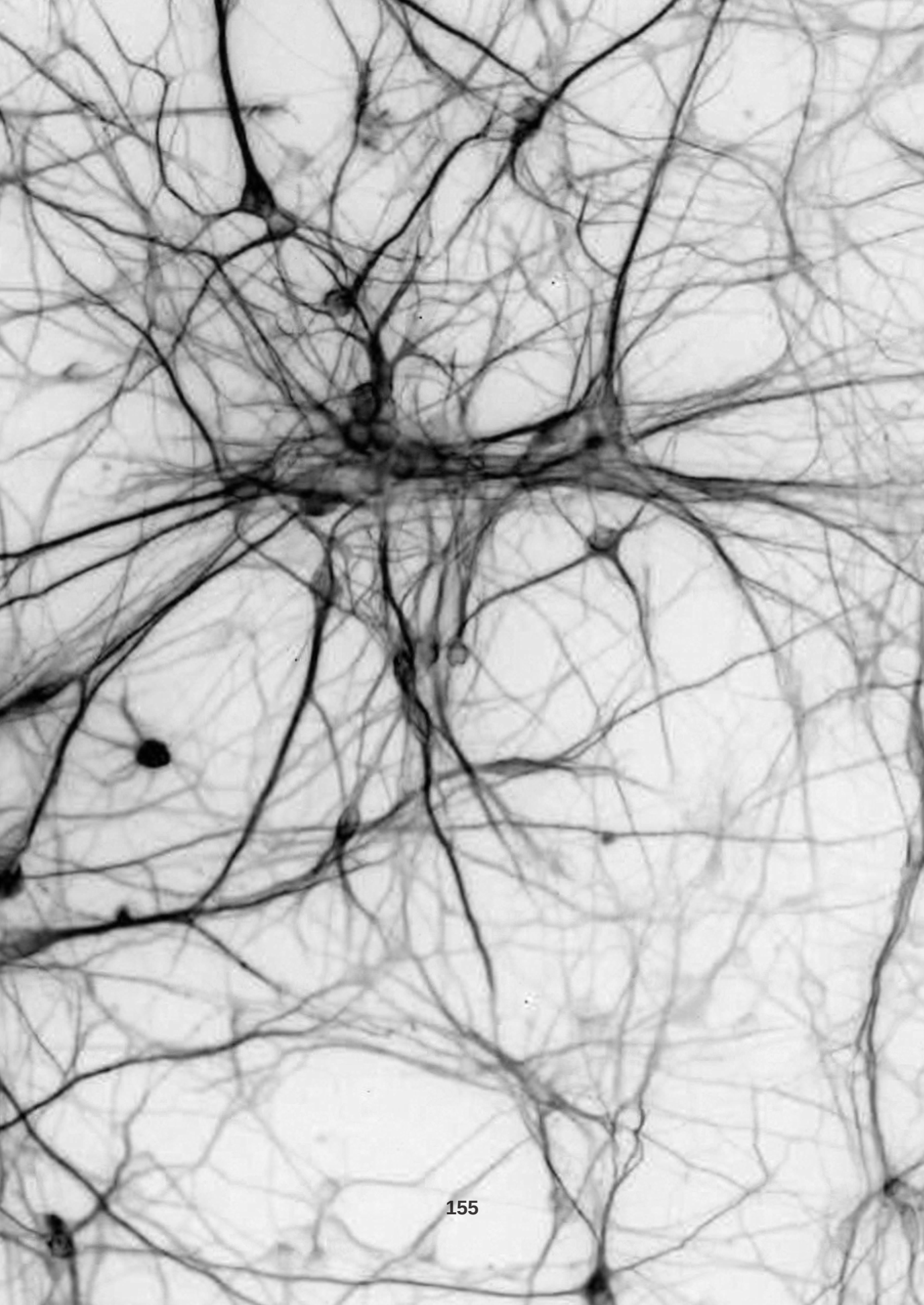

BIBLIOGRAPHY

9. BIBLIOGRAPHY

1. Global, regional, and national burden of multiple sclerosis 1990-2016: a systematic analysis for the Global Burden of Disease Study 2016. Lancet Neurol. England; 2019;18:269–285.

2. Goldenberg MM. Multiple sclerosis review. P T [online serial]. 2012;37:175–184. Accessed at: http://www.pubmedcentral.nih.gov/articlerender.fcgi?artid=3351877&tool=pmcentrez&rendertype=abstract.

3. Hauser SL, Oksenberg JR. The Neurobiology of Multiple Sclerosis: Genes, Inflammation, and Neurodegeneration. Neuron. 2006;52:61–76.

4. Kasper LH, Shoemaker J. Multiple sclerosis immunology: The healthy immune system vs the MS immune system. Neurology. 2010;74.

5. Sospedra M, Martin R. Immunology of Multiple Sclerosis. Semin Neurol. 2016;36:115–127.

6. Soldan SS, Lieberman PM. Epstein–Barr virus and multiple sclerosis. Nat Rev Microbiol. Springer US; 2023;21:51–64.

7. Harbo HF, Gold R, Tintoré M. Sex and gender issues in multiple sclerosis. Ther Adv Neurol Disord. England; 2013;6:237–248.

8. Olsson T, Barcellos LF, Alfredsson L. Interactions between genetic, lifestyle and environmental risk factors for multiple sclerosis. Nat Rev Neurol [online serial]. Nature Publishing Group; 2016;13:26–36. Accessed at: http://dx.doi.org/10.1038/nrneurol.2016.187.

9. Boiko A, Vorobeychik G, Paty D, Devonshire V, Sadovnick D. Early onset multiple sclerosis: a longitudinal study. Neurology. United States; 2002;59:1006–1010.

10. Tremlett H, Devonshire V. Is late-onset multiple sclerosis associated with a

worse outcome? Neurology. United States; 2006;67:954–959.

11. Lublin FD, Reingold SC, Cohen JA, et al. Defining the clinical course of multiple sclerosis: the 2013 revisions. Neurology. United States; 2014;83:278–286.

12. Thompson AJ, Banwell BL, Barkhof F, et al. Diagnosis of multiple sclerosis: 2017 revisions of the McDonald criteria. Lancet Neurol. England; 2018;17:162–173.

13. Lassmann H, Brück W, Lucchinetti CF. The immunopathology of multiple sclerosis: An overview. Brain Pathol. 2007;17:210–218.

14. Lassmann H. Multiple sclerosis pathology. Cold Spring Harb Perspect Med. 2018;8:1–16.

15. Dutta R, Trapp BD. Pathogenesis of axonal and neuronal damage in multiple sclerosis. Neurology. 2007;68.

16. Miller DH, Barkhof F, Frank JA, Parker GJM, Thompson AJ. Measurement of atrophy in multiple sclerosis: pathological basis, methodological aspects and clinical relevance. Brain. England; 2002;125:1676–1695.

17. Lassmann H, Van Horssen J, Mahad D. Progressive multiple sclerosis: Pathology and pathogenesis. Nat Rev Neurol [online serial]. Nature Publishing Group; 2012;8:647–656. Accessed at: http://dx.doi.org/10.1038/nrneurol.2012.168.

18. Frischer JM, Bramow S, Dal-Bianco A, et al. The relation between inflammation and neurodegeneration in multiple sclerosis brains. Brain. 2009;132:1175–1189.

19. Kutzelnigg A, Lucchinetti CF, Stadelmann C, et al. Cortical demyelination and diffuse white matter injury in multiple sclerosis. Brain. England; 2005;128:2705–2712.

20. Hohlfeld R, Wekerle H. Autoimmune concepts of multiple sclerosis as a basis for selective immunotherapy: from pipe dreams to (therapeutic) pipelines. Proc Natl Acad Sci U S A. United States; 2004;101 Suppl:14599–14606.

21. Filippi M, Bar- A, Piehl F, et al. Multiple sclerosis. Epub 2018.:1–27.

22. Trapp BD, Nave K-A. Multiple Sclerosis: An Immune or Neurodegenerative Disorder? Annu Rev Neurosci [online serial]. 2008;31:247–269. Accessed at: http://www.annualreviews.org/doi/10.1146/annurev.neuro.30.051606.094313 .

23. Dendrou CA, Fugger L, Friese MA. Immunopathology of multiple sclerosis. Nat Rev Immunol [online serial]. Nature Publishing Group; 2015;15:545–558. Accessed at: http://dx.doi.org/10.1038/nri3871.

24. van der Star BJ, Vogel DY, Kipp M, Puentes F, Baker D, Amor S. In vitro and in vivo models of multiple sclerosis. CNS Neurol Disord Drug Targets [online serial]. 2012;11:570–588. Accessed at: http://www.ncbi.nlm.nih.gov/pubmed/22583443.

25. Chen W, Sivaprasad U, Tabata Y, et al. Neuroprotective effects of apigenin against inflammation, neuronal excitability and apoptosis in an induced pluripotent stem cell model of Alzheimer's disease. Sci Rep [online serial]. Nature Publishing Group; 2016;11:1–16. Accessed at: http://www.jimmunol.org/cgi/doi/10.4049/jimmunol.182.2.1167.

26. McFarland HF, Martin R. Multiple sclerosis: A complicated picture of autoimmunity. Nat Immunol. 2007;8:913–919.

27. Jadidi-Niaragh F, Mirshafiey A. Th17 Cell, the new player of neuroinflammatory process in multiple sclerosis. Scand J Immunol. 2011;74:1–13.

28. Häggmark A, Byström S, Ayoglu B, et al. Antibody-based profiling of cerebrospinal fluid within multiple sclerosis. Proteomics. 2013;13:2256–2267.

29. Steinman L, Zamvil S. Transcriptional analysis of targets in multiple sclerosis. Nat Rev Immunol. Nature Publishing Group; 2003;3:483.

30. Tzartos JS, Friese MA, Craner MJ, et al. Interleukin-17 production in central nervous system-infiltrating T cells and glial cells is associated with active disease in multiple sclerosis. Am J Pathol. 2008;172:146–155.

31. Siffrin V, Radbruch H, Glumm R, et al. In Vivo Imaging of Partially Reversible Th17 Cell-Induced Neuronal Dysfunction in the Course of Encephalomyelitis. Immunity. Elsevier; 2018;33:424–436.

32. Segal BM. Th17 cells in autoimmune demyelinating disease. Semin Immunopathol. 2010;32:71–77.

33. Wagner CA, Roqué PJ, Mileur TR, Liggitt D, Goverman JM. Myelin-specific CD8+ T cells exacerbate brain inflammation in CNS autoimmunity. J Clin Invest. United States; 2020;130:203–213.

34. Ellwardt E, Zipp F. Molecular mechanisms linking neuroinflammation and neurodegeneration in MS. Exp Neurol. 2014;262:8–17.

35. Hauser SL, Waubant E, Arnold DL, et al. B-Cell Depletion with Rituximab in Relapsing–Remitting Multiple Sclerosis. N Engl J Med. Massachusetts Medical Society; 2008;358:676–688.

36. Vogel DYS, Vereyken EJF, Glim JE, et al. Macrophages in inflammatory multiple sclerosis lesions have an intermediate activation status. J Neuroinflammation [online serial]. 2013;10:809. Accessed at: https://doi.org/10.1186/1742-2094-10-35.

37. Filippi M, Bar-Or A, Piehl F, et al. Multiple sclerosis. Nat Rev Dis Prim [online serial]. Springer US; 2018;4:1–27. Accessed at: http://dx.doi.org/10.1038/s41572-018-0041-4.

38. Mandolesi G, Gentile A, Musella A, et al. Synaptopathy connects inflammation and neurodegeneration in multiple sclerosis. Nat Rev Neurol. 2015;11:711–

724.

39. Schäfers M, Sorkin L. Effect of cytokines on neuronal excitability. Neurosci Lett. Ireland; 2008;437:188–193.

40. Rossi S, Furlan R, De Chiara V, et al. Interleukin-1β causes synaptic hyperexcitability in multiple sclerosis. Ann Neurol. United States; 2012;71:76–83.

41. Rossi S, Motta C, Studer V, et al. Tumor necrosis factor is elevated in progressive multiple sclerosis and causes excitotoxic neurodegeneration. Mult Scler. England; 2014;20:304–312.

42. Dutta R, Trapp B. Mechanisms of neuronal dysfunction and degeneration in multiple sclerosis. Prog Neurobiol [online serial]. 2011;93:1–12. Accessed at: http://www.sciencedirect.com/science/article/pii/S030100821000170X.

43. Platt SR. The role of glutamate in central nervous system health and disease – A review. Vet J [online serial]. 2007;173:278–286. Accessed at: https://www.sciencedirect.com/science/article/pii/S1090023305002893.

44. Stover JF, Pleines UE, Morganti-Kossmann MC, Kossmann T, Lowitzsch K, Kempski OS. Neurotransmitters in cerebrospinal fluid reflect pathological activity. Eur J Clin Invest. England; 1997;27:1038–1043.

45. Sarchielli P, Greco L, Floridi A, Floridi A, Gallai V. Excitatory amino acids and multiple sclerosis: evidence from cerebrospinal fluid. Arch Neurol. United States; 2003;60:1082–1088.

46. Kostic M, Zivkovic N, Stojanovic I. Multiple sclerosis and glutamate excitotoxicity. Rev Neurosci. 2013;24:71–88.

47. Pitt D, Werner P, Raine CS. Glutamate excitotoxicity in a model of multiple sclerosis. Nat Med [online serial]. 2000;6:67–70. Accessed at: http://www.ncbi.nlm.nih.gov/cgi-bin/Entrez/referer?http://library.medicine.nature.com/server-

java/Propub/medicine/nm0100_67.fulltext.

48. Schwarz K, Schmitz F. Synapse Dysfunctions in Multiple Sclerosis. Int J Mol Sci. 2023;24.

49. Waxman SG. Ion channels and neuronal dysfunction in multiple sclerosis. Arch Neurol. 2002;59:1377–1380.

50. Waxman SG. Sodium channels as molecular targets in multiple sclerosis. J Rehabil Res Dev. United States; 2002;39:233–242.

51. Friese MA, Schattling B, Fugger L. Mechanisms of neurodegeneration and axonal dysfunction in multiple sclerosis. Nat Rev Neurol [online serial]. Nature Publishing Group; 2014;10:225–238. Accessed at: http://dx.doi.org/10.1038/nrneurol.2014.37.

52. Wegner C, Esiri MM, Chance SA, Palace J, Matthews PM. Neocortical neuronal, synaptic, and glial loss in multiple sclerosis. Neurology. United States; 2006;67:960–967.

53. De Stefano N, Matthews PM, Filippi M, et al. Evidence of early cortical atrophy in MS: relevance to white matter changes and disability. Neurology. United States; 2003;60:1157–1162.

54. Calabrese M, Agosta F, Rinaldi F, et al. Cortical lesions and atrophy associated with cognitive impairment in relapsing-remitting multiple sclerosis. Arch Neurol. United States; 2009;66:1144–1150.

55. Dutta R, Chang A, Doud MK, et al. Demyelination causes synaptic alterations in hippocampi from multiple sclerosis patients. Ann Neurol. United States; 2011;69:445–454.

56. Gonsette RE. Oxidative stress and excitotoxicity: A therapeutic issue in multiple sclerosis? Mult Scler. 2008;14:22–34.

57. Gonsette RE. Neurodegeneration in multiple sclerosis: The role of oxidative

stress and excitotoxicity. J Neurol Sci. 2008;274:48–53.

58. Hametner S, Wimmer I, Haider L, Pfeifenbring S, Brück W, Lassmann H. Iron and neurodegeneration in the multiple sclerosis brain. Ann Neurol. United States; 2013;74:848–861.

59. Lassmann H, Van Horssen J. The molecular basis of neurodegeneration in multiple sclerosis. FEBS Lett [online serial]. Federation of European Biochemical Societies; 2011;585:3715–3723. Accessed at: http://dx.doi.org/10.1016/j.febslet.2011.08.004.

60. Fischer MT, Wimmer I, Höftberger R, et al. Disease-specific molecular events in cortical multiple sclerosis lesions. Brain. England; 2013;136:1799–1815.

61. Gunasekar PG, Kanthasamy AG, Borowitz JL, Isom GE. NMDA Receptor Activation Produces Concurrent Generation of Nitric Oxide and Reactive Oxygen Species: Implications for Cell Death. J Neurochem. 2002;65:2016–2021.

62. Dutta R, McDonough J, Yin X, et al. Mitochondrial dysfunction as a cause of axonal degeneration in multiple sclerosis patients. Ann Neurol. United States; 2006;59:478–489.

63. Friese MA, Schattling B, Fugger L. Mechanisms of neurodegeneration and axonal dysfunction in multiple sclerosis. Nat Rev Neurol. Nature Publishing Group; 2014;10:225–238.

64. Torkildsen O, Myhr KM, Bø L. Disease-modifying treatments for multiple sclerosis - a review of approved medications. Eur J Neurol. 2016;23:18–27.

65. Limmroth V, Putzki N, Kachuck NJ. The interferon beta therapies for treatment of relapsing-remitting multiple sclerosis: are they equally efficacious? A comparative review of open-label studies evaluating the efficacy, safety, or dosing of different interferon beta formulations alone or . Ther Adv Neurol Disord. England; 2011;4:281–296.

66. Comi G, Filippi M, Wolinsky JS. European/Canadian multicenter, double-blind, randomized, placebo-controlled study of the effects of glatiramer acetate on magnetic resonance imaging--measured disease activity and burden in patients with relapsing multiple sclerosis. European/Canadian GI. Ann Neurol. United States; 2001;49:290–297.

67. Kappos L, Radue E-W, O'Connor P, et al. A placebo-controlled trial of oral fingolimod in relapsing multiple sclerosis. N Engl J Med. United States; 2010;362:387–401.

68. Lassiter G, Melancon C, Rooney T, et al. Ozanimod to Treat Relapsing Forms of Multiple Sclerosis: A Comprehensive Review of Disease, Drug Efficacy and Side Effects. Neurol Int. Switzerland; 2020;12:89–108.

69. Ruggieri S, Quartuccio ME, Prosperini L. Ponesimod in the Treatment of Relapsing Forms of Multiple Sclerosis: An Update on the Emerging Clinical Data. Degener Neurol Neuromuscul Dis. New Zealand; 2022;12:61–73.

70. Dubey D, Kieseier BC, Hartung HP, et al. Dimethyl fumarate in relapsing-remitting multiple sclerosis: rationale, mechanisms of action, pharmacokinetics, efficacy and safety. Expert Rev Neurother. England; 2015;15:339–346.

71. O'Connor P, Wolinsky JS, Confavreux C, et al. Randomized trial of oral teriflunomide for relapsing multiple sclerosis. N Engl J Med. United States; 2011;365:1293–1303.

72. Giovannoni G, Soelberg Sorensen P, Cook S, et al. Efficacy of Cladribine Tablets in high disease activity subgroups of patients with relapsing multiple sclerosis: A post hoc analysis of the CLARITY study. Mult Scler. England; 2019;25:819–827.

73. Polman CH, O'Connor PW, Havrdova E, et al. A randomized, placebo-controlled trial of natalizumab for relapsing multiple sclerosis. N Engl J Med. United States; 2006;354:899–910.

74. Heming M, Wiendl H. Learning multiple sclerosis immunopathogenesis from anti-CD20 therapy. Proc Natl Acad Sci U S A. United States; 2023;120:e2221544120.

75. Krämer J, Bar-Or A, Turner TJ, Wiendl H. Bruton tyrosine kinase inhibitors for multiple sclerosis. Nat Rev Neurol. Springer US; 2023;19:289–304.

76. Pinteac R, Montalban X, Comabella M. Chitinases and chitinase-like proteins as biomarkers in neurologic disorders. Neurol. Neuroimmunol. neuroinflammation 2021.

77. Comabella M, Montalban X. Body fluid biomarkers in multiple sclerosis. Lancet Neurol. 2014;13:113–126.

78. Paul A, Comabella M, Gandhi R. Biomarkers in Multiple Sclerosis. Cold Spring Harb Perspect Med. United States; 2019;9.

79. Delcoigne B, Manouchehrinia A, Barro C, et al. Blood neurofilament light levels segregate treatment effects in multiple sclerosis. Neurology. United States; 2020;94:e1201–e1212.

80. Barro C, Healy BC, Liu Y, et al. Serum GFAP and NfL Levels Differentiate Subsequent Progression and Disease Activity in Patients With Progressive Multiple Sclerosis. Neurol Neuroimmunol NeuroInflammation. 2023;10.

81. Comabella M, Fernández M, Martin R, et al. Cerebrospinal fluid chitinase 3-like 1 levels are associated with conversion to multiple sclerosis. Brain. 2010;133:1082–1093.

82. Cantó E, Reverter F, Morcillo-Suárez C, et al. Chitinase 3-like 1 plasma levels are increased in patients with progressive forms of multiple sclerosis. Mult Scler. England; 2012;18:983–990.

83. Canto E, Tintore M, Villar LM, et al. Chitinase 3-like 1: Prognostic biomarker in clinically isolated syndromes. Brain. 2015;138:918–931.

84. Hinsinger G, Galéotti N, Nabholz N, et al. Chitinase 3-like proteins as diagnostic and prognostic biomarkers of multiple sclerosis. Mult Scler J [online serial]. SAGE Publications Ltd STM; 2015;21:1251–1261. Accessed at: https://doi.org/10.1177/1352458514561906.

85. Modvig S, Degn M, Roed H, et al. Cerebrospinal fluid levels of chitinase 3-like 1 and neurofilament light chain predict multiple sclerosis development and disability after optic neuritis. Mult Scler. England; 2015;21:1761–1770.

86. Martínez MAM, Olsson B, Bau L, et al. Glial and neuronal markers in cerebrospinal fluid predict progression in multiple sclerosis. Mult Scler J [online serial]. SAGE Publications Ltd STM; 2015;21:550–561. Accessed at: https://doi.org/10.1177/1352458514549397.

87. Burman J, Raininko R, Blennow K, Zetterberg H, Axelsson M, Malmeström C. YKL-40 is a CSF biomarker of intrathecal inflammation in secondary progressive multiple sclerosis. J Neuroimmunol. Netherlands; 2016;292:52–57.

88. Gil-Perotin S, Castillo-Villalba J, Cubas-Nuñez L, et al. Combined Cerebrospinal Fluid Neurofilament Light Chain Protein and Chitinase-3 Like-1 Levels in Defining Disease Course and Prognosis in Multiple Sclerosis. Front Neurol. 2019;10:1008.

89. Håkansson I, Tisell A, Cassel P, et al. Neurofilament levels, disease activity and brain volume during follow-up in multiple sclerosis. J Neuroinflammation. 2018;15:209.

90. Matute-Blanch C, Río J, Villar LM, et al. Chitinase 3-like 1 is associated with the response to interferon-beta treatment in multiple sclerosis. J Neuroimmunol [online serial]. Elsevier B.V.; 2017;303:62–65. Accessed at: http://dx.doi.org/10.1016/j.jneuroim.2016.12.006.

91. Alcolea D, Vilaplana E, Pegueroles J, et al. Relationship between cortical thickness and cerebrospinal fluid YKL-40 in predementia stages of

Alzheimer's disease. Neurobiol Aging. United States; 2015;36:2018–2023.

92. Baldacci F, Toschi N, Lista S, et al. Two-level diagnostic classification using cerebrospinal fluid YKL-40 in Alzheimer's disease. Alzheimers Dement. United States; 2017;13:993–1003.

93. Janelidze S, Hertze J, Zetterberg H, et al. Cerebrospinal fluid neurogranin and YKL-40 as biomarkers of Alzheimer's disease. Ann Clin Transl Neurol. 2016;3:12–20.

94. Janelidze S, Mattsson N, Stomrud E, et al. CSF biomarkers of neuroinflammation and cerebrovascular dysfunction in early Alzheimer disease. Neurology. 2018;91:e867–e877.

95. Craig-Schapiro R, Perrin RJ, Roe CM, et al. YKL-40: a novel prognostic fluid biomarker for preclinical Alzheimer's disease. Biol Psychiatry. 2010;68:903–912.

96. Kester MI, Teunissen CE, Sutphen C, et al. Cerebrospinal fluid VILIP-1 and YKL-40, candidate biomarkers to diagnose, predict and monitor Alzheimer's disease in a memory clinic cohort. Alzheimers Res Ther. 2015;7:59.

97. Alcolea D, Martínez-Lage P, Sánchez-Juan P, et al. Amyloid precursor protein metabolism and inflammation markers in preclinical Alzheimer disease. Neurology. United States; 2015;85:626–633.

98. Teunissen CE, Elias N, Koel-Simmelink MJA, et al. Novel diagnostic cerebrospinal fluid biomarkers for pathologic subtypes of frontotemporal dementia identified by proteomics. Alzheimer's Dement (Amsterdam, Netherlands). 2016;2:86–94.

99. Wennström M, Surova Y, Hall S, et al. The Inflammatory Marker YKL-40 Is Elevated in Cerebrospinal Fluid from Patients with Alzheimer's but Not Parkinson's Disease or Dementia with Lewy Bodies. PLoS One. 2015;10:e0135458.

100. Thompson AG, Gray E, Thézénas M-L, et al. Cerebrospinal fluid macrophage biomarkers in amyotrophic lateral sclerosis. Ann Neurol. 2018;83.

101. Thompson AG, Gray E, Bampton A, Raciborska D, Talbot K, Turner MR. CSF chitinase proteins in amyotrophic lateral sclerosis. J Neurol Neurosurg Psychiatry. 2019;90:1215–1220.

102. Abu-Rumeileh S, Vacchiano V, Zenesini C, et al. Diagnostic-prognostic value and electrophysiological correlates of CSF biomarkers of neurodegeneration and neuroinflammation in amyotrophic lateral sclerosis. J Neurol. Epub 2020.

103. Gille B, De Schaepdryver M, Dedeene L, et al. Inflammatory markers in cerebrospinal fluid: Independent prognostic biomarkers in amyotrophic lateral sclerosis? J Neurol Neurosurg Psychiatry. 2019;90:1338–1346.

104. Vu L, An J, Kovalik T, Gendron T, Petrucelli L, Bowser R. Cross-sectional and longitudinal measures of chitinase proteins in amyotrophic lateral sclerosis and expression of CHI3L1 in activated astrocytes. J Neurol Neurosurg Psychiatry. Epub 2020.:350–358.

105. Andrés-Benito P, Domínguez R, Colomina MJ, Llorens F, Povedano M, Ferrer I. YKL40 in sporadic amyotrophic lateral sclerosis: cerebrospinal fluid levels as a prognosis marker of disease progression. Aging (Albany NY) [online serial]. Impact Journals; 2018;10:2367–2382. Accessed at: https://pubmed.ncbi.nlm.nih.gov/30215603.

106. Illán-Gala I, Alcolea D, Montal V, et al. CSF sAPPβ, YKL-40, and NfL along the ALS-FTD spectrum. Neurology. 2018;91:E1619–E1628.

107. Park HY, Jun C-D, Jeon S-J, et al. Serum YKL-40 levels correlate with infarct volume, stroke severity, and functional outcome in acute ischemic stroke patients. PLoS One. United States; 2012;7:e51722.

108. Chen X-L, Li Q, Huang W-S, et al. Serum YKL-40, a prognostic marker in patients with large-artery atherosclerotic stroke. Acta Neurol Scand. Denmark;

2017;136:97–102.

109. Kjaergaard AD, Bojesen SE, Johansen JS, Nordestgaard BG. Elevated plasma YKL-40 levels and ischemic stroke in the general population. Ann Neurol. 2010;68:672–680.

110. Kjaergaard AD, Johansen JS, Bojesen SE, Nordestgaard BG. Elevated plasma YKL-40, lipids and lipoproteins, and ischemic vascular disease in the general population. Stroke. 2015;46:329–335.

111. Rathcke CN, Thomsen SB, Linneberg A, Vestergaard H. Variations of CHI3L1, levels of the encoded glycoprotein YKL-40 and prediction of fatal and non-fatal ischemic stroke. PLoS One. 2012;7.

112. Ridker PM, Chasman DI, Rose L, Loscalzo J, Elias JA. Plasma levels of the proinflammatory chitin-binding glycoprotein YKL-40, variation in the chitinase 3-like 1 gene (CHI3l1), and incident cardiovascular events. J Am Heart Assoc. 2014;3:1–17.

113. Bonneh-Barkay D, Zagadailov P, Zou H, et al. YKL-40 expression in traumatic brain injury: An initial analysis. J Neurotrauma. 2010;27:1215–1223.

114. Carabias CS, Gomez PA, Panero I, et al. Chitinase-3-Like Protein 1, Serum Amyloid A1, C-Reactive Protein, and Procalcitonin Are Promising Biomarkers for Intracranial Severity Assessment of Traumatic Brain Injury: Relationship with Glasgow Coma Scale and Computed Tomography Volumetry. World Neurosurg. United States; 2020;134:e120–e143.

115. Shahim P, Tegner Y, Marklund N, et al. Astroglial activation and altered amyloid metabolism in human repetitive concussion. Neurology. 2017;88:1400–1407.

116. Llorens F, Thüne K, Tahir W, et al. YKL-40 in the brain and cerebrospinal fluid of neurodegenerative dementias. Mol Neurodegener. 2017;12:83.

117. Abu-Rumeileh S, Steinacker P, Polischi B, et al. CSF biomarkers of

neuroinflammation in distinct forms and subtypes of neurodegenerative dementia. Alzheimer's Res Ther. Alzheimer's Research & Therapy; 2019;12:1–15.

118. Villar-Piqué A, Schmitz M, Hermann P, et al. Plasma YKL-40 in the spectrum of neurodegenerative dementia. J Neuroinflammation. Journal of Neuroinflammation; 2019;16:1–5.

119. Funkhouser JD, Aronson NN. Chitinase family GH18: Evolutionary insights from the genomic history of a diverse protein family. BMC Evol Biol. 2007;7:1–16.

120. Guan S-P, Mok Y-K, Koo K-N, Chu K-L, Wong WS. Chitinases: Biomarkers for Human Diseases. Protein Pept Lett. 2009;16:490–498.

121. Patel S, Goyal A. Chitin and chitinase: Role in pathogenicity, allergenicity and health. Int J Biol Macromol [online serial]. Elsevier B.V.; 2017;97:331–338. Accessed at: http://dx.doi.org/10.1016/j.ijbiomac.2017.01.042.

122. Deutschmann C, Roggenbuck D, Schierack P. The loss of tolerance to CHI3L1 - A putative role in inflammatory bowel disease? Clin Immunol. United States; 2019;199:12–17.

123. Yeo IJ, Lee CK, Han SB, Yun J, Hong JT. Roles of chitinase 3-like 1 in the development of cancer, neurodegenerative diseases, and inflammatory diseases. Pharmacol Ther [online serial]. Elsevier Inc.; 2019;203:107394. Accessed at: https://doi.org/10.1016/j.pharmthera.2019.107394.

124. Di Rosa M, Malaguarnera G, De Gregorio C, Drago F, Malaguarnera L. Evaluation of CHI3L-1 and CHIT-1 expression in differentiated and polarized macrophages. Inflammation. 2013;36:482–492.

125. Di Rosa M, Malaguarnera L. Chitotriosidase: A new inflammatory marker in diabetic complications. Pathobiology. 2016;83:211–219.

126. Libreros S, Iragavarapu-Charyulu V. YKL-40/CHI3L1 drives inflammation on

the road of tumor progression. J Leukoc Biol. United States; 2015;98:931–936.

127. Geng B, Pan J, Zhao T, et al. Chitinase 3-like 1-CD44 interaction promotes metastasis and epithelial-to-mesenchymal transition through β-catenin/Erk/Akt signaling in gastric cancer. J Exp Clin Cancer Res. Journal of Experimental & Clinical Cancer Research; 2018;37:1–20.

128. Shao R, Hamel K, Petersen L, et al. YKL-40, a secreted glycoprotein, promotes tumor angiogenesis. Oncogene [online serial]. Nature Publishing Group; 2009;28:4456–4468. Accessed at: http://dx.doi.org/10.1038/onc.2009.292.

129. Hakala BE, White C, Recklies AD. Human cartilage gp-39, a major secretory product of articular chondrocytes and synovial cells, is a mammalian member of a chitinase protein family. J Biol Chem. United States; 1993;268:25803–25810.

130. Lee CG, Hartl D, Lee GR, et al. Role of breast regression protein 39 (BRP-39)/chitinase 3-like-1 in Th2 and IL-13-induced tissue responses and apoptosis. J Exp Med. 2009;206:1149–1166.

131. Di Rosa M, Tibullo D, Saccone S, et al. CHI3L1 nuclear localization in monocyte derived dendritic cells [online]. Immunobiology Elsevier GmbH.; 2015. Accessed at: http://dx.doi.org/10.1016/j.imbio.2015.09.023.

132. Huang C, Huang B, Bi F, et al. Profiling the genes affected by pathogenic TDP-43 in astrocytes. J Neurochem. 2014;129:932–939.

133. Chen Y, Zhang S, Wang Q, Zhang X. Tumor-recruited M2 macrophages promote gastric and breast cancer metastasis via M2 macrophage-secreted CHI3L1 protein. J Hematol Oncol. Journal of Hematology & Oncology; 2017;10:1–13.

134. Kim DH, Park HJ, Lim S, et al. Regulation of chitinase-3-like-1 in T cell elicits Th1 and cytotoxic responses to inhibit lung metastasis. Nat Commun [online

serial]. Springer US; 2018;9. Accessed at: http://dx.doi.org/10.1038/s41467-017-02731-6.

135. Kognole AA, Payne CM. Inhibition of Mammalian Glycoprotein YKL-40. J Biol Chem. 2017;292:2624–2636.

136. He CH, Lee CG, DelaCruz CS, et al. Chitinase 3-like 1 regulates cellular and tissue responses via IL-13 receptor α2. Cell Rep [online serial]. Elsevier; 2013;4:830–841. Accessed at: http://dx.doi.org/10.1016/j.celrep.2013.07.032.

137. Lee CM, He CH, Nour AM, et al. IL-13Rα2 uses TMEM219 in chitinase 3-like-1-induced signalling and effector responses. Nat Commun [online serial]. Nature Publishing Group; 2016;7:1–12. Accessed at: http://dx.doi.org/10.1038/ncomms12752.

138. Zhou Y, He CH, Herzog EL, et al. Chitinase 3-like-1 and its receptors in Hermansky-Pudlak syndrome-associated lung disease. J Clin Invest. 2015;125:3178–3192.

139. Zhou Y, He CH, Yang DS, et al. Galectin-3 Interacts with the CHI3L1 Axis and Contributes to Hermansky–Pudlak Syndrome Lung Disease. J Immunol. 2018;200:2140–2153.

140. Cao Y, Rudrakshala J, Williams R, et al. CRTH2 Mediates Profibrotic Macrophage Differentiation and Promotes Lung Fibrosis. Am J Respir Cell Mol Biol. United States; 2022;67:201–214.

141. Francescone RA, Scully S, Faibish M, et al. Role of YKL-40 in the angiogenesis, radioresistance, and progression of glioblastoma. J Biol Chem. 2011;286:15332–15343.

142. Low D, Subramaniam R, Lin L, et al. Chitinase 3-like 1 induces survival and proliferation of intestinal epithelial cells during chronic inflammation and colitis-associated cancer by regulating S100A9. Oncotarget [online serial]. Impact Journals LLC; 2015;6:36535–36550. Accessed at:

https://pubmed.ncbi.nlm.nih.gov/26431492.

143. Bonneh-Barkay D, Wang G, Starkey A, Hamilton RL, Wiley CA. In vivo CHI3L1 (YKL-40) expression in astrocytes in acute and chronic neurological diseases. J Neuroinflammation. 2010;7:1–8.

144. Querol-Vilaseca M, Colom-Cadena M, Pegueroles J, et al. YKL-40 (Chitinase 3-like I) is expressed in a subset of astrocytes in Alzheimer's disease and other tauopathies. J Neuroinflammation. Journal of Neuroinflammation; 2017;14:1–10.

145. Bonneh-Barkay D, Bissel SJ, Kofler J, Starkey A, Wang G, Wiley CA. Astrocyte and macrophage regulation of YKL-40 expression and cellular response in neuroinflammation. Brain Pathol. 2012;22:530–546.

146. Singh SK, Bhardwaj R, Wilczynska KM, Dumur CI, Kordula T. A complex of nuclear factor I-X3 and STAT3 regulates astrocyte and glioma migration through the secreted glycoprotein YKL-40. J Biol Chem. 2011;286:39893–39903.

147. Hyvärinen T, Hagman S, Ristola M, et al. Co-stimulation with IL-1β and TNF-α induces an inflammatory reactive astrocyte phenotype with neurosupportive characteristics in a human pluripotent stem cell model system. Sci Rep. 2019;9:1–15.

148. Singh SK, Bhardwaj R, Wilczynska KM, Dumur CI, Kordula T. A complex of nuclear factor I-X3 and STAT3 regulates astrocyte and glioma migration through the secreted glycoprotein YKL-40. J Biol Chem. 2011;286:29893–29903.

149. Ku BM, Lee YK, Ryu J, et al. CHI3L1 (YKL-40) is expressed in human gliomas and regulates the invasion, growth and survival of glioma cells. Int J Cancer. 2011;128:1316–1326.

150. Moreno-Rodriguez M, Perez SE, Nadeem M, Malek-Ahmadi M, Mufson EJ.

Frontal cortex chitinase and pentraxin neuroinflammatory alterations during the progression of Alzheimer's disease. J Neuroinflammation. Journal of Neuroinflammation; 2020;17:1–15.

151. Sanfilippo C, Longo A, Lazzara F, et al. CHI3L1 and CHI3L2 overexpression in motor cortex and spinal cord of sALS patients. Mol Cell Neurosci. 2017;85:162–169.

152. Wurm J, Behringer SP, Ravi VM, et al. Astrogliosis Releases Pro-Oncogenic Chitinase 3-Like 1 Causing MAPK Signaling in Glioblastoma. Cancers (Basel) [online serial]. MDPI; 2019;11:1437. Accessed at: https://pubmed.ncbi.nlm.nih.gov/31561550.

153. Li L, Tian E, Chen X, et al. GFAP Mutations in Astrocytes Impair Oligodendrocyte Progenitor Proliferation and Myelination in an hiPSC Model of Alexander Disease. Cell Stem Cell. 2018;23:239-251.e6.

154. Jiang W, Zhu F, Xu H, et al. CHI3L1 signaling impairs hippocampal neurogenesis and cognitive function in autoimmune-mediated neuroinflammation. Epub 2023.

155. Starossom SC, Campo Garcia J, Woelfle T, et al. Chi3l3 induces oligodendrogenesis in an experimental model of autoimmune neuroinflammation. Nat Commun. 2019;10.

156. Matute-Blanch C, Calvo-Barreiro L, Carballo-Carbajal I, et al. Chitinase 3-like 1 is neurotoxic in primary cultured neurons. Sci Rep. 2020;10:1–6.

157. Im JH, Yeo IJ, Park PH, et al. Deletion of Chitinase-3-like 1 accelerates stroke development through enhancement of Neuroinflammation by STAT6-dependent M2 microglial inactivation in Chitinase-3-like 1 knockout mice. Exp Neurol [online serial]. Elsevier; 2020;323:113082. Accessed at: https://doi.org/10.1016/j.expneurol.2019.113082.

158. Wiley CA, Bonneh-Barkay D, Dixon CE, et al. Role for mammalian chitinase

3-like protein 1 in traumatic brain injury. Neuropathology. 2015;35:95–106.

159. Bonneh-Barkay D, Wang G, Laframboise WA, Wiley CA, Bissel SJ. Exacerbation of experimental autoimmune encephalomyelitis in the absence of breast regression protein 39/chitinase 3-like 1. J Neuropathol Exp Neurol [online serial]. 2012;71:948–958. Accessed at: https://pubmed.ncbi.nlm.nih.gov/23041842.

160. Cantó E, Espejo C, Costa C, Montalban X, Comabella M. Breast regression protein-39 is not required for experimental autoimmune encephalomyelitis induction. Clin Immunol [online serial]. Elsevier B.V.; 2015;160:133–141. Accessed at: http://dx.doi.org/10.1016/j.clim.2015.06.004.

161. Choi JY, Yeo IJ, Kim KC, et al. K284-6111 prevents the amyloid beta-induced neuroinflammation and impairment of recognition memory through inhibition of NF-KB-mediated CHI3L1 expression. J Neuroinflammation. Journal of Neuroinflammation; 2018;15:1–13.

162. Gordon J, Amini S, White MK. Neuronal Cell Culture. Methods Mol Biol [online serial]. 2013;1078:35–44. Accessed at: http://link.springer.com/10.1007/978-1-62703-640-5.

163. Tomita S, Stein V, Stocker TJ, Nicoll RA, Bredt DS. Bidirectional synaptic plasticity regulated by phosphorylation of stargazin-like TARPs. Neuron. 2005;45:269–277.

164. Basarsky TA, Parpura V, Haydon PG. Hippocampal synaptogenesis in cell culture: Developmental time course of synapse formation, calcium influx, and synaptic protein distribution. J Neurosci. 1994;14:6402–6411.

165. Koesters AG, Rich MM, Engisch KL. Homeostatic Synaptic Plasticity of Miniature Excitatory Postsynaptic Currents in Mouse Cortical Cultures Requires Neuronal Rab3A. {eLife} Sciences Publications, Ltd; Epub 2023 Sep. Accessed at: https://doi.org/10.7554/elife.90261.1.

166. Martínez-Mármol R, Barneda-Zahonero B, Soto D, et al. FAIM-L regulation of XIAP degradation modulates Synaptic Long-Term Depression and Axon Degeneration. Sci Rep. Nature Publishing Group; 2016;6:1–16.

167. Tibau E, Valencia M, Soriano J. Identification of neuronal network properties from the spectral analysis of calcium imaging signals in neuronal cultures. Front Neural Circuits. 2013;7:1–16.

168. Stetter O, Battaglia D, Soriano J, Geisel T. Model-Free Reconstruction of Excitatory Neuronal Connectivity from Calcium Imaging Signals. PLoS Comput Biol. 2012;8.

169. Murmu RP, Li W, Holtmaat A, Li J-Y. Dendritic Spine Instability Leads to Progressive Neocortical Spine Loss in a Mouse Model of Huntington's Disease. J Neurosci. 2013;33:12997–13009.

170. Lee D-Y, Jeon GS, Shim Y-M, Seong S-Y, Lee K-W, Sung J-J. Modulation of SOD1 Subcellular Localization by Transfection with Wild- or Mutant-type SOD1 in Primary Neuron and Astrocyte Cultures from ALS Mice. Exp Neurobiol. Korea (South); 2015;24:226–234.

171. Giralt A, Brito V, Chevy Q, et al. Pyk2 modulates hippocampal excitatory synapses and contributes to cognitive deficits in a Huntington's disease model. Nat Commun. 2017;8.

172. Dragunow M. The adult human brain in preclinical drug development. Nat Rev Drug Discov. England; 2008;7:659–666.

173. Takahashi K, Tanabe K, Ohnuki M, et al. Induction of Pluripotent Stem Cells from Adult Human Fibroblasts by Defined Factors. Cell. 2007;131:861–872.

174. Valadez-Barba V, Cota-Coronado A, Hernández-Pérez OR, et al. iPSC for modeling neurodegenerative disorders. Regen Ther. 2020;15:332–339.

175. Al Abbar A, Ngai SC, Nograles N, Alhaji SY, Abdullah S. Induced Pluripotent Stem Cells: Reprogramming Platforms and Applications in Cell Replacement

Therapy. Biores Open Access. United States; 2020;9:121–136.

176. Dolmetsch R, Geschwind DH. The human brain in a dish: The promise of iPSC-derived neurons. Cell [online serial]. Elsevier Inc.; 2011;145:831–834. Accessed at: http://dx.doi.org/10.1016/j.cell.2011.05.034.

177. Barak M, Fedorova V, Pospisilova V, et al. Human iPSC-Derived Neural Models for Studying Alzheimer's Disease: from Neural Stem Cells to Cerebral Organoids. Stem Cell Rev Reports [online serial]. Springer US; 2022;18:792–820. Accessed at: https://doi.org/10.1007/s12015-021-10254-3.

178. Comella-Bolla A, Orlandi JG, Miguez A, et al. Human Pluripotent Stem Cell-Derived Neurons Are Functionally Mature In Vitro and Integrate into the Mouse Striatum Following Transplantation. Mol. Neurobiol. Molecular Neurobiology; 2020.

179. Hemmati-Brivanlou A, Melton D. Vertebrate neural induction. Annu Rev Neurosci. United States; 1997;20:43–60.

180. Urbán N, Guillemot F. Neurogenesis in the embryonic and adult brain: Same regulators, different roles. Front Cell Neurosci. 2014;8:1–19.

181. Monuki ES, Porter FD, Walsh CA. Patterning of the dorsal telencephalon and cerebral cortex by a roof plate-lhx2 pathway. Neuron. 2001;32:591–604.

182. Weick JP. Functional Properties of Human Stem Cell-Derived Neurons in Health and Disease. Stem Cells Int. 2016;2016.

183. Itskovitz-Eldor J, Schuldiner M, Karsenti D, et al. Differentiation of human embryonic stem cells into embryoid bodies compromising the three embryonic germ layers. Mol Med. England; 2000;6:88–95.

184. Chambers SM, Fasano CA, Papapetrou EP, Tomishima M, Sadelain M, Studer L. Highly efficient neural conversion of human ES and iPS cells by dual inhibition of SMAD signaling. Nat Biotechnol. 2009;27:275–280.

185. Han SSW, Williams LA, Eggan KC. Constructing and Deconstructing Stem Cell Models of Neurological Disease. Neuron [online serial]. Elsevier Inc.; 2011;70:626–644. Accessed at: http://dx.doi.org/10.1016/j.neuron.2011.05.003.

186. Zhang Y, Pak CH, Han Y, et al. Rapid single-step induction of functional neurons from human pluripotent stem cells. Neuron. Epub 2013.

187. Estévez-Priego E, Moreno-Fina M, Monni E, Kokaia Z, Soriano J, Tornero D. Long-term calcium imaging reveals functional development in hiPSC-derived cultures comparable to human but not rat primary cultures. Stem Cell Reports. 2023;18:205–219.

188. Kirwan P, Turner-Bridger B, Peter M, et al. Development and function of human cerebral cortex neural networks from pluripotent stem cells in vitro. Dev. 2015;142:3178–3187.

189. Wainger BJ, Kiskinis E, Mellin C, et al. Intrinsic membrane hyperexcitability of amyotrophic lateral sclerosis patient-derived motor neurons. Cell Rep. United States; 2014;7:1–11.

190. Ebert AD, Yu J, Rose FFJ, et al. Induced pluripotent stem cells from a spinal muscular atrophy patient. Nature. England; 2009;457:277–280.

191. Abeliovich A, Hammond R. Midbrain dopamine neuron differentiation: Factors and fates. Dev Biol [online serial]. 2007;304:447–454. Accessed at: https://www.sciencedirect.com/science/article/pii/S0012160607000656.

192. Cheung AYL, Horvath LM, Grafodatskaya D, et al. Isolation of MECP2-null Rett Syndrome patient hiPS cells and isogenic controls through X-chromosome inactivation. Hum Mol Genet. England; 2011;20:2103–2115.

193. Marchetto MCN, Carromeu C, Acab A, et al. A model for neural development and treatment of Rett syndrome using human induced pluripotent stem cells. Cell. United States; 2010;143:527–539.

194. Nguyen HN, Byers B, Cord B, et al. LRRK2 mutant iPSC-derived DA neurons demonstrate increased susceptibility to oxidative stress. Cell Stem Cell. United States; 2011;8:267–280.

195. Carola G, Malagarriga D, Calatayud C, et al. Parkinson's disease patient-specific neuronal networks carrying the LRRK2 G2019S mutation unveil early functional alterations that predate neurodegeneration. npj Park Dis. 2021;7:1–14.

196. Paşca SP, Portmann T, Voineagu I, et al. Using iPSC-derived neurons to uncover cellular phenotypes associated with Timothy syndrome. Nat Med. United States; 2011;17:1657–1662.

197. Ludtmann MHR, Angelova PR, Horrocks MH, et al. α-synuclein oligomers interact with ATP synthase and open the permeability transition pore in Parkinson's disease. Nat Commun [online serial]. Springer US; 2018;9. Accessed at: http://dx.doi.org/10.1038/s41467-018-04422-2.

198. Duan L, Bhattacharyya BJ, Belmadani A, Pan L, Miller RJ, Kessler JA. Stem cell derived basal forebrain cholinergic neurons from Alzheimer's disease patients are more susceptible to cell death. Mol Neurodegener. 2014;9:1–14.

199. Liu Q, Waltz S, Woodruff G, et al. Effect of potent γ-secretase modulator in human neurons derived from multiple presenilin 1-induced pluripotent stem cell mutant carriers. JAMA Neurol. United States; 2014;71:1481–1489.

200. Carcamo-Orive I, Hoffman GE, Cundiff P, et al. Analysis of Transcriptional Variability in a Large Human iPSC Library Reveals Genetic and Non-genetic Determinants of Heterogeneity. Cell Stem Cell. United States; 2017;20:518-532.e9.

201. Hu B-Y, Weick JP, Yu J, et al. Neural differentiation of human induced pluripotent stem cells follows developmental principles but with variable potency. Proc Natl Acad Sci U S A. United States; 2010;107:4335–4340.

202. Rivetti di Val Cervo P, Besusso D, Conforti P, Cattaneo E. hiPSCs for predictive modelling of neurodegenerative diseases: dreaming the possible. Nat Rev Neurol [online serial]. Springer US; 2021;17:381–392. Accessed at: http://dx.doi.org/10.1038/s41582-021-00465-0.

203. Stein JL, de la Torre-Ubieta L, Tian Y, et al. A quantitative framework to evaluate modeling of cortical development by neural stem cells. Neuron. 2014;83:69–86.

204. Vaskova EA, Stekleneva AE, Medvedev SP, Zakian SM. "Epigenetic memory" phenomenon in induced pluripotent stem cells. Acta Naturae. Russia (Federation); 2013;5:15–21.

205. Quintana E, Coll C, Salavedra-Pont J, et al. Cognitive impairment in early stages of multiple sclerosis is associated with high cerebrospinal fluid levels of chitinase 3-like 1 and neurofilament light chain. Eur J Neurol. England; 2018;25:1189–1191.

206. Miquel-Serra L, Duarri A, Muñoz Y, et al. Generation of six multiple sclerosis patient-derived induced pluripotent stem cell lines. Stem Cell Res [online serial]. The Authors; 2017;24:155–159. Accessed at: https://doi.org/10.1016/j.scr.2017.06.001.

207. García-Díaz Barriga G, Giralt A, Anglada-Huguet M, et al. 7,8-dihydroxyflavone ameliorates cognitive and motor deficits in a Huntington's disease mouse model through specific activation of the PLCγ1 pathway. Hum Mol Genet. England; 2017;26:3144–3160.

208. Orlandi JG, Fernández-García S, Comella-Bolla A, et al. NETCAL: An interactive platform for large-scale, NETwork and population dynamics analysis of CALcium imaging recordings. Epub 2017 Nov 12. Accessed at: https://zenodo.org/record/1119026. Accessed July 24, 2023.

209. Fernández-García S, Orlandi JG, García-Díaz Barriga GA, et al. Deficits in coordinated neuronal activity and network topology are striatal hallmarks in

Huntington’s disease. BMC Biol. England; 2020;18:58.

210. Grewe BF, Langer D, Kasper H, Kampa BM, Helmchen F. High-speed in vivo calcium imaging reveals neuronal network activity with near-millisecond precision. Nat Methods. United States; 2010;7:399–405.

211. Montalà-Flaquer M, López-León CF, Tornero D, et al. Rich Dynamics and Functional Organization on Topographically Designed Neuronal Networks *in vitro*. SSRN Electron J. Epub 2022.

212. Bastian M, Heymann S, Jacomy M. Gephi: An Open Source Software for Exploring and Manipulating Networks. Proc Third Int ICWSM Conf [online serial]. Epub 2009.:361–362. Accessed at: http://www.aaai.org/ocs/index.php/ICWSM/09/paper/view/154.

213. Blondel VD, Guillaume J-L, Lambiotte R, Lefebvre E. Fast unfolding of communities in large networks. J Stat Mech Theory Exp [online serial]. 2008;2008:P10008. Accessed at: https://dx.doi.org/10.1088/1742-5468/2008/10/P10008.

214. Smyth GK. Linear models and empirical bayes methods for assessing differential expression in microarray experiments. Stat Appl Genet Mol Biol. Germany; 2004;3:Article3.

215. Gu Z, Hübschmann D. simplifyEnrichment: A Bioconductor Package for Clustering and Visualizing Functional Enrichment Results. Genomics Proteomics Bioinformatics [online serial]. 2023;21:190–202. Accessed at: https://www.sciencedirect.com/science/article/pii/S1672022922000730.

216. Livak KJ, Schmittgen TD. Analysis of relative gene expression data using real-time quantitative PCR and the 2(-Delta Delta C(T)) Method. Methods. United States; 2001;25:402–408.

217. Zhou Y, Zhou B, Pache L, et al. Metascape provides a biologist-oriented resource for the analysis of systems-level datasets. Nat Commun. England;

2019;10:1523.

218. Libreros S, Garcia-Areas R, Shibata Y, Carrio R, Torroella-Kouri M, Iragavarapu-Charyulu V. Induction of proinflammatory mediators by CHI3L1 is reduced by chitin treatment: Decreased tumor metastasis in a breast cancer model. Int J Cancer. 2012;131:377–386.

219. Eurich K, Segawa M, Toei-Shimizu S, Mizoguchi E. Potential role of chitinase 3-like-1 in inflammation-associated carcinogenic changes of epithelial cells. World J Gastroenterol. 2009;15:5249–5259.

220. Stankiewicz TR, Linseman DA. Rho family GTPases: Key players in neuronal development, neuronal survival, and neurodegeneration. Front Cell Neurosci. 2014;8:1–14.

221. Gagnon KB, Delpire E. Sodium Transporters in Human Health and Disease. Front Physiol. 2021;11:1–18.

222. Ferrer I, Garcia-Esparcia P, Carmona M, et al. Olfactory receptors in non-chemosensory organs: The nervous system in health and disease. Front Aging Neurosci. 2016;8:1–17.

223. Tracey TJ, Steyn FJ, Wolvetang EJ, Ngo ST. Neuronal lipid metabolism: Multiple pathways driving functional outcomes in health and disease. Front Mol Neurosci. 2018;11:1–25.

224. Koseoglu MM, Norambuena A, Sharlow ER, Lazo JS, Bloom GS. Aberrant Neuronal Cell Cycle Re-Entry: The Pathological Confluence of Alzheimer's Disease and Brain Insulin Resistance, and Its Relation to Cancer. J Alzheimers Dis. Netherlands; 2019;67:1–11.

225. Han H, Shim H, Shin D, et al. TRRUST: A reference database of human transcriptional regulatory interactions. Sci Rep. Nature Publishing Group; 2015;5:1–11.

226. Cerezo EL, Houles T, Lié O, et al. RIOK2 phosphorylation by RSK promotes

synthesis of the human small ribosomal subunit. PLoS Genet. United States; 2021;17:e1009583.

227. Kumar R, Francis V, Kulasekaran G, Khan M, Armstrong GAB, McPherson PS. A cell-based GEF assay reveals new substrates for DENN domains and a role for DENND2B in primary ciliogenesis. Sci Adv. United States; 2022;8:eabk3088.

228. King PD, Lubeck BA, Lapinski PE. Nonredundant functions for Ras GTPase-activating proteins in tissue homeostasis. Sci Signal. United States; 2013;6:re1.

229. Pedraza N, Ortiz R, Cornadó A, Llobet A, Aldea M, Gallego C. KIS, a kinase associated with microtubule regulators, enhances translation of AMPA receptors and stimulates dendritic spine remodeling. J Neurosci Off J Soc Neurosci. United States; 2014;34:13988–13997.

230. Woitecki AMH, Müller JA, van Loo KMJ, Sowade RF, Becker AJ, Schoch S. Identification of Synaptotagmin 10 as Effector of NPAS4-Mediated Protection from Excitotoxic Neurodegeneration. J Neurosci Off J Soc Neurosci. United States; 2016;36:2561–2570.

231. Yang M-H, Chen Y-MA, Tu S-C, et al. Utilizing an Animal Model to Identify Brain Neurodegeneration-Related Biomarkers in Aging. Int J Mol Sci. Switzerland; 2021;22.

232. Hall S, Surova Y, Öhrfelt A, Blennow K, Zetterberg H, Hansson O. Longitudinal Measurements of Cerebrospinal Fluid Biomarkers in Parkinson's Disease. Mov Disord. 2016;31:898–905.

233. Hermansson L, Yilmaz A, Axelsson M, et al. Cerebrospinal fluid levels of glial marker YKL-40 strongly associated with axonal injury in HIV infection. J Neuroinflammation. 2019;16:16.

234. Rolstad S, Jakobsson J, Sellgren C, et al. CSF neuroinflammatory biomarkers

in bipolar disorder are associated with cognitive impairment. Eur Neuropsychopharmacol [online serial]. Elsevier; 2015;25:1091–1098. Accessed at: http://dx.doi.org/10.1016/j.euroneuro.2015.04.023.

235. Sellebjerg F, Börnsen L, Ammitzbøll C, et al. Defining active progressive multiple sclerosis. Mult Scler [online serial]. Danish Multiple Sclerosis Center, Department of Neurology, Rigshospitalet, University of Copenhagen, Copenhagen, Denmark.; 2017;23:1727–1735. Accessed at: http://europepmc.org/abstract/MED/28831853.

236. Gabriel E, Ramani A, Karow U, et al. Recent Zika Virus Isolates Induce Premature Differentiation of Neural Progenitors in Human Brain Organoids. Cell Stem Cell. United States; 2017;20:397-406.e5.

237. Xu X, Tay Y, Sim B, et al. Reversal of Phenotypic Abnormalities by CRISPR/Cas9-Mediated Gene Correction in Huntington Disease Patient-Derived Induced Pluripotent Stem Cells. Stem cell reports. United States; 2017;8:619–633.

238. Bardy C, Van Den Hurk M, Eames T, et al. Neuronal medium that supports basic synaptic functions and activity of human neurons in vitro. Proc Natl Acad Sci U S A. 2015;112:E2725–E2734.

239. Hedegaard A, Monzón-Sandoval J, Newey SE, Whiteley ES, Webber C, Akerman CJ. Pro-maturational Effects of Human iPSC-Derived Cortical Astrocytes upon iPSC-Derived Cortical Neurons. Stem cell reports. United States; 2020;15:38–51.

240. Lin YC, Koleske AJ. Mechanisms of synapse and dendrite maintenance and their disruption in psychiatric and neurodegenerative disorders. Annu Rev Neurosci. 2010;33:349–378.

241. Falke E, Nissanov J, Mitchell TW, Bennett DA, Trojanowski JQ, Arnold SE. Subicular dendritic arborization in Alzheimer's disease correlates with neurofibrillary tangle density. Am J Pathol. United States; 2003;163:1615–

1621.

242. Sfakianos MK, Eisman A, Gourley SL, et al. Inhibition of Rho via Arg and p190RhoGAP in the postnatal mouse hippocampus regulates dendritic spine maturation, synapse and dendrite stability, and behavior. J Neurosci Off J Soc Neurosci. United States; 2007;27:10982–10992.

243. Dillon C, Goda Y. The actin cytoskeleton: integrating form and function at the synapse. Annu Rev Neurosci. United States; 2005;28:25–55.

244. Tashiro A, Yuste R. Regulation of dendritic spine motility and stability by Rac1 and Rho kinase: evidence for two forms of spine motility. Mol Cell Neurosci. United States; 2004;26:429–440.

245. Toksoz D, Merdek KD. The Rho small GTPase: Functions in health and disease. Histol Histopathol. 2002;17:915–927.

246. Aspenström P. Fast-cycling Rho GTPases. Small GTPases [online serial]. Taylor & Francis; 2020;11:248–255. Accessed at: https://doi.org/10.1080/21541248.2017.1391365.

247. Estévez-Priego E, Teller S, Granell C, Arenas A, Soriano J. Functional strengthening through synaptic scaling upon connectivity disruption in neuronal cultures. Netw Neurosci. 2020;4:1160–1180.

248. Turrigiano GG, Nelson SB. Homeostatic plasticity in the developing nervous system. Nat Rev Neurosci. 2004;5:97–107.

249. Targa Dias Anastacio H, Matosin N, Ooi L. Neuronal hyperexcitability in Alzheimer's disease: what are the drivers behind this aberrant phenotype? Transl Psychiatry. Springer US; 2022;12.

250. Centonze D, Muzio L, Rossi S, Furlan R, Bernardi G, Martino G. The link between inflammation, synaptic transmission and neurodegeneration in multiple sclerosis. Cell Death Differ [online serial]. Nature Publishing Group; 2010;17:1083–1091. Accessed at: http://dx.doi.org/10.1038/cdd.2009.179.

251. Caramia MD, Palmieri MG, Desiato MT, et al. Brain excitability changes in the relapsing and remitting phases of multiple sclerosis: a study with transcranial magnetic stimulation. Clin Neurophysiol Off J Int Fed Clin Neurophysiol. Netherlands; 2004;115:956–965.

252. Carrasco M, Rabaneda LG, Murillo-Carretero M, et al. Glycine N-methyltransferase expression in the hippocampus and its role in neurogenesis and cognitive performance. Hippocampus. United States; 2014;24:840–852.

253. Yang C-P, Wang H-A, Tsai T-H, et al. Characterization of the neuropsychological phenotype of glycine N-methyltransferase−/− mice and evaluation of its responses to clozapine and sarcosine treatments. Eur Neuropsychopharmacol [online serial]. 2012;22:596–606. Accessed at: https://www.sciencedirect.com/science/article/pii/S0924977X11003348.

254. Cambray S, Pedraza N, Rafel M, Garí E, Aldea M, Gallego C. Protein kinase KIS localizes to RNA granules and enhances local translation. Mol Cell Biol. United States; 2009;29:726–735.

255. Song Y, Li C, Jin L, et al. RIOK2 is negatively regulated by miR-4744 and promotes glioma cell migration/invasion through epithelial-mesenchymal transition. J Cell Mol Med. England; 2020;24:4494–4509.

256. Qu L, Pan C, He S-M, et al. The Ras Superfamily of Small GTPases in Non-neoplastic Cerebral Diseases. Front Mol Neurosci. Switzerland; 2019;12:121.

257. Koudinov AR, Koudinova N V. Cholesterol homeostasis failure as a unifying cause of synaptic degeneration. J Neurol Sci [online serial]. 2005;229–230:233–240. Accessed at: https://www.sciencedirect.com/science/article/pii/S0022510X04004575.

258. Zhong J. RAS and downstream RAF-MEK and PI3K-AKT signaling in neuronal development, function and dysfunction. Biol Chem. Germany; 2016;397:215–222.

259. Zenke K, Muroi M, Tanamoto K-I. IRF1 supports DNA binding of STAT1 by promoting its phosphorylation. Immunol Cell Biol. United States; 2018;96:1095–1103.

260. Plaisier CL, O'Brien S, Bernard B, et al. Causal Mechanistic Regulatory Network for Glioblastoma Deciphered Using Systems Genetics Network Analysis. Cell Syst [online serial]. Elsevier Inc.; 2016;3:172–186. Accessed at: http://dx.doi.org/10.1016/j.cels.2016.06.006.

261. Rawlings JS, Rosler KM, Harrison DA. The JAK/STAT signaling pathway. J Cell Sci. 2004;117:1281–1283.

262. Clark DN, Begg LR, Filiano AJ. Unique aspects of IFN-γ/STAT1 signaling in neurons. Immunol Rev. 2022;311:187–204.

263. Kim IJ, Beck HN, Lein PJ, Higgins D. Interferon γ Induces Retrograde Dendritic Retraction and Inhibits Synapse Formation. J Neurosci. 2002;22:4530–4539.

264. Pavlinek A, Matuleviciute R, Sichlinger L, et al. Interferon-γ exposure of human iPSC-derived neurons alters major histocompatibility complex I and synapsin protein expression. Front Psychiatry. 2022;13.

265. Li X, Hong X, Wang Y, et al. Tau accumulation triggers STAT 1-dependent memory deficits by suppressing NMDA receptor expression . EMBO Rep. 2019;20:1–18.

266. Hsu WL, Ma YL, Hsieh DY, Liu YC, Lee EH. STAT1 negatively regulates spatial memory formation and mediates the memory-impairing effect of Aβ. Neuropsychopharmacology. Nature Publishing Group; 2014;39:746–758.

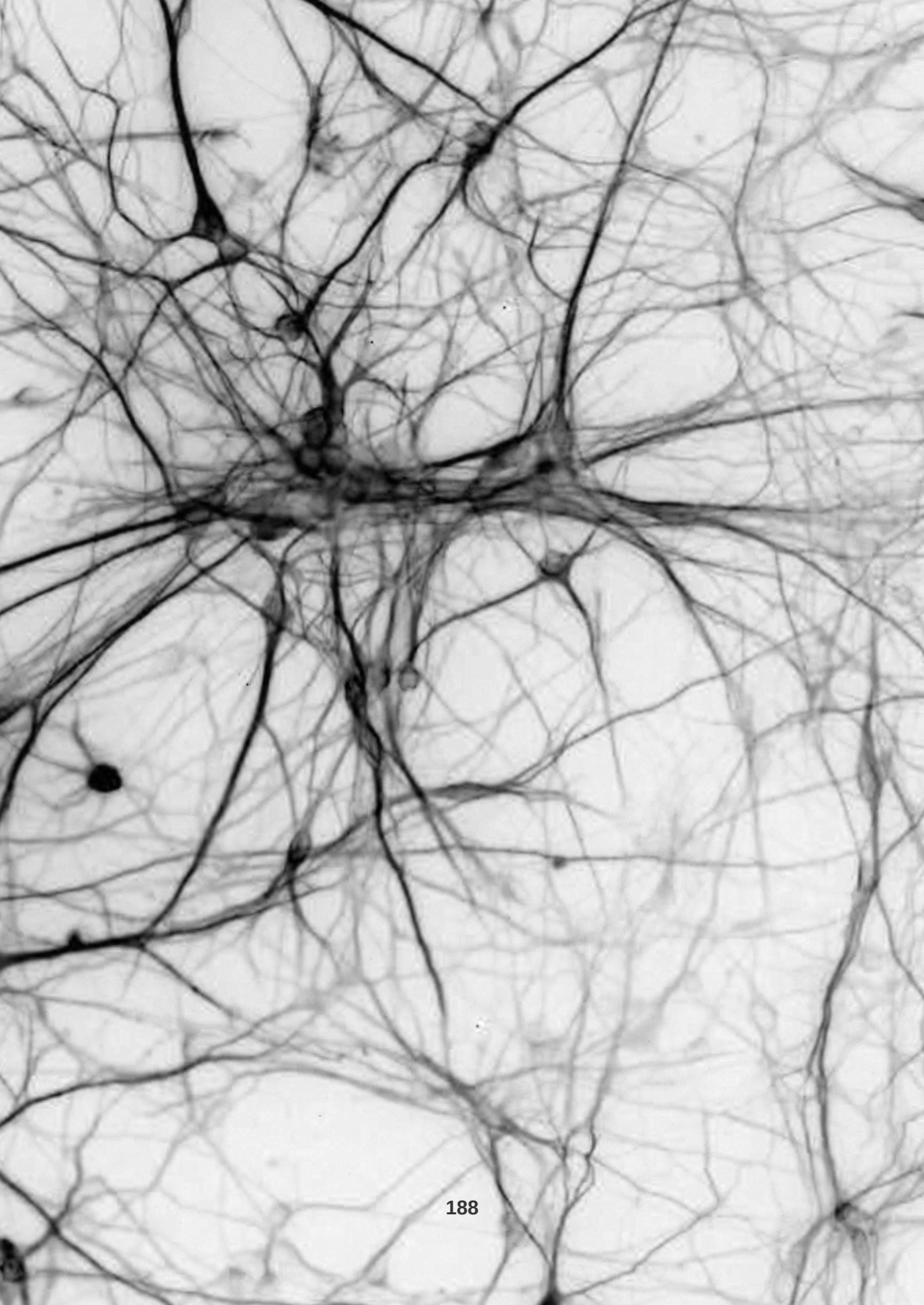

ANNEXES

10. ANNEXES

Supplemental table 1. WB buffers composition

Buffer	Composition
RIPA	150 mM sodium chloride 1% Triton-X-100 0.5% sodium deoxycholate (SDS) 50 mM Tris, pH 8.0
Electrophoresis	25 mM Tris-HCl 192 mM Glycine 20% SDS
Transference	48 mM Tris-HCl 39 mM glycine 20% methanol
TBST	20 mM Tris-HCl pH 7.6 150 mM NaCl 0.1% Tween

Supplemental Table 2. Pathway and processes enrichment of up-regulated DEGs p<0.01 at 12 hours

Description	GO	LogP	Hits
receptor ligand activity	GO:0048018	-5.04	AREG|EDA|IFNA21|CCL24|STC1|INHBE
signaling receptor activator activity	GO:0030546	-5	AREG|EDA|IFNA21|CCL24|STC1|INHBE
signaling receptor regulator activity	GO:0030545	-4.78	AREG|EDA|IFNA21|CCL24|STC1|INHBE
NABA SECRETED FACTORS	M5883	-4.69	AREG|EDA|IFNA21|CCL24|INHBE
cytokine activity	GO:0005125	-4.07	AREG|IFNA21|CCL24|INHBE
Cytokine-cytokine receptor interaction	hsa04060	-3.7	EDA|IFNA21|CCL24|INHBE
Overview of proinflammatory and profibrotic mediators	WP5095	-3.55	AREG|IFNA21|CCL24
NABA MATRISOME ASSOCIATED	M5885	-3.1	AREG|EDA|IFNA21|CCL24|INHBE
cytokine receptor binding	GO:0005126	-2.62	EDA|IFNA21|CCL24
response to cAMP	GO:0051591	-4.02	AQP1|AREG|STC1
response to organophosphorus	GO:0046683	-3.55	AQP1|AREG|STC1
response to glucocorticoid	GO:0051384	-3.43	AQP1|AREG|STC1
response to purine-containing compound	GO:0014074	-3.42	AQP1|AREG|STC1
response to corticosteroid	GO:0031960	-3.23	AQP1|AREG|STC1
apical part of cell	GO:0045177	-2.97	AQP1|EDA|ITPR3|STC1
response to steroid hormone	GO:0048545	-2.54	AQP1|AREG|STC1
positive regulation of GTPase activity	GO:0043547	-2.61	CCL24|RALGPS2|RASGEF1C
regulation of GTPase activity	GO:0043087	-2.26	CCL24|RALGPS2|RASGEF1C
regulation of cellular component size	GO:0032535	-2.27	AQP1|CCL24|CARMIL1

regulation of actin filament-based process	GO:0032970	-2.18	CCL24|STC1|CARMIL1
gland development	GO:0048732	-2.08	AREG|EDA|RAG1

Abbreviations: AQP1 - Aquaporin 1, AREG – Amphiregulin, CARMIL1 - capping protein regulator and myosin 1 linker 1, CCL24 - C-C motif chemokine ligand 24, EDA - Ectodysplasin A, IFNA21 - Interferon alpha-21, INHBE - Inhibin subunit beta E, ITPR3 - Inositol 1,4,5-trisphosphate receptor type 3, RAG1 - Recombination activating gene 1, RALGPS2 - Ral GEF with PH domain and SH3 binding motif 2, RASGEF1C - RasGEF domain family member 1C, STC1 - Stanniocalcin

Supplemental Table 3. Pathway and processes enrichment of down-regulated DEGs p<0.01 at 12 hours

Description	GO	LogP	Hits
regulation of RNA splicing	GO:0043484	-3.19	AHNAK|TADA2B|TADA1
lytic vacuole	GO:0000323	-2.32	BORCS6|AHNAK|NEU4|C6orf120
lysosome	GO:0005764	-2.32	BORCS6|AHNAK|NEU4|C6orf120

Abbreviations: AHNAK - AHNAK Nucleoprotein, BORCS6 - BLOC-1 Related Complex Subunit 6, C6orf120 - Chromosome 6 Open Reading Frame 120, NEU4 - Neuraminidase 4, TADA1 - Transcriptional Adaptor 1, TADA2B - Transcriptional Adaptor 2B

Supplemental Table 4. Pathway and processes enrichment of up-regulated DEGs p<0.01 at 24 hours

Description	GO	_LogP_MyList	Hits
chemical synaptic transmission	GO:0007268	-3.69	CHRNA3|GRID2|KCND2|SV2C|VPS54|CHRFAM7A|SYT10
anterograde trans-synaptic signaling	GO:0098916	-3.69	CHRNA3|GRID2|KCND2|SV2C|VPS54|CHRFAM7A|SYT10
regulation of postsynaptic membrane potential	GO:0060078	-3.64	CHRNA3|GRID2|KCND2|CHRFAM7A
trans-synaptic signaling	GO:0099537	-3.59	CHRNA3|GRID2|KCND2|SV2C|VPS54|CHRFAM7A|SYT10
synaptic signaling	GO:0099536	-3.42	CHRNA3|GRID2|KCND2|SV2C|VPS54|CHRFAM7A|SYT10
excitatory postsynaptic potential	GO:0060079	-3.08	CHRNA3|GRID2|CHRFAM7A
chemical synaptic transmission, postsynaptic	GO:0099565	-2.96	CHRNA3|GRID2|CHRFAM7A
regulation of membrane potential	GO:0042391	-2.75	CHRNA3|GRID2|KCND2|MTMR2|CHRFAM7A|TMEM161B
Neuronal System	R-HSA-112316	-2.16	CHRNA3|KCND2|EPB41L5|CHRFAM7A|SYT10
cerebellum morphogenesis	GO:0021587	-3.54	GRID2|GNPAT|SLC25A46
hindbrain morphogenesis	GO:0021575	-3.45	GRID2|GNPAT|SLC25A46
cell junction assembly	GO:0034329	-2.87	CDH12|CDH13|GRID2|GNPAT|SLC25A46
cerebellum development	GO:0021549	-2.44	GRID2|GNPAT|SLC25A46
synapse assembly	GO:0007416	-2.37	GRID2|GNPAT|SLC25A46
cell junction organization	GO:0034330	-2.37	CDH12|CDH13|GRID2|GNPAT|MTMR2|SLC25A46
myelination	GO:0042552	-2.34	GNPAT|MTMR2|SLC25A46
metencephalon development	GO:0022037	-2.33	GRID2|GNPAT|SLC25A46
ensheathment of neurons	GO:0007272	-2.32	GNPAT|MTMR2|SLC25A46
axon ensheathment	GO:0008366	-2.32	GNPAT|MTMR2|SLC25A46
sensory perception of smell	GO:0007608	-3.42	OR2D2|OR4L1|OR2L13|OR5F1|SYT10|OR52H1|OR8H3
sensory perception of chemical stimulus	GO:0007606	-3.02	OR2D2|OR4L1|OR2L13|OR5F1|SYT10|OR52H1|OR8H3
Expression and translocation of olfactory receptors	R-HSA-9752946	-3.01	OR2D2|OR4L1|OR2L13|OR5F1|OR52H1|OR8H3

Olfactory Signaling Pathway	R-HSA-381753	-2.97	OR2D2|OR4L1|OR2L13|OR5F1|OR52H1|OR8H3
detection of chemical stimulus involved in sensory perception of smell	GO:0050911	-2.78	OR2D2|OR4L1|OR2L13|OR5F1|OR52H1|OR8H3
Olfactory transduction	hsa04740	-2.74	OR2D2|OR4L1|OR2L13|OR5F1|OR52H1|OR8H3
detection of chemical stimulus involved in sensory perception	GO:0050907	-2.56	OR2D2|OR4L1|OR2L13|OR5F1|OR52H1|OR8H3
detection of stimulus	GO:0051606	-2.48	ANO3|OR2D2|OR4L1|OR2L13|OR5F1|OR52H1|OR8H3
detection of chemical stimulus	GO:0009593	-2.43	OR2D2|OR4L1|OR2L13|OR5F1|OR52H1|OR8H3
detection of stimulus involved in sensory perception	GO:0050906	-2.28	OR2D2|OR4L1|OR2L13|OR5F1|OR52H1|OR8H3
Sensory Perception	R-HSA-9709957	-2.02	OR2D2|OR4L1|OR2L13|OR5F1|OR52H1|OR8H3
response to calcium ion	GO:0051592	-3.02	TSHB|VPS54|CPNE4|SYT10
response to salt	GO:1902074	-2.29	CHRNA3|TSHB|VPS54|CPNE4|SYT10
sodium ion transport	GO:0006814	-2.69	SLC13A1|ASIC5|SLC10A5|SLC9A4
sodium ion transmembrane transport	GO:0035725	-2.15	SLC13A1|ASIC5|SLC9A4
locomotory behavior	GO:0007626	-2.59	CALB1|CHRNA3|KCND2|SLC25A46
behavior	GO:0007610	-2.05	CALB1|CHRNA3|KCND2|VPS54|SLC25A46|LRRC66
oogenesis	GO:0048477	-2.58	TNFAIP6|FBXO5|PAQR5
female gamete generation	GO:0007292	-2.01	TNFAIP6|FBXO5|PAQR5
regulation of reproductive process	GO:2000241	-2.50	OVGP1|FBXO5|CCDC87|CLXN
lipid transport	GO:0006869	-2.46	SLCO1A2|ZDHHC5|VPS54|ANO3|SLC10A5
lipid localization	GO:0010876	-2.28	SLCO1A2|ZDHHC5|VPS54|ANO3|SLC10A5
dephosphorylation	GO:0016311	-2.41	MTMR2|TPTE2|UBLCP1|DUSP19
aminoglycan metabolic process	GO:0006022	-2.27	OVGP1|TNFAIP6|CHST15
cell-cell junction assembly	GO:0007043	-2.19	CDH12|CDH13|GNPAT
Cell-Cell communication	R-HSA-1500931	-2.19	CDH12|CDH13|SKAP2

cell-cell adhesion via plasma-membrane adhesion molecules	GO:0098742	-2.14	CDH12|CDH13|GRID2|DCHS2

Abbreviations: ANO3 - Anoctamin 3, ASIC5 - Acid-Sensing Ion Channel Subunit Family Member 5, CALB1 - Calbindin 1, CDH12 - Cadherin 12, CDH13 - Cadherin 13, CHRFAM7A - Cholinergic Receptor Nicotinic Alpha 7 Subunit and FAM7A Hybrid, CHRNA3 - Cholinergic Receptor Nicotinic Alpha 3 Subunit, CHST15 - Carbohydrate Sulfotransferase 15, CLXN – Calaxin, CPNE4 - Copine 4, DCHS2 - Dachsous Cadherin-Related 2, DUSP19 - Dual-Specificity Phosphatase 19, EPB41L5 - Erythrocyte Membrane Protein Band 4.1 Like 5, FBXO5 - F-Box Protein 5, GNPAT - Glyceronephosphate O-Acyltransferase, GRID2 - Glutamate Receptor Ionotropic Delta-2, KCND2 - Potassium Voltage-Gated Channel Subfamily D Member 2, LRRC66 - Leucine-Rich Repeat-Containing Protein 66, MTMR2 - Myotubularin-Related Protein 2, OR2D2 - Olfactory Receptor Family 2 Subfamily D Member 2, OR4L1 - Olfactory Receptor Family 4 Subfamily L Member 1, OR5F1 - Olfactory Receptor Family 5 Subfamily F Member 1, OR52H1 - Olfactory Receptor Family 52 Subfamily H Member 1, OR8H3 - Olfactory Receptor Family 8 Subfamily H Member 3, OVGP1 - Oviductal Glycoprotein 1, PAQR5 - Progestin and AdipoQ Receptor Family Member V, SLC10A5 - Solute Carrier Family 10 Member 5, SLC13A1 - Solute Carrier Family 13 Member 1, SLC25A46 - Solute Carrier Family 25 Member 46, SLC9A4 - Solute Carrier Family 9 Member A4, SKAP2 - Src Kinase-Associated Phosphoprotein 2, SLCO1A2 - Solute Carrier Organic Anion Transporter Family Member 1A2, SYT10 - Synaptotagmin 10, TMEM161B - Transmembrane Protein 161B, TNFAIP6 - Tumor Necrosis Factor Alpha-Induced Protein 6, TPTE2 - Transmembrane Phosphoinositide 3-Phosphatase and Tensin Homolog 2, UBLCP1 - Ubiquitin-Like Domain-Containing CTD Phosphatase 1, VPS54 - VPS54 Subunit of GARP Complex, ZDHHC5 - Zinc Finger DHHC-Type Containing 5

Supplemental Table 5. Pathway and processes enrichment of down-regulated DEGs p<0.01 at 24 hours

Description	GO	_LogP_MyList	Hits
apical plasma membrane	GO:0016324	-3.43	ATP4B|CD44|MPP3|SLC2A1|SLC5A6|OCEL1
import across plasma membrane	GO:0098739	-3.16	ATP4B|SLC2A1|SLC5A6|SLC15A3
apical part of cell	GO:0045177	-3.08	ATP4B|CD44|MPP3|SLC2A1|SLC5A6|OCEL1
import into cell	GO:0098657	-2.82	ATP4B|SLC2A1|SLC5A6|SLC15A3
basal part of cell	GO:0045178	-2.30	CD44|KRT14|SLC2A1|SLC5A6
monocarboxylic acid transport	GO:0015718	-2.25	SLC2A1|SLC5A6|SLC16A5
negative regulation of cysteine-type endopeptidase activity involved in apoptotic process	GO:0043154	-3.29	CD44|MMP9|PAX2
negative regulation of cysteine-type endopeptidase activity	GO:2000117	-3.05	CD44|MMP9|PAX2
negative regulation of proteolysis	GO:0045861	-2.98	CD44|CST6|EFNA1|MMP9|PAX2
negative regulation of peptidase activity	GO:0010466	-2.67	CD44|CST6|MMP9|PAX2
regulation of peptidase activity	GO:0052547	-2.49	CD44|CST6|EFNA1|MMP9|PAX2
negative regulation of endopeptidase activity	GO:0010951	-2.26	CD44|MMP9|PAX2
regulation of proteolysis	GO:0030162	-2.13	CD44|CST6|EFNA1|MELTF|MMP9|PAX2
regulation of endopeptidase activity	GO:0052548	-2.12	CD44|EFNA1|MMP9|PAX2
negative regulation of hydrolase activity	GO:0051346	-2.08	CD44|CST6|MMP9|PAX2
lens development in camera-type eye	GO:0002088	-3.03	CRYBB1|CRYBB3|PITX3
camera-type eye development	GO:0043010	-2.09	CRYBB1|CRYBB3|PAX2|PITX3
regulation of glucose metabolic process	GO:0010906	-2.69	IGF2|MLYCD|GNMT
carbohydrate metabolic process	GO:0005975	-2.39	IGF2|SLC2A1|GNMT|A3GALT2|BRAT1
Ras signaling pathway	hsa04014	-2.61	EFNA1|IGF2|IKBKG|CALML5
Estrogen signaling pathway	hsa04915	-2.36	KRT14|MMP9|CALML5

Fluid shear stress and atherosclerosis	hsa05418	-2.35	MMP9|IKBKG|CALML5
Pathways in cancer	hsa05200	-2.06	IGF2|MMP9|SLC2A1|IKBKG|CALML5
Apoptosis	hsa04210	-2.37	LMNA|IKBKG|TUBA3E
chemotaxis	GO:0006935	-2.13	EFNA1|XCR1|PLP2|SEMA3G|PREX1
taxis	GO:0042330	-2.12	EFNA1|XCR1|PLP2|SEMA3G|PREX1
locomotion	GO:0040011	-2.06	EFNA1|XCR1|PLP2|SEMA3G|PREX1
negative regulation of cell differentiation	GO:0045596	-2.13	EFNA1|IGF2|MMP9|PITX3|FOXP3|SEMA3G
positive regulation of peptidyl-tyrosine phosphorylation	GO:0050731	-2.03	CD44|EFNA1|IGF2
carbohydrate derivative catabolic process	GO:1901136	-2.10	CD44|MLYCD|NEIL2
mesenchymal cell differentiation	GO:0048762	-2.09	EFNA1|PAX2|SEMA3G
stem cell differentiation	GO:0048863	-2.02	KRT14|PAX2|SEMA3G

Abbreviations: A3GALT2 - Alpha-1,3-galactosyltransferase 2, ATP4B - ATPase H+/K+ transporting subunit beta, BRAT1 - BRCA1-associated ATM activator 1, CALML5 - Calmodulin-like protein 5, CD44 - Cluster of Differentiation 44, CST6 - Cystatin E/M, CRYBB1 - Beta-crystallin B, CRYBB3 - Beta-crystallin B3, EFNA1 - Ephrin-A1, FOXP3 - Forkhead box protein P3, GNMT - Glycine N-methyltransferase, IGF2 - Insulin-like growth factor 2, IKBKG - Inhibitor of nuclear factor kappa-B kinase subunit gamma, KRT14 - Keratin 14, LMNA - Lamin A/C, MELTF – Melanotransferrin, MMP9 - Matrix metalloproteinase 9, MLYCD - Malonyl-CoA decarboxylase, MPP3 - MAGUK P55 Scaffold Protein 3, NEIL2 - Nei-like DNA glycosylase 2, OCEL1 - Occludin/ELL Domain Containing 1, PAX2 - Paired box protein 2, PITX3 - Paired-like homeodomain transcription factor 3, PLP2 - Proteolipid protein 2, PREX1 - Phosphatidylinositol-3,4,5-trisphosphate-dependent Rac exchange factor 1, SLC15A3 - Solute carrier family 15 member 3, SLC16A5 - Solute carrier family 16 member 5, SLC2A1 - Solute carrier family 2 member 1, SLC5A6 - Solute carrier family 5 member 6, SEMA3G - Semaphorin 3G, TUBA3E - Tubulin alpha-3E chain, XCR1 - X-C motif chemokine receptor 1

Supplemental Table 6. GO CC enrichment of DEGs p<0.05 at 12 hours

ID	Description	NES	pvalue	p.adjust	core_enrichment
GO:0031253	cell projection membrane	1,60	$2,7904^{E-05}$	0,03361025	AQP1/SLC3A1/PLEK/TRPM6/GNAT2/CDKL5/MTMR9/SCIMP/SLC7A9/CDHR1/KCNC3/EPHA2/ARHGEF4/TACR3/TESC/LCP1/DRD2/SLC6A19/REG1A/DIAPH1/TIRAP/CNGA2/SLC34A1/OPRM1/MCHR1/ITGB3/GABRA4/SLC28A3/SLC26A3/RHO/SNAP29/WLS/TAS2R4/USH2A/GNA12/SLC22A5/SCARB1/EPB41L3/DOCK8/GABRG1/SLC11A2/ADORA2A/GNAT1/PTPRH/SLC6A18/SH3YL1/TRPV4/C2CD5/RAB35/SLC34A3/GABRA2/SLC17A3/PTPRJ/CA9/MYO1D/GABRA5/SLC9A3/GABRG3/TWF1/TMEM231/VEZT/JCAD/ANTXR1/HIP1R/PDE6H/SLC22A12/FSCN1/KANK1/ITGAV/PLEK2/BBS7/GABARAPL1/ITGA8/GABRA6/ARL13B/MTMR6/CASK/GPR157/PDE4A/GABRA1/CNGA4/CUBN/GNA13/CLCN3/SHISA7/PTH1R/PALM/MOSMO/TIAM1/AKAP5/PLEKHO1/EZR
GO:0098798	mitochondrial protein-containing complex	-1,65	$6,3096^{E-05}$	0,03361025	DAP3/PPIF/VDAC1/MRPL58/MRPL9/MRPS21/DNAJC19/MRPS30/NDUFV1/ROMO1/ATP5F1D/MRPS26/NDUFA8/TIMM17A/PMPCB/NDUFB8/MRPL33/MTERF4/NDUFB3/TOMM22/NDUFS6/UQCRHL/HSD17B10/CYC1/BAX/ATP5MJ/MICOS10/MTX1/MRPL23/GRPEL2/DNA2/ATP5MG/SMDT1/NDUFA4L2/COX6A1/MRPS35/TIMM22/ATP5PF/UQCRC1/BCS1L/NDUFA1/MRPL14/AFG3L2/TIMM9/ATP5MC3/NDUFB11/MRPS22/MRPL57/TIMM23/TRMT10C/MICU3/NDUFB7/WDR93/SDHA/HADHA/SUCLG2/MRPL46/NDUFA6/COX6A2/MRPS11/MRPL35/TOMM7/NDUFC1/FOXRED1/MRPL19/UQCRFS1/NDUFB10/MRPL20/MRPL47/TIMM50/UQCRH/NDUFA13/MRPS33/MRPL2/PHB/IMMP1L/TIMM17B/MRPL54/TIMM13/MALSU1/TIMM21/TOMM5/COX4I1/MRPS31/MRPS34/POLG2/MRPL18/MRPL22/MRPL40/NDUFB4/MRPL36/TOMM70/MCCC2
GO:0031526	brush border membrane	1,98	$7,4359^{E-05}$	0,03361025	AQP1/SLC3A1/TRPM6/SLC7A9/SLC6A19/SLC34A1/SLC28A3/SLC26A3/GNA12/SLC22A5/SLC11A2/SLC6A18/SLC34A3/SLC17A3/SLC9A3/SLC22A12/CUBN/GNA13/PTH1R/CDHR5/AMN/CD36/SLC28A2/SLC26A4
GO:0098862	cluster of actin-based cell projections	1,74	0,00013	0,03851084	AQP1/DOCK4/SLC3A1/ITPR3/TRPM6/PLS1/ELMOD3/DNM1L/CDC14A/SLC7A9/CDH23/TMPRSS15/SLC6A19/PLEC/GRXCR1/SLC34A1/IFT20/SLC28A3/SLC26A3/USH2A/GNA12/SLC22A5/SNX5/LOXHD1/SLC11A2/MYO15A/SLC6A18/DAB1/SLC34A3/SLC17A3/MYO1D/SLC9A3
GO:0097225	sperm midpiece	2,07	0,00014	0,03851084	AKAP3/TACR3/DEFB1/SLC26A3/RHO/TACR2/AKAP4/TCP11/CFAP69/IFT27/SQSTM1/CFAP65

Supplemental Table 7. GO CC enrichment of DEGs p<0.05 at 24 hours

ID	Description	NES	pvalue	p.adjust	core_enrichment
GO:0098982	GABA-ergic synapse	2,40	$3,85^{E-08}$	$3,87^{E-05}$	CALB1/CDH13/PTPRO/ATP2B1/NLGN3/KCND2/PCLO/NLGN2/SLITRK1/NLGN4Y/CBLN4/GABRA5/GUCY1A1/SV2A/GABRA4/MDGA1/SLITRK2/ABHD6/PCDH17/PLCB1/IGSF9B/FLOT1/GABRG2/PHB/LRRTM1/NLGN4X/CSPG5/SLC6A17/GABBR1/ERC2/GABRA3
GO:0005581	collagen trimer	-2,29	$5,71^{E-08}$	$3,87^{E-05}$	FCN3/COL5A2/C1QTNF8/MARCO/C1QL1/DCN/COL2A1/COLEC12/EMILIN1/COL1A2/SFTPA1/COL1A1/C1QB/COL18A1/COL8A1/COL6A3/COL20A1/OTOL1/COL24A1/COL9A3/EMILIN2/COL9A1/C1QL2/COL27A1/COL13A1/COL5A1/C1QC/LUM/C1QL3/ADIPOQ/COL8A2/C1QTNF7/C1QTNF2/COL10A1/COL19A1/COLEC10/COL4A2/FCN1/GLDN/COLQ/COL23A1/COL22A1
GO:0097060	synaptic membrane	1,78	$1,44^{E-07}$	$6,53^{E-05}$	MTMR2/CHRM3/GRID2/CHRNA3/ATP2B1/CHRM2/NLGN3/NLGN1/GRIN2A/KCND2/GABRQ/CNTNAP1/CHRNE/SORCS3/GABRA2/NLGN2/SLITRK1/SCN2A/NLGN4Y/GABRA5/KCNA3/P2RY4/KCTD16/CNTN6/KCNMA1/DMD/STX3/UNC13A/GPC4/LRRC4C/DGKI/TIAM1/GABRA4/SLITRK2/CACNG2/ABHD6/GLRA2/SHC4/PCDH17/GRIK2/LIN7A/EPHA7/UNC13B/ZNRF2/EFNB3/CHRM5/GRIK1/SYT7/GRIN3A/ADORA1/SRGAP2/GABRA1/IGSF9B/SHISA6/ANXA1/GABRG2/GPHN/ABHD17B/CACNG4/NECTIN3/RIMS2/ANK3/ATAD1/SHISA9/PHB/LRRTM1/LRRTM4/NLGN4X/CSPG5/DAGLB/NCSTN/CACNG7/DNM1L/ADCY8/STRN/ADAM22/GABRP/SLC8A1/CHRNA6/TRAPPC4/PLPPR4/FMR1/GRIP1/DCC/ITSN2/GABBR1/ADAM23/MAGEE1/SYNJ1/CNIH2/CDH8/LRRTM3/ERC2/CHRNA4/SEMA4F/GABRA3/CNKSR2/SYP/SIGMAR1/PCDH8/CDH9/GRM5/GRM3/STXBP1/HTR1B/ZDHHC17/SLC6A2/GABRB2/KCNC3/SNCAIP/ABHD17C/CDH2/DNM1/DLG2/GABBR2/GRIA4/KCNC2/KCNC1/SLC6A4/LIN7B/UTRN/CACNG5/GPM6A/CLSTN2/SLC6A5/CNTN1/SEMA4C/GABRA6/GABRB1/CHRNA2/LHFPL4/GABRR3/CACNA1C/GRIK3/NSG1/GRIA1
GO:0045211	postsynaptic membrane	1,82	$1,25^{E-06}$	0,000423	CHRM3/GRID2/CHRNA3/CHRM2/NLGN3/NLGN1/GRIN2A/KCND2/GABRQ/CHRNE/SORCS3/GABRA2/NLGN2/SLITRK1/NLGN4Y/GABRA5/KCNA3/KCTD16/KCNMA1/DMD/LRRC4C/TIAM1/GABRA4/SLITRK2/CACNG2/ABHD6/GLRA2/SHC4/PCDH17/GRIK2/LIN7A/EPHA7/EFNB3/CHRM5/GRIK1/GRIN3A/ADORA1/SRGAP2/GABRA1/IGSF9B/SHISA6/GABRG2/GPHN/ABHD17B/CACNG4/NECTIN3/ANK3/ATAD1/SHISA9/LRRTM1/LRRTM4/NLGN4X/CSPG5/DAGLB/CACNG7/STRN/ADAM22/GABRP/SLC8A1/CHRNA6/TRAPPC4/PLPPR4/FMR1/GRIP1/DCC/GABBR1/MAGEE1/CNIH2/LRRTM3/CHRNA4/SEMA4F/GABRA3/CNKSR2/SIGMAR1/PCDH8/CDH9/GRM5/GRM3/GABRB2/KCNC3/ABHD17C/CDH2/DNM1/DLG2/GABBR2/GRIA4/KCNC2/SLC6A4/LIN7B/UTRN/CACNG5/CLSTN2/CNTN1/SEMA4C/GABRA6/GABRB1/CHRNA2/LHFPL4/GABRR3/CACNA1C/GRIK3/NSG1/GRIA1
GO:0098878	glutamatergic synapse	1,72	$3,17^{E-06}$	0,000861	GRID2/CALB1/CDKL5/PTPRO/ERBIN/ATP2B1/NLGN3/NLGN1/GRIN2A/EPS15/KCND2/CAMKV/SORCS3/PCLO/SLITRK1/BCR/SCN2A/NLGN4Y/SH3GL3/ADGRL3/CDH1/KCNA3/GUCY1A1/SPARC/P2RY4/STX3/SV2A/CADPS/GPC4/SRC/LRRC4C/TIAM1/SLITRK2/CACNG2/ABHD6/PCDH17/GRIK2/EPHA7/EFNB3/PLCB1/CDH11/GRIN3A/PPP3CB/RHOA/PPP1R9A/ARPC5L/SHISA6/RAB8A/FLOT1/CTTNBP2/CDK5/ABHD17B/CACNG4/PRKCZ/FZD9/ARF4/ATAD1/SHISA9/PHB/LRRTM1/PPP3CC/NLGN4X/CSPG5/ACTN1/CACNG7/DRP2/ADCY8/JAK2/ADAM22/SYN2/TNIK/SLC6A17/PLPPR4/GRIP1/ADAM23/SH3GL1/CNIH2/CDH8/LRRTM3/ERC2/PPP1CC/PLCB4/CNKSR2/PCDH8/DLGAP3/GRM3/STXBP1/PLEKHA5

GO:0062023	collagen-containing extracellular matrix	-1,56	$2,31^{E-05}$	0,005225	FREM1/MMRN2/EGFLAM/APOA4/GREM1/SFRP1/CLEC14A/NTN1/C17orf58/MATN1/AMTN/FREM3/CSTB/ANXA6/SERPINB12/PXDN/LAMB4/FCN3/ADAMTS3/MFAP4/COL5A2/MATN4/LGALS3BP/SERPINB1/MGP/MXRA7/CSPG4/ANGPTL4/CHADL/ACHE/TGFB1/LAMA4/DCN/ANGPTL5/COL2A1/SERPINE2/WNT8A/CTSZ/AMELX/EMILIN1/RBP3/AZGP1/COL1A2/AHSG/HSPG2/COL1A1/ADAMTSL4/NTN5/GDF15/SFRP2/SOST/C1QB/COL18A1/COL8A1/THBS1/COL6A3/MFGE8/VTN/FREM2/RTBDN/VWA2/COL20A1/PZP/GPC1/OTOL1/AMBP/COL24A1/COL9A3/EMILIN2/COL9A1/MXRA5/BGN/PLOD3/COL27A1/COL13A1/LMAN1L/LRRC15/LGALS3/ORM2/NDP/SERPINE1/EMILIN3/VWC2/MUC2/COL5A1/ZP1/SNORC/CCN2/EGFL7/ICAM1/C1QC/LUM/HPX/TGFB3/CTSC/SRPX2/ZG16/CCN1/TGM4/SHH/ADIPOQ/COL8A2/P3H2/COL10A1/CLC/CRELD1/MST1/ADAMTS10/MMP28/VWF/MDK/CXCL12/WNT2/COL19A1/CLEC3B/FBLN1/F2/FGL2/S100A8/EGFL6/COCH/ADAMTS1/IMPG2/HTRA1/F12/PCOLCE/SSC5D/PRTN3/PODN/FIBCD1/MYOC/MMP2/RARRES2/LGALS9/COMP/ELN/TNXB/COL4A2/APOE/PF4/ENTPD2/IGFBP7/FCN1/SERPINF2/COLQ/ACAN/COL23A1/LAMC3/MMP9/LEFTY2/FMOD/FGFBP3
GO:0099240	intrinsic component of synaptic membrane	1,83	$3,27^{E-05}$	0,006329	GRID2/ATP2B1/NLGN3/NLGN1/GRIN2A/KCND2/SORCS3/NLGN2/SLITRK1/SCN2A/GABRA5/KCNA3/P2RY4/CNTN6/GPC4/LRRC4C/GABRA4/SLITRK2/CACNG2/ABHD6/PCDH17/EPHA7/EFNB3/SYT7/ADORA1/SHISA6/GPHN/ABHD17B/CACNG4/NECTIN3/SHISA9/LRRTM1/CSPG5/NCSTN/CACNG7/ADCY8/ADAM22/SLC8A1/PLPPR4/DCC/ADAM23/CNIH2/LRRTM3/GABRA3/PCDH8/CDH9/GRM3/HTR1B/GABRB2/CDH2/SLC6A4/CACNG5/GPM6A/CLSTN2/SLC6A5/CNTN1
GO:0099699	integral component of synaptic membrane	1,81	$5,17^{E-05}$	0,008758	GRID2/ATP2B1/NLGN3/NLGN1/GRIN2A/KCND2/SORCS3/NLGN2/SLITRK1/SCN2A/GABRA5/KCNA3/P2RY4/LRRC4C/GABRA4/SLITRK2/CACNG2/ABHD6/PCDH17/EPHA7/EFNB3/SYT7/ADORA1/SHISA6/CACNG4/NECTIN3/SHISA9/LRRTM1/CSPG5/NCSTN/CACNG7/ADCY8/ADAM22/SLC8A1/PLPPR4/DCC/ADAM23/CNIH2/LRRTM3/GABRA3/PCDH8/CDH9/GRM3/HTR1B/GABRB2/CDH2/SLC6A4/CACNG5/GPM6A/CLSTN2/SLC6A5
GO:0022626	cytosolic ribosome	-1,92	$9,91^{E-05}$	0,014932	DDX3X/RPS18/RPS15A/RPL22/RPL34/MCTS1/RPL10L/RPL38/RPL24/RPS16/APOD/RPS5/RPL27/RPSA/RPS24/RPS23/MRPS11/RPL26L1/RPL21/LARP4/RPL26/RPL12/RPS25/RPS12/RPL37/RPS29/RPL35A/ISG15/EIF2A/RPL18/RPS27/RPL37A/RPL19/RPL10A/RPS10/RPL29/RPS4Y2/RPL18A/RPLP1/RPL11/RPS28/RPL36AL/RPS26/RPS19/RPS15/HBA1
GO:0098936	intrinsic component of postsynaptic membrane	1,79	0,00012	0,016386	GRID2/NLGN3/NLGN1/GRIN2A/KCND2/SORCS3/NLGN2/SLITRK1/GABRA5/KCNA3/LRRC4C/GABRA4/SLITRK2/CACNG2/ABHD6/PCDH17/EPHA7/EFNB3/ADORA1/SHISA6/ABHD17B/CACNG4/NECTIN3/SHISA9/LRRTM1/CSPG5/CACNG7/ADAM22/SLC8A1/PLPPR4/DCC/CNIH2/LRRTM3/GABRA3/PCDH8/CDH9/GRM3/GABRB2/CDH2/SLC6A4/CACNG5/CLSTN2/CNTN1
GO:0099055	integral component of postsynaptic membrane	1,79	0,00017	0,021444	GRID2/NLGN3/NLGN1/GRIN2A/KCND2/SORCS3/NLGN2/SLITRK1/GABRA5/KCNA3/LRRC4C/GABRA4/SLITRK2/CACNG2/ABHD6/PCDH17/EPHA7/EFNB3/ADORA1/SHISA6/CACNG4/NECTIN3/SHISA9/LRRTM1/CSPG5/CACNG7/ADAM22/SLC8A1/PLPPR4/DCC/CNIH2/LRRTM3/GABRA3/PCDH8/CDH9/GRM3/GABRB2/CDH2/SLC6A4/CACNG5/CLSTN2
GO:0016459	myosin complex	-1,93	0,00030	0,033918	MYH7/CGNL1/MYO1C/MYH2/MYH14/MYH9/MYH1/LIMCH1/MYO7B/MYL5/CCDC102A/MYO18B/MYLPF/MYO3B/MYO10/MYO1A/MYL9/MYH13/MYH3/MYH6/MYO5C/CGN
GO:0035976	transcription factor AP-1 complex	-1,76	0,00032	0,033918	FOS/JUND/JUNB

GO:0044391	ribosomal subunit	-1,69	0,00045	0,043418	DDX3X/RPS18/RPS15A/MRPL52/MRPS16/RPL22/RPL34/MRPL43/MRPL28/MCTS1/RPL10L/MRPL33/RPL38/MRPL46/RPL24/MRPL47/RPS16/RPS5/MRPL24/RPL27/RPSA/RPS24/RPS23/MRPL27/MRPS11/RPL26L1/RPL21/RBM3/MRPS31/MRPS27/MRPS35/LARP4/MRPL55/MRPS36/MRPL22/RPL26/RPL12/RPS25/MALSU1/RPS12/RPL37/MRPL37/MRPL41/RPS29/RPL35A/ISG15/EIF2A/RPL18/MTRFR/MRPL20/MRPS26/MRPL38/MRPS34/RPS27/RPL37A/MRPL57/RPL19/RPL10A/RPS10/MRPL17/MRPL4/NDUFAB1/RPL29/MRPL21/MRPL30/RPS4Y2/MRPS18C/RPL18A/RPLP1/MRPL23/RPL11/RPS28/RPL36AL/RPS26/NSUN3/RPS19/RPS15/HBA1

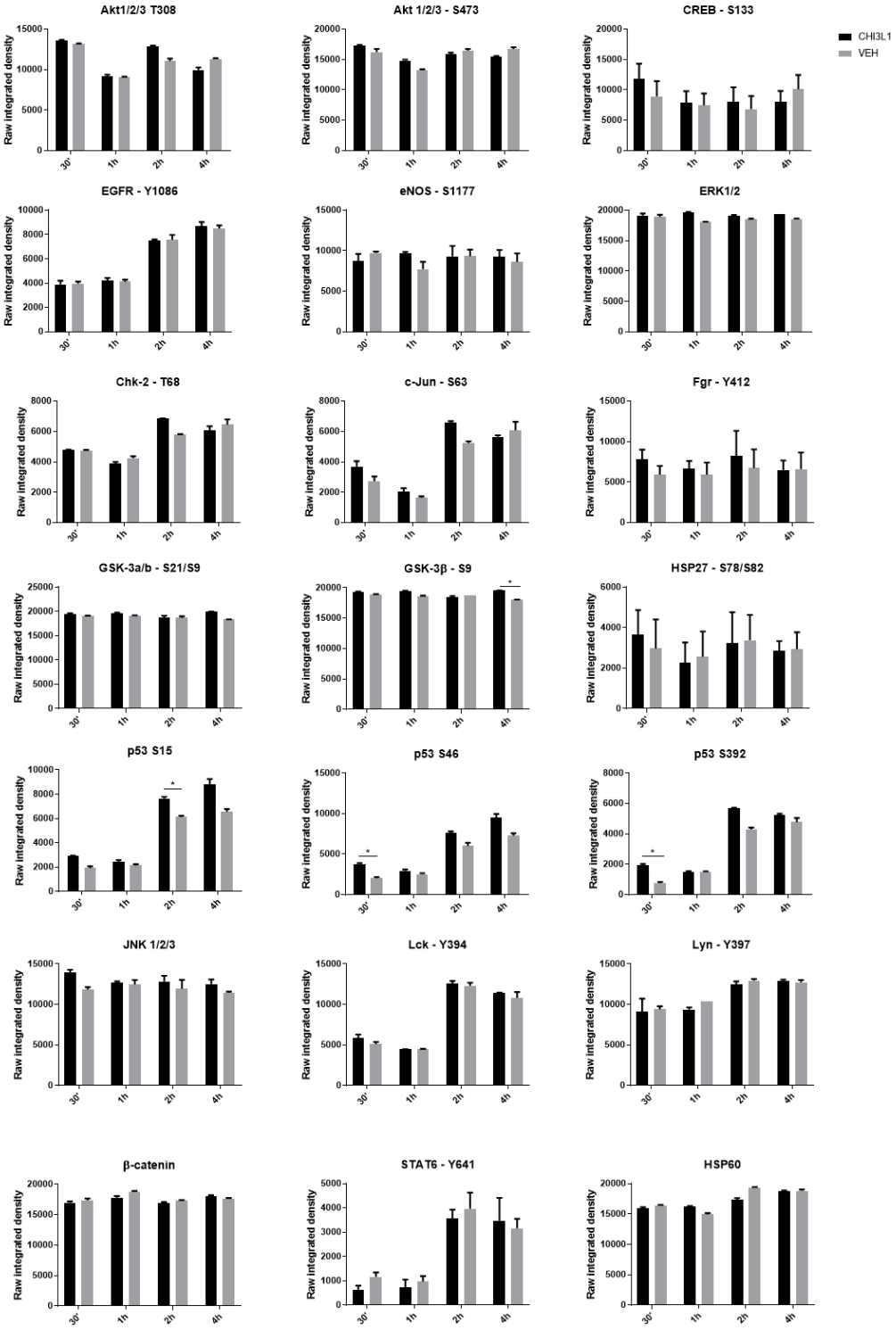
CHI3L1
VEH
Akt1/2/3 T308
Akt 1/2/3 - S473
CREB - S133
EGFR - Y1086
eNOS - S1177
ERK1/2
Chk-2 - T68
c-Jun - S63
Fgr - Y412
GSK-3a/b - S21/S9
GSK-3β - S9
HSP27 - S78/S82
p53 S15
p53 S46
p53 S392
JNK 1/2/3
Lck - Y394
Lyn - Y397
β-catenin
STAT6 - Y641
HSP60
Raw integrated density
30'
1h
2h
4h

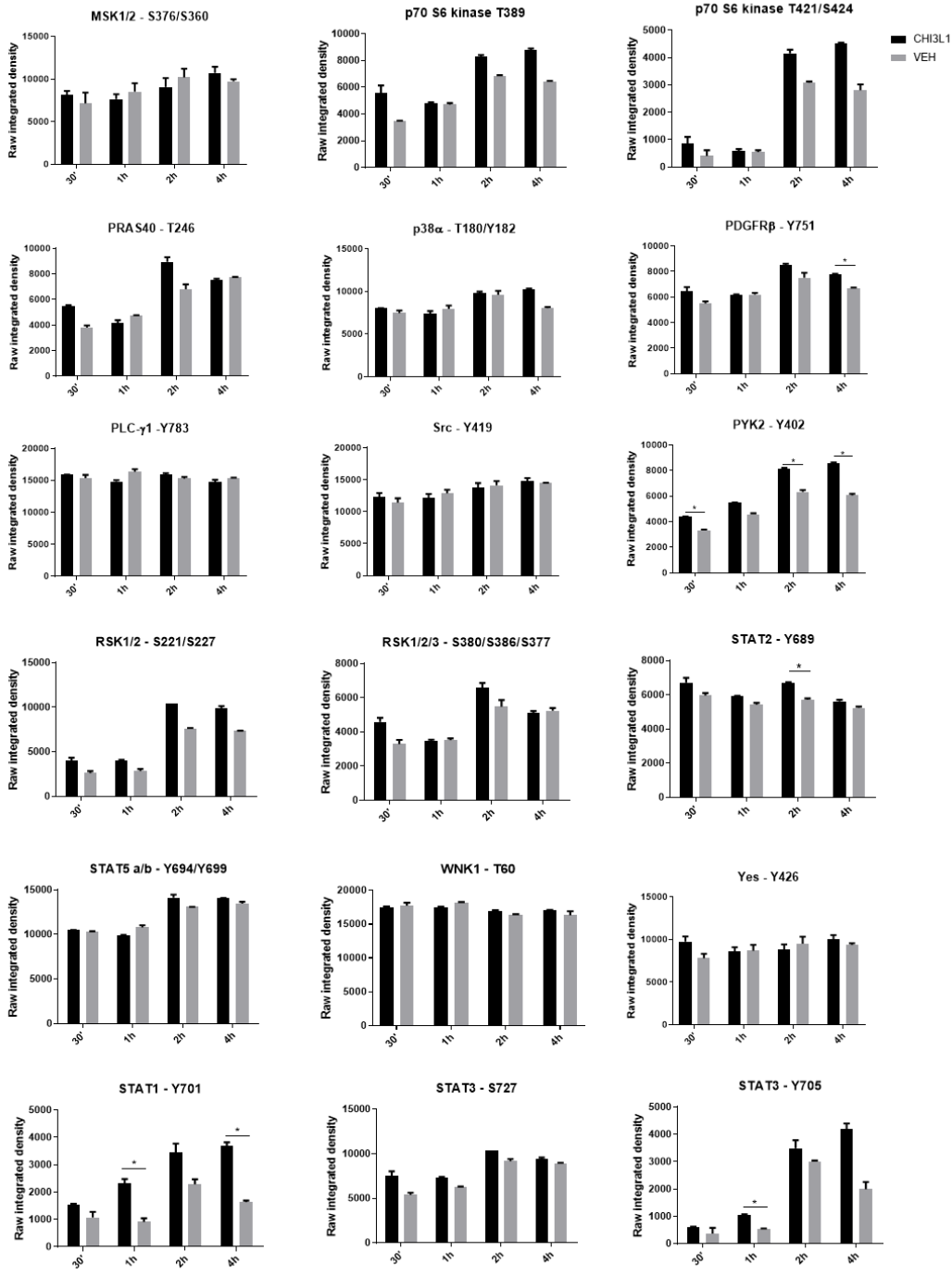
MSK1/2 - S376/S360
p70 S6 kinase T389
p70 S6 kinase T421/S424
CHI3L1
VEH
PRAS40 - T246
p38α - T180/Y182
PDGFRβ - Y751
PLC-γ1 -Y783
Src - Y419
PYK2 - Y402
RSK1/2 - S221/S227
RSK1/2/3 - S380/S386/S377
STAT2 - Y689
STAT5 a/b - Y694/Y699
WNK1 - T60
Yes - Y426
STAT1 - Y701
STAT3 - S727
STAT3 - Y705
Raw integrated density
30'
1h
2h
4h

Supplemental Figure 1. Human Phosphokinase Array results. hiPSC-derived neurons (MS-10 D28) were exposed to CHI3L1 at a concentration of 300 ng/ml, or vehicle (PBS), for 30 minutes, 1 hour, 2 hours, and 4 hours. The presented graphs display integrated pixel density values, derived from two replicates for each specific condition. Statistical analysis was conducted with a Two-Way ANOVA with Greenhouse-Geisser Correction, followed by Bonferroni post hoc analysis. The experimental design encompassed variations in treatment and time. Post hoc comparisons were performed between CHI3L1-treated versus vehicle-treated conditions at each time point. The data are presented as mean ± SD. *$p<0.05$